The systematics of oxygen isotopes in chironomids (Insecta: Diptera): a tool for reconstructing past climate

Alexander Lombino

University College London

Faculty of Social and Historical Sciences

Department of Geography

Thesis submitted for the degree of Doctor of Philosophy

September 2014

Table of Contents

Table of Tables

Table of Figures

11

14

Declaration

I, Alexander Lombino, confirm the work presented in this thesis is my own. Where information has been derived from other sources, I confirm that this has been indicated in this thesis.

Alexander Lombino

September 2014

Acknowledgements

Abstract

Oxygen isotope ratios have become an indispensable tool in elucidating past climates. In recent years the chitinous remains of chironomid larvae (Insecta: Diptera: Chironomidae), which are abundant in most lacustrine sediments, have received increasing attention as a proxy for reconstructing the oxygen isotope composition of past lake waters ($\delta^{18}O_{lakewater}$). The interpretation of stratigraphic changes in the oxygen isotopic composition of chironomid remains ($\delta^{18}O_{chironomid}$) is underpinned by the fundamental assumption that $\delta^{18}O_{chironomid}$ is primarily reflective of $\delta^{18}O_{lakewater}$, which itself is intimately associated with climate. In this investigation a series of laboratory and field-based calibration studies were conducted, with the aim of contributing to the development of $\delta^{18}O_{chironomid}$ as a tool in palaeoclimate reconstructions. All analyses were performed on purified chironomid remains using a high temperature conversion elemental analyser (TC/EA) coupled, via a ConFlo III open split interface unit, to a Delta V Advantage isotope ratio mass spectrometer (IRMS). Compositional heterogeneity and exogenous contamination are known to have a deleterious influence on $\delta^{18}O$ determinations from chitinous remains, including chironomids. In order to produce meaningful $\delta^{18}O_{chironomid}$ measurements, non-amino polysaccharide impurities present in chironomid samples were eliminated through a series of liquid solvent-based extractions (2:1 DCM: MeOH, 0.25M HCl, 0.25M NaOH) performed at 20°C for 24 hours. The chosen reaction conditions were based on the results of a systematic study evaluating the influence of chemical pre-treatments on the $\delta^{18}O$ of contemporary chironomid head capsules isolated from commercially grown larvae. To date the absence of a standardised pre-treatment procedure has hindered inter-laboratory comparisons, therefore it is recommended that analysts employ a similar protocol in the future. Laboratory and field-based calibration studies indicate that the interpretation of $\delta^{18}O_{chironomid}$ is not straightforward, with signals influenced to varying degrees by $\delta^{18}O_{lakewater}$, temperature and secondary factors (e.g. diet). The findings of these calibration studies were used to construct a novel chironomid-carbonate palaeothermometer, which was applied to $\delta^{18}O_{chironomid}$ and $\delta^{18}O_{bulk\_carbonate}$ records obtained from a Late-glacial sediment sequence

(Hawes Water, UK). Although the general climate trends reported by this approach are generally in good agreement with other palaeoclimate reconstructions from the region, absolute temperature estimates were unrealistically low (ranging between −9 and +11°C). Based on the limited available data the spurious temperature estimates were attributed to diagenetic alteration. The strong correlation observed between the two independent $\delta^{18}O$ records indicates that diagenetic alterations are likely to have retained some of the original isotopic signature. Despite the efforts of this investigation it is clear that this approach remains in its infancy, with further extensive calibration studies necessary. However, the results presented in this thesis demonstrate that in suitable limnological settings $\delta^{18}O_{chironomid}$ has great potential for elucidating past climates.

Chapter 1 Background and context

1.1 Project rationale

The earth's climate is unequivocally changing. Instrumental and historical records from across the globe reveal that average land and ocean surface temperatures have increased by ~0.85°C between 1880 and 2012 (IPCC 5th assessment report, 2013). The potential consequences of climate change (e.g. more frequent extreme weather events, rising sea levels and migrating ecosystems and resources) are likely to pose a serious threat to biodiversity and have far-reaching socio-economic implications (IPCC 5th assessment report, 2013). As a consequence, climate change has become one of the most prominent scientific, economic and political issues facing modern society. However, policy-making processes aimed at mitigating and adapting to the challenges of climate change have been hampered by uncertainties surrounding its likely rate and magnitude (Alley 2003). In order to gain a better insight into the likely effects of future climate change a more comprehensive understanding of long-term climate perturbations is necessary (Overpeck 2007).

Instrumental and historical records lack sufficient temporal (<150 years) and spatial resolution to provide an adequate perspective of past climatic variations, where natural forcing (e.g. solar, volcanic and orbital) and feedback mechanisms act on centennial to millennial time-scales. The development of physical, biological and geochemical proxies capable of providing climatic information over these time-scales is fundamental for improving our understanding of the climate system, permitting the development of more sophisticated global climate models (Fricke & O'Neil 1999; Hargreaves & Annan 2009; Jones *et al.,* 2009). In recent decades, facilitated by the advent and development of mass spectrometry techniques, stable isotope geochemistry has revolutionised our understanding of past environments (e.g. temperature, hydrological status, rainfall, salinity, productivity and nutrient cycling). Traditionally stable isotope based studies concerned with reconstructing past environments have been restricted to a

limited number of elements, including, hydrogen (^{1}H, ^{2}H), carbon (^{12}C, ^{13}C), nitrogen (^{14}N, ^{15}N), oxygen (^{16}O, ^{18}O) and sulphur (^{32}S, ^{34}S). Recent attempts to quantify palaeoclimates have focused on the interpretation of oxygen isotope ratios (^{18}O/^{16}O) in a variety of different organic and inorganic materials preserved in natural archives (e.g. ice cores (Jouzel *et al.,* 1997), speleothems (Fleitmann *et al.*, 2004; Hopley *et al.,* 2009), corals (Juillet-Leclerc *et al.,* 2009, tree rings (Loader *et al.,* 2008; McCarroll & Loader 2004), peat bogs (Daley *et al.,* 2010) marine (Waelbroeck *et al.,* 2002; Shackleton 1967) and lake sediments (Leng & Marshall 2004)). This approach has become an indispensable tool in deciphering past temperatures, since the seminal works of Urey (1947) and McCrea (1950) first highlighted the potential of oxygen isotopes in ocean palaeothermometry.

In the terrestrial realm, lake sediments are recognised as one of the most valuable archives for assessing past climates. The physical and/or biological responses of a lake system to climate perturbations are often preserved in their sediments, which can be dated to a reasonable degree of accuracy (Battarbee 2000; Birks *et al.,* 2000; Fritz 1996; Lotter *et al.,* 1997). Stuiver (1970) was among the first to realise that certain materials in lacustrine sediments had the potential to preserve information of the oxygen isotope composition of the lake water ($\delta^{18}O_{lakewater}$) at the time of formation. In limnologically suitable locations $\delta^{18}O_{lakewater}$ is strongly correlated with the oxygen isotopic composition of precipitation ($\delta^{18}O_{precipitation}$), which itself is intimately linked with climate (Dansgaard 1964). Historically, $\delta^{18}O_{lakewater}$ records have been generated using a limited number of inorganic and organic materials preserved in lacustrine sediments (e.g. endogenic mineral precipitates, fossil floral and faunal remains) (Andersen *et al.,* 2001; von Grafenstein *et al.,* 1996; 1999; 2013; Leng *et al.,* 2006; Leng & Barker 2006; Leng & Marshall 2004; Sauer *et al.,* 2001). Despite being one of the most abundant and resilient components found in lacustrine sediments, the remains of aquatic invertebrates have received relatively little attention as a tool for inferring past $\delta^{18}O_{lakewater}$ (e.g. Gröcke *et al.,* 2006; Heiri *et al.,* 2012;

Leng & Henderson 2013; Miller 1991; Motz 2000; Nielson & Bowen 2010; Verbruggen *et al.,* 2010a; 2010b; 2011; Wang *et al.,* 2009; Wooller *et al.,* 2004; 2008). This thesis aims to contribute to the on going development of the analysis of oxygen isotope ratios in chironomid (Insecta: Diptera: Chironomidae) remains as a tool for reconstructing past climates in the terrestrial realm. This approach has the potential to be combined with complementary $\delta^{18}O$ records to provide quantitative palaeotemperature estimates.

1.2 Stable isotope geochemistry: an introduction

In order to provide an adequate context for this thesis a brief introduction to stable isotopes will be provided in this section. For a more comprehensive review of the applications of stable isotope geochemistry in palaeoclimate reconstructions see Criss (1999), Koch (1998), Hoefs (2009) and Leng & Marshall (2004).

1.2.1 Notation, abundance and distribution

All atoms are composed of a nucleus, made up of protons and neutrons, surrounded by a cloud of electrons. Isotopes are defined as nuclides of an element that chemically are virtually identical to one another (i.e. have the same atomic number), but which display detectible disparities in their physiochemical properties arising from differences in atomic mass (Criss 1999; Hoefs 2009). The total quantity of stable isotopes on earth is fixed, with the majority of elements having at least two naturally occurring stable isotopes. Lighter elements (e.g. hydrogen: ^{1}H, ^{2}H, ^{3}H, carbon: ^{12}C, ^{13}C, nitrogen: ^{14}N, ^{15}N and oxygen: ^{16}O, ^{17}O, ^{18}O) have traditionally been the focus of the majority of stable isotope analyses since the proportional differences in mass between the isotopes of these elements is greatest, and therefore easiest to detect (Criss 1999). However, technical innovations in mass spectrometry have facilitated the analyses of isotopes from other elements (e.g. calcium: ^{40}Ca, ^{42}Ca, ^{43}Ca, ^{44}Ca, ^{46}Ca, silicon: ^{28}Si, ^{29}Si, ^{30}Si and sulphur: ^{32}S, ^{33}S, ^{34}S, ^{36}S).

Stable isotope measurements are commonly reported as a ratio between the relative abundances of the different isotopes, defined by the following expression:

$$R = \frac{\textbf{Abundance of Rare Isotope}}{\textbf{Abundance of Common Isotope}}$$

Relative differences in isotopic ratios of compounds can be determined far more precisely than absolute values. Therefore, according to convention

stable isotope ratios are commonly reported as relative differences between samples and a known standard in terms of parts per thousand (‰), using the delta notation (δ):

$$\delta_{Sample} = \left(\frac{R_{sample} - R_{Standard}}{R_{Standard}} \right) \times 1000$$

where R_{sample} is the isotopic ratio of the sample and $R_{standard}$ is the isotopic ratio of the standard. In samples with a positive δ value, the ratio between 'heavy' and 'light' isotopic forms is higher than in the standard; whereas the opposite is true in samples with a negative δ value.

Isotope fractionations (partitioning of isotope species), occurring during chemical, physical and/or biological processes, are responsible for creating variability in the distribution of stable isotopes of a given element. The dominant processes in the cycling of C, N, O, H and S within the biosphere are associated with characteristic fractionations, making stable isotopes useful environmental proxies (Criss 1999; Gat *et al.,* 2000; Hoefs 2009). The two most important phenomena responsible for creating isotopic fractionations in nature are briefly summarised below:

a) **Equilibrium isotope effects** occur during the exchange of isotopes among substances in bi-directional chemical reactions, where mass is conserved (Koch 1998). Equilibrium fractionations are a function of bond type and are strongly related to the laws of thermodynamics, with greater fractionation observed at lower temperatures. As a consequence heavy isotope species tend to accumulate in a particular component of a system where they are bound most strongly (Hayes 1983).

b) **Kinetic isotope effects** occur due to differences in the reaction rates of isotopes and are normally associated with unidirectional and incomplete reactions (e.g. evaporation and diffusion), where both

the bond strength and isotope velocity are important factors (Criss 1999; Hoefs 2009). Continual discrimination against heavier isotope species during kinetic isotope effects, results in the enrichment of the lighter isotopes in the product (Criss 1999; Hoefs 2009).

The fractionation of isotopes between two phases/substances (e.g. liquid water and water vapour) can be defined by a fractionation factor:

$$\alpha_{p-s} = \frac{R_p}{R_S}$$

where α_{p-s} is the fractionation observed between the two phases/substances, R_p is the ratio of heavy to light isotopes in the product and, R_S is the ratio of heavy to light isotopes in the substrate. Isotope effects are generally small (α = ~1) for most reactions, thus authors often report the difference in ‰ between two phases rather than the fractionation factor itself:

$$\varepsilon_{B/A} = (\alpha_{B/A} - 1) \times 1000$$

where ε is the result of the fractionation process, and is referred to as enrichment. If $\varepsilon > 0$ then the heavy isotope is described as being depleted in compound B with respect to A (Criss 1999; Hoefs 2009).

Isotope fractionations can be predicted by the laws of thermodynamics, which describe that at a given energy state molecules with a higher mass will have a lower diffusion velocity and collision frequency (the prerequisites for a chemical reaction), compared to molecules with a lower mass:

$$kT = \frac{1}{2}mv^2$$

Equation 4

where k = Boltzmann constant, T = absolute temperature, m = molecular mass, v = average molecular velocity. Moreover, molecules containing a higher proportion of heavier isotopes will require more kinetic energy to overcome the net attractive forces (binding energies) in order to change state/phase, compared to molecules containing a higher proportion of lighter isotopes (Gat *et al.,* 2000; Hoefs 2009).

1.3 Palaeoclimate application of oxygen isotopes in lacustrine sediments

1.3.1 Oxygen isotope systematics

Oxygen is one of the most abundant elements on earth. It has three naturally occurring stable isotopes; ^{16}O (99.763% abundance), ^{17}O (0.0375% abundance) and ^{18}O (0.1995% abundance) (Nier 1950). The ratio of $^{18}O/^{16}O$ (relative amount), the two most common forms, varies spatially and temporally in nature, related to changes in climate. Therefore, scientists can infer past climates from stratigraphic changes in $^{18}O/^{16}O$ preserved in proxy archives. Oxygen isotopes are particularly well suited as a tool for inferring past climates for four key reasons:

I. Small differences in oxygen isotope ratios of a compound can be measured precisely by an isotope ratio mass spectrometer (IRMS), as a result of large differences between the abundances of the different isotopic forms.

II. Oxygen typically forms compounds that are well preserved over geological time scales.

III. The relationship between the fractionation of oxygen isotopes in certain mineral precipitates (i.e. carbonates) and temperature can be quantified experimentally and empirically.

IV. Oxygen isotope records are largely unaffected by lags associated with changes in floral and faunal communities.

Two main internationally accepted scales have been developed for oxygen isotope analysis: the Vienna Pee Dee Belemnite (V-PDB) and Vienna Standard Mean Ocean Water (V-SMOW) scales. The use of the different scales depends on the type of material being measured. Oxygen isotope analyses of low temperature carbonates are reported relative to the V-PDB scale; whereas most other oxygen isotope analyses (waters, organic matter, silicates, phosphates, sulphates) are reported relative to the V-SMOW scale (Hoefs 2009).

1.3.2 Natural variations of oxygen isotopes in the hydrological cycle

The stable isotopic composition of meteoric waters have long been recognised as powerful palaeoclimate tracers. Water molecules (H_2O) are composed of two hydrogen atoms (^1H and D (deuterium)) and one oxygen (^{16}O, ^{17}O, ^{18}O) atom. Out of the possible isotopic combinations creating water molecules, only three are found in measurable amounts in nature; $^1H_2^{16}O$ (atomic weight = 18), $^1HD^{16}O$ (atomic weight = 19), $^1H_2^{18}O$ (atomic weight = 20). In this section the spatial distribution of isotopes in precipitation and the main hydrological processes determining the isotopic composition of precipitation (rain, snow and hail) are briefly explored.

The International Atomic Energy Agency (IAEA), in collaboration with the World Meteorological Organization (WMO), established the Global Network of Isotopes in Precipitation (GNIP) in the early 1960's. This network was responsible for mapping the isotopic composition of monthly precipitation across the globe. The database created by the network demonstrated that the distribution of $\delta^{18}O$ and δD in precipitation is characterised by a systematic linear relationship, referred to as the global meteoric water line (GMWL) (Craig 1961):

$$\delta D = 8 \times \delta^{18}O + 10$$

Equation 5

The slope (~8) of the GMWL reflects the temperature-dependant equilibrium fractionation of heavy isotopes between water vapour and precipitation; whereas the intercept (also referred to as the deuterium excess) reflects kinetic isotope fractionations during evaporative processes and can be used to infer water vapour source(s) (Dansgaard 1964; Leng *et al.,* 2006).

An extended account of the variables controlling the oxygen isotopic composition of precipitation ($\delta^{18}O_{precipitation}$) is beyond the scope of this study (see Clark & Fritz 1997 for review). In brief, $\delta^{18}O_{precipitation}$ can be considered to be reflective of the water vapour source(s), modified by isotope

fractionations accompanying phase transitions (evaporation-condensation-freezing) during the passage of water molecules through the hydrological cycle (Darling *et al.,* 2003; 2006; Gat 1996; Rozanski *et al.,* 1993). During the migration of an air mass from low latitudes, where the global evaporative flux is concentrated, to higher latitudes, adiabatic cooling induces condensation of water vapour to form clouds. In the clouds, water droplets coalesce with one another before eventually falling to the surface of the earth as precipitation. During the migration of an air mass rainout results in the progressive depletion of heavy isotopes in the remaining vapour, following a Rayleigh-type distillation model (Jouzel *et al.,* 2000) (Figure 1-1).
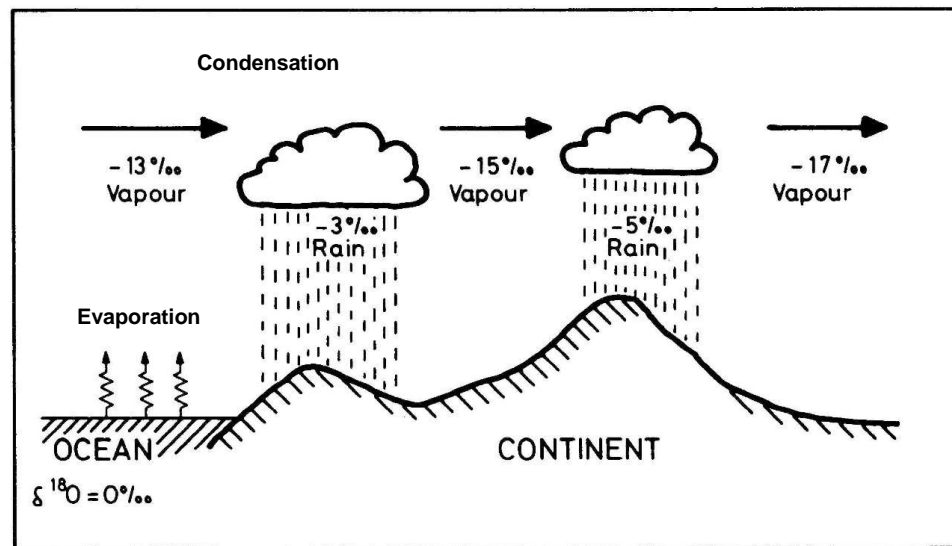
Figure 1-1: Schematic diagram of oxygen isotope fractionation in the hydrological cycle. Differences in the diffusivity of water molecules containing ^{16}O and ^{18}O result in fractionations during the passage of water through the hydrological cycle (Hoefs 2009).

In mid-high latitudes $\delta^{18}O_{precipitation}$ is highly correlated with mean annual air temperature (MAT) (Dansgaard 1964). The global relationship between $\delta^{18}O_{precipitation}$ and temperature (known as the 'Dansgaard relationship') is ~ +0.2 to +0.7‰°C^{-1} (Dansgaard 1964), with an average coefficient of ~ +0.6‰°C^{-1} (Rozanski *et al.,* 1993).

$\delta^{18}O_{precipitation}$ can also be influenced by a number of other mutually related factors including:

Altitude effects- Increases in altitude induce adiabatic cooling by advection, resulting in the progressive depletion of heavy isotopes in an air mass. Vertical $\delta^{18}O_{precipitation}$ gradients vary between -0.15 to $-0.5‰/100m^{-1}$ (Poage & Chamberlain 2001).

Amount effects- This effect is commonly observed in tropical low latitude locations (between 20°N and 20°S) where seasonal variations in temperature are minimal and convection-driven rainfall events are common (Dansgaard 1964; Rozanski *et al.,* 1993). Preferential depletion of heavy isotope species during a storm event can result in enrichment of ^{16}O. Consequently, there is a strong inverse correlation between $\delta^{18}O_{precipitation}$ and the amount of precipitation (Dansgaard 1964; Rozanski *et al.,* 1993).

Continentality- This effect results in the progressive depletion of heavy isotope species during the migration of an air mass in-land (Alley & Cuffey 2001). Continental effects depend on both topography and climate. An isotope gradient of $\sim -2.0‰/1000km^{-1}$ can be observed in modern day precipitation across Europe (Rozanski *et al.,* 1993).

Seasonal effects- Mid-high latitudes are characterised by marked seasonal variations in $\delta^{18}O_{precipitaion}$, with values becoming more negative in the winter compared to the summer (Rozanski *et al.,* 1993). The seasonal variability in $\delta^{18}O_{precipitaion}$ is driven by temperature-dependant changes in; i) available atmospheric water vapour, ii) the evapotranspiration flux, which amplifies seasonal differences in the amount of water vapour in the atmosphere, and iii) changes in the prevailing air mass source and circulation patterns (Gat 1996; Rozanski *et al.,* 1993).

The combined effects of these mutually related factors produce distinct isotopic differences in meteoric waters across the globe (Darling *et al.,* 2006). The basic mechanisms responsible for controlling the isotopic composition of precipitation are today relatively well defined (e.g. Dansgaard 1964; Darling *et al.,* 2006; Gat 1996; Rozanski *et al.,* 1993).

1.3.3 Natural variations in $\delta^{18}O_{lakewater}$

In comparison to the oceans, freshwater systems are far more sensitive to changes in isotopic composition. In mid-high latitudes, $\delta^{18}O_{lakewater}$ at hydrologically open sites (i.e. large, catchment area/surface area ratio (>20), short residence time) is primarily reflective of precipitation received by the lake, with values plotting on, or close to, the GMWL (Figure 1-2) (Alley & Cuffey 2001; Clark & Fritz 1997; Henderson & Holmes 2009; Leng & Marshall 2004; Sauer *et al.,* 2001). In contrast, $\delta^{18}O_{lakewater}$ in hydrologically closed sites (i.e. small catchment, no effective outflow, long residence times) is primarily reflective of precipitation: evaporation, with values displaced from the GMWL. Deviations from the GMWL occur as a result of local meteorological or hydrological factors (Rozanski *et al.,* 1993). The majority of hydrologically closed lakes lose water via evaporation, which is influenced by wind speed, temperature and humidity (Hostetler & Benson 1994). In such circumstances, a local evaporative line (LEL) can be used to describe the co-varying relationship between $\delta^{18}O$ and δD in lake water (Figure 1-2). The lower gradient of the LEL compared to GMWL arises due to differences in the rate of fractionation of water molecules during kinetic (evaporative) process (Araguás Araguás *et al.,* 2000).
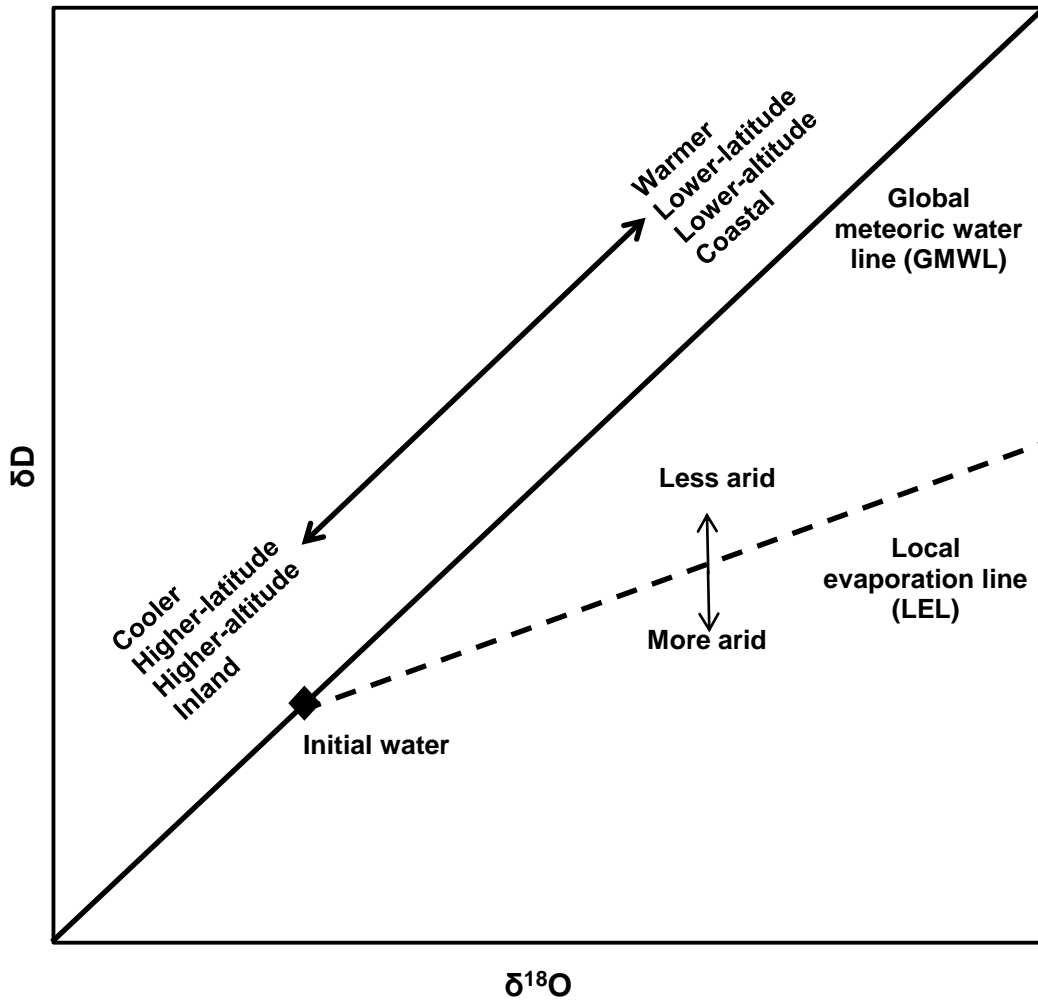
Figure 1-2: Plot of $\delta^{18}O$ vs δD depicting major controls on isotopic composition of lake water. Deviations from the Global meteoric water line (MWL) are reflective of local meteorological or hydrological factors at a particular site.

Lakes are complex dynamic systems that are connected to the hydrological cycle through surface and sub-surface inflows/outflows and precipitation/evaporation fluxes, with the response of a lake to environmental change likely to vary (Talbot 1990). Consequently, $\delta^{18}O_{lakewater}$ is more accurately described as reflecting the hydrological balance between the inputs (e.g. precipitation, groundwater, and surface run-off) and outputs (e.g. groundwater loss, evaporation and outflows), modified by a wide range of interlinked local environmental parameters specific to the lake in question (e.g. climate, atmospheric circulation patterns, hydrological conditions and catchment characteristics) (Anderson *et al.,* 2001; Buhay *et al.,* 2012; Darling *et al.,* 2006; Leng & Marshall 2004).

1.3.4 Variations in oxygen isotopes in compounds preserved in lacustrine sediments

The isotopic composition of components preserved in lacustrine sediments can provide a valuable insight into the prevailing environmental conditions during their formation. Stratigraphic variability in $\delta^{18}O$ records generated from endogenic (e.g. calcite precipitated in the water column in response to photosynthetic activity) and accretionary biogenic (e.g. skeletal structures of ostracods and molluscs) carbonate precipitates have routinely been employed in palaeoclimate reconstructions (Andersen *et al.,* 2001; von Grafenstein *et al.,* 1996; 1999; 2013; Ito *et al.,* 2003; Leng *et al.,* 2006; Leng & Marshall 2004). However, carbonate sequences in non-alkaline, dilute, open lakes, which are common in high latitudes, are often incomplete or difficult to interpret (Gröcke *et al.,* 2006; Sauer *et al.,* 2001; Wooller *et al.,* 2004). The high latitudes are widely believed to have played an important role in driving past climate change (e.g. Shackleton 2000), consequently palaeoclimate reconstructions from these regions are of great interest. More recently alternative proxies have been explored in areas with a dearth of preserved carbonate remains. For example, biogenic silica (e.g. diatoms) has become an increasingly popular $\delta^{18}O_{lakewater}$ proxy (Lamb *et al.,* 2005; 2007; Leng *et al.,* 2006; Leng & Barker 2006; Swann *et al.,* 2006). However, biogenic silica requires extensive purification prior to $\delta^{18}O$ analysis since analytical procedures (typically fluorination) liberate oxygen from all the components present within a sample (Morley *et al.,* 2005; Lamb *et al.,* 2007).

In cases of equilibrium precipitation, the oxygen isotope composition of inorganic compounds ($\delta^{18}O_{inorganic}$) formed in a lake can be considered to reflect $\delta^{18}O_{lakewater}$ modified by temperature-dependant isotope fractionations. However, in practice the interpretation of $\delta^{18}O_{inorganic}$ is complicated because both $\delta^{18}O_{lakewater}$ and temperature are influenced by changes in climate (Leng *et al.,* 2006; Leng & Marshall 2004). Furthermore, disequilibrium effects may cause disparities between the isotopic composition of the lake water and the mineral precipitate (Figure 1-3) (see Leng *et al.,* 2006; Leng & Marshall 2004).
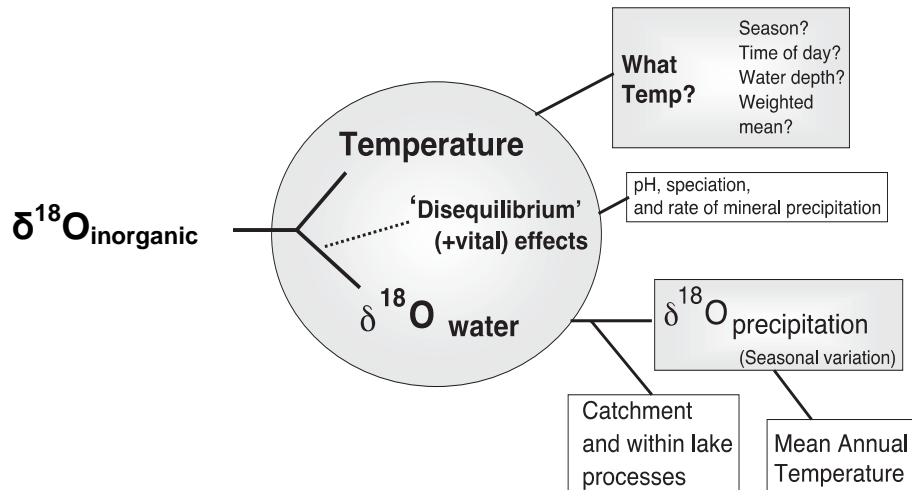
Figure 1-3: Controls on the oxygen isotope composition of inorganic compounds ($\delta^{18}O_{inorganic}$) preserved in lacustrine sediments. In cases of equilibrium, $\delta^{18}O_{inorganic}$ is reflective of $\delta^{18}O_{lakewater}$ modified by temperature-dependant fractionations and disequilibrium effects (Leng & Marshall 2004).

Organic compounds preserved in lacustrine sediments potentially offer a more direct approach for inferring past $\delta^{18}O_{lakewater}$, since they are anticipated to be largely independent of kinetic (temperature related) and disequilibrium effects (Leng *et al.,* 2006). For example, $\delta^{18}O_{aquatic\_cellulose}$ records have been used to infer past $\delta^{18}O_{lakewater}$ (e.g. Anderson *et al.,* 2001; Edwards & McAndrews 1989; Epstein *et al.,* 1977; DeNiro & Epstein 1981; Sauer *et al.,* 2001; Wolfe *et al.,* 2007). However, the reproducibility and reliability of $\delta^{18}O_{aquatic\_cellulose}$ determinations can be compromised by the presence of terrestrial cellulose, which is often enriched in ^{18}O compared to aquatic cellulose (Sauer *et al.,* 2001). Supplementary elemental data can be used to constrain the interpretation of cellulose sources, with low C/N ratios (<10) interpreted to reflect predominantly aquatic derived organic matter (Wolfe *et al.,* 2001). However, Sauer *et al.* (2001) argued that elemental ratios are insufficient criteria for interpreting the origin of cellulose.

Technical innovations in continuous flow stable isotope mass spectrometry (e.g. Farquhar *et al.,* 1997; Kornexl *et al.,* 1999; Koziet 1997) have facilitated the diversification and expansion of materials used for oxygen isotope determinations. The chitinous remains of chironomid larvae (Insecta: Diptera:

Chironomidae) have recently received increasing attention as a $\delta^{18}O_{lakewater}$ proxy (e.g. Heiri *et al.,* 2012; Verbruggen *et al.,* 2010; 2010b; 2011; Wang *et al.,* 2008; 2009; Wooller *et al.,* 2004; 2008). This approach is underpinned by the assumption that the oxygen isotope composition of chironomid remains ($\delta^{18}O_{chironomid}$) is reflective of $\delta^{18}O_{lakewater}$ in which the larvae grew. Since aquatic fauna primarily metabolise dissolved oxygen from their habitat water and because isotopic exchange is thought to be negligible in these exoskeletal fragments following biosynthesis, the remains of aquatic insects are potentially capable of retaining information of their biochemical heritage (Gröcke *et al.,* 2006; Heiri *et al.,* 2012; Miller 1991; Motz 2000; Nielson & Bowen 2010; Schimmelmann 2010; Schimmelmann & DeNiro 1986; Schimmelmann *et al.,* 1986; Verbruggen *et al.,* 2010a; 2010b; 2011 Wang *et al.,* 2009; Wooller *et al.,* 2004; 2008). Furthermore, since chironomid remains are easily identified under a light microscope the approach should be less susceptible to contamination from semi-terrestrial/terrestrial taxa or sedimentary components, which often have a deleterious influence on $\delta^{18}O$ determinations in other biomolecules. Consequently this approach is potentially less technically challenging than oxygen isotope analysis in other organic and inorganic compounds.

1.4 Chironomids in palaeoclimate reconstructions

This section will provide a brief introduction to chironomid biology and ecology. This will be followed by a review of the development of oxygen isotope analysis in chironomid remains. A comprehensive overview of the application of stable isotopes (O, C, H and N) in chironomid remains can be found in Heiri *et al.* (2012).

1.4.1 Biology and ecology

Chironomidae are a taxonomically diverse family of non-biting flies (Insecta: Diptera) comprised of eleven subfamilies and estimated to contain ~15,000 species worldwide (Armitage *et al.,* 1995). As larvae, chironomids are ubiquitous in virtually all aquatic biomes, occupying an unparalleled number of habitats (Brooks & Birks 2001; Brooks 2006; Ferrington 2008; Langdon *et al.,* 2004; Oliver 1971; Velle *et al.,* 2005). The broad-scale distribution of chironomids is restricted to a specific set of environmental conditions, predominantly driven by temperature (Brooks 2000; Brooks *et al.,* 2007; Eggermont & Heiri 2012; Kurek 2008; Płóciennik *et al.,* 2011; Self 2010; Velle *et al.,* 2005).

Chironomids are holometabolous (undergo metamorphism), developing from an egg through four larval instar stages, the first three of which are restricted to the aquatic realm, before emerging into the terrestrial realm as a winged adult (Figure 1-4).
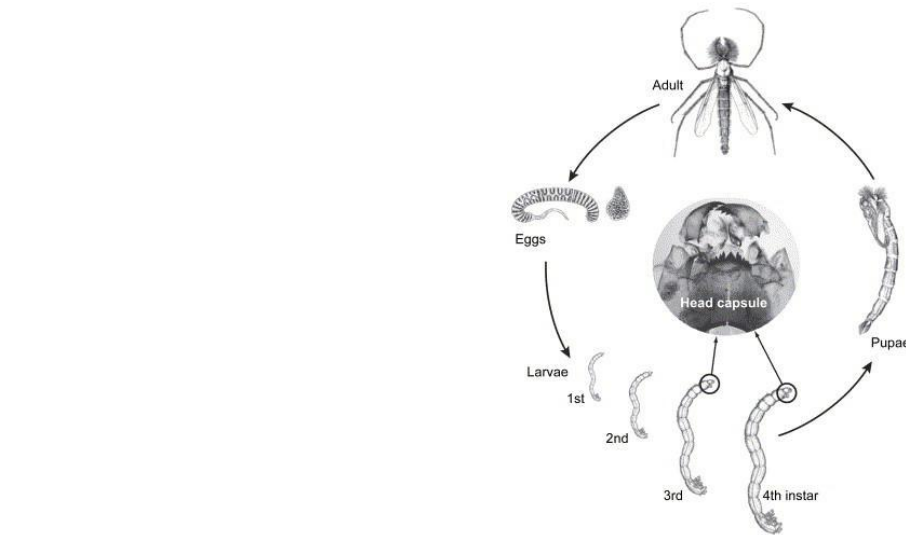
Figure 1-4: Schematic representation of the chironomid life cycle from Ruiz *et al.,* (2006).

Each developmental stage of the chironomid life cycle will now be discussed in more detail.

Egg stage- Eggs are laid (several hundred at a time) in a hydrophilous gelatinous matrix directly into water or attached to a suitable substrate. The gelatinous matrix offers protection and a source of nourishment for the embryonic pro-larvae and the newly hatched larvae (Oliver 1971).

Larval stage- This stage assumes a disproportionate importance in the life cycle, relative to the other stages, encompassing four progressively lengthening periods of growth, each defined by exoskeletal ecdysis (periodic molting of the head capsule) (Walker 1987). The early instar stage is largely planktonic, permitting dispersal, whereas the latter instars are generally sedentary.

Mature chironomid larvae can generally be described as having elongate nine-segmented soft cylindrical bodies (2-30mm in length), which bear a fully developed non-retractile, strongly sclerotized, chitinous head capsule (Figure 1-5) (Brooks *et al.,* 2007).

head capsule

anterior parapods

anal or procercal setae

posterior parapods

anal tubules

Chironominae larva (*Chironomus*)
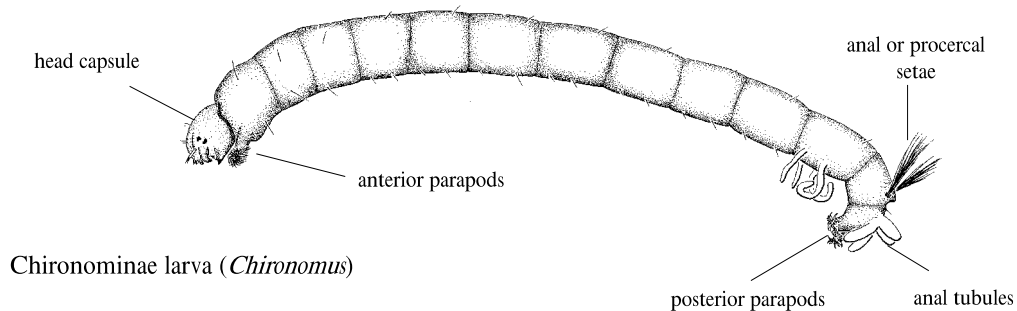
Figure 1-5: Schematic diagram of chironomid larvae (typically 2-30mm in length) showing key morphological characteristics from Epler (2001).

Larvae typically inhabit the uppermost sediments of both littoral and profundal environments, within silken tubes constructed from specialised organs (Brooks *et al.,* 2007). Larvae may also be found clinging on or burrowing into aquatic macrophytes, woody debris or other invertebrates, as well as living freely within the water column (Brooks *et al.,* 2007; Bouchard & Ferrington 2008; Oliver 1971; Płóciennik *et al.,* 2011).

Pupal stage- This stage typically persists only a few hours or days and involves the morphological rearrangement of larva in preparation for adult emergence (Armitage *et al.,* 1995; Oliver 1971). At maturity pupa migrate to the water surface where the adult emerges into the terrestrial realm, leaving the discarded pupal case on the surface of the water (Bouchard & Ferrington 2008; Pinder 1986; Walker 1987).

Imago- The reproductive aspects of the life cycle are completed during this stage (Oliver, 1971). Adult emergence within a population is synchronised with changes in external stimuli (e.g. temperature and photoperiod), which maximises copulation potential (Oliver 1971; Pinder 1986). The adult stage persists anywhere between a few days to a week (Oliver 1971; Pinder 1986).

The duration of the chironomid life cycle varies greatly among taxa, with growth (i.e. the increase in larval body size) and development (i.e. progression through the life cycle) predominately under the control of temperature (Walker 1987). Laboratory rearing experiments have demonstrated a strong positive correlation between chironomid development and water temperature, up to a certain threshold (Ward & Cummins 1979). Temperature may also have an indirect influence on chironomid growth and development through the alteration of lake productivity, dissolved oxygen concentration, thermal stratification, pH and salinity (Pinder 1986).

Chironomid larvae are generally found in lake sediments all year round. In temperate climates chironomid adults typically emerge into the terrestrial realm in spring or late summer, triggered by changes in water temperature and light intensity (Johnson & Pejler 1987). The number of generations within a population per year (voltinism) increases with MAT, with species from low latitudes typically being multivoltine (multiple generations per year) whilst those in temperate locations are most likely to be univoltine (single generation per year) or bivoltine (two generation per year).

1.4.2 Chironomid-inferred temperature (CI-T) models

The chitinous head capsules of chironomid larvae, shed during ecdysis or from deceased individuals, are often one of the most abundant macro-invertebrate remains encountered in lacustrine sediments. These remains are readily identifiable at least to a generic level, based on distinctive morphological characteristics (Brooks *et al.,* 2007). Since chironomids are sensitive environmental indicators, fossil assemblages can be enumerated to infer changes in past environmental conditions (e.g. Brooks & Birks 2001; Brooks 2006; Langdon *et al.,* 2004; Walker & Cwynar 2006).

Walker & Mathewes (1987) were among the first to suggest that mean July air temperature was a dominant driver of the distribution of chironomid taxa. This observation facilitated the development of chironomid-inferred temperature (CI-T) models, to quantitatively infer past temperature from

stratigraphic changes in the taxonomic composition of chironomid assemblages (e.g. Brooks & Birks 2001; Lotter *et al.,* 1998; Walker *et al.,* 1991; Walker & Cwynar 2006; Walker & Mathewes 1987). CI-T models are derived from regionally-calibrated training sets, which empirically link contemporaneous taxonomic distributions and abundances to temperature (Brooks & Birks 2001; Eggermont & Heiri 2012). CI-T models generally produce estimates in accordance with other palaeoclimate reconstructions (Brooks 2006; Eggermont & Heiri 2012; Heiri *et al.,* 2007; Walker & Cwynar 2006) and instrumental records (Larocque & Hall 2003). However, disparities have been observed due to difficulties in disentangling the response of chironomid communities to changes in temperature (Bigler *et al.,* 2002; Brooks 2006; Brooks & Birks 2001; Eggermont & Heiri 2012; Velle *et al.,* 2010).

Although the broad-scale geographical distribution of chironomid taxa is mainly driven by temperature, in-lake variables have also been observed to influence chironomid distribution (Walker & Mathews 1989; Walker *et al.,* 1991). As a consequence chironomid assemblages can also be used to infer past changes in pH (Henrikson *et al.,* 1982), salinity (Eggermont *et al.,* 2006), water depth (Hofmann 1998; Korhola *et al.,* 2000), hypolimnetic anoxia (Little & Smol 2001; Quinlan *et al.,* 1998) and trophic status associated with changes in total phosphorous and chlorophyll-a (Brodersen & Lindegaard 1999; Brooks & Birks 2001; Lotter *et al.,*1998; Zhang *et al.,* 2006).

1.4.3 Oxygen isotope analyses of chironomid head capsules: a tool in palaeoclimate reconstructions

In a pioneering study Wooller *et al.* (2004) demonstrated that the oxygen isotope composition of chironomids ($\delta^{18}O_{chironomid}$), was highly correlated with interpolated regional $\delta^{18}O_{precipitation}$ ($r^2 = 0.96$) from North American lakes across a broad climatic range (Figure 1-6). However, this study was only based on surface sediments collected from four lakes and no information regarding $\delta^{18}O_{lakewater}$ was provided, making the assessment of oxygen isotope fractionation between chironomid head capsules and lake water ($\alpha^{18}O_{chironomid\text{-}lakewater}$) impossible. In a more extensive field-based study, spanning 31 stratified lakes across Europe (41-69°N latitude), Verbruggen *et al.* (2011) also observed robust linear relationships between $\delta^{18}O_{chironomid}$, inferred $\delta^{18}O_{precipitation}$ ($r^2 = 0.79$) and $\delta^{18}O_{lakewater}$ ($r^2 = 0.95$).
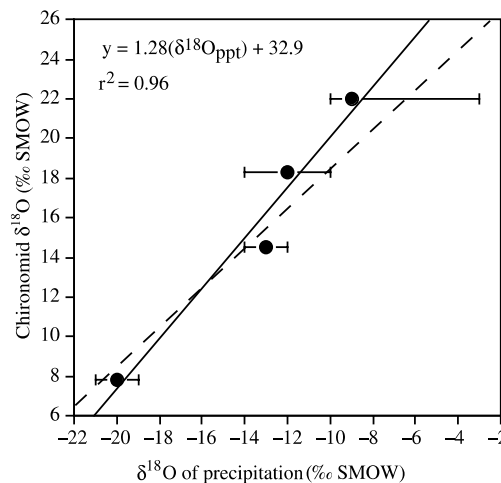
Figure 1-6: Calibration of $\delta^{18}O_{chironomid}$ vs. inferred $\delta^{18}O_{precipitation}$, where the constant fractionation line (dashed line) displays a lower slope than the regression line (solid line). Assuming constant fractionation between chironomid head capsules and water, $\alpha = 1.028$ (Wooller *et al.*, 2004).

The authors of these studies speculated that; i) the remains of chironomid larvae are in isotopic equilibrium with their habitat water and, ii) the imprinting of the $\delta^{18}O_{lakewater}$ signal in chironomids is largely independent of temperature dependant fractionations and vital effects. As a result they suggest stratigraphic changes in $\delta^{18}O_{chironomid}$ can be used to infer past $\delta^{18}O_{lakewater}$ directly.

Wooller *et al.* (2004) were the first to infer past temperature changes from a $\delta^{18}O_{chironomid}$ record spanning the last 10,000 years. The results of this study were largely in accordance with chironomid inferred summer water temperature (SWT) and independent MAT records from the period (Wooller *et al.,* 2004). The same authors also produced another down-core record, in which $\delta^{18}O_{chironomid}$ variability was attributed to changes in the seasonality of precipitation and the origin of air masses delivering precipitation to the study area (Wooller *et al.,* 2008).

Verbruggen *et al.* (2011) demonstrated that $\delta^{18}O_{chironomid}$ successfully tracked stratigraphic changes in $\delta^{18}O_{bulk\_carbonate}$ from a Late-glacial sediment sequence (Rotsee, Switzerland) (Figure 1-7). Therefore, $\delta^{18}O_{chironomid}$ records can compliment carbonate-derived $\delta^{18}O$ records and provide an opportunity to generate $\delta^{18}O$ records from sites where carbonate sequences are absent or incomplete. Furthermore, the coupling of organic and inorganic $\delta^{18}O$ archives from the same stratigraphic sequence offers a potentially powerful quantitative approach for reconstructing past temperatures (e.g. Buhay *et al.,* 2012; Rozanski *et al.,* 2010). This approach is underpinned by the fundamental assumption that $\delta^{18}O_{chironomid}$ is an uncorrupted proxy for $\delta^{18}O_{lakewater}$ and that the two independent $\delta^{18}O$ archives are formed simultaneously from the same waters. Providing that $\delta^{18}O_{lakewater}$ can be accurately inferred from $\delta^{18}O_{chironomid}$, calcification temperature can be predicted based on the laws of thermodynamics.
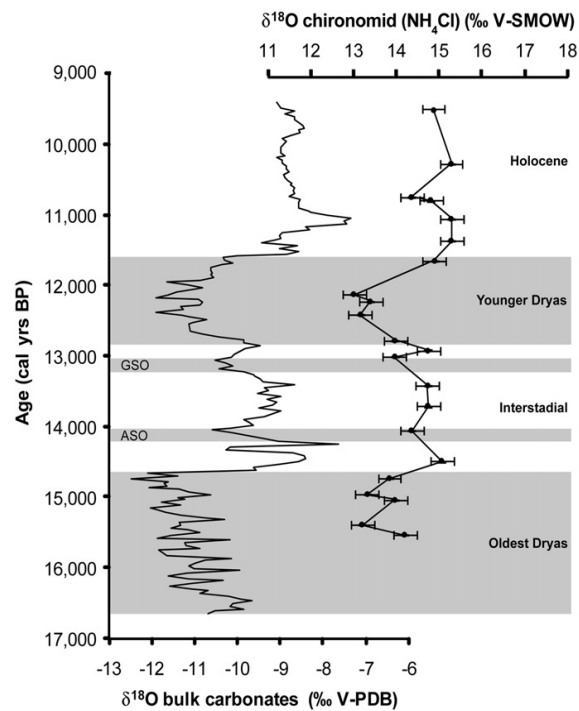
Figure 1-7: Stable oxygen isotope record of bulk carbonate (left curve) and chironomids (right curve) from Late-glacial sediments Rotsee, Switzerland. Grey areas indicate cold periods (from Verbruggen *et al.,* 2011). The chironomid remains were treated with 2M ammonium chloride (NH$_4$Cl) to eliminate carbonate contamination.

Remaining challenges

In order for $\delta^{18}O_{chironomid}$ to become a quantitative tool in the reconstruction of past $\delta^{18}O_{lakewater}$, and therefore past climates, the proxy needs to be calibrated. Many aspects regarding the application and interpretation of this proxy remain under developed. The most important remaining considerations are: i) the development of standardised sample preparation and analytical procedures, ii) rigorous calibration of the contemporary relationship between $\delta^{18}O_{chironomid}$, $\delta^{18}O_{lakewater}$ and temperature to confirm the absence of temperature dependant $\alpha^{18}O_{chironomid-H2O}$ and iii) the development of palaeotemperature estimates from $\delta^{18}O$ measurements of co-existing chironomid and carbonate samples. The absence of a standardised protocol for the preparation of chironomid remains for $\delta^{18}O$ analyses has restricted the application of this approach. It is expected that once the methodology has been developed and necessary calibration studies produced this approach will increase in popularity (Heiri *et al.,* 2012).

1.5 Project aims

This thesis aims to contribute to the on going development of $\delta^{18}O_{chironomid}$ as a tool for reconstructing past climates, with particular attention paid to:

a) **The evaluation of molybdenum as an alternative to glassy-carbon in high temperature pyrolysis reduction reactors during $\delta^{18}O$ analyses of organic compounds (Chapter 2).**

b) **Development of a standardised protocol for the preparation of chironomid remains for $\delta^{18}O$ analyses (Chapter 3).**

c) **Laboratory and field-based calibrations of the relationships between $\delta^{18}O_{chironomid}$, $\delta^{18}O_{H2O}$ and temperature (Chapter 4).**

d) **The development of Late-glacial palaeotemperature reconstruction based on stratigraphic changes in $\delta^{18}O_{chironomid}$ and $\delta^{18}O_{bulk\_carbonate}$ (Chapter 5)**.

Specific objectives are developed in the individual chapters. The overall findings and their implications are explored in the following chapters and summarised in Chapter 6.

Chapter 2 Analytical developments: the search for improved precision of oxygen isotope determinations in oxygen-bearing organic compounds

2.1 Introduction

Effective and reliable continuous-flow oxygen isotope analyses from organic compounds can be achieved through the coupling of a high temperature pyrolysis unit (HTP) to a continuous flow isotope ratio mass spectrometer (IRMS) (Figure 2-1).
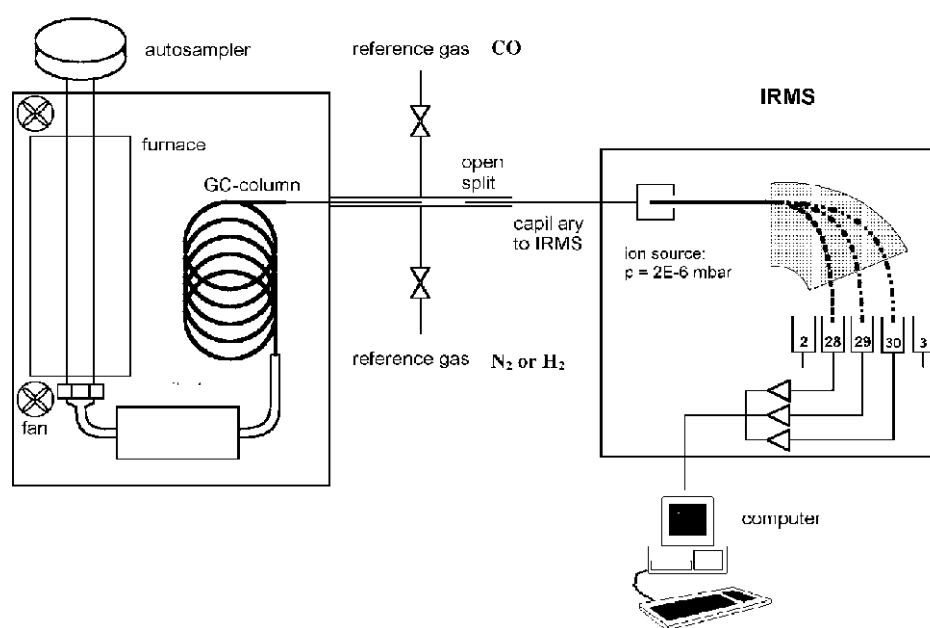
Figure 2-1: Schematic representation of a high temperature pyrolysis (HTP) unit coupled to an IRMS (Gehre & Strauch 2003).

A prerequisite of HTP techniques is the quantitative thermal decomposition (pyrolysis) of a sample into a single oxygen-bearing gas at temperatures in excess of ~1200°C, with carbon monoxide (CO) being the thermodynamically favoured product (Brand *et al.,* 2009; Kornexl *et al.,* 1999; Farquhar *et al.,* 1997; Gehre & Strauch 2003). Providing that the thermal decomposition of the sample is quantitative, the CO gas produced can be considered to be isotopically representative of the sample (Brenna *et al.,* 1997). The thermal decomposition of an organic compound can be described by the following generalised formula:

O-Compound (solid) + C (solid) → CO (gas) + Residues (solid, gas, liquid)

Following flash pyrolysis, the gaseous products (including H, N_2 CO) are swept through a isothermal gas chromatography column (5 Å molecular sieve, 80-100 mesh), which separates the gases based on molecular mass (Brand 1996; Koziet 1997; Werner & Brand 2001). A small proportion of the gaseous transient is admitted to the IRMS, via an interface unit, where it is ionized before being accelerated across an electrical potential gradient and focused into a beam by a series of electrostatically charged lenses. The positively charged ions present in the beam interact with a magnetic field in the flight tube, with the flight path radii of individual atoms proportional to their mass. Eventually these ions strike a series of collectors (Faraday Cups) at the end of the flight tube, where individual ionic impacts are converted into a voltage. The isotopic composition of the sample gas is determined by monitoring the ion current intensities of relevant masses (i.e. *m/z* 28 and 30 for oxygen isotope determinations), with the relative differences between the ion current ratios of the sample, reference material and calibrated reference gases calculated on an internationally agreed scale (Gehre & Strauch 2003; Hagopian & Jahren 2012; Werner & Brand 2001).

HTP systems typically utilise a tube-in-tube reduction reactor composed of a glassy-carbon-lined alumina (Al_2O_3) column situated inside a vertical furnace, held at temperatures in excess of 1200°C (Figure 2-2) (Accoe *et al.,* 2008; Gehre *et al.,* 2004; Gehre & Strauch 2003; Koziet 1997; Werner 2003). The

reactor is partially filled with glassy carbon granules, which help prime sample reduction, up to the hottest part of the reactor where a graphite crucible is positioned (Boschetti & Iacumin 2005). The glassy carbon liner provides an oxidation barrier between the gaseous pyrolytic products, the granular glassy carbon bed and the Al_2O_3 tube, reducing the formation of long-lived or permanent oxide complexes (Gygli 1993; Kornexl *et al.,* 1999; Werner & Brand 2001; Werner 2003).
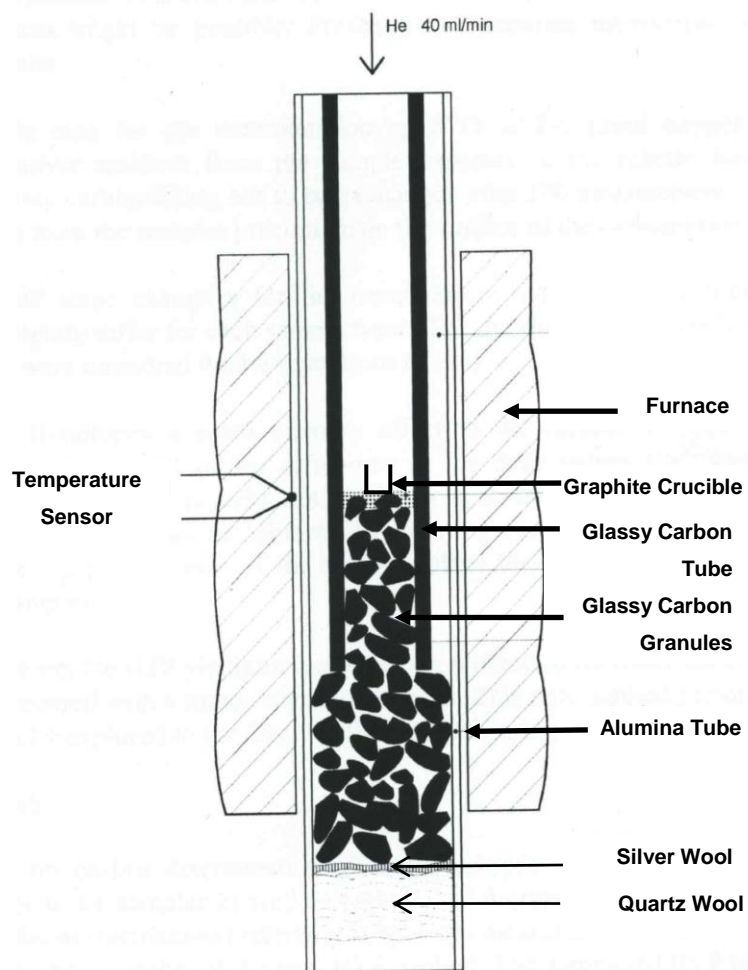
Figure 2-2: Schematic representation of a standard tube-in-tube pyrolysis reactor adopted in high temperature pyrolysis (HTP) units. Image modified from Kornexl *et al.* (1999).

However, glassy-carbon-lined HTP reduction reactors are commonly associated with several problems: i) low/variable yields (i.e. non-quantitative sample conversion into CO), ii) memory effects, iii) peak tailing as a result of improper flushing of the gaseous pyrolytic products caused by the bypassing of the carbon bed, and iv) high backgrounds arising from unwanted reactions between the glassy carbon liner and the outer Al_2O_3 tube at elevated temperatures (Lombino *et al.,* 2012). These problems have a deleterious influence on the analytical precision of $\delta^{18}O$ determinations (Farquhar *et al.,* 1997; Kornexl *et al.,* 1999; Lombino *et al.,* 2012).

2.2 δ^{18}O analysis of organic compounds: problems with pyrolysis in molybdenum-lined reactors[1]

In an attempt to improve the analytical precision associated with δ^{18}O$_{organic}$ measurements the performance of a molybdenum (Mo)-lined reduction reactor was evaluated. In this section a modified version of a manuscript published in the Journal Rapid Communications in Mass Spectrometry (Lombino *et al.,* 2012; see appendix A-I for full manuscript), evaluating the performance of a Mo-lined reduction reactor during δ^{18}O$_{organic}$ determinations, will be presented. The manuscript was produced in collaboration with Prof. Tim Atkinson (Department of Earth Sciences, University College London) and Dr. Steve Firth (Department of Chemistry, University College London), who both provided analytical support and guidance during the production of this article. This investigation was undertaken at University College London's Bloomsbury Environment Isotope Facility (BEIF), using a high temperature conversion elemental analyser (TC/EA), coupled via a ConFlo III open split interface to a Delta^{XP} IRMS (all units from ThermoFisher Scientific, Bremen, Germany).

2.2.1 Reactor configuration and testing

The tested reduction reactor was composed of an Al$_2$O$_3$ tube (internal diameter 13mm; outer diameter 17mm; length 470mm) lined with 0.1mm thick Mo-foil (99.95% purity) (supplied by SerCon, Crewe, UK). The reactor was partially filled with a 60mm deep bed of coarse (3-4mm) glassy carbon granules, supported within the hottest zone of the reactor by a folded Mo-plug (Figure 2-3a).

The configuration of the Mo-reactor was constrained by the construction of the TC/EA furnace, resulting in significant differences from the reactor employed in Stuart-Williams *et al.* (2008). The most striking difference being the broadness of the relative hot-zones, as shown in Figure 2-3b, and a wider Al$_2$O$_3$ tube (i.d. 16mm). Based on the available information it was

---

[1] Published as: Lombino *et al.,* 2012

inferred that the glassy carbon bed in Stuart-Williams *et al.* (2008) was approximately twice as deep as the one tested in this pilot (~110–120mm).

Stable isotope determinations were conducted on silver encased aliquots (150µg ± 10µg) of two internationally distributed reference materials, IAEA 601 ($\delta^{18}O_{V-SMOW}$: +23.3‰), IAEA 602 ($\delta^{18}O_{V-SMOW}$: +71.4‰) (International Atomic Energy Agency, Vienna, Austria) and a benzoic acid laboratory standard (Benzoesäure; Hekatek HE 33822501). The majority of analyses during performance testing were conducted at 1400°C, however furnace temperatures were systematically varied (1350-1430°C) independently to He carrier gas flow rate (60 to 90 mLmin^{-1}) in search of improved precision.
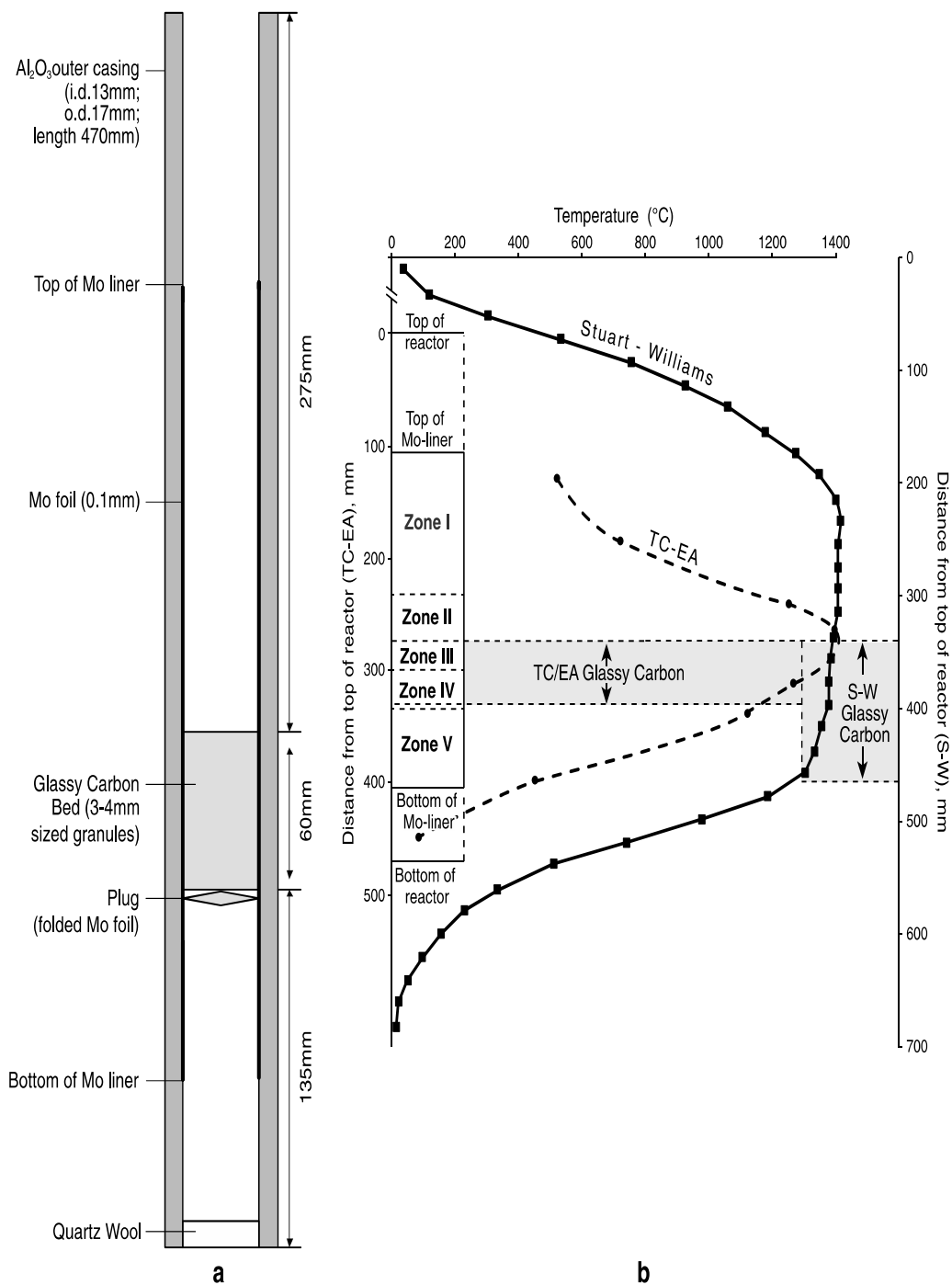
Figure 2-3: (a) Construction of the Mo-lined reactor for the TC/EA system. (b) Comparison between the temperature profiles and glassy carbon bed thickness for the TC/EA and the Mo-lined reactor used by Stuart-Williams *et al.* (2008). The vertical scales are offset so that the tops of the glassy carbon beds are aligned. Zones of corrosion damage in TC/EA reactor shown on the left (Lombino *et al.*, 2012).

2.2.2 Reactor performance

Stuart-Williams *et al.* (2008) reported that the typical analytical precision associated with $\delta^{18}O_{organic}$ determinations using Mo-lined reactors was <0.25‰ (1σ). However, the reproducibility of $\delta^{18}O$ determinations in this investigation was between 0.4-3‰ (1σ). Moreover, $\delta^{18}O$ determinations were associated with severe scale compression of up to 20‰ during memory trials conducted at 1400°C, but under varying carrier gas flow rates (60 to 90 mLmin^{-1}) (see Appendix A-II). CO yield per unit weight of carbon in benzoic acid was also observed to be variable under different constant flow rate regimes (Figure 2-4).
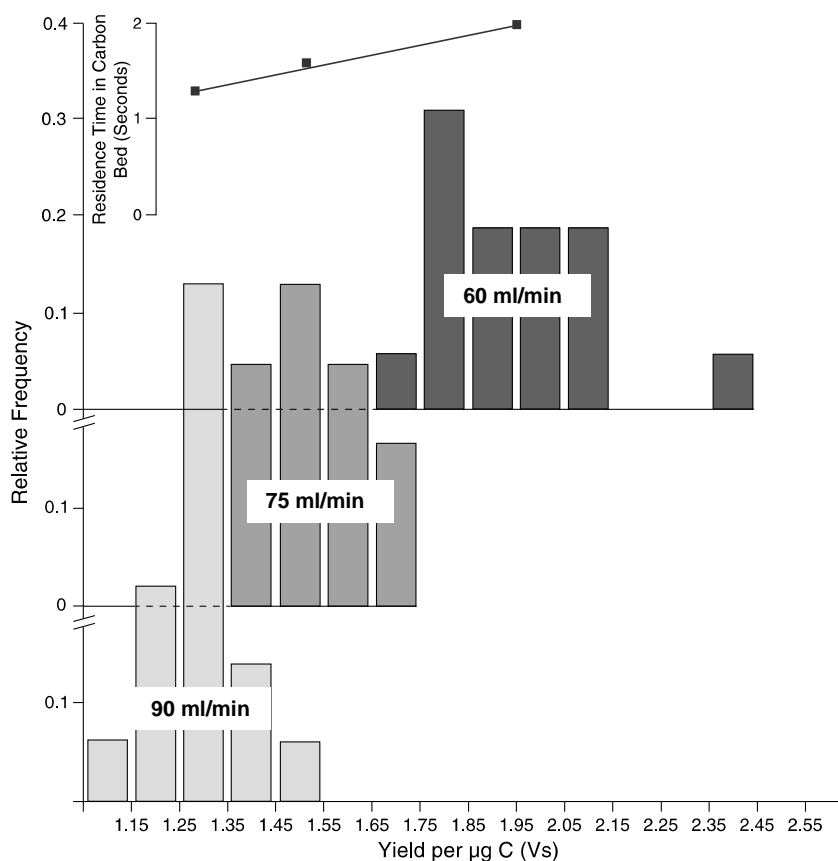
Figure 2-4: Variability of CO gas yield with carrier gas flow rate and inferred residence time in contact with glassy carbon at temperatures in excess of 1100°C. Histogram show grouped data from individual analyses; square symbols show mean for each flow rate plotted against inferred residence time (Lombino *et al.,* 2012).

The apparent isotope fractionation in the modified reactor indicates that quantitative reduction of sample O into CO was not achieved in the tested system. Non-quantitative sample reduction can either be due to incomplete pyrolysis or the partitioning of oxygen into phases other than gaseous CO. Given the relative chemical simplicity of benzoic acid and the high reactor temperatures, incomplete pyrolysis appears unlikely. Sample reduction to CO_2 could potentially account for the partitioning of oxygen, however its absence from the gases emerging from the reactor indicated that the partitioning was most likely to have been into a non-gaseous phase. In order to investigate this hypothesis the elemental composition of sections from two used Mo-lined reactors were analysed by scanning electron microscopy energy-dispersive X-ray spectroscopy (SEM-EDX) (Goldstein *et al.,* 1992) and Raman spectroscopy (Gilson & Hendra 1970).

2.2.3 Examination and analysis of used reactors

Two used reactors were gently broken open using a hammer. The Mo-liners had become brittle and were severely corroded and pitted, particularly in the hottest part of the furnace. Based on visual examination both liners displayed similar characteristic zonation. The elemental compositions of each of these zones are described below (Figure 2-5a)

> **Zone I**- spanned the upper 130mm of the Mo-liner. Temperatures in this part of the reactor ranged from 450-1150°C (Figure 2-3b). The Mo in the zone had a violet/brown lustre, consistent with MoO_2 (Cotton & Wilkinson 1966; Heslop & Jones 1976; Partington 1958; Sidwick 1950) (Figure 2-5a). No SEM-EDAX or Ramen spectroscopy data is available from this section.

> **Zone II**- spanned approximately 40mm. The zone was characterised by a bronze/gold patina (Figure 2-5a), which gave way to a band of bright metal. The metal band corresponds to the region just above the carbon bed. EDX spectra from the inner

55

surface of the Mo-liner indicates the presence of elemental Mo (30 atom%) and O (69 atom%), similar proportional contributions plus trace amounts of Al characterise the outer surface of the Mo-liner as well.

Globular residues found adhering to the inner surface of the Mo-liner in the lower section of this zone were composed of Ag (90 atom%) and elemental C (10 atom%) (Figure 2-5b), these must have originated from the splashing of molten silver during pyrolysis.

Zone III- spanned approximately 25mm and corresponds with the upper part of the carbon bed where temperatures were >1350°C (Figure 2-3b). The Mo-liner in this zone showed extensive pitting and dulling with surface encrustations both on inner and outer surfaces (Figure 2-5a). Encrustations found on the inner surface of the Mo-liner were mainly comprised of elemental Mo (85 atom%) and O (15 atom%). EDX spectra of encrustations found on the outer surface of the Mo-liner indicate the presence of elemental O (58 atom%), Al (29 atom%), N (10 atom%) and Mo (2 atom%) (Figure 2-5c).

The inner surface of the Al_2O_3 tube was stained black in this zone and extended into Zone IV, above and below this deposit the Al_2O_3 retained its original white colour. Raman spectroscopy showed the presence of graphitic carbon within these black deposits.

Zone IV- spans the lower 35mm of the carbon bed, where temperatures exceed 1100°C (Figure 2-3b). The inner surface of the Mo-liner was dulled and covered by metallic globules (Figure 2-5a), up to several mm in diameter, composed of Ag (51 atom%) along with substantial proportions of elemental C (32 atom%), and O (15 atom%) (Figure 2-5d).

Zone V- spans the cooler (400 – 1100°C) region below the Mo-plug (Figure 2-3b). Both inner and outer Mo-liner surfaces carried a patina of Mo-oxides (Mo: 41 atom%, O: ~ 52 atom%) on which fine closely spaced hemispherical globules composed of Ag (77 atom%) and elemental C (19 atom%) were deposited (Figure 2-5e). Increased fining and density of the globules could be observed with increasing distance.
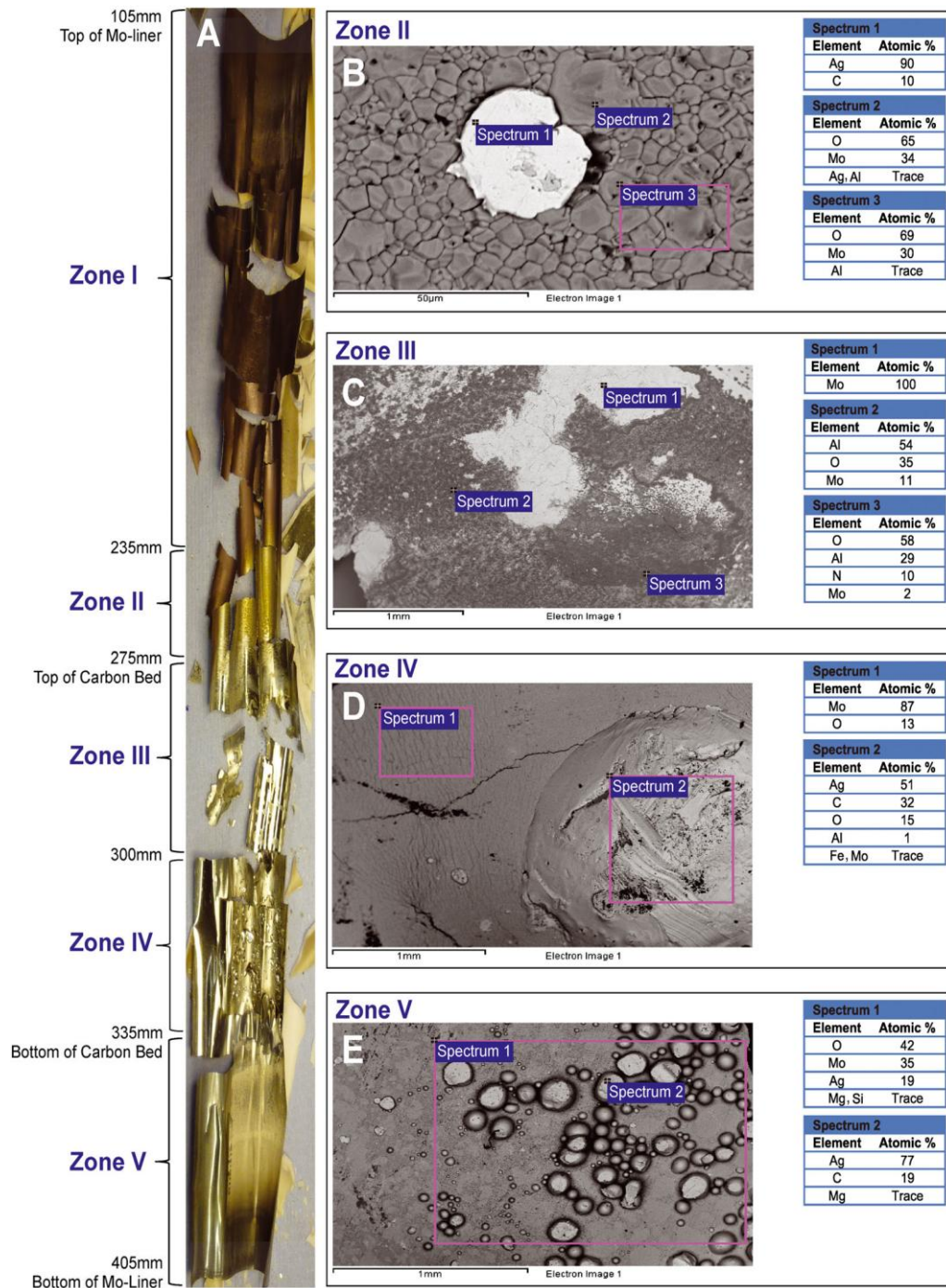
Figure 2-5: **A)** **Photograph** **of** **used** **Mo-liner.** (B) SEM image and EDX analysis of inner liner surface from Zone II, showing silver globule (spectrum 1) adhering to mosaic-like patina of Mo-oxides (spectra 2 and 3). (C) SEM image and EDX analyses of outer liner surface from Zone III, showing areas of light-coloured Mo metal (spectrum 1) and darker patina containing Al and Mo oxides and a nitrogen-bearing phase (spectrum 3). (D) SEM image and EDX analyses of the inner surface from Zone IV, showing cracked patina of Mo-oxide (spectrum 1), plus 2 mm diameter blob of silver containing carbon and oxygen (spectrum 2). (E) SEM image and EDX analyses of inner liner surface from Zone V with ~0.1mm globules of silver containing carbon (spectrum 2) on a patina of Mo-oxide. Spectrum 1 contains both components (Lombino *et al.,* 2012).

2.2.4 Discussion

Mo-oxide patinas were ubiquitous throughout the length of the tested Mo-lined reactors. There are three potential sources of oxygen within the reactor: a) diffusion of atmospheric oxygen through the Al_2O_3 tube at elevated temperatures, b) self-diffusion of oxygen from the Al_2O_3 or direct interactions between the Al_2O_3 tube and Mo at elevated temperatures or, c) oxygen-bearing gaseous products of pyrolysis. Extensive patination and corrosion observed on the inner surface of the Mo-liners is suggestive that the genesis of the oxygen, within our system, is likely to have originated from within the reactor. The other two potential sources of oxygen (a and b) are likely to have also contributed to the formation of Mo-oxides and corrosion of the Mo-liner, to some degree. For example, the presence of nitrogen on the outer surface of the Mo-liner in Zone III (Figure 2-5c) is suggestive of the diffusion of air through the Al_2O_3 tube.

The oxygen bearing products produced during the pyrolysis of benzoic acid could include CO, CO_2 and H_2O, however the latter two will be reduced to CO in the presence of excess carbon at elevated temperatures. Consequentially, CO and H_2 are the principal gases expected inside the Mo-liner, along with the He carrier gas. Mo metal is known to react with gaseous CO to produce Mo-oxides and carbon (Reaction I below) (Sidwick 1950). The principal oxides of Mo are MoO_2 and MoO_3. The melting points (MP) and boiling points (BP) of these oxides are far lower than the expected maximum temperatures in the heart of the reactor (MoO_2 MP 782°C, BP 1257°C; MoO_3 MP 795°C, BP 1155°C; see Cotton & Wilkinson 1966; Heslop & Jones 1976; Partington 1958; Sidgwick 1950), consequently these oxides could theoretically exist in their vaporised form within the hot zone of the reactor, condensing to form patinas in the cooler parts. The consumption of oxygen during the formation of MoO can potentially explain the observed variability in CO yields per unit weight of carbon (Figure 2-4) and will directly contribute to isotopic fractionation of the remaining CO. This fractionation is unlikely to have been the sole cause of the scale

59

compression observed in our system, as this would require the degree of fractionation to vary systematically with sample $\delta^{18}O$. An alternative scenario could be isotopic exchange between gaseous CO and Mo-oxide reservoirs that have accumulated over time in the reactor. The other principal gas present in the reactor is H_2, which is known to react with MoO_2 at temperatures in excess of 500°C to form Mo-metal and water (Cotton & Wilkinson 1966; Holleman & Wiberg 2001) (Reaction II). At temperatures in excess of 1000°C the water produced during pyrolysis will be partially reduced on glassy carbon, re-forming as H_2 and CO (Reaction III). Thus Mo and C in the reactor will take part in a circular series of reactions with the gases present:
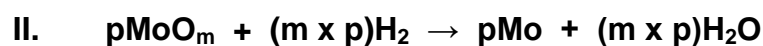
I.   (m x n)CO + nMo $\rightarrow$ nMoO$_m$ + (m x n)C (Sidwick 1950)

II.   pMoO$_m$ + (m x p)H$_2$ $\rightarrow$ pMo + (m x p)H$_2$O

III.   (m x p)H$_2$O + (m x p)C $\rightarrow$ (m x p)H$_2$ + (m x p)CO.

Reaction I will sequester a portion of the oxygen in the original CO into Mo-oxides. Reaction II followed by III will return some of this oxygen as CO. This back conversion will only be complete if n=p in the above scheme, and also that Reaction III runs to completion. If both criteria are met, the Mo-liner will be corroded, but would not be associated with any Mo-oxide patinas. The presence of MoO patinas throughout the length of both studied Mo-liners strongly suggests that the return of gaseous CO is incomplete in this case (p<n). In standard HTP reduction reactors (Figure 2-2), reaction III only runs to completion in temperatures in excess of 1350 – 1400°C (Gehre *et al.,* 2004; Gehre & Strauch 2003), with catalysis by Ni being required at lower temperatures. This suggests that there is scope for additional isotopic fractionation of the final CO leaving the reactor, through kinetic effects in both Reactions II and III. It is

speculated that the varying scale compressions observed in $\delta^{18}O$ of the final CO may be a function of differential fractionations between Reaction I and Reactions II and III, as well as the degree of inequality p<n and other possible factors. The latter include the possibility that Reactions II and III take place over a range of temperatures as the gases stream downwards from the hottest zone into cooler regions and Mo-oxides condense from the vapour to the liquid and solid phases. Once the Mo-liner has been pierced by corrosion due to Reaction I, as seems to have occurred quite quickly in this pilot, some of the gases and vapours may migrate down the annulus between the Mo-liner and the outer Al_2O_3 tube, where there is no access to solid carbon apart from that produced by Reaction I. The presence of graphitic carbon on the inner surface of the Al_2O_3 tube in the hottest part of the reactor supports the occurrence of this reaction. As a consequence of the migration of these gases into the annulus the majority of water produced in Reaction II will not be converted back in CO and H_2. In the core of the reactor, where carbon is abundant, Reaction III can be expected to run to completion in Zone III where the local temperature is high enough, but may not do so in the cooler lower part of the carbon bed (Zone IV), and cannot do so where carbon is absent (Zone V). The yield of CO gas, its isotopic composition and resultant scale compression, are likely to depend upon the interplay of reaction rates, local temperatures, carrier gas flow rates and the residence times of the gases in the parts of the reactor that are most favourable for Reactions II and III. The condition of the reactor liner, especially whether it is pierced by corrosion, and the amount of Mo-oxide deposit that has built up over time are further factors. The Mo-oxide deposit is a potential locus for Reaction II, so the fractionation it causes in the final output of CO may depend on the whole history of reactor use and the $\delta^{18}O$ values of the samples that have been analysed previously, as there will be a memory of these in the Mo-oxide $\delta^{18}O$.

If the scheme of reactions envisaged is correct, then successful, accurate analysis of organic compounds using Mo-lined reduction reactors would

require conditions such that Reactions II and III can return all oxygen to gaseous CO, so that Mo-oxides would not build up in the reactor. This is most likely to be achieved if the sample gases have a long residence time in contact with carbon in the hottest part of the reactor, optimising recovery of oxygen to CO via Reaction III. Such conditions appear to have been met in the HTP system utilised by Stuart-Williams *et al.* (2008), who managed to achieve excellent precision without scale compression using this approach. As can be seen from Figure 2-3b the reactor used by Stuart-Williams *et al.* (2008) had a broader hot-zone and larger diameter than the reactor tested in this pilot. Rough estimations, based on figures provided by Stuart-Williams *et al.* (2008), suggests that if volumetric gas flows were equal in the two systems, the gas residence time in the hottest part of Stuart-Williams' reactor was 2-3 times greater than the configuration tested in this study. Therefore, it is hypothesised that residence time of gas in contact with carbon at ~1400°C is critical to the performance of the Mo-lined reduction reactors.

A possible line of development for HTP units, which have a narrow hot-zone (Figure 2-3b), might be to inactivate the Mo surface of the liner. Mo is known to form a variety of carbides by reaction with CO (Gillet *et al.,* 1976) and a coating of these might inhibit the corrosion reactions with the metal. Borda (1985) describes the use of Mo-carbide-coated carbon as a catalyst for the conversion of oxygen in organic compounds into CO at 1080°C. Inactivation might also slow down corrosion of the outside surface of the Mo-liner by oxygen diffusion through the alumina tube or by direct reaction with the Al_2O_3. Direct measurement of air diffusion through the alumina tubes under operating temperatures would also help to establish the relative importance of these sources of oxygen in causing the corrosion observed in this study.

2.2.5 Conclusion

No previously published studies have investigated the chemical composition of HTP reactors after use. Mo-liners are relatively inexpensive and easy to fabricate but they are apparently unsuitable for use in the TC/EA system in the configuration tested by this study. The principal reason for this appears to be the production and build-up of Mo-oxides as a patina or coating on the liner as a result of the reaction between Mo-metal and CO gas, causing poor precision and variable CO yields. To some extent the loss of CO is compensated for by reactions between Mo-oxides and hydrogen gas derived from the sample, producing water, followed by reduction of the water to CO and H_2 by reaction with glassy carbon. However, these restoring reactions probably introduce further fractionation effects and may be responsible for scale compression observed in testing. Despite all this, it is possible to obtain a precision of <0.25‰ during $\delta^{18}O$ analyses using Mo-liners, as demonstrated by Stuart-Williams *et al.* (2008). From comparison of reactor designs, it is concluded that the depth of the hot zone and the time that the pyrolysis products spend within it are critical factors, although diffusion of atmospheric oxygen through the walls of the alumina tubes may also contribute. Analysts intending to develop a Mo-lined HTP system should ensure that their furnace and reactor design follow those of Stuart-Williams *et al.* (2008) and provide a residence time at ~1400°C for the produced gases of at least 4 seconds. The approximate residence times in the system tested in this pilot varied from ~1.3 to ~2 seconds, which was not sufficient to promote quantitative conversion of oxygen from the sample into CO. Although Mo-lined reactors have potential for $\delta^{18}O$ determinations within some HTP systems, it is clear that the chemistry of reactions is not straightforward.

2.3 Oxygen isotope determinations of chironomid head capsules

Following the negative experiences with Mo-lined reduction reactors and time constraints, this line of method development was abandoned in favour of standard HTP techniques. Although the search for improved analytical precision ultimately proved fruitless, it did provide a valuable opportunity to become intimately associated with analytical procedures.

All oxygen isotope analyses of chironomid remains were performed at Durham University's Stable Isotope Biogeochemistry Laboratory (SIBL), using a TC/EA coupled to a Delta V Advantage IRMS, via a ConFlo III open split interface (all units from ThermoFisher Scientific). The TC/EA was equipped with a zero-blank auto-sampler (Costech International, Milan, Italy) and an integrated GC column (5 Å molecular sieve), which was held at 60°C to maximise chromatographic separation. All analyses were performed without dilution, due to limited sample sizes.

2.3.1 Reproducibility and calibration

All results presented in this thesis are normalised to the V-SMOW scale by calibration against three international reference materials IAEA 600, 601 and 602 (measured vs. expected r^2 >0.99), which were monitored regularly throughout each sample run. The isotopic values of the chosen standards bracketed the expected sample range. For each standard, average measured values and standard deviations are shown in Table 2-1.

Table 2-1: Measured values and 1σ for the international reference materials together with their published values. All values are presented in ‰ vs. the V-SMOW scale.

	Published $\delta^{18}O$	Measured $\delta^{18}O$	n
IAEA 600	−3.5	−2.5 ±0.64	60
IAEA 601	+23.3	+25.8 ± 0.40	60
IAEA 602	+71.4	+71.8 ± 0.59	60

The precision of $\delta^{18}O$ analyses in this investigation was between ±0.40-0.64‰ (1σ), based on repeated analysis of reference materials. Unless otherwise stated this range is used as an estimate of analytical uncertainty throughout this thesis.

Chapter 3 Methodological development: the evaluation of optimal sample size and the geochemical influence of chemical pre-treatments on chironomid head capsules

The reproducibility and reliability of $\delta^{18}O$ determinations from insect cuticles can be compromised by compositional heterogeneity (Schimmelmann 2010; Schimmelmann & DeNiro 1986) and exogenous contamination (Verbruggen *et al.,* 2010a). Since HTP techniques are largely indiscriminate, resulting in the conversion of all oxygen bearing organic compounds present within a sample into CO gas during pyrolysis, sample heterogeneity can alter the original $\delta^{18}O$ values masking climate-driven changes (see Section 2.1) (Gehre & Strauch 2003; Verbruggen *et al.,* 2010a; 2011). In order to produce meaningful $\delta^{18}O$ measurements, efforts should be made to limit the abundance of non-amino-polysaccharide impurities present within a sample. Strategies employed to reduce sample heterogeneity should maintain the isotopic integrity of the original sample or introduce a systematic offset that can be corrected for (Nielson & Bowen 2010; Schimmelmann 2010).

3.1.1 Chapter Aims and Objectives

This chapter aims to develop a standardised protocol for the preparation of sub-fossil, fossil and contemporary chironomid remains for $\delta^{18}O$ analysis. This will be achieved by: -

- Ascertaining optimal sample size required for reproducible $\delta^{18}O_{chironomid}$ analyses.
- Systematically investigating the geochemical influences associated with different reagent types, concentration, reaction temperature and exposure duration.

3.2 Sample size analysis

Prior to evaluating the geochemical influences of chemical pre-treatments on chironomid remains, the optimal sample size required for reproducible $\delta^{18}O_{chironomid}$ measurements needs to be established. The amount of sample required for online $\delta^{18}O$ analysis varies depending on the measured substrate and instrument sensitivity (Hagopian & Jahren 2012; Heiri *et al.,* 2012). The isolation of chironomid head capsules from lacustrine sediments is often the most time consuming step in chironomid-based studies, as a result the establishment of the optimal weight required for reproducible $\delta^{18}O_{chironomid}$ analyses was one of the most important steps during the early stages of this project.

Sample size requirements were assessed through the repeated (x3) analyses of chironomid head capsules across a range of different weights (10-100µg) (Figure 3-1). For this purpose, chironomid head capsules were manually isolated from commercially sourced whole freeze-dried *Chironomus riparius* larvae (King British, UK). Based on communication with the supplier it was assumed that these larvae were subjected to similar conditions during growth. Digestive tracts and muscle tissue were carefully detached from the head capsules using a scalpel, to avoid contamination by organic material potentially present in the larval gut. Samples ranging from 10-100µg (±2µg) were weighed out into silver capsules (6 x 4mm, Elemental Microanalysis) and analysed.
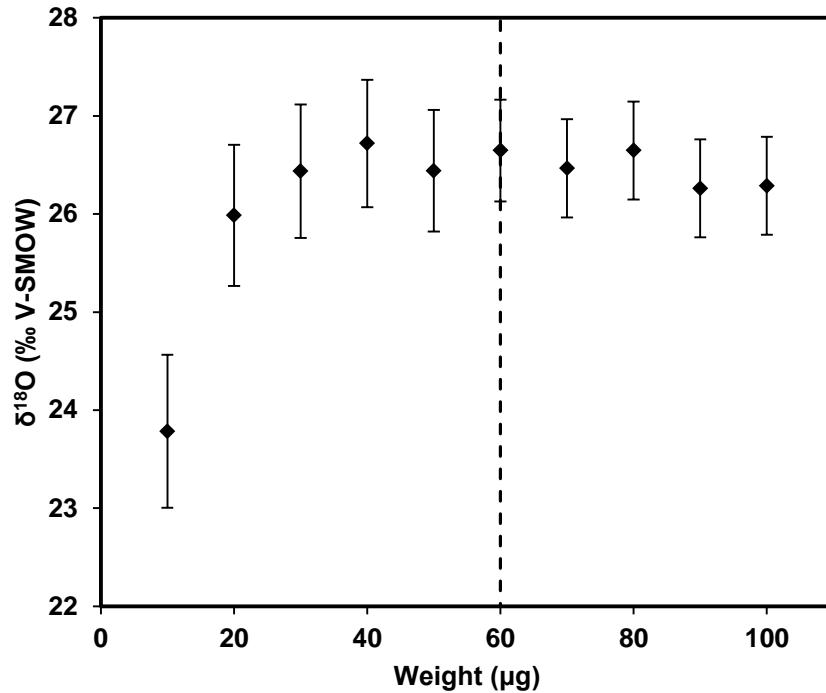
Figure 3-1: δ^{18}O values of chironomid head capsules isolated from commercially grown _Chironomus riparius_ larvae (King British, UK) plotted against sample weight (see appendix B-I for raw data). Error bars represent 1σ (0.8 - 0.5) in each weight. Dashed line represents the optimal sample weight required for reproducible analyses.

A minimum sample size of >20µg was required to produce reproducible δ^{18}O$_{chironomid}$ measurements, based on analyses with no sample dilution (Figure 3-1; see appendix B-I for raw data). However, given the scatter observed in δ^{18}O$_{chironomid}$ across the different weights (_1σ_ = 0.8-0.5‰) it was decided that a minimum weight of 60 ±10µg would be used throughout this investigation. Chironomid head capsules vary greatly in size and weight depending on species and developmental stage making the estimation of a minimum number of fossil head capsules necessary for an individual measurement difficult (Heiri _et al.,_ 2012); based on experiences throughout this investigation between 10-50 head capsules are necessary to achieve the desired weight.

3.3 An introduction to chitin

In order to provide adequate context for the remainder of this chapter a brief introduction into chitin will now follow.

3.3.1 Chemical structure of chitin

Chitin is a linear amino-polysaccharide composed of N-acetyl-β-D-glucosamine (2-acetamido-2-deoxy-β-D-glucose) monomers held together by β- (1→4)-glycosidic linkages (Figure 3-2) (Acosta *et al.,* 1993; Abdullin *et al.,* 2008; Das & Ganesh 2010; Majtán *et al.,* 2007; Percot *et al.,* 2003a; 2003b). The idealised chemical structure of chitin is rarely found in nature, with its stoichiometric formula variable between two end-members; fully acetylated chitin ($C_8H_{13}O_5N$) and the partially de-acetylated derivative chitosan ($C_6H_{11}O_4N$) (Gröcke *et al.,* 2006).
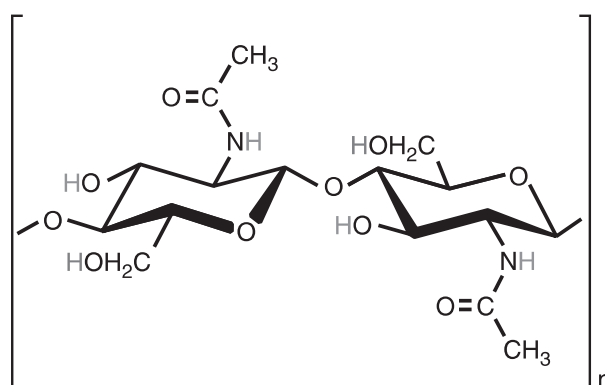
Figure 3-2: Theoretical molecular structure of chitin ($C_8H_{13}O_5N$) (Gröcke *et al.,* 2006).

Chitin bears a strong chemical resemblance to cellulose, differing only in the substitution of a hydroxyl group at the C-2 position with an acetamido group (Acosta *et al.,* 1993; Cohen 1987; 2001; Das & Ganesh 2010; Dutta *et al.,* 2002; 2004; Einbu 2007; Gröcke *et al.,* 2006; Hogenkamp 2006; Kurita 2006; Merzendorfer & Zimoch 2003; Ravi-Kumar 1999; Schimmelmann 2010; Zhang *et al.,* 2000).

Chitin exhibits a highly ordered, crystalline structure and can be found in nature in three polymorphic forms (α-chitin, β-chitin and γ-chitin; see Figure 3-3). Each of these polymorphs have unique physical properties owing to differences in the degree of hydration, crystal cell size, number of chitin chains per unit cell and structural arrangement of chitin chains (Acosta *et al.,* 1993; Einbu 2007; Kramer & Koga 1986; Nation 2008).

α-chitin   β-chitin   γ-chitin
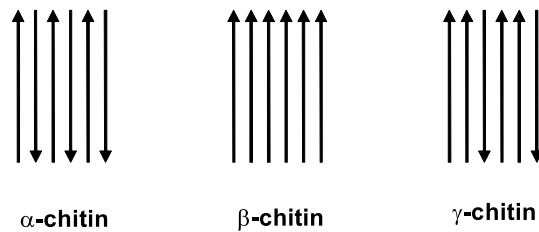
Figure 3-3: Polymorphic forms of chitin found in nature (α-chitin, β-chitin and γ-chitin). Adjacent chitin chains in the α-and β-forms are arranged in an antiparallel and parallel manner respectively, while every third chain has the opposite orientation to the two preceding chains in the γ-form (Carlström 1957; Einbu 2007; Hogenkamp 2006; Merzendorfer 2006; Merzendorfer & Zimoch 2003).

The antiparallel arrangement of chitin molecules in the α-form permits tight packaging of chitin chains to form microfibrils (Merzendorfer & Zimoch 2003; Nation 2008). α-chitin is commonly found in structures where extreme mechanical strength and stability is required (e.g. exoskeletons) (Einbu 2007; Rinaudo 2006). In contrast chitin chains in β and γ-forms are less tightly packed and subsequently contain fewer intra- and inter-chain hydrogen bonds (Merzendorfer & Zimoch 2003). The reduced packing tightness and increased degree of hydration in these polymorphs improves the flexibility of the chitinous structure (e.g. in insect cocoons) (Einbu 2007; Hogenkamp 2006; Merzendorfer & Zimoch 2003; Rinaudo 2006).

3.3.2 Chitin in nature

Chitin is one of the most abundant amino-polysaccharides in the biosphere and forms an essential extracellular structural component in a wide variety of invertebrate groups (e.g. Arachnida, Arthropoda, Brachiopoda, Mollusca) (Andersen 1979; Aranaz *et al.,* 2009; Cohen 1987; 2001; Hogenkamp 2006; Majtán *et al.,* 2007; Merzendorfer 2006; Merzendorfer & Zimoch 2003; Miller 1991). Chitin is particularly conspicuous in insect cuticles, where it accounts for ~10-50% of the overall biomass (Acosta *et al.,* 1993; Andersen 1979; Kurita 2006; Majtán *et al.,* 2007; Zhang *et al.,* 2000). Insect cuticles are complex composite structures, composed of three main layers (Figure 3-4) (Andersen 1979; Barbakadze *et al.,* 2006; Nation 2008; Neville 1975):
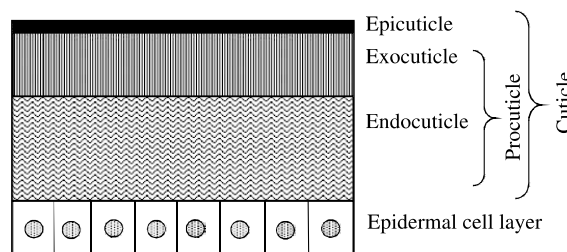
Figure 3-4: Cross-section of typical multi-layered insect cuticle (Barbakadze *et al.,* 2006).

Epidermal cells- These cells are responsible for the secretion of chitin, protein and some lipids under hormonal control during cuticle synthesis (Nation 2008).

Procuticle (divided into the exocuticle and endocuticle)- This layer is composed of successive lamella (or sheets) of chitin microfibrils/rods embedded within a largely proteinaceous matrix, in a similar arrangement to steel re-enforced concrete (Figure 3-5) (Einbu 2007; Nation 2008).

Epicuticle- The impermeable non-chitnous outmost layer of an insect cuticle.

72
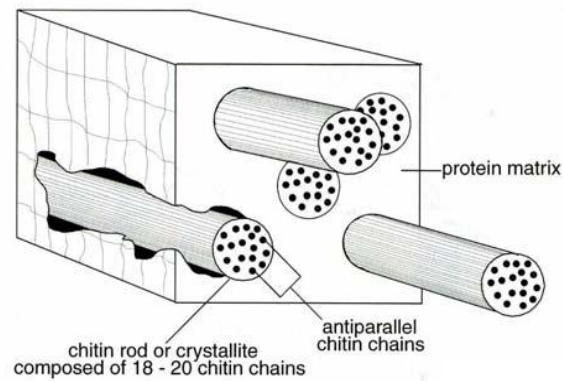
Figure 3-5: Diagram of chitin rod set within a protein matrix in insect cuticle (Nation 2008).

The structural rigidity of insect cuticles is enhanced through cross-linking (sclerotization) of protein and chitin moieties, via extensive covalent bonding between the amine and carbonyl groups of adjacent chitin chains, as well as cross-linking with phenol and quinone compounds (e.g. catecholamines and histidine moieties) (Figure 3-6) (Einbu 2007; Hopkins & Kramer 1992; Merzendorfer & Zimoch 2003; Nation 2008). The chemical composition and degree of sclerotization of insect cuticles varies greatly among different species and even within different developmental stages (Nation 2008). For an extensive review of sclerotization in insects see Hopkins and Kramer (1992).
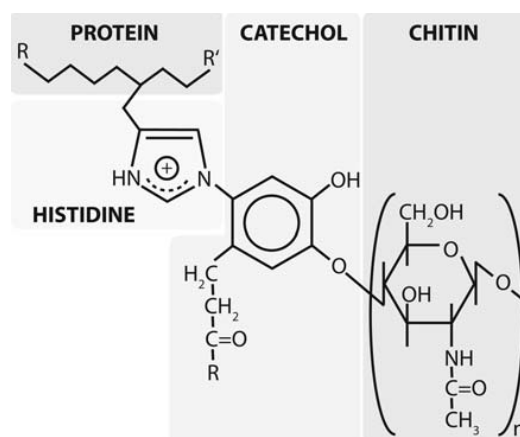
Figure 3-6: Chemical structure of chitin linked to proteins in insect cuticles through catecholamines and histidine moieties (Verbruggen *et al.,* 2010a).

73

3.3.3 Chitin biosynthesis in insects

Insect cuticles have a limited capacity to keep pace with growth, consequently insects must periodically shed their cuticles (ecdysis) (Merzendorfer & Zimoch 2003; Nation 2008). Although chitin is one of the most abundant biopolymers on the planet the biosynthesis of chitin remains poorly defined (Merzendorfer 2006). Chitin biosynthesis appears to follow an orderly sequence of multifaceted, interconnected, intracellular and extracellular reactions (Figure 3-7) (Cohen 1987; 2001). The process is initiated by the cytoplasmic biotransformation of simple metabolites (e.g. glucose, fructose, glucosamine, trehalose) into the substrate uridine diphospho-*N*-acetyl-glucosamine (UDP-GlcNAc), which is used in the polymerisation of N-acetyl-β-D-glucosamine monomers in a reaction catalysed by the membrane-integral enzyme chitin synthase (Andersen 1979; Cohen 1987; 2001; Merzendorfer & Zimoch 2003; Merzendorfer 2006). Nascent chitin polymers (α, β or γ-chitin) are extruded into the extracellular space where they spontaneously undergo crystallisation, forming chitin microfibrils of varying length and diameter (Andersen 1979; Cohen 1987; 2001; Merzendorfer & Zimoch 2003; Nation 2008).
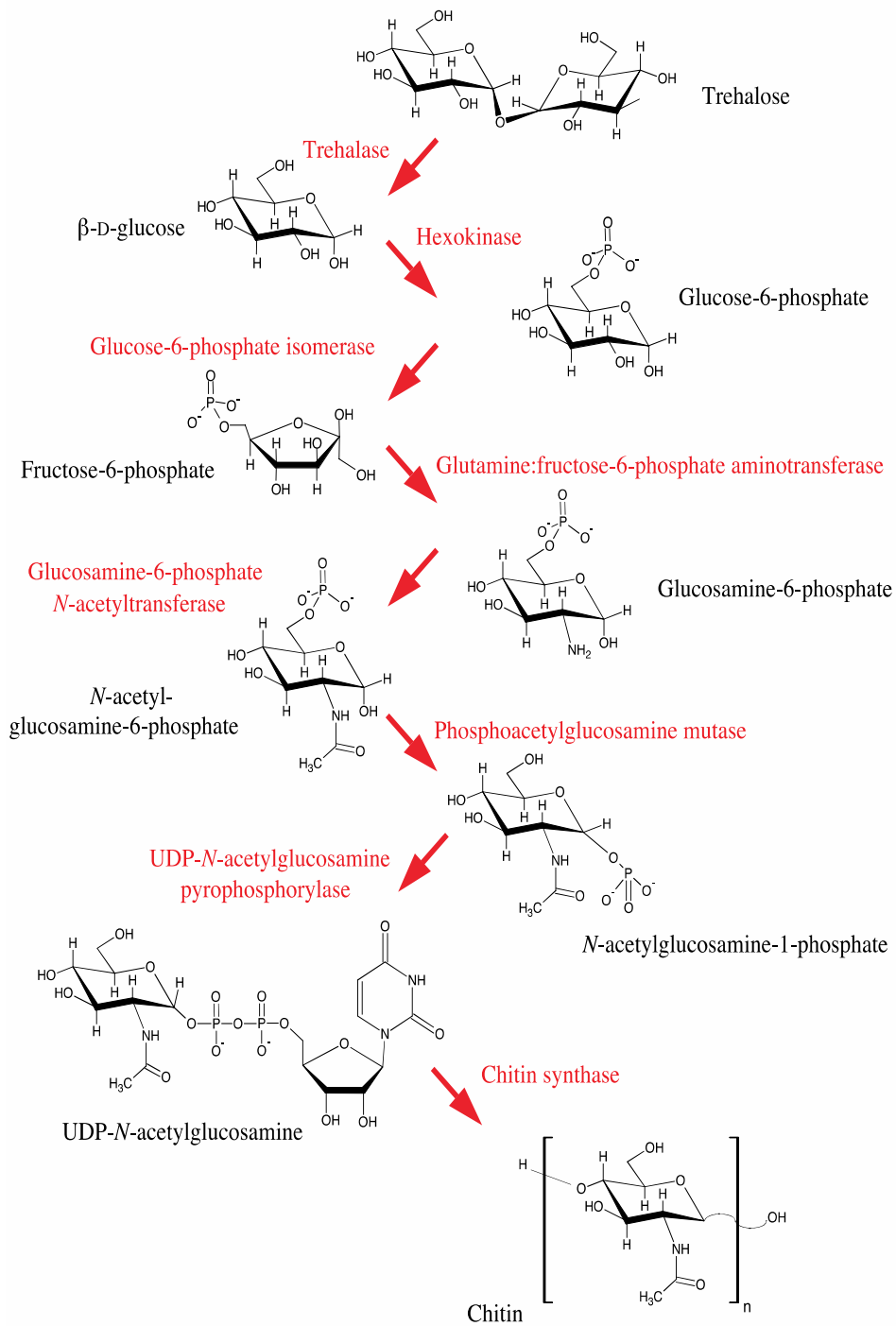
Figure 3-7: Anticipated chemical pathway of chitin biosynthesis in insects (Merzendorfer & Zimoch 2003).

3.4 Preparation of chironomid remains for δ^{18}O analysis

The use of chitin monomer units, such as D-glucosamine hydrochloride (GlcN.HCl), as a substrate for stable isotope analyses can potentially circumvent the inherent issues associated with the analysis of insect cuticles (Schimmelmann & DeNiro 1986; Schimmelmann *et al.,* 1986). In brief, the preparation of GlcN.HCl involves the hydrolysis of mineral and proteinaceous moieties using HCl and NaOH, followed by ion-exchange chromatography purification (Schimmelmann 2010). However, the preparation of GlcN.HCl is labour-intensive and results in the addition of one oxygen atom, originating from water, to each GlcN.HCl molecule (Schimmelmann 2010). Furthermore, the preparation of GlcN.HCl is associated with substantial sample weight loss (> 95%) precluding the use of this substrate where samples are limited (Hodgins *et al.,* 2001; Motz 2000; Tripp *et al.,* 2004).

Alternatively, since chitin is largely insoluble in most organic solvents, non-amino-polysaccharide impurities present within a sample (both compositional and exogenous) can be largely decomposed via a series of liquid solvent-based extractions, yielding a residual chitin rich "isolate" (Schimmelmann 2010). Although the purified residual will invariably contain some covalently-bound impurities, it should represent a more suitable substrate for stable isotope analysis compared to chitinous biomass (Nielson & Bowen 2010; Schimmelmann 2010).

The purification of insect cuticles typically involves three main stages, broadly categorised as:

Decolouration- The elimination of waxes, oils, pigments and resins present within the epicuticle. This is typically achieved using an organic solvent solution such as dichloromethane: methanol (DCM: MeOH).

Demineralisation- The elimination of acid-soluble moieties (e.g. catechols or carbonate in the case of crustaceans) present within the cuticle (Zhang *et al.,* 2000) and exogenous contamination (e.g. endogenic carbonates). HCl is the preferred reagent and is typically applied at a concentration of between 0.25 and 2M for 1-48 hours at temperatures varying from 0 to 100°C (Charoenvuttitham *et al.,* 2006; Einbu 2007; Percot *et al.,* 2003a, 2003b; Zhang *et al.,* 2000).

Deproteination - The elimination of base-soluble moieties (e.g. proteins) present within the cuticle. NaOH is the preferred reagent for deproteinisation and is applied at a concentration of 1M for 1-72 hours at temperatures ranging from 50-100°C (Einbu 2007; Percot *et al.,* 2003a, 2003b). Complete hydrolysis can only be achieved through more aggressive treatments (e.g. 5% NaOH at 100°C) (Brine & Austin 1981; Kurita 2006; Nation 2008).

A similar multi-stage chemical pre-treatment was successfully adopted by Nielson & Bowen (2010) to limit non-amino-polysaccharide impurities in *Artemia franciscana* prior to $\delta^{18}O$ analyses (see Nielson & Bowen 2010). However, previous studies have demonstrated that great care is required during the preparation of chironomid remains for $\delta^{18}O$ analyses. Verbruggen *et al.* (2010a) reported that alkaline- (10% KOH, 2 hours, 20°C; 28% KOH, 24 hours, 70°C) and acid-based (30% HCl, 1 hour, 40% HF, 2 hours, 20°C) chemical pre-treatments induce significant alterations in chironomid head capsule geochemistry and morphology (Figure 3-8). Consequently the authors of this study recommended that chemical pre-treatments should be avoided altogether during the preparation of chironomid head capsules for $\delta^{18}O$ analysis (Verbruggen *et al.,* 2010a). However, in a more recent publication the same authors recognised the importance of eliminating exogenous contamination in order to produce reliable $\delta^{18}O_{chironomid}$ measurements (Verbruggen *et al.,* 2011).
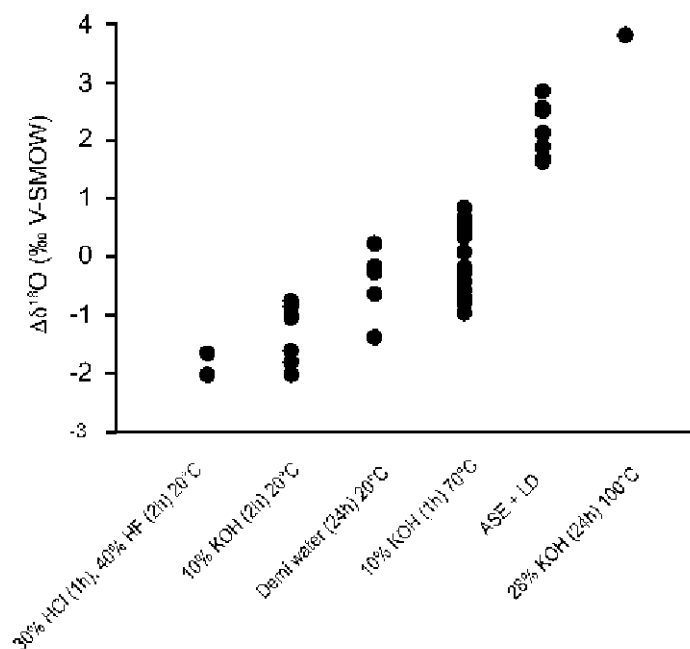
Figure 3-8: Effects of different chemical pre-treatments on the δ^{18}O of head capsules of *Chironomus riparius* larvae. Values are plotted as deviations from reference treatment (10% KOH, 1 hour, 70°C). Note that ASE+LD treatment refers to a chemical pre-treatment commonly employed for the purification of cellulose, involving accelerated solvent extraction (ASE) and successive treatment with sodium chlorite and glacial acetic. Image from Heiri *et al.* (2012) originally adapted from Verbruggen *et al.* (2010a).

3.4.1 Materials and methods

In this investigation the geochemical influence associated with reagents used during decolouration (DCM: MeOH), demineralisation (HCl) and deproteination (NaOH) were evaluated using an isotopically well-characterised, purified shrimp chitin standard ($\delta^{18}O$ = +27.9 ±0.3‰; Sigma-Aldrich, C9752, St. Louis, MO, USA) and a chironomid standard, consisting of head capsules isolated from commercially sourced freeze-dried larvae grown under the same conditions (see Section 3.2). The efficiency of each purification stage is known to be a function of reaction conditions (Abdullin *et al.,* 2008; Charoenvuttitham *et al.,* 2006; Percot *et al.,* 2003a, 2003b), therefore reagent concentration (0.25M and 1M), reaction duration (1 and 24 hours) and temperature (20°C and 70°C) were varied systematically in order to optimise reaction conditions (Table 3-1). Sub-samples were exposed to MiliQ water ($\delta^{18}O$ V-SMOW = −6.9‰) to represent chemically untreated samples for comparison.

Sample aliquots (1000-2000µg) were exposed to the relevant chemical solutions (1ml) in sealed 1.5ml plastic Eppendorf tubes, which were left in either a water bath set at 20°C or in an oven set at 70°C, for 1 or 24 hours. Following chemical exposure for the desired period, samples were centrifuged, at 12000 r.p.m for 10 minutes, and the reagent solution pipetted off. The samples were then repeatedly (x3) rinsed with MiliQ water, before being freeze-dried for 5 days. Residual material from each experiment was re-weighed, to calculate the weight loss associated with each treatment. The pre-treated samples then underwent $\delta^{18}O$ analysis at SIBL, Durham University, using standard HTP techniques (see Section 2.1), to establish the isotopic differences between untreated and treated samples ($\Delta^{18}O_{untreated-treated}$). It should be noted that no attempts were made to determine the effectiveness of each treatment at removing different moieties present in the cuticle. The experiment was not replicated due to time constraints, however replicate $\delta^{18}O$ analyses were performed for each of the tested conditions where sufficient material was available.

Table 3-1: Matrix of different pre-treatments tested in this investigation.

Treatment	Concentration			Temperature (°C)		Duration (hours)	
	2:1	0.25M	1M	20	70	1	24
DCM: MeOH	X			X		X	
	X			X			X
	X				X	X	
	x				x		X
HCl	N/A	X		X		X	
		X		X			X
		X			X	X	
		X			X		X
			X	X		X	
			X	X			X
			X		X	X	
			X		X		X
NaOH	N/A	X		X		X	
		X		X			X
		X			X	X	
		X			X		X
			X	X		X	
			X	X			X
			X		X	X	
			X		X		X
DCM: MeOH + HCl + NaOH	X	X		X		X	
	X	X		X			X
	X	X			X	X	
	X	X			X		X
	X		X	X		X	
	X		X	X			X
	X		X		X	X	
	X		X		X		X
Control	N/A			X		X	
				X			X
					X	X	
					X		X

3.5   Results and discussion

3.5.1   Sample weight loss

The average weight loss associated with each of the purification stages is presented in Table 3-2 for both sample materials. It should be noted that some of the weight loss observed in each experiment is likely to have been attributed to sample loss during solution pipetting and weighing. An average sample weight loss of ~40% was observed in control treatments for both sample materials, which was used as an estimate of error introduced during sample preparation. Assuming that this error was systematic, several semi-quantitative conclusions can be drawn from the average weight loss data.

The average weight loss associated with each purification stage is virtually indistinguishable from the control treatment for purified chitin standard (Table 3-2). In contrast, the average weight loss observed in contemporary chironomid head capsules varied across the different purification procedures. For example, exposure to DCM: MeOH treatments resulted in an average weight loss of ~60%, while the NaOH treatments were associated with an average weight loss of ~80% (Table 3-2). Based on these results it can be inferred that DCM: MeOH-soluble moieties (e.g. lipids, waxes and/or pigments) and NaOH-soluble moieties (e.g. proteins) form a significant component in contemporary chironomid head capsules. These findings are consistent with Verbruggen *et al.* (2010a), who reported near equal proportions of chitin and protein derived moieties in sub-fossil chironomid head capsules. Average weight loss associated with HCl-based treatments was virtually indistinguishable from the control treatments, indicating that acid soluble moieties form a relatively minor component in both materials.

Table 3-2: Average weight loss and $\delta^{18}O$ data associated with each of the tested pre- treatments (see appendix B-II for raw data).

Treatment	Chitin Powder				Chironomid Head Capsules			
	Average Weight Loss (%)	$\delta^{18}O$	1σ	Average $\Delta^{18}O_{untreated-treated}$	Average Weight Loss (%)	$\delta^{18}O$	1σ	Average $\Delta^{18}O_{untreated-treated}$
DCM:MeOH	42	+28.5	0.3	−0.6	58	+14.1	1.5	0.4
HCl	48	+28.9	0.1	−1.0	42	+15.4	1.1	−1.0
NaOH	38	+28.7	0.4	−0.8	83	+17.6	2.2	−3.2
DCM:MeOH + HCl + NaOH	50	+28.8	0.7	−0.9	86	+15.9	1.6	−1.5
Control	40	+27.9	0.3		46	+14.5	0.9	

3.5.2 Chemical treatment impact on δ^{18}O

The geochemical influence associated with each of the purification stages tested in this investigation is presented in Figure 3-9 as an average deviation of treated samples from untreated samples ($\Delta^{18}O_{untreated-treated}$).
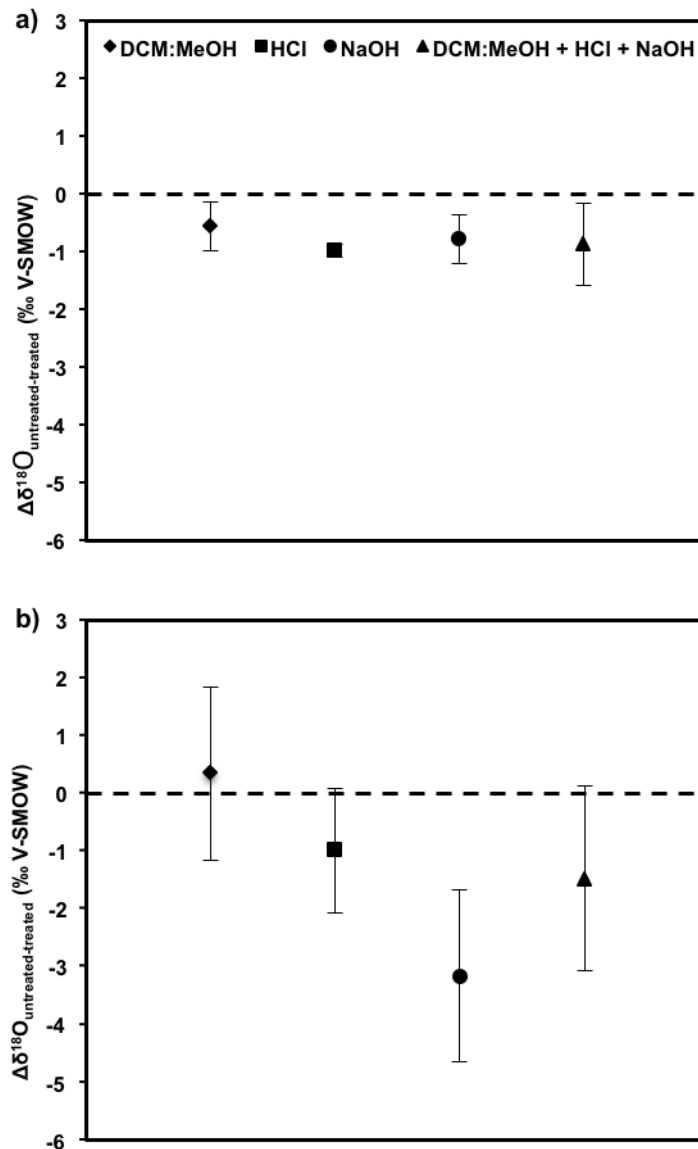
Figure 3-9: a) Average $\Delta^{18}O_{untreated-treated}$ observed in chitin standard and b) contemporary head capsules. Error bars represent 1σ across the treatments tested in each purification stage. It should be noted that no statistical analysis could be performed to assess the relationships between the different treatments as the data was drawn from a non-homogenous data set (i.e. each symbol represents an average from all of the tested conditions).

$\Delta^{18}O_{untreated-treated}$ for each individual tested reaction condition is presented in Figure 3-10.
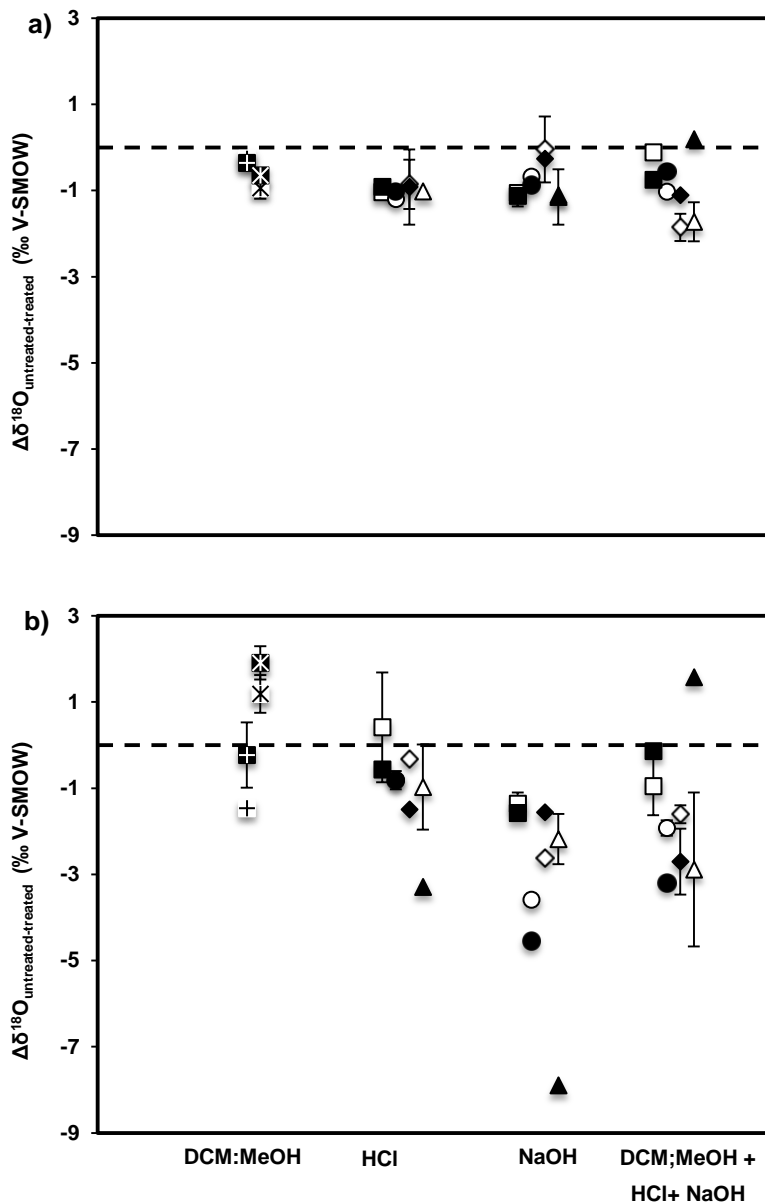
Figure 3-10: a) $\Delta^{18}O_{untreated-treated}$ **for each of the tested reaction conditions for chitin standard and b) chironomid remains. White symbols represent 1 hour treatments; black symbols represent 24 hour treatments. Black cross- 24 hour, 20°C; black star- 24 hour, 70°C; white cross- 1 hour, 20°C; white star- 1 hour, 70°C, square- 0.25M, 20°C; circle- 0.25M, 70°C; diamond- 1M, 20°C; triangle- 1M, 70°C. Each symbol represents average value for treatment type where repeat measurements were possible. Error bars represent 1σ of replicated analysis.**

The following section describes the effects of each of the tested pre-treatments on $\delta^{18}O$ vales in both sample materials.

DCM: MeOH

The tested DCM: MeOH-based treatments were on average associated with a $\Delta^{18}O_{untreated-treated}$ of ~ −0.6‰ and ~ +0.4‰ for the chitin standard and contemporary head capsules respectively (Table 3-2). The offsets observed in both sample materials are largely indistinguishable from analytical error (±0.30-0.45‰) and 1σ of $\delta^{18}O$ measurements in the respective control groups.

The tested DCM: MeOH treatments were observed to introduce variability in $\delta^{18}O$ determinations of contemporary head capsules (1σ = 1.5‰). The average $\Delta^{18}O_{untreated-treated}$ was +1.9 ±0.4‰ in contemporary head capsules exposed to hot (70°C), prolonged (24 hours) DCM: MeOH treatment; whereas the average $\Delta^{18}O_{untreated-treated}$ was −1.5‰ in contemporary head capsules exposed to cold (20°C), short (1 hour) treatments (Figure 3-10). Considering the relatively high average sample weight loss (see Table 3-2), a potential mechanism responsible for creating the observed isotopic variability is the selective removal of ^{18}O enriched solvent-soluble moieties.

HCl

The tested HCl-based treatments were associated with an average $\Delta^{18}O_{untreated-treated}$ of ~ +1.0‰ in both sample materials, although analysis of the chitin standard exposed to the most extreme reaction conditions (1M, 24 hours, 70°C) was not possible due to excessive sample loss. Extensive acid hydrolysis at elevated temperatures is known to catalyse de-acetylation (cleaving of the glycosidic bonds between chitin monomer units) producing chitosan, which is soluble in acidic aqueous solutions (Acosta *et al.,* 1993; Aranaz *et al.,* 2009; Das & Ganesh 2010; Einbu 2007; Hodgins *et al.,* 2001; Nielson & Bowen 2010; Schimmelmann 2010; Tripp *et al.,* 2004; Verbruggen *et al.,* 2010a).

The similarity in the magnitude of the offsets observed in both sample materials indicates that isotope exchange is likely to be the primary mechanism for the observed variability in $\delta^{18}O$ measurements, since acid soluble moieties should not be present in the purified chitin standard. The lowering of sample pH is known to promote isotope exchange between the 'freely exchangeable' oxygen atoms within the acetyl group and/or the hydroxyl oxygen bound to the glucose ring in organic matter, with the OH' group in the water used to dilute the acid (Hodgins *et al.,* 2001; Nielson & Bowen 2010; Schimmelmann 2010; Verbruggen *et al.,* 2010a). The relative proportion of freely exchangeable and non-exchangeable O-atoms will differ among different types of organic molecules. Chemical attack by H^+ will alter the macromolecular structure of organic molecules releasing oxygen-bearing fragments, increasing potential sites for isotope exchange. This process may be selective to a degree and is apparently strongly correlated with reaction conditions (Figure 3-10).

NaOH

The NaOH treatments tested in this investigation were associated with an average $\Delta^{18}O_{untreated\text{-}treated}$ of ~ −0.8‰ and ~ −3.2‰ for the chitin standard and contemporary head capsules respectively (Table 3-2). Once again the offset observed in the chitin standard is largely indistinguishable from analytical error (±0.30-0.45‰) and 1σ of $\delta^{18}O$ measurements in the control group. In contrast the offset observed in contemporary head capsules is much larger.

The primary mechanism responsible for creating variability in $\delta^{18}O$ determinations of chironomid head capsules is likely to be the selective removal of base soluble moieties (e.g. mainly proteins), which appear to be isotopically lighter than the residual bulk material. Prolonged exposure to concentrated NaOH treatment at elevated temperatures is associated with a $\Delta^{18}O_{untreated\text{-}treated}$ of ~ −8.0‰. A similar magnitude of offset was observed in Verbruggen *et al.* (2010a) in chironomid remains exposed to 'harsh' basic treatments (e.g. 28% KOH for 24 hours at 100°C) (see Figure 3-8). However, NaOH treatments are associated with high average sample weight loss of up

to ~ 90% in contemporary remains exposed to 'harsh' reaction conditions. Therefore, a balance must be struck between the complete elimination of base soluble moieties and the preservation of sufficient samples to perform $\delta^{18}O$ analyses.

DCM: MeOH+ HCl+ NaOH

Samples subjected to each of the purification stages were on average associated with a $\Delta^{18}O_{untreated-treated}$ of ~ −0.9‰ and ~ −1.5‰ for the chitin standard and contemporary head capsules respectively. In contrast to the chitin standard, the $\Delta^{18}O_{untreated-treated}$ in contemporary head capsules is greater than the analytical error (±0.30-0.45‰) and 1σ of $\delta^{18}O$ measurements in the control group (see Table 3-2). The magnitude of $\Delta^{18}O_{untreated-treated}$ in contemporary head capsules is about half the sum of the offsets observed in each individual treatment as outlined above.

3.6 Standardisation of the preparation of chironomid head capsules for $\delta^{18}O$ analysis

The results presented in this investigation demonstrate that each of the tested purification stages are sensitive to reaction conditions, with harsh (e.g. 1M, 24 hours, 70°C) conditions likely to provoke the removal of soluble moieties, a degree of isotope exchange and/or chitin de-acetylation. Isotope exchange will result in the overprinting of the original oxygen isotope ratios, leading to spurious palaeoclimate interpretations. In order to limit these detrimental effects reagent concentration (2:1 or 0.25M), exposure duration (24 hours) and reaction temperature (20°C) were standardised. The standardisation of reaction conditions significantly reduced $\delta^{18}O$ variability observed in the chitin standard (standardised $1\sigma = 0.4$; unstandardised $1\sigma = 0.7$) and the chironomid head capsules (standardised $1\sigma = 0.7$; unstandardised $1\sigma = 1.6$). The average $\Delta^{18}O_{untreated\text{-}treated}$ for the chitin standard and contemporary head capsules exposed to the standardised pre-treatment is presented in Figure 3-11.
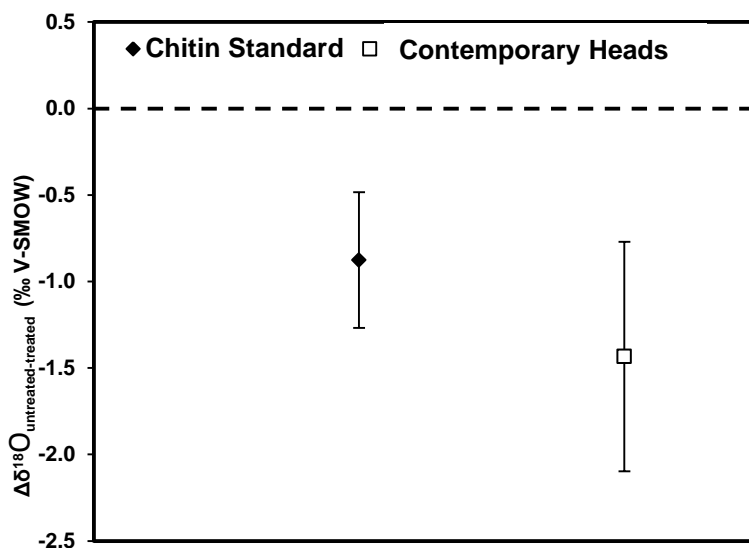
Figure 3-11: Plot of average $\Delta^{18}O_{untreated\text{-}treated}$ for chitin standard (diamond) and head capsule standard (square) subjected to the chosen standardised chemical pre-treatment (sequential soaking in 2:1 DCM: MeOH, 0.25M HCl, 0.25M NaOH solutions for 24 hours at 20°C). Error bars represent 1σ of replicated analysis (n = 6 for both materials). Dashed line represents average repeated control $\delta^{18}O$ measurement.

The average $\Delta^{18}O_{untreated\text{-}treated}$ in the chitin standard exposed to the standardised pre-treatment was −0.9‰ (n=6), which encompasses both analytical and preparatory uncertainties. Isotope exchange is likely to be the primary mechanism responsible for creating this offset, given that extensive de-acetylation is not evident and that the original material contains few compositional impurities (*pers.comm.*Sigma-Aldrich; 20 August 2013). Consequently, one may conclude that the standardised pre-treatment procedure is associated with ~ −0.9‰ offset. The average $\Delta^{18}O_{untreated\text{-}treated}$ of contemporary head capsules exposed to the standardised pre-treatment was −1.4‰ (n=6). Since ~ −0.9‰ of this offset is likely to have been due to isotope exchange, the remaining ~ −0.6‰ offset can be considered to be caused by the selective removal of impurities, most likely compositional in the instance of contemporary remains tested in this investigation. $\delta^{18}O$ determinations of samples treated using a standardised multi-stage procedure were statistically different from untreated samples in both tested sample materials ($p < 0.01$). Consequently it may be necessary to apply a +0.9‰ correction during $\delta^{18}O$ analyses of samples treated using this procedure.

The current absence of a standardised protocol for the preparation of chironomid remains for $\delta^{18}O$ analyses has restricted the application of $\delta^{18}O_{chironomid}$ in palaeoclimate reconstructions and hindered inter-laboratory comparisons (Wang *et al.,* 2008; Verbruggen *et al.,* 2010a). It is hoped that the procedure described in this chapter can form the basis for the standardisation of preparatory procedures in future $\delta^{18}O_{chirononmid}$ analysis. However, additional systematic studies are required in order to fully assess the effectiveness of the adopted procedure at limiting non-amino polysaccharide impurities by comparing chemical composition of the standard materials before and after treatment (e.g. pyrolysis-GC/MS analysis), while studies are also required to assess the influence of different types of exogenous contamination (e.g. carbonate and silicate) on $\delta^{18}O_{chironomid}$ determinations.

Chapter 4 Towards a mechanistic understanding of the incorporation of oxygen isotopes in chironomid head capsules: laboratory and field-based calibration of $\delta^{18}O_{chironomid}$, $\delta^{18}O_{lakewater}$ and temperature.

4.1 Overview

In order for $\delta^{18}O_{chironomid}$ to become a quantitative tool for reconstructing past $\delta^{18}O_{lakewater}$ and, indirectly past climates, it is first necessary to refine our understanding of the inherent fractionations associated with the incorporation of environmental isotopic signatures into chironomid head capsules. Oxygen isotope fractionations between chironomid head capsules and habitat water ($\alpha^{18}O_{chironomid-H2O}$) are poorly defined. In their pioneering study, Wooller *et al.* (2004) concluded that $\alpha^{18}O_{chironomid-H2O}$ was constant and largely indistinguishable from oxygen isotope fractionation in aquatic cellulose ($\alpha^{18}O_{aquatic\ cellulose-H2O}$ = 1.025-1.028) (e.g. Edwards & McAndrews 1989; Wolfe *et al.,* 2001). The apparent similarity between $\alpha^{18}O_{chironomid-H2O}$ and $\alpha^{18}O_{aquatic\ cellulose-H2O}$ suggests that common biochemical reactions are likely to govern fractionation in both organic compounds. Since $\alpha^{18}O_{aquatic\ cellulose-H2O}$ is largely independent of kinetic (temperature related) and disequilibrium effects, one may assume that the same is true for chironomids, based on the findings presented in Wooller *et al.* (2004). Although it should be noted that Wooller *et al.* (2004) did not account for secondary effects associated with atmospheric circulation patterns, hydrological conditions and catchment characteristics, which can alter $\delta^{18}O_{precipitation}$ during transportation to the lake or while in the lake (see Sections 1.3.2 and 1.3.3). Consequently their assessments require experimental verification.

In this chapter the relationship between $\delta^{18}O_{chironomid}$, habitat water $\delta^{18}O$ and temperature was evaluated in a series of laboratory and field-based calibration studies, with these results forming the foundations for the interpretation of stratigraphic changes in $\delta^{18}O_{chironomid}$ (Chapter 5).

4.1.1 Chapter aims and objectives

This chapter aims to improve the mechanistic understanding of the incorporation of oxygen isotopes in chironomid head capsules and refine the characterisation of the relationship between $\delta^{18}O_{chironomid}$, $\delta^{18}O_{lakewater}$ and temperature in contemporary chironomid remains. This will be achieved by: -

- Accurately measuring $\alpha^{18}O_{chironomid-H2O}$ as a function of temperature in a series of controlled laboratory experiments (Section 4.2).
- Investigating the relationship between $\delta^{18}O_{chironomid}$ and $\delta^{18}O_{lakewater}$ in a spring-fed pond, known to be subjected to negligible temporal variations in water chemistry and $\delta^{18}O_{lakewater}$ (Section 4.3).
- Investigating $\delta^{18}O_{chironomid}$ in a series of lakes that experience seasonal variations in $\delta^{18}O_{lakewater}$, water chemistry and temperature (Section 4.4).

The calibration of relationships between $\delta^{18}O_{chironomid}$, $\delta^{18}O_{lakewater}$ and temperature in contemporary settings is fundamental to the development of this approach as a tool in palaeoclimate reconstructions.

4.2 An *in vitro* assessment of the influence of temperature on oxygen isotope fractionation between chironomid head capsules and water

4.2.1 Rearing experiments

Laboratory studies are an excellent model for examining the influence of different parameters on the stable isotopic composition of a compound (Gannes *et al.,* 1997). In this investigation, *Chironomus riparius* larvae were reared from eggs (supplied by Huntington Life Sciences Ltd) in glass Erlenmeyer flasks, containing 2 litres of bottled mineral water and 500g of sand (combusted at 550°C for six hours to eliminate extraneous food sources). The flasks were situated inside isothermal cabinets (Natural History Museum, London) set at different constant temperatures (5, 10, 15, 20, 25°C) (Figure 4-1). Replicate experiments at each of the test temperatures were conducted concurrently in the same isothermal cabinet to minimise temperature variations between replicate experiments.

Figure 4-1: Erlenmeyer flasks located inside an isothermal cabinet (NHM, London).

The flasks were kept in complete darkness to prohibit photosynthetic activity and were loosely sealed with aluminium foil to limit evaporation. Each flask was typically provided with 1.5ml suspension of finely ground Tetramin fish food flakes, every other day. The food suspension was made weekly, by blending 4g of fish food flakes with one litre of water. Rationing was adjusted

according to water quality and larval behaviour as the decomposition of uneaten food can lead to increased microbial activity and reduced dissolved oxygen concentration, which may hinder larval development. Since no aeration could be provided to the flasks inside the isothermal cabinets, water quality was maintained through regular partial water replacements. One litre of water was siphoned off each flask weekly and replaced with stock mineral water stored at the relevant temperature, to ensure satisfactory dissolved oxygen concentration and maintain optimal environmental conditions for growth and development.

Experiments were terminated once the majority of larvae had reached the final instar stages, with experiment duration varying depending on larval growth rates.

4.2.2 Sampling

Water samples- Water samples were taken regularly throughout the experiments to track changes in $\delta^{18}O$. Samples were filtered using disposable cellulose acetate filters (0.2μm pore size) and were stored at 4°C, in 5ml screw top glass vials with no headspace.

Stable isotope analyses of water samples were undertaken at the 'Lifer' stable isotope laboratory, Department of Earth, Ocean and Ecological Sciences, University of Liverpool. Oxygen ($^{18}O/^{16}O$) and hydrogen ($D/^1H$) isotope ratios were determined simultaneously using a Picarro WS-CRDS system, with the results presented in this thesis being the average of at least 8 sequential injections of 2μl of water. Results were normalised onto the V-SMOW scale using internationally distributed standards. Internal precision was $< 0.08‰$ for $\delta^{18}O$ and $< 0.4‰$ for δD measurements.

Water Chemistry- Camlab Handylab 1 battery powered hand-held meters attached to a data logger were used to measure electrical conductivity (μScm^{-1}), dissolved oxygen concentration (mgL^{-1}) and pH of the growth water in each experiment, at near weekly intervals. The meters were calibrated before use in accordance with manufacturer's procedures. It should be noted that water chemistry measurements were performed prior to the partial water replacements.

Tinytalk (TK-0040) data loggers were used to monitor water temperature at hourly intervals in one of the flasks in each of the isothermal cabinets, due to an insufficient number of loggers. However, it is assumed that temperature variations between flasks in the same cabinet were negligible.

Chironomid Larvae- The contents of each flask were washed through a 1mm mesh sieve and chironomid larvae were isolated from the retained residue, using fine tipped forceps. The larvae were frozen whole, with freezing assumed to have no influence on $\delta^{18}O_{chironomid}$ (Verbruggen *et al.,* 2010a).

Following defrosting, head capsules were manually isolated from larval bodies under a stereo-microscope (x25 magnification) using a mounted needle and fine tipped forceps. Care was taken to remove as much of the digestive tract and muscle tissue as possible from the head capsules, which then underwent chemical pretreatment following the procedures outlined in Section 3.6, prior to $\delta^{18}O$ analysis (Section 2.3).

4.2.3 Results and Discussion

Temperature, chemistry and δ¹⁸O of the growth water

The maintenance of constant conditions during this investigation proved problematic, particularly at higher temperatures where the oxygen demands of the chironomid larvae were increased due to enhanced metabolic activity. A summary of mean water chemistry (pH, dissolved oxygen concentration and electrical conductivity), temperature and $\delta^{18}O_{H2O}$ from each experiment is provided in Table 4-1.

Table 4-1: Mean $\delta^{18}O$, pH, dissolved oxygen concentration and electrical conductivity in each of the rearing experiments. Temperature measurements were not taken from replicate flasks due an insufficient number of data loggers. An additional flask was reared at 15°C during a preliminary study.

Temperature (°C)	$\delta^{18}O_{H2O}$ (‰ V-SMOW)	pH	Dissolved Oxygen (mgL^{-1})	Electrical Conductivity (µScm^{-1})
5.6 ± 0.4	−7.4 ± 0.18	7.2 ± 0.2	7.3 ± 1.5	230 ± 12
	−7.5 ± 0.12	7.3 ± 0.1	7.2 ± 1.4	237 ± 10
10.5 ± 0.4	−7.6 ±0.18	7.4 ± 0.2	7.1 ± 1.3	256 ± 18
	−7.5 ±0.21	7.2 ± 0.2	7.2 ± 1.4	259 ± 25
15.2 ± 0.4	−7.3 ±0.07	7.4 ± 0.2	6.7 ± 1.9	247 ± 18
	−7.4 ±0.11	7.3 ± 0.2	6.2 ± 2.3	259 ± 14
	−7.5 ±0.15	7.3 ± 0.1	6.4 ± 1.9	259 ± 16
20.2 ± 0.3	−7.3 ±0.16	7.6 ± 0.1	6.8 ± 1.0	250 ± 7
	−7.3 ±0.14	7.6 ± 0.0	6.8 ± 1.1	252 ± 8
24.9 ± 0.5	−7.3 ±0.25	7.5 ± 0.2	6.1 ± 1.8	292 ± 17

The evolution of water chemistry, temperature and $\delta^{18}O_{H2O}$ throughout the duration of each experiment is presented in Figure 4-2.

a)

b)

5°C'

c)   10°C

d)

10°C'

e)

15°C

f) 15°C'
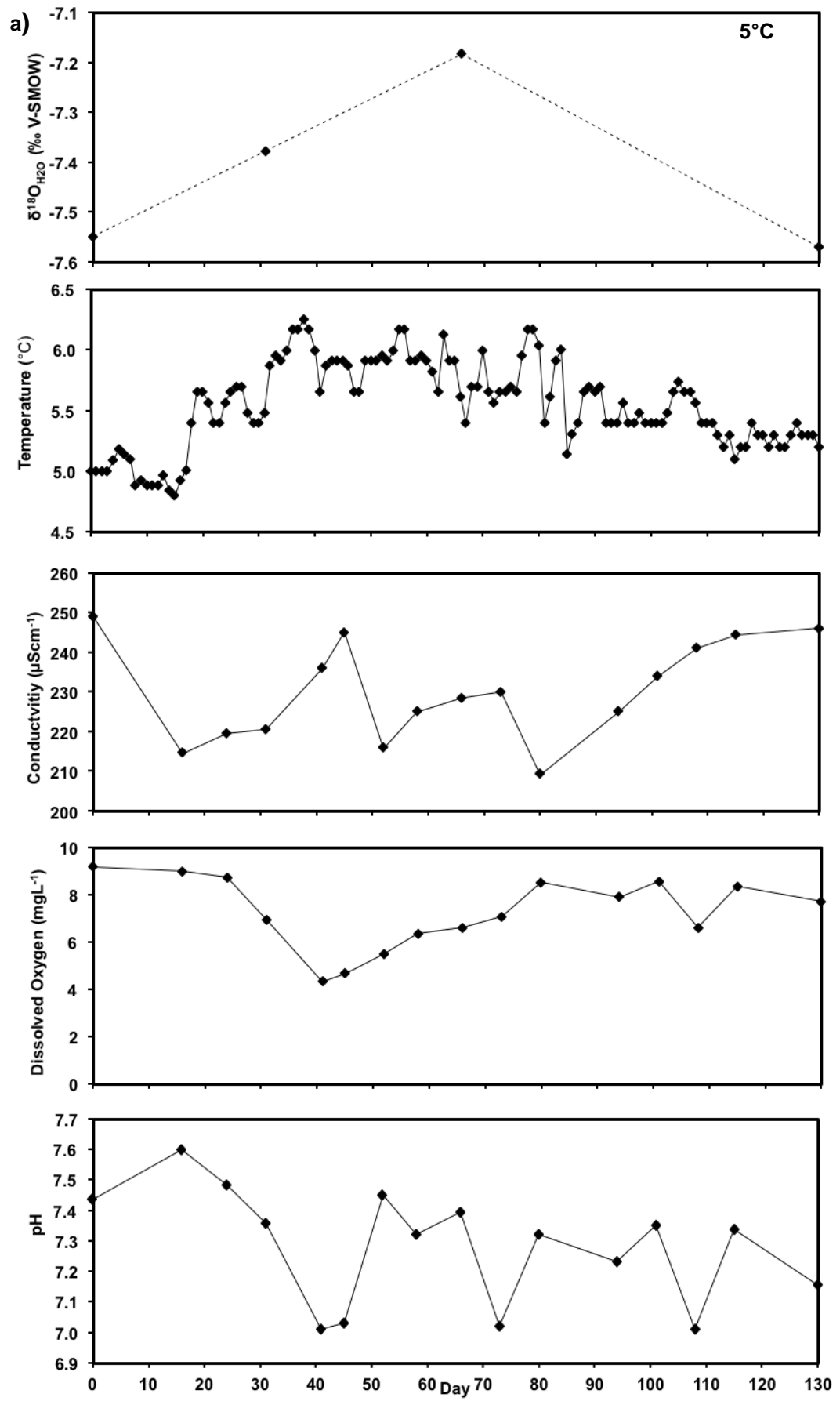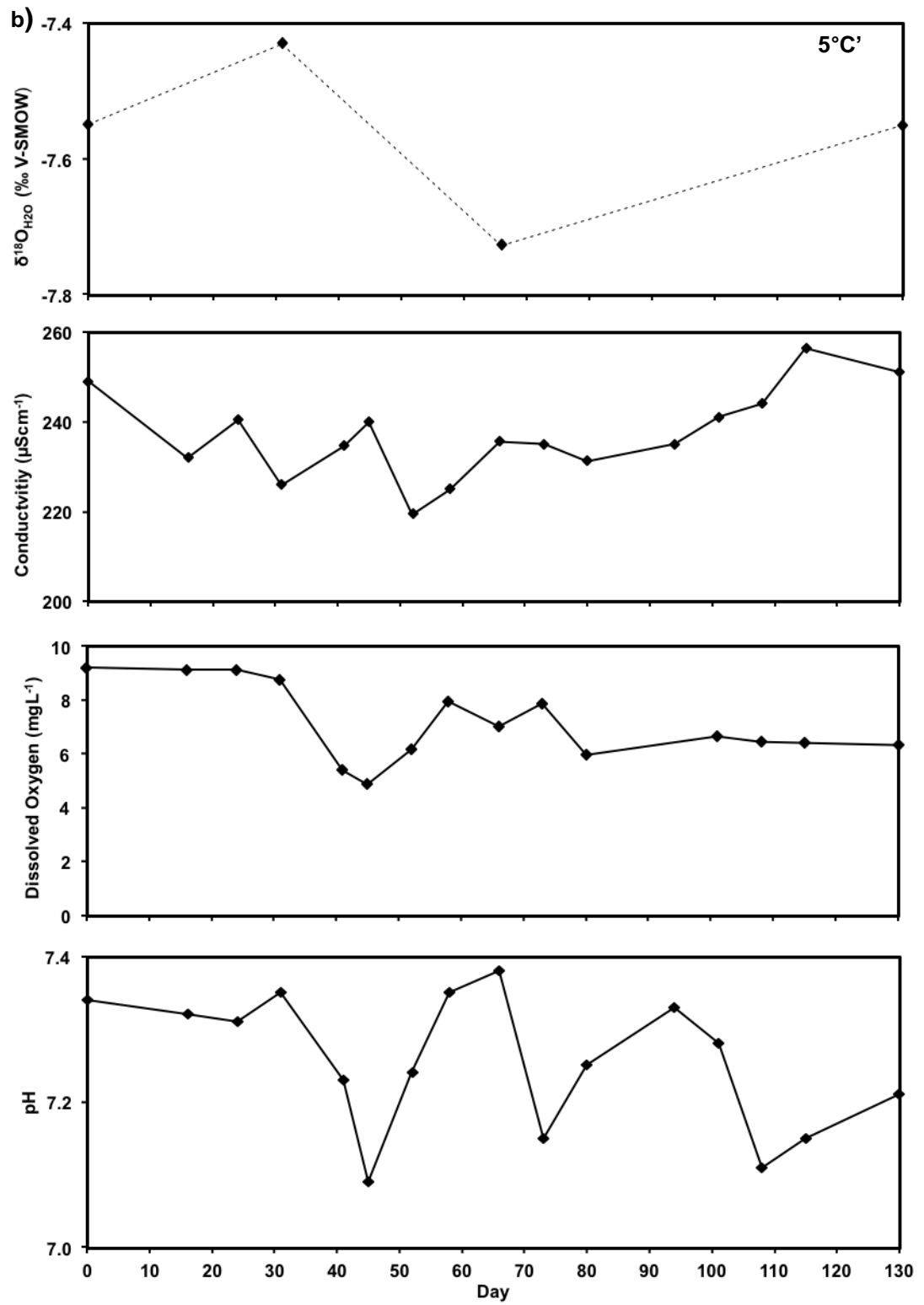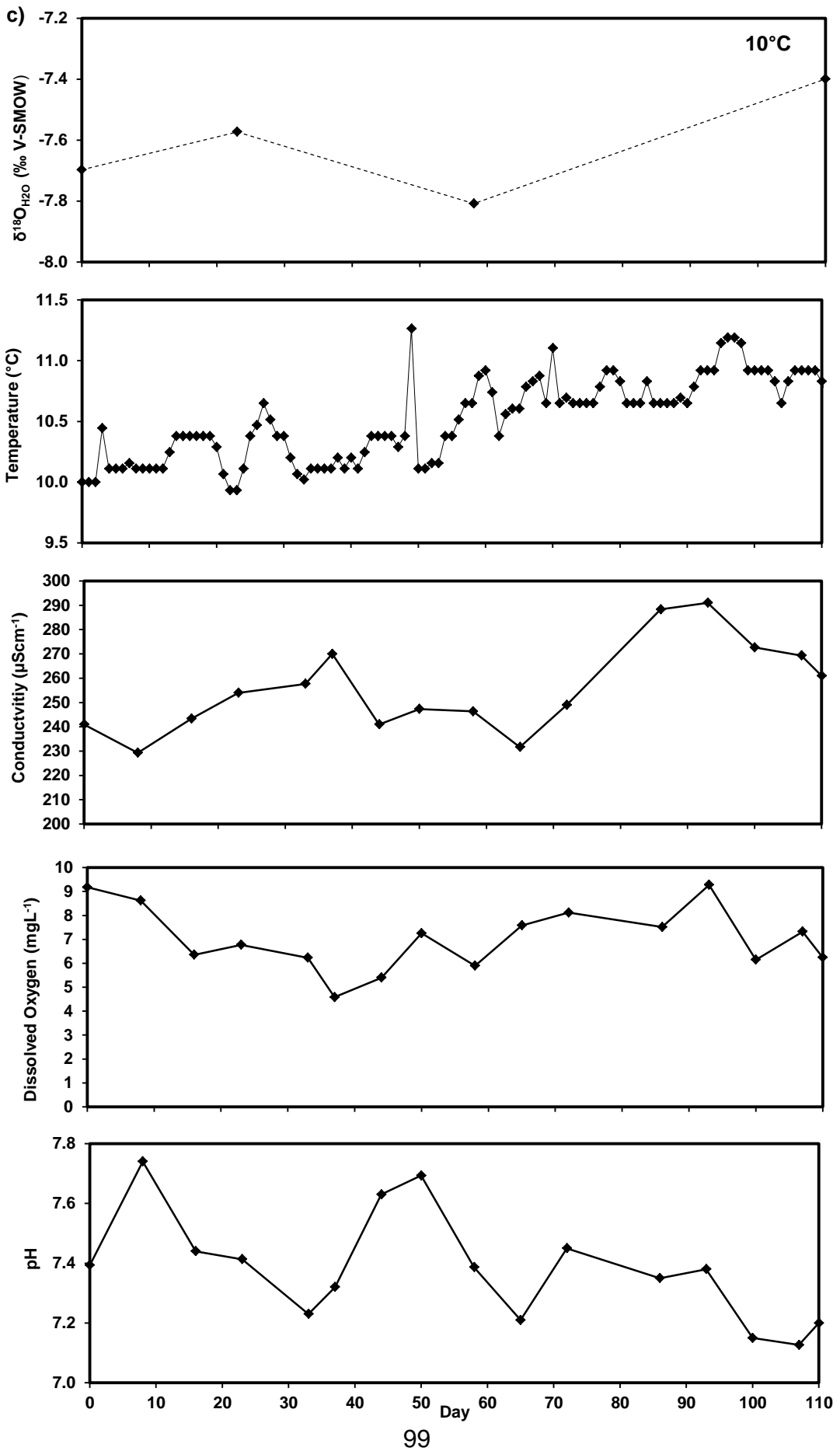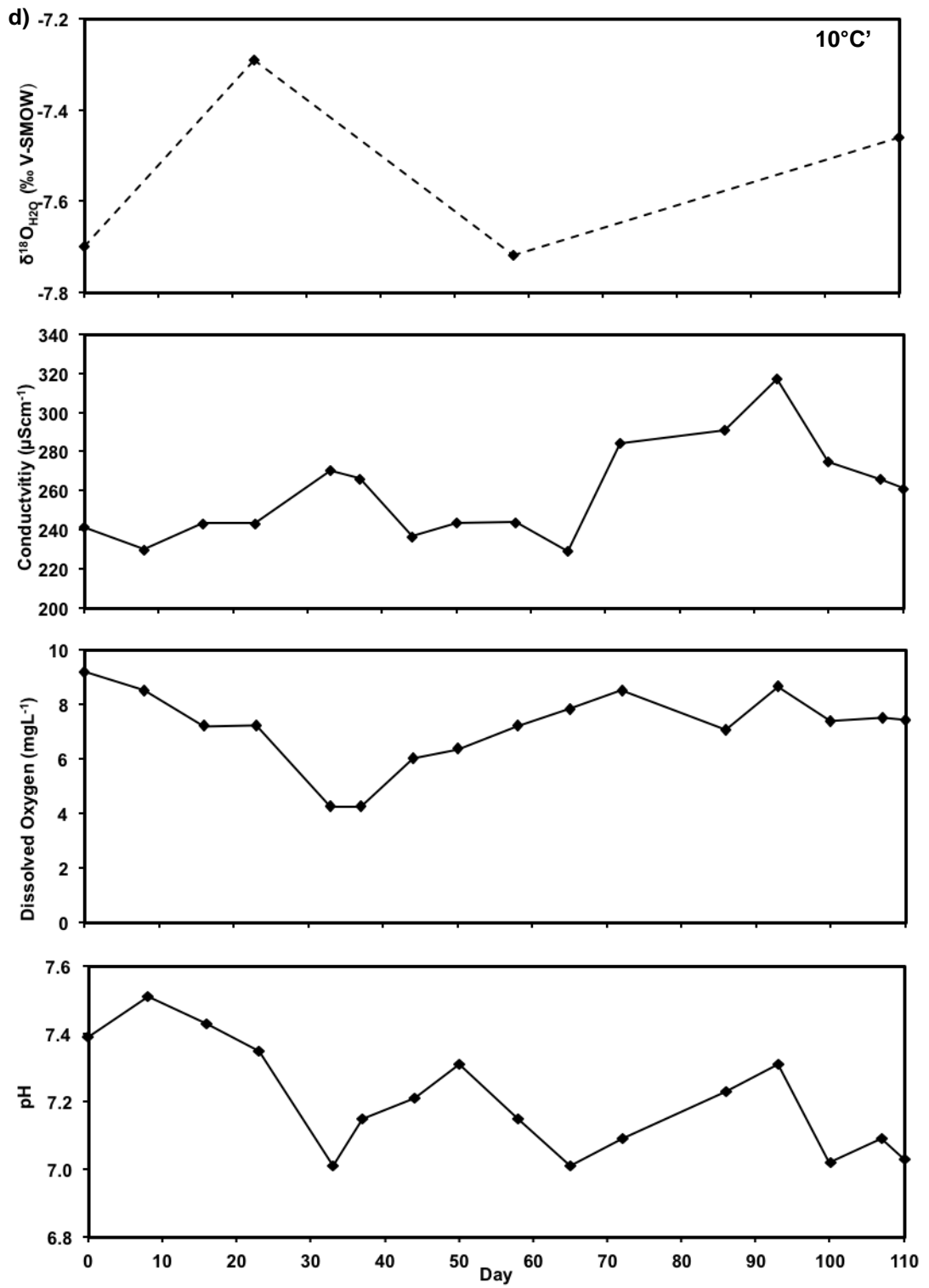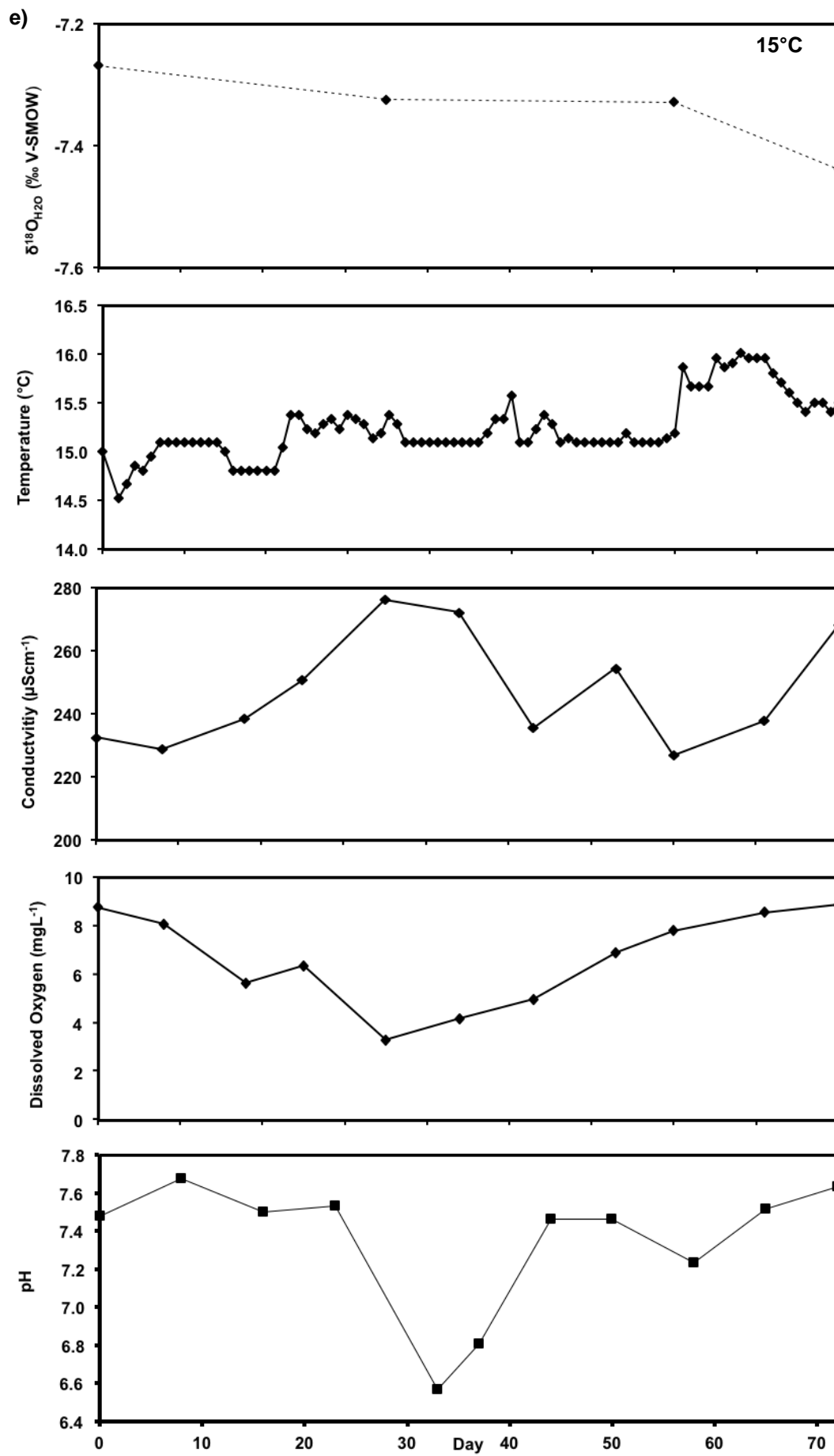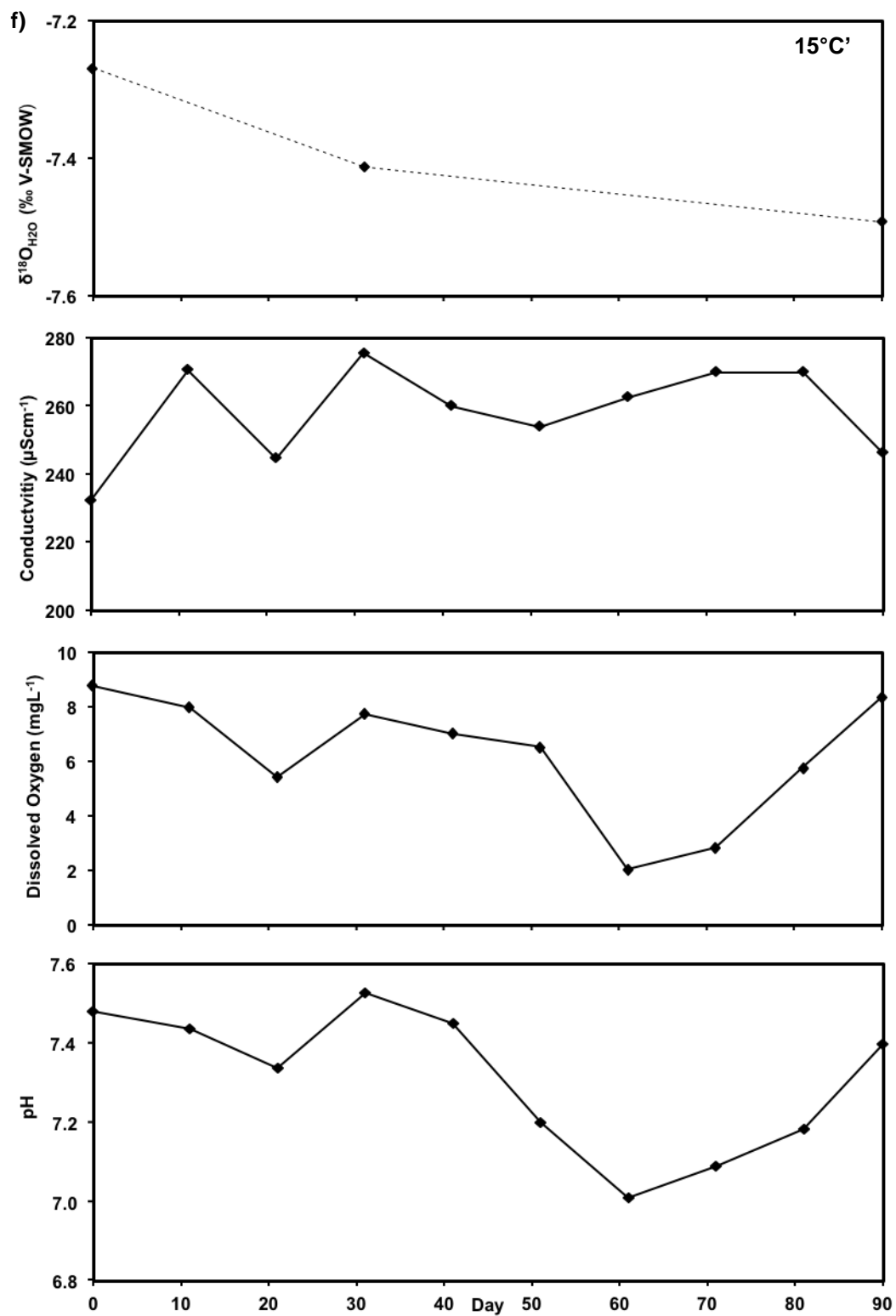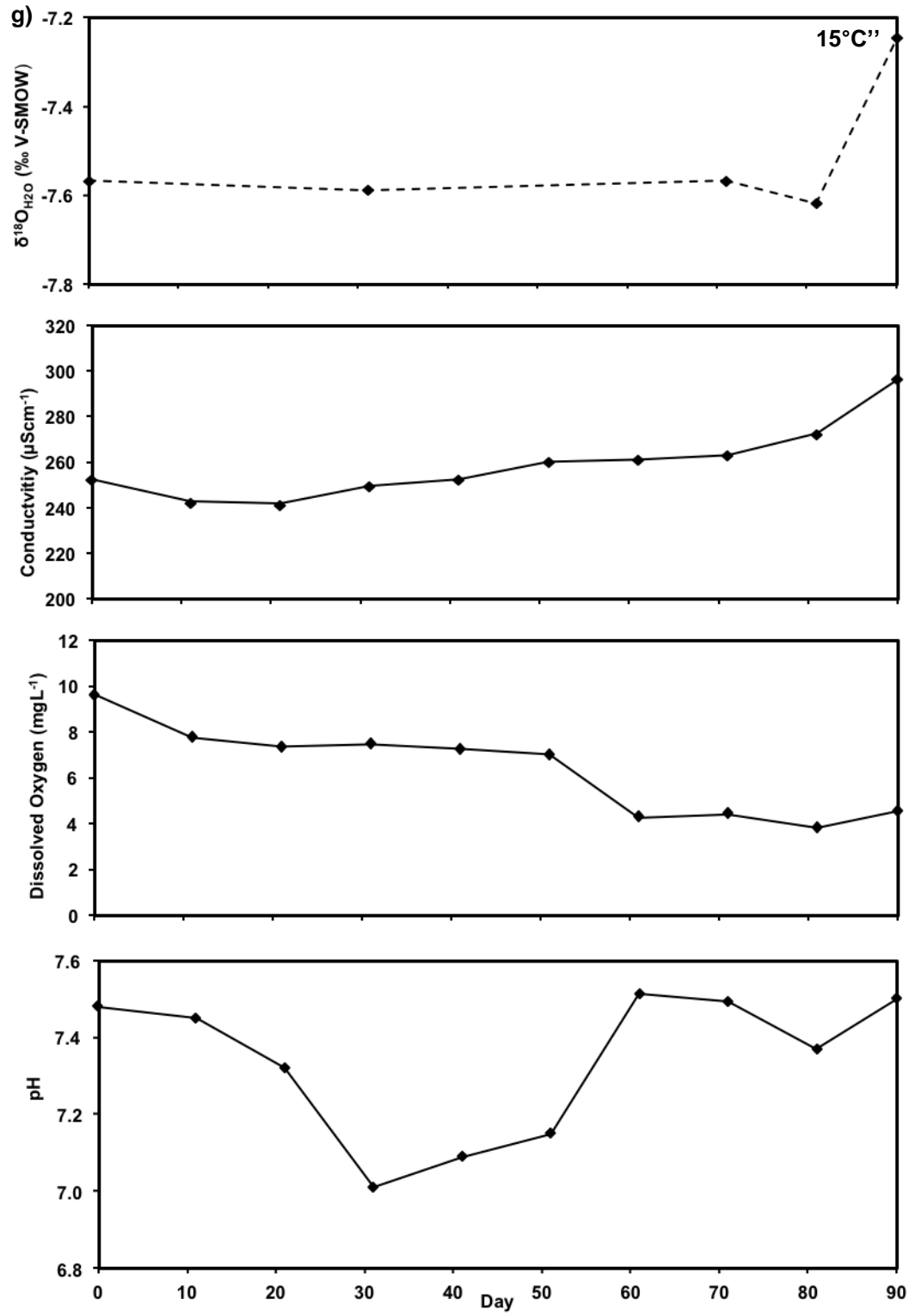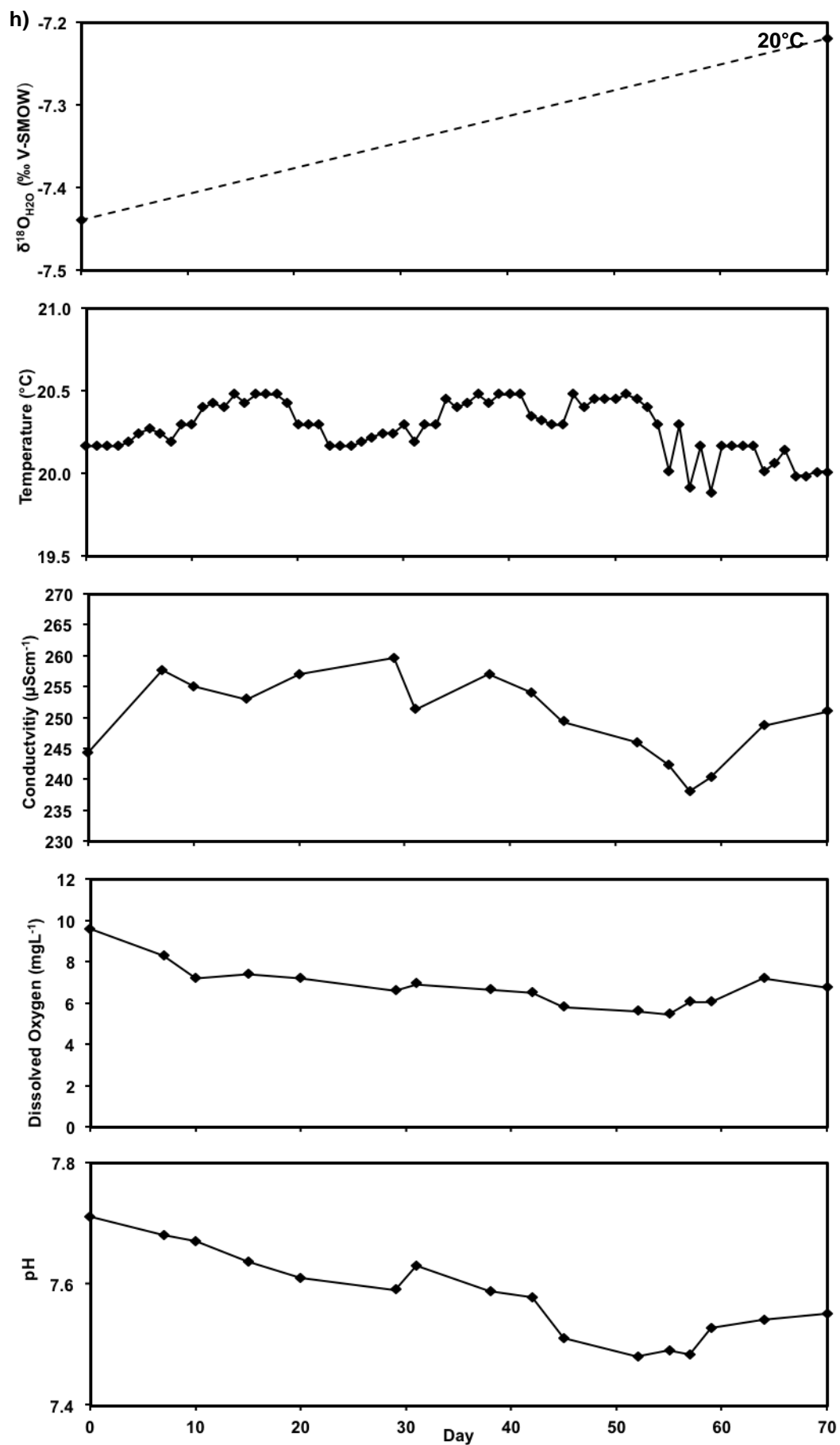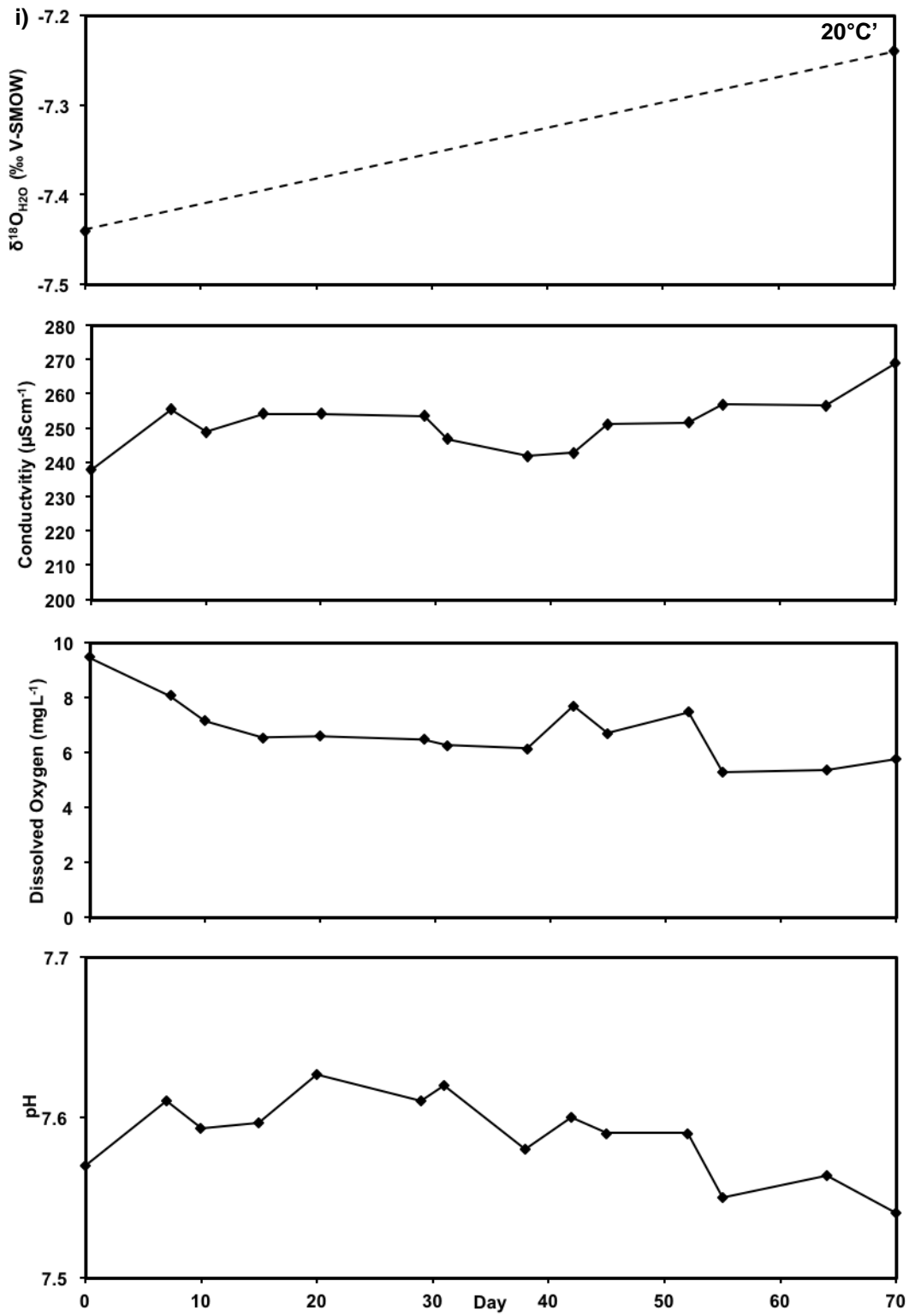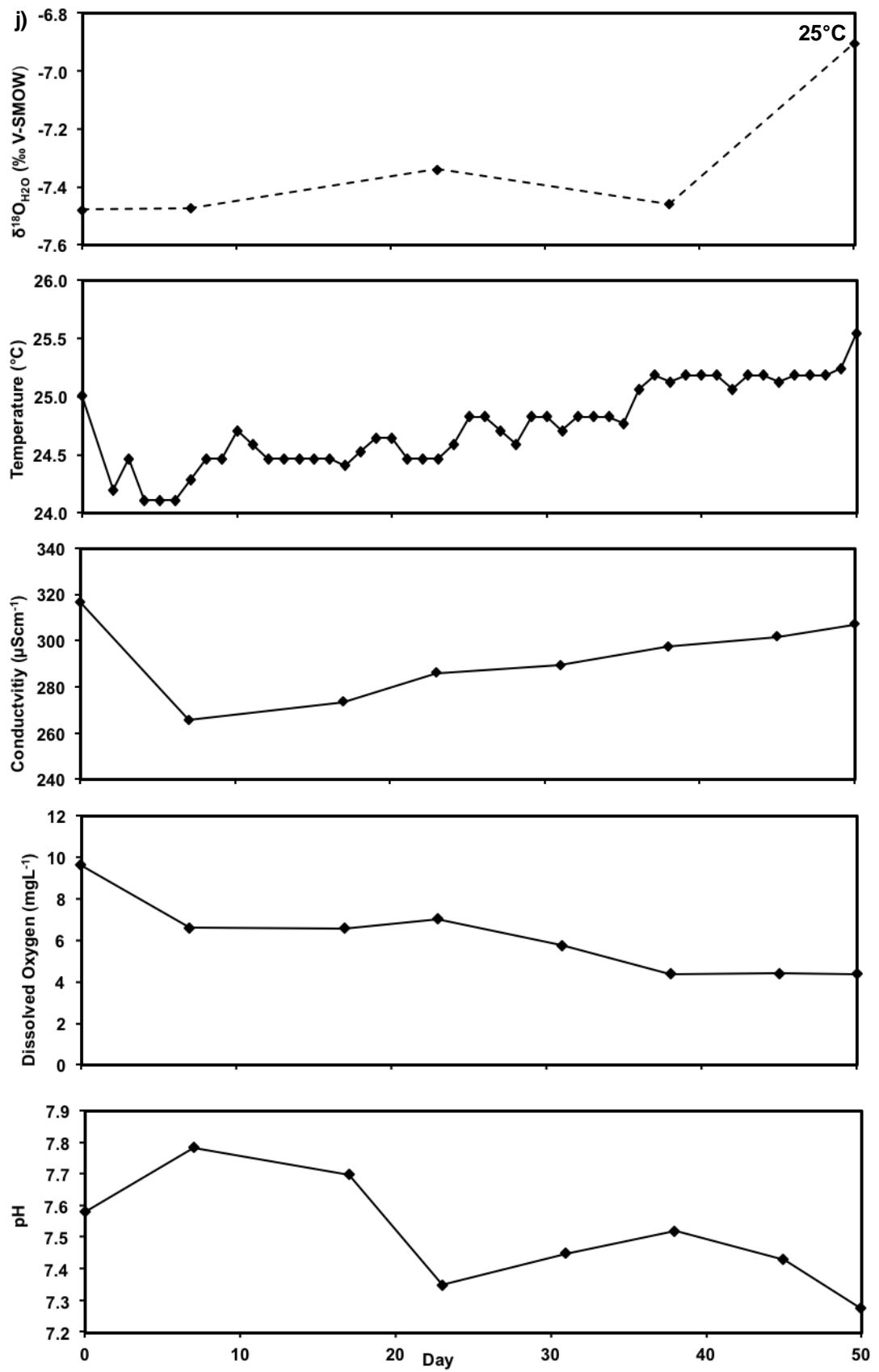
Figure 4-2: a-j evolution of water chemistry and stable isotope data throughout the duration of each experiment. ' and " denote replicate cultures.

Since no significant mortality events were observed throughout the duration of this investigation, conditions are assumed to have remained within the ecological tolerances of the *Chironomus riparius* larvae; however it should be noted that eggs failed to hatch in one of the cultures at 25°C. Water temperature ($1\sigma = \pm0.3 - 0.5$°C), pH ($1\sigma = \pm0.1 - 0.2$), and $\delta^{18}O_{H2O}$ ($1\sigma = \pm0.1 - 0.3$‰) remained essentially constant in each experiment, although limited evaporative enrichment was apparent in nearly all of the flasks (Figure 4-2). The observed variability in $\delta^{18}O_{H2O}$ ($1\sigma \pm0.1 - 0.3$‰) in this investigation is considerably lower than the variation reported in a similar controlled laboratory study, in which $\delta^{18}O_{H2O}$ varied by 1.1 to 1.8‰ (1σ) in experiments that ran for ~8 weeks (Wang *et al.,* 2009). Dissolved oxygen concentration fluctuated in each experiment, which is likely to have been associated with changes in the metabolic processes (e.g. respiration) in the chironomid larvae and the decomposition of uneaten food.

Experiment duration

Temperature has a profound influence on chironomid physiology, with the duration of each experiment varying at different temperatures. Larval development was slowest in experiments conducted at 5°C and fastest at 25°C. A summary of the time for *Chironomus riparius* larvae to reach the 4th instar stage is provided in Table 4-2.

Table 4-2: *Chironomus riparius* larvae development time (from eggs to 4th instar stage) at different constant temperatures.

Temperature (°C)	Larval Development Time (Days)
5	130
10	110
15	90
20	70
25	50

Temperature dependence of $\alpha^{18}O_{chironomid\text{-}H2O}$

Oxygen isotope analyses were performed on chironomid head capsules isolated from larvae reared at different constant temperatures and exposed to a series of liquid solvent-based extractions (2:1 DCM: MeOH, 0.25M HCl, 0.25M NaOH) for 24 hours at 20°C. The results of the experiment are summarised in Table 4-3. The oxygen isotope composition of the purified chironomid head capsules ranged between +13.8-16.3‰ across the tested temperatures, even though $\delta^{18}O_{H2O}$, water chemistry and diet all remained essentially constant. This variability is considerably larger than the reported analytical precision of ±0.4-0.6‰ (Section 2.3.1). On average $\delta^{18}O_{chironomid}$ measurements were ~ +1.3‰ lower in larvae reared at 25°C than in larvae reared at 5°C, with $\alpha^{18}O_{chironomid\text{-}H2O}$ varying between 1.021-1.024 across the tested temperature range [note that $\alpha^{18}O_{chironomid\text{-}H2O} = (1000 + \delta^{18}O_{chironomid})/(1000 + \delta^{18}O_{H2O})$] (Table 4-3).

Table 4-3: Average $\delta^{18}O_{H2O}$ throughout the duration of each experiment and $\delta^{18}O_{chironomid}$ from each of the tested temperatures. ' denotes repeat experiments conducted at a particular temperature. * denotes pilot study included in the analyses. Note analyses were only performed on larvae reared in one of the flasks at 5°C due to analytical difficulties at Durham University.

Temperature (°C)	Average $\delta^{18}O_{H2O}$ (‰ V-SMOW)	$\delta^{18}O_{chironomid}$ (‰ V-SMOW)	$\alpha^{18}O_{chironomid\text{-}H2O}$
5	−7.4 ± 0.2	+16.8	1.024
10	−7.6 ± 0.2	+16.1	1.024
10'	−7.6 ± 0.2	+15.6	1.023
15	−7.5 ± 0.2	+15.9	1.024
15'	−7.3 ± 0.1	+16.3	1.024
15*	−7.3 ± 0.1	+15.7	1.023
20	−7.3 ± 0.1	+13.8	1.021
20'	−7.3 ± 0.2	+15.0	1.022
25	−7.3 ± 0.3	+14.9	1.022

Under the controlled laboratory conditions tested in this investigation a robust correlation is observed between $\alpha^{18}O_{chironomid-H2O}$ and temperature (R= 0.73; $r^2 = 0.53$; $p < 0.05$; n= 9), with the uncertainty of the calibration (standard error of the estimate) being 0.6 (Figure 4-3).
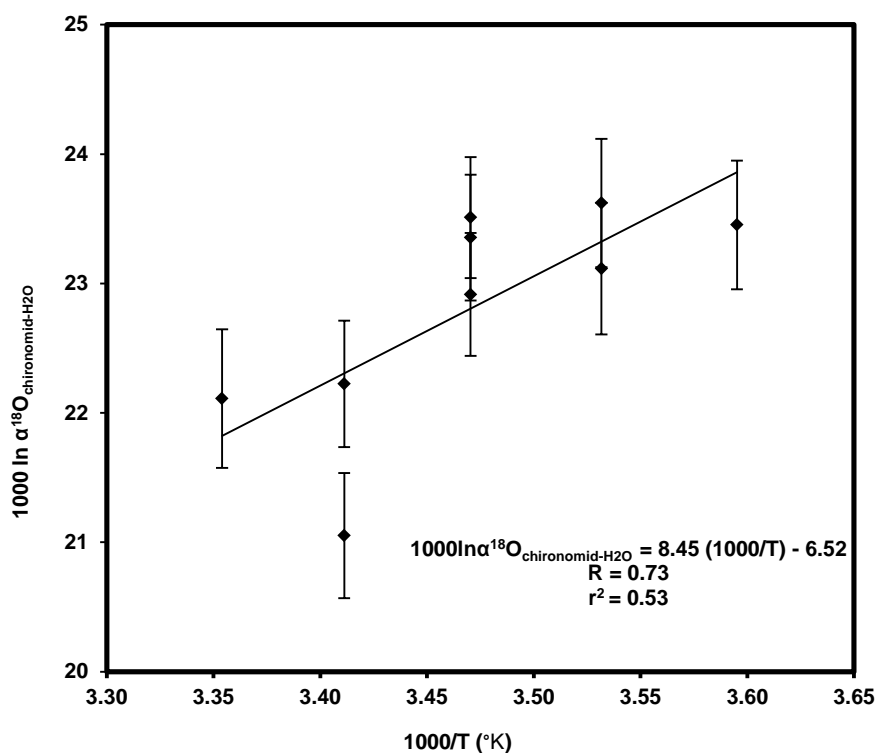
Figure 4-3: 1000.ln $\alpha^{18}O_{chironomid-H2O}$ as a function of inverse temperature. Temperature decreasing from left to right. Error bars represent 1σ.

The reduction in $\alpha^{18}O_{chironomid-H2O}$ with increasing temperature, between 5 and 25°C, is consistent with the laws of thermodynamics (Section 1.2.1) and can be defined by the following fractionation equation:

$$1000 \ln \alpha^{18}O_{chironomid-H2O} = 8.45(1000\ T^{-1}) - 6.52$$

Equation 6

where T is temperature in Kelvin (i.e. °C + 273.18).

The systematic variability of $\alpha^{18}O_{chironomid-H2O}$, implies that temperature plays a secondary role in influencing $\delta^{18}O_{chironomid}$ signals. The coefficient of the linear regression between $\delta^{18}O_{chiornomid}$ and temperature is substantially lower

($\sim$ −0.1‰/°C^{-1}) than in mineral precipitates, where oxygen isotope fractionation has been well defined experimentally and empirically in carbonates (−0.24‰/°C^{-1}; Kim & O'Neil 1997) and is less well-defined in biogenic silica ($\sim$ −0.2 to −0.5‰/°C^{-1}; Brandriss *et al.*, 1998; Juillet-Leclerc & Labeyrie 1987; Leng & Barker 2006).

All results plot within 1σ of analytical uncertainty, except for one of the rearing experiments at 20°C. The reason for the disparity between the two rearing experiments at this temperature is not known, but could be related to additional dietary contributions from microorganisms originating from the decomposition of excess food. The statistical strength of the relationship between $\alpha^{18}O_{chironomid-H2O}$ and temperature can be improved by removing this apparent outlier (R = 0.81; r^2 = 0.66; *p* < 0.05; n= 8). Furthermore, standard error of the estimate is reduced to 0.4 while the gradient and intercept of the linear regression is substantially changed so that:

$$1000 \ln \alpha^{18}O_{chironomid-H2O} = 6.29\,(1000\,T^{-1}) + 1.16$$

Equation 7

Given the relatively small size of the data set (n=9), it was decided that the most pragmatic approach would be to retain this apparent outlier. Replicate samples for each of the rearing experiments have been prepared, but at the time of writing had not been analysed due to analytical difficulties at Durham University. The results from the replicate analyses will help establish whether the apparent outlier should be retained or excluded from the data set.

The consistency of the findings of this investigation was assessed in relation to the results obtained by Wang *et al.* (2009) (Figure 4-4). In their study, *Chironomus dilutus* larvae were reared under controlled laboratory conditions (23°C with a constant diet) in waters with different $^{18}O/^{16}O$ ratios. The study reported a strong correlation between $\delta^{18}O_{chironomid}$ (whole larvae) and $\delta^{18}O_{H2O}$. The results presented in this section bisect the linear regression observed between $\delta^{18}O_{chironomid}$ (whole larvae) and $\delta^{18}O_{H2O}$ in Wang *et al.*

(2009), with measurements from rearing experiments conducted at temperatures above/close to 23°C plotting below the line, and measurements from rearing experiments conducted at temperatures below 23°C plotting above the line.
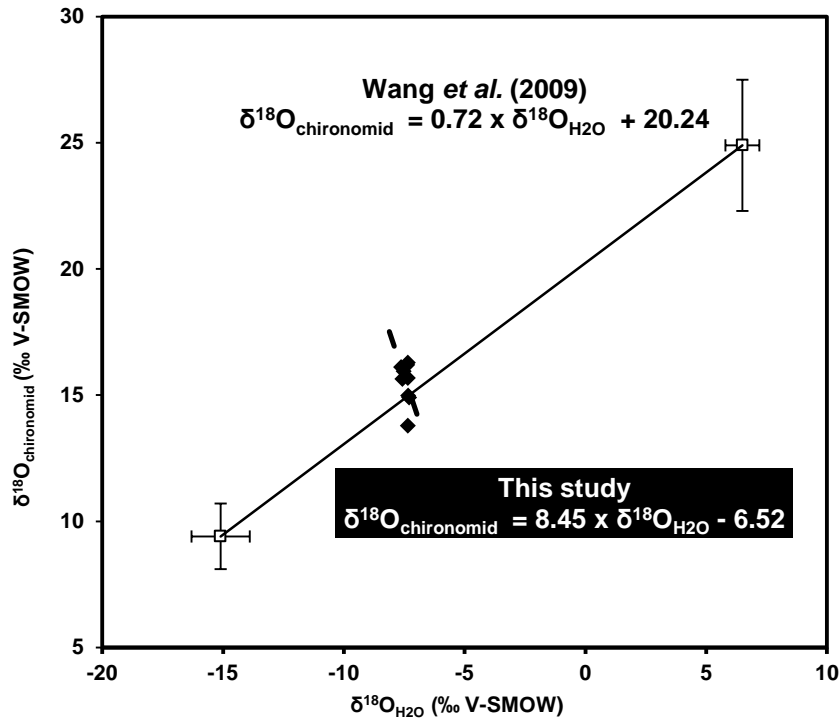
Figure 4-4: Open squares represent mean $\delta^{18}O_{chironomid}$ (whole larvae) vs. $\delta^{18}O_{H2O}$ from Wang *et al.* (2009). Black diamonds represent average $\delta^{18}O_{chironomid}$ reared at different temperatures vs. $\delta^{18}O_{H2O}$, from this study.

This section documents the first experimental calibration of the relationship between $\alpha^{18}O_{chironomid-H2O}$ and temperature (between 5 and 25°C). Precipitation processes in inorganic systems (e.g. carbonate and silicate) are known to be associated with temperature-dependant oxygen isotope fractionations. However, temperature is largely anticipated to have a negligible influence on oxygen isotope fractionation in organic matter (e.g. DeNiro & Epstein 1981; Wolfe *et al.,* 2001). The results from this investigation indicate that temperature may influence $\alpha^{18}O_{chironomid-H2O}$ in larvae reared under controlled conditions. However, it should be noted that the coefficient ($\sim -0.1‰/°C^{-1}$) of the observed relationship is significantly smaller than the analytical error associated with the measurements. Since

111

this data set is relatively small it is recommended that further laboratory- and field-based calibration studies should be performed to validate these findings. It is hoped that the results presented in this section will eventually form part of a larger data set permitting the empirical characterisation of the relationship between $\alpha^{18}O_{chironomid\text{-}H2O}$ and temperature, which is essential to the development of this approach as a tool for reconstructing past climates. The implications of the findings in terms of palaeoclimate reconstructions are discussed further in Section 4.5.

4.3 An investigation of $\delta^{18}O_{chironomid}$ in a near constant natural environment

4.3.1 Site description

Greywell Moor Nature Reserve (latitude 51.25°N longitude – 0.96°W), situated 70km west-southwest of London in the village of Greywell (Hampshire, UK), is an area of managed heathland surrounded by arable farmland (Figure 4-5). After an initial inspection of a series of groundwater fed ponds within the reserve, a ~10m diameter, shallow (< 1m deep), roughly circular pond (herein referred to as Greywell Pond) was chosen for monitoring between May 2011-2013 since it contained the most abundant chironomid community. The chosen pond has no discernible outflow, draining through seepage into an adjacent marsh area before ultimately feeding the River Whitewater (Keatings *et al.,* 2002). A previous monitoring program by Keatings *et al.* (2002) indicated that pond water $\delta^{18}O$, temperature and chemistry remained essentially constant between December 1996 and March 1998 (see Table 4-4). Although laboratory studies are an excellent model for examining the influence of different parameters on $\delta^{18}O_{chironomid}$ they are rarely able to fully simulate the complex biological requirements of an organism, potentially hindering "normal" growth. Greywell pond provides an ideal "natural culture" for assessing the relationship between $\delta^{18}O_{chironomid}$ and $\delta^{18}O_{lakewater}$ due to the stability of pond water $\delta^{18}O$, temperature and chemistry at the site.
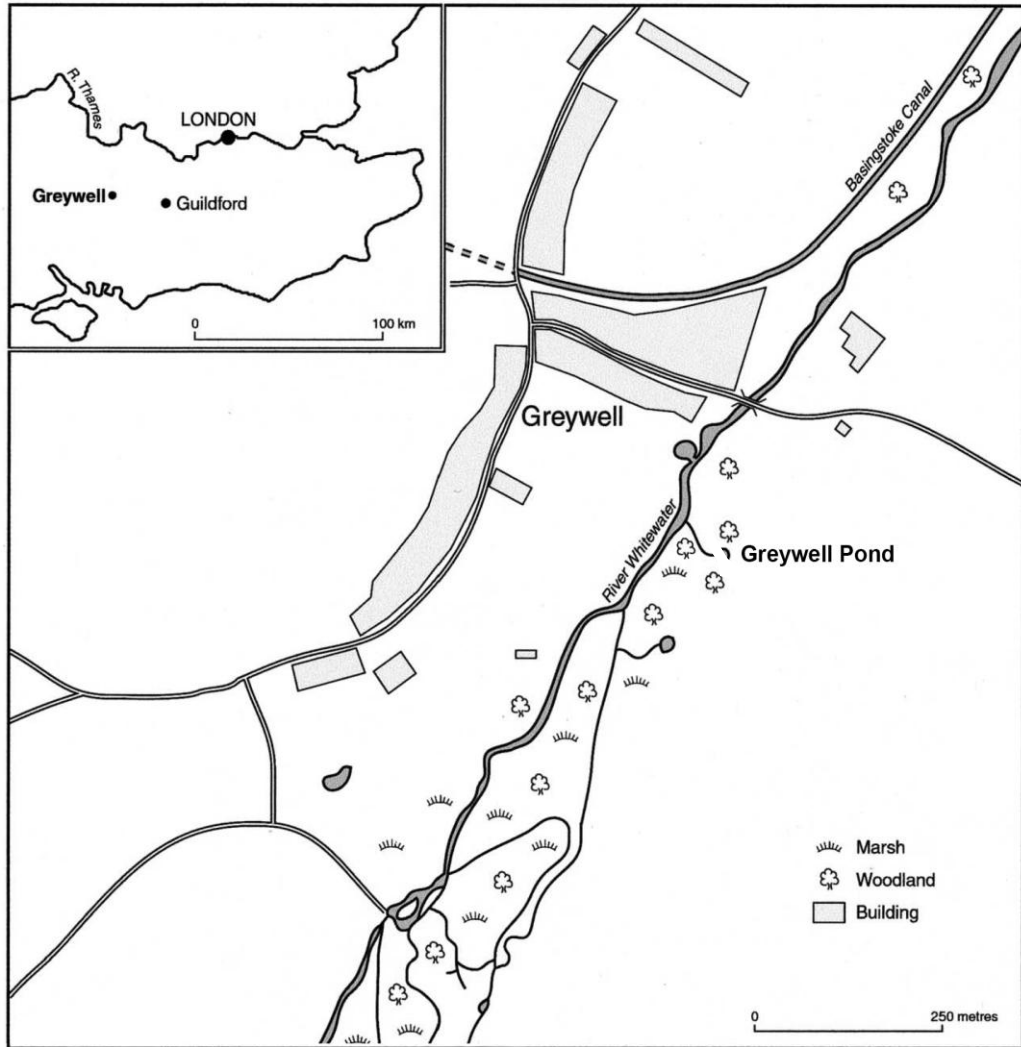
Figure 4-5: Greywell Pond (latitude 51.25°N longitude – 0.96°W). Image modified from Keatings *et al.* (2002).

Records of average monthly temperature and precipitation between 1981-2010 were obtained from the Met office database for Odiham meteorological station (latitude 51.24°N longitude – 0.94°W; 118m above mean sea level), which is the closest meteorological station to the reserve located 1.8 miles south-east of Greywell. Mean monthly air temperature varied seasonally, with maximum values reported in July (21.9°C) and minimum values in February (1.3°C) (Figure 4-6). Precipitation is generally evenly distributed throughout the year, with the highest monthly average in October (87.2mm) and lowest in June (48.5mm) (Figure 4-6).
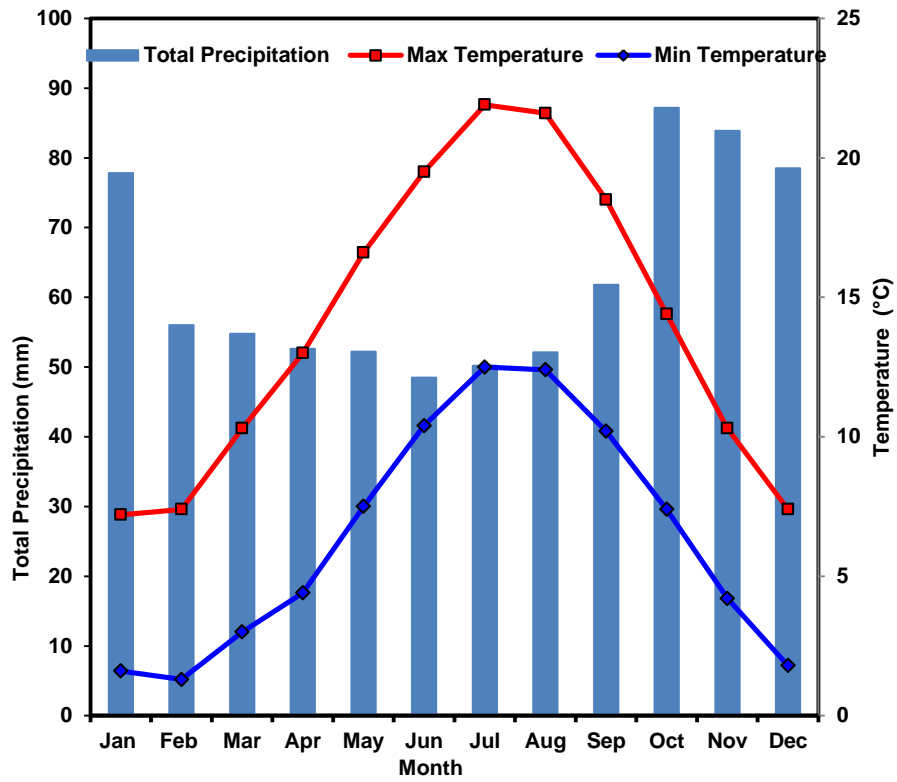
Figure 4-6: Mean minimum and maximum monthly temperature and total monthly precipitation for Odiham (nearest station to Greywell) between 1981 and 2010 (Met Office).

4.3.2 Sampling

Water samples- Water samples were collected at elbow depth from the centre of the pond (deepest part) in polyethylene bottles at monthly intervals. On return to the laboratory the water samples were filtered using disposable cellulose acetate filters (0.2µm pore size) and stored at 4°C, in 5ml screw top glass vials with no head space, prior to stable isotope analysis at the University of Liverpool (see Section 4.2.2).

Water Chemistry- Camlab Handylab 1 battery powered hand-held meters attached to a data logger were used to measure electrical conductivity (μScm^{-1}), dissolved oxygen concentration (mgL^{-1}) and pH of the pond water. The meters were calibrated before use in accordance with manufacturer's procedures. Repeated measurements (x3) were taken from three roughly equidistant locations along a transect bisecting the pond, with average values presented in this thesis.

Water temperature was measured hourly between December 2011 and May 2013, with a Tinytag Aquatic 2 (TG-4100) data logger (accuracy ±0.2°C for measurements between 0°C and 70°C). The logger was first installed into the pond in September 2011, however it failed to record any data until December 2011 due to a programming malfunction.

Chironomid Larvae- Chironomid larvae were isolated from surface sediments washed through a metal sieve (mesh size 1mm) *in situ*, using fine-tipped forceps. The larvae were retained in ambient lake water, before being frozen whole on return to the laboratory. No attempts were made to differentiate species or instar stage due to low sample abundance, although the coarse sieve size is likely to have resulted in the preferential retention of larger 3rd and 4th instars, since the smaller 1st and 2nd instars will have passed through the mesh.

Following defrosting, head capsules were manually isolated from larval bodies (Section 4.2.2) before undergoing chemical pretreatment (see Section 3.6 for purification procedure) and $\delta^{18}O$ analysis (Section 2.3).

4.3.3 Results & discussion

Water chemistry

Mean, minimum and maximum values for water chemistry (May 2011-2013) and temperature (December 2011-May 2013) are presented in Table 4-4, alongside data collected by Keatings *et al.* (2002).

Table 4-4: Mean, minimum and maximum values for monthly water chemistry (May 2011-2013) and average monthly water temperature (December 2011- May 2013) from Greywell Pond. Data presented alongside measurements made by Keatings *et al.* (2002).

	May 2011- 2013 (This study)			March 1997- Feb 1998 (Keatings *et al.,* 2002)		
	Mean	Min	Max	Mean	Min	Max
pH	7.0	6.7	7.3	6.87	6.75	6.97
Dissolved Oxygen (mgL^{-1})	5.8	3.2	8.0	N/A	N/A	N/A
Conductivity (µScm^{-1})	627	577	660	506	498	514
Temperature (°C)	10.4	10.0	10.6	11.0	10.2	12.3

Pond water chemistry and temperature remained essentially constant over the duration of the study (Table 4-4 and Figure 4-7). In particular, average monthly water temperature only exhibited small variations over the monitoring period, ranging from 10 to 10.6°C. The results from this investigation are consistent with the findings of Keatings *et al.* (2002) (Table 4-4), with discrepancies between the studies potentially arising due to differences in equipment and methodologies adopted.

117
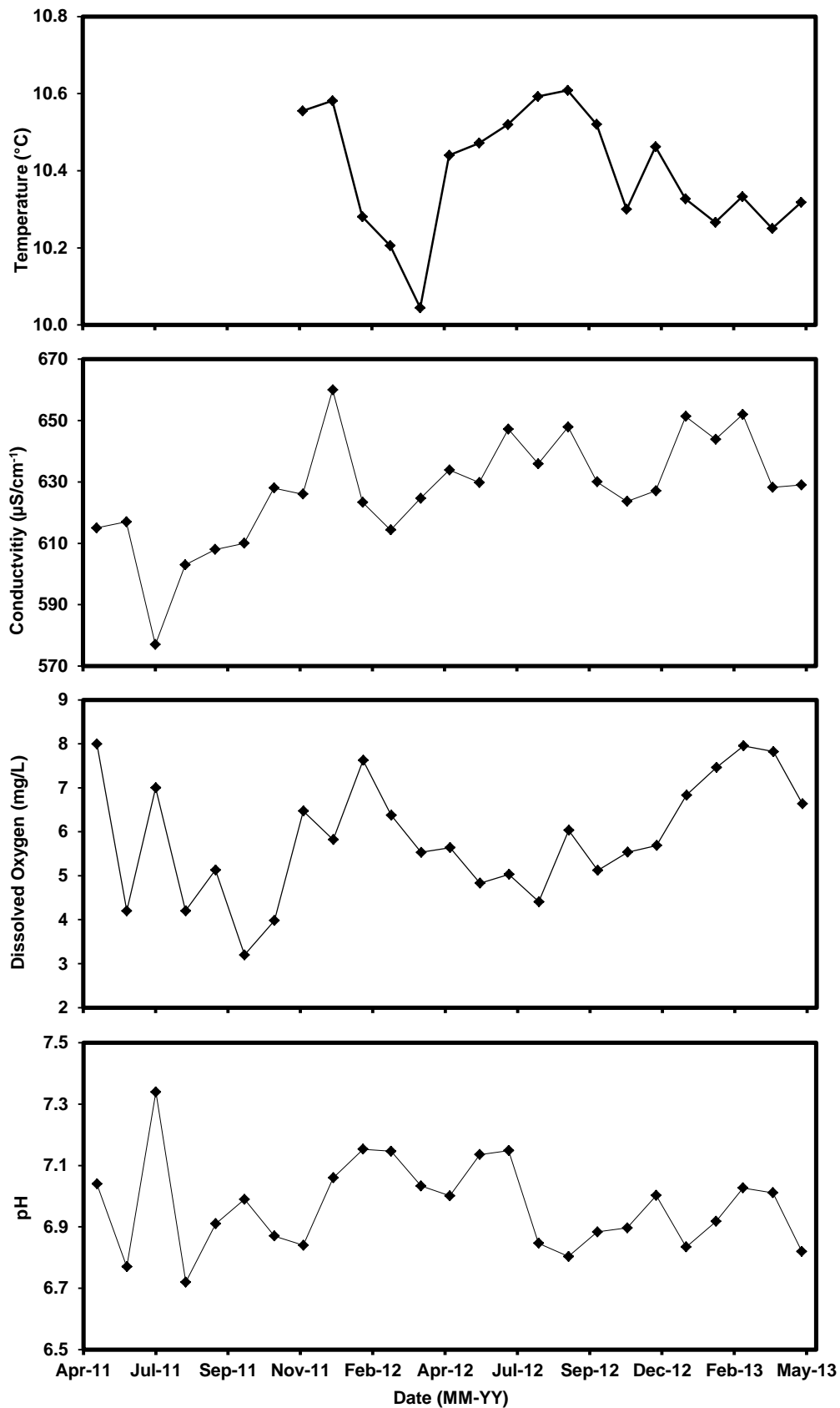
Figure 4-7: Evolution of mean monthly pH, conductivity, dissolved oxygen and temperature from Greywell Pond. Each of the variables remain largely stable throughout the sample period supporting the findings of Keatings *et al.* (2002).

118

$\delta^{18}O_{lakewater}$

Stable isotope analyses were performed on water samples collected from Greywell Pond at roughly monthly intervals between May 2011 and April 2013, with values ranging between −7.2 to −6.9‰. Average $\delta^{18}O_{lakewater}$ measurements (−7.1‰ ± 0.1) are largely indistinguishable from the values reported in Keatings *et al.* (2002). The values are also consistent with non-evaporated meteoric waters from this part of England (Darling *et al.,* 1996), with monthly $\delta^{18}O_{lakewater}$ plotting on or close to the GMWL (Figure 4-8). The stability of $\delta^{18}O_{lakewater}$ is principally due to the short residence time of water (~100 minutes) at Greywell Pond (Keatings *et al.,* 2002).
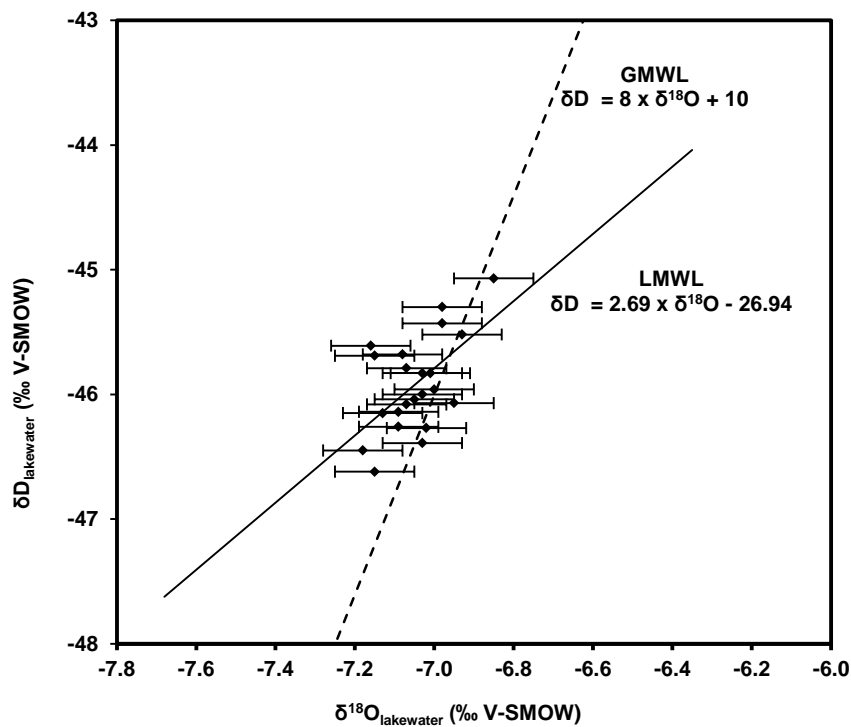
Figure 4-8: Relationship between $\delta^{18}O$ and δD of pond water between May 2011- April 2013. Error bars represent internal precision (±0.1‰) of $\delta^{18}O_{lakewater}$ determinations. Dashed line represents GMWL and solid line represents the LMWL on to which the data from the site plots.

Negligible seasonal variations in $\delta^{18}O_{lakewater}$ were observed at the site throughout the sampling period (see Figure 4-9)
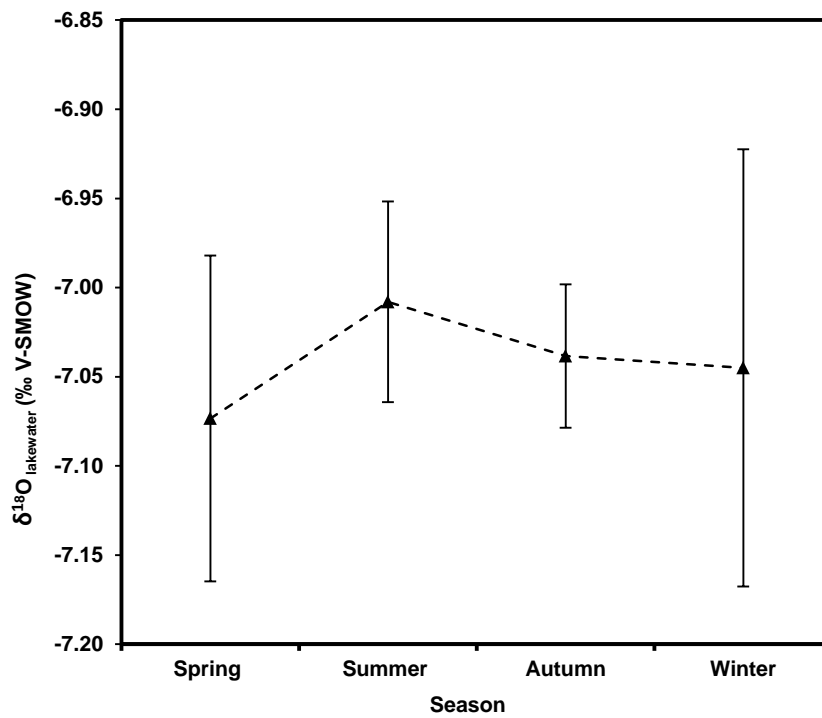
Figure 4-9: The evolution of $\delta^{18}O_{lakewater}$ during spring (March, April, May), summer (June, July, August), autumn (September, October, November) and winter (December, January and February) throughout the monitoring period. Error bars represent 1σ of seasonal variability observed $\delta^{18}O_{lakewater}$ measurements.

δ^{18}*O*$_{chironomid}$

Oxygen isotope analyses were performed on a total of nine purified chironomid samples (see Section 3.6 for purification procedure) collected from Greywell Pond between July 2011 and April 2013. Replicates for each sample were prepared for analysis, however at the time of writing these had not been analysed due to laboratory difficulties at Durham University. Since replicate $δ^{18}O_{chironomid}$ analyses were not available, an estimate of analytical uncertainty was based on repeated analyses of IAEA 601 ($1σ = ± 0.40‰$) (see Section 2.3.1) as its accepted value is closest to the measured $δ^{18}O_{chironomid}$ values.

The oxygen isotope composition of purified chironomid head capsules varied throughout the duration of the monitoring period, ranging between +16.1-18.2‰ ($α^{18}O_{chironomid-lakewater}$ = 1.023-1.025) (Figure 4-10a). The most striking feature of the seasonal evolution of the $δ^{18}O_{chironomid}$ signal is the negative isotope shift of ~ −1.6‰ between spring and summer (Figure 4-10b).
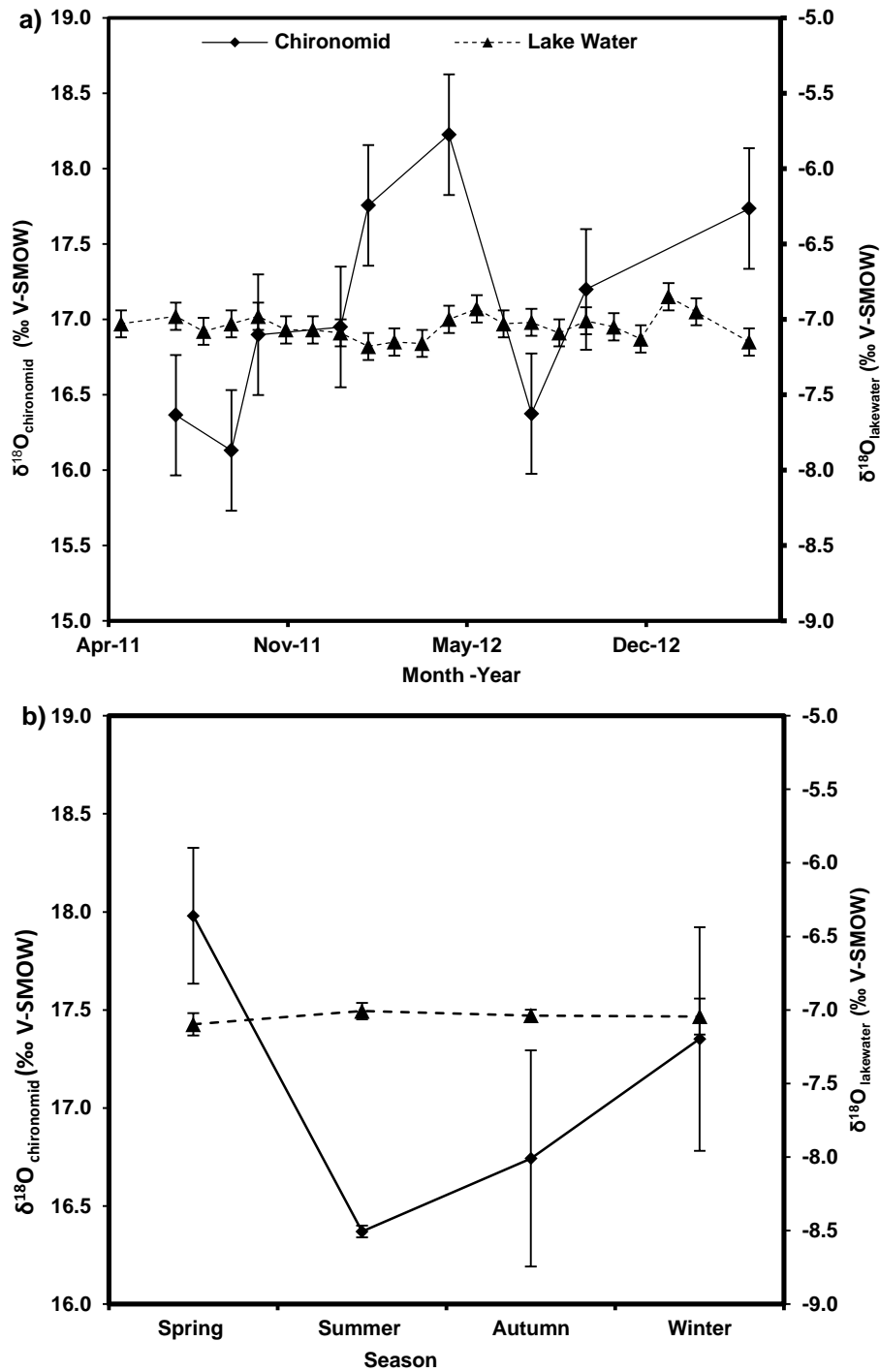
Figure 4-10: a) Monthly and b) seasonal evolution of $\delta^{18}O_{chironomid}$ and $\delta^{18}O_{lakewater}$ over the monitoring period; spring (March, April, May), summer (June, July, August), autumn (September, October, November) and winter (December, January and February). The most striking feature of the seasonal evolution of $\delta^{18}O_{chironomid}$ signal is the negative isotope shift (~ −1.6‰) observed between spring and summer.

No significant correlation was observed between $\delta^{18}O_{chironomid}$ and $\delta^{18}O_{lakewater}$, average monthly air temperature, average monthly water temperature, monthly pH, monthly electrical conductivity or monthly dissolved oxygen concentration (Table 4-5).

Table 4-5: Correlation between $\delta^{18}O_{chironomid}$ and monthly $\delta^{18}O_{lakewater}$, average monthly air temperature, average monthly water temperature, pH, electrical conductivity, and dissolved oxygen concentration.

	R	r^2	p	n
$\delta^{18}O_{lakewater}$	−0.44	0.20	> 0.05	9
Air Temperature	−0.59	0.34	> 0.05	9
Water Temperature	−0.72	0.52	> 0.05	6
pH	0.05	0.00	> 0.05	9
Electrical Conductivity	0.40	0.16	> 0.05	9
Dissolved Oxygen Concentration	0.15	0.02	> 0.05	9

Wang *et al.* (2009) demonstrated that ~70% of oxygen atoms in chironomid biomass (whole larvae) are derived from habitat water under controlled laboratory conditions. The origin of the remaining ~30% is unclear, but is likely to be mainly comprised of ingested food (Wang *et al.,* 2009). Similarly, Nielsen & Bowen (2010) reported that ~10-30% of oxygen in the chitinous remains of *Artemia franciscana* is derived directly from diet. Since $\delta^{18}O_{lakewater}$, temperature and water chemistry at the site remained essentially constant; the observed variability in $\delta^{18}O_{chironomid}$ may reflect seasonal changes in the isotopic composition of diet ($\delta^{18}O_{diet}$). Based on the proportional contributions (~10-30%), changes in $\delta^{18}O_{diet}$ in the order of ~4-16‰ would have been necessary to facilitate the observed seasonal

variability in $\delta^{18}O_{chironomid}$ (Figure 4-10b). The influence of diet on $\delta^{18}O_{chironomid}$ cannot be quantitatively assessed in this investigation; however a conceptual framework examining the feasibility of the required magnitude of change in $\delta^{18}O_{diet}$ will now be constructed.

Chironomid larvae are typically omnivores, deriving nourishment from a combination of phytoplankton, zooplankton and sedimented detrital material (including associated microorganisms) (Armitage *et al.,* 1995; Epler 2001; Oliver 1971; Walker 1987). The relative abundance of these components varies seasonally in most lakes. Phytoplankton and zooplankton are likely to make up a significant proportion of larval diets during the spring and summer months. In contrast, during the autumn and winter, larval diets are anticipated to be primarily composed of organic detritus and associated microorganisms. Typically the organic detritus in most lakes is composed of particles that have formed within the water column (Jones & Grey 2004) and therefore should be isotopically reflective of lake water. However, at Greywell Pond terrestrial leaf litter shed by deciduous trees (mainly *Corylus*) surrounding the pond is likely to have formed a significant proportion of the available organic detritus.

The isotopic composition of terrestrial plants are typically ^{18}O enriched in comparison to aquatic plants, as a result of enhanced evapotranspiration (kinetic isotope fractionation) (Sauer *et al.,* 2001; Sensuła *et al.,* 2006). The magnitude of the typical offset between terrestrial and aquatic plants described in Sensuła *et al.* (2006) is consistent with the $\delta^{18}O_{diet}$ offset necessary to facilitate the observed variability in $\delta^{18}O_{chironomid}$ at Greywell Pond (Table 4-6).

Table 4-6: Average δ^{18}O of plants collected within the same ecosystem from Sensuła *et al.* (2006). Terrestrial plants are on average 4‰ heavier than aquatic plants.

δ^{18}O (‰ V-SMOW)

Terrestrial plants	28.98
Semi-submerged plants	26.81
Submerged plants	24.62

In temperate regions chironomid populations typically pass through two generations per year (bivoltine), with the main emergences occurring in the spring and late summer/early autumn (Tokeshi 1995). The development rate of *Chironomus riparius* larvae under controlled laboratory conditions at 10°C, the average monthly water temperature at Greywell Pond, was ~4 months (see Table 4-2). If a similar development time is assumed for the chironomid larvae at Greywell Pond, adults emerging in the late summer/ early autumn are likely to have completed the majority of their life cycle during the spring/ early summer. In contrast, adults emerging in the spring will have completed the majority of their life cycle during the previous autumn, overwintering as 3rd/4th instars.

Growth and development can be temporarily arrested or slowed during unfavourable conditions, in a process known as diapause. This survival strategy is commonly adopted in poikilotherms (an organisms who's internal body temperature varies) such as Chironomidae (Armitage *et al.,* 1995; Brooks *et al.,* 1997; Hahn & Denlinger 2011). The initiation and termination of diapause can be triggered by changes in a number of different environmental stimuli (e.g. temperature, photoperiod, dissolved oxygen concentration, food abundance and/or quality) (Armitage *et al.,* 1995). Diapause offers a survival advantage, permitting the synchronisation of life cycles with periods suitable for growth, development and reproduction (Hahn & Denlinger 2011). Insects generally adopt two main strategies in mitigating the energetic costs associated with diapause: a) they accumulate micronutrient reserves (e.g.

carbohydrate, protein and lipid) prior to the onset of diapause and b) they limit metabolic activity during diapause (Nation 2008; Pinder 1986). Feeding, and even restricted growth, may still occur during diapause in some insects along with the synthesis of amino acids required to support anabolic activities, catabolic respiratory metabolism and postdiapause development (Godlewski *et al.,* 2001; Hahn & Derlinger 2011; Sonoda *et al.,* 2007). Following the termination of diapause, larval development re-commences with the metabolism of the remaining polysaccharide reserves, e.g. trehalose and glycogen, accumulated prior to and during diapause.

Given the envisaged seasonal change in $\delta^{18}O_{diet}$ at Greywell Pond, polysaccharides synthesised during the autumn and winter will differ isotopically from those synthesised during the spring or summer. This may potentially explain the observed variability in $\delta^{18}O_{chironomid}$ signals. The increase in average seasonal $\delta^{18}O_{chironomid}$ from summer to winter (Figure 4-10b) may indicate a gradual proportional change in the relative contribution of terrestrial and aquatic components in the chironomid larvae diet. The hypothesis outlined above could not be experimentally verified in this investigation. The implications of the findings in terms of palaeoclimate reconstructions are discussed in greater detail in Section 4.5.

An alternative argument is that the observed variability in $\delta^{18}O_{chironomid}$ may be related to vital effects. Seasonal variability in $\delta^{13}C$ and $\delta^{15}N$ signals from chironomid larvae has been attributed to vital effects in previous studies (e.g. Grey *et al.,* 2004). However, since chironomid species were not identified in this investigation, this hypothesis could not be explored.

4.4 An investigation of $\delta^{18}O_{chironomid}$ in a series of lakes from the Attenborough Nature Reserve

4.4.1 Site description

The Attenborough Nature Reserve (~170ha) (latitude 52.53°N longitude -1.24°W) is located within the catchment of the River Trent, 7km southwest of the city of Nottingham (East Midlands, UK) (Figure 4-11). The reserve, a designated Site of Special Scientific Interest (SSSI), contains a series of semi-connected, shallow (maximum depth 5.2m) former gravel pits that have been allowed to fill naturally following the termination of gravel extraction (Sayer & Roberts 2001). Drier areas of scrub and grassland as well as native woodland separate the lakes. Four of the lakes within the reserve were chosen for monthly monitoring between June 2011 and May 2013: Main Pond (extracted 1939-1960), Church Pond (extracted 1962-1965), Clifton Pond (extracted 1964-1968) and Beeston Pond (extracted 1941-1951). A summary of the basic physical characteristics of each lake is provided in Table 4-7.

Table 4-7: Summary of physical lake characteristics (modified from Jones *et al., in prep*).

Pond	Area (ha)	Max Depth (m)	Inflow	Outflow
Main	24	5.0	Yes	Yes
Beeston	0.9	2.7	Yes	Yes
Church	9.6	5.2	No	No
Clifton	18.6	3.3	No	No
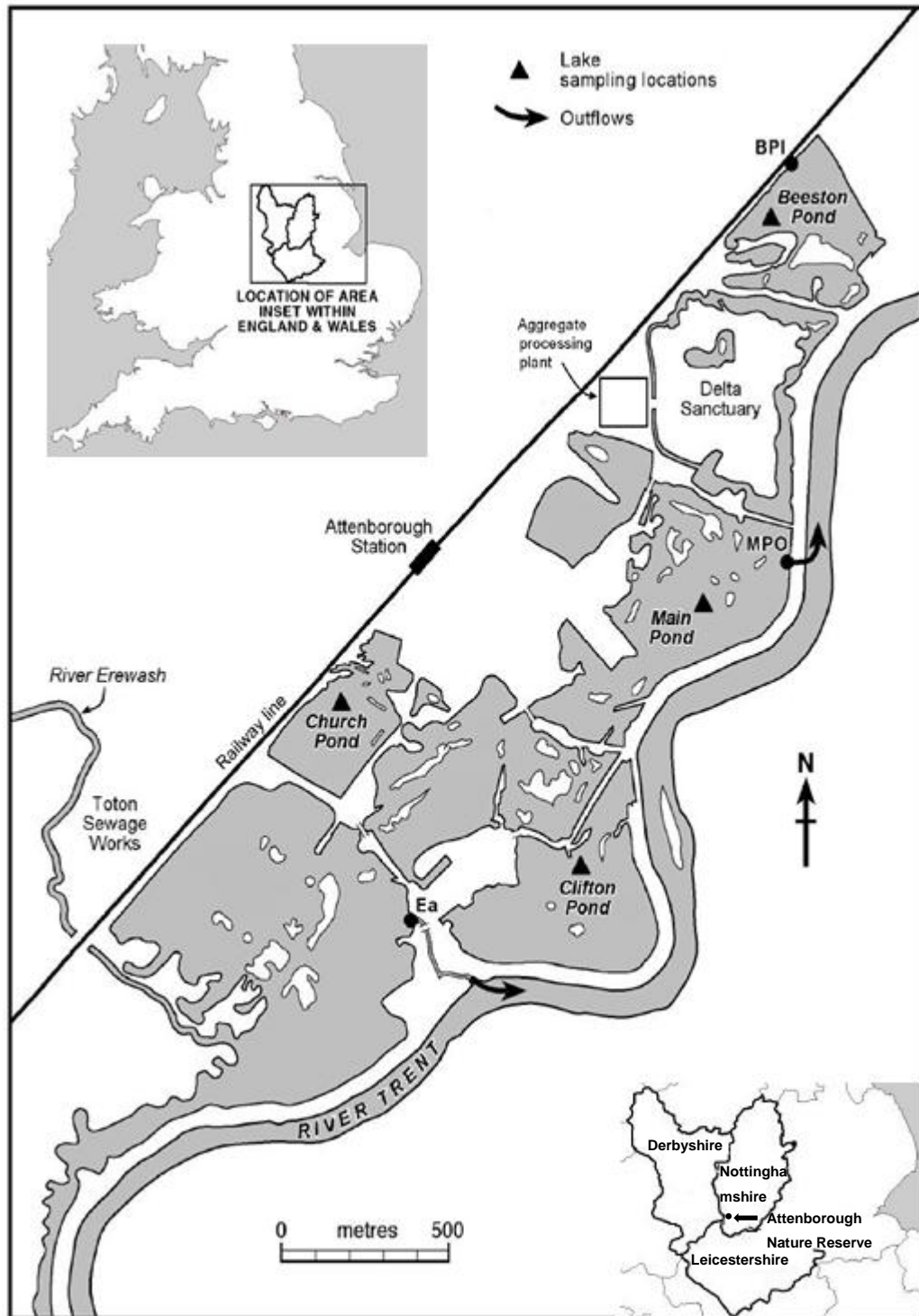
Figure 4-11: Attenborough Nature Reserve (latitude 52.53°N longitude −1.24°W), Nottingham, UK. The reserve is close to the confluence of the River Trent and River Erewash. Marked on the map (black triangle) are the approximate sampling locations in each of the monitored lakes (map modified from Cross 2009).

Main and Beeston ponds are both hydrologically open systems, with surface inflows and outflows. Main Pond can essentially be considered as a wide section of river, with water from the River Erewash flowing through it before entering the River Trent (Jones *et al., in prep*). In contrast Church and Clifton ponds are both isolated from the main lake chain, as well as one another, with no surface inflows or outflows. The lakes provide a perfect opportunity to assess the relationship between $\delta^{18}O_{chironomid}$ and $\delta^{18}O_{lakewater}$ in hydrologically different natural settings subjected to essentially the same climatic, geographical and geological conditions.

Meteorological data for the monitoring period was obtained from an automated weather station at the University of Nottingham's Sutton Bonnington Campus (*pers. comm. Matt Jones*), which is approximately ~11 miles south of the nature reserve. Mean monthly air temperatures varied seasonally, with maximum (16.8°C) and minimum (2.3°C) mean values recorded in the summer and early spring respectively.

Monthly total rainfall ranged from 8 to 112mm over the sampling period. The seasonal distribution of precipitation was fairly even, with the highest total amount of precipitation observed during summer months (356mm), while the lowest amount of precipitation was recorded during spring (291mm). Both total monthly precipitation and mean monthly temperature compared well with average meteorological data from the East Midlands (1981-2010) (Figure 4-12).
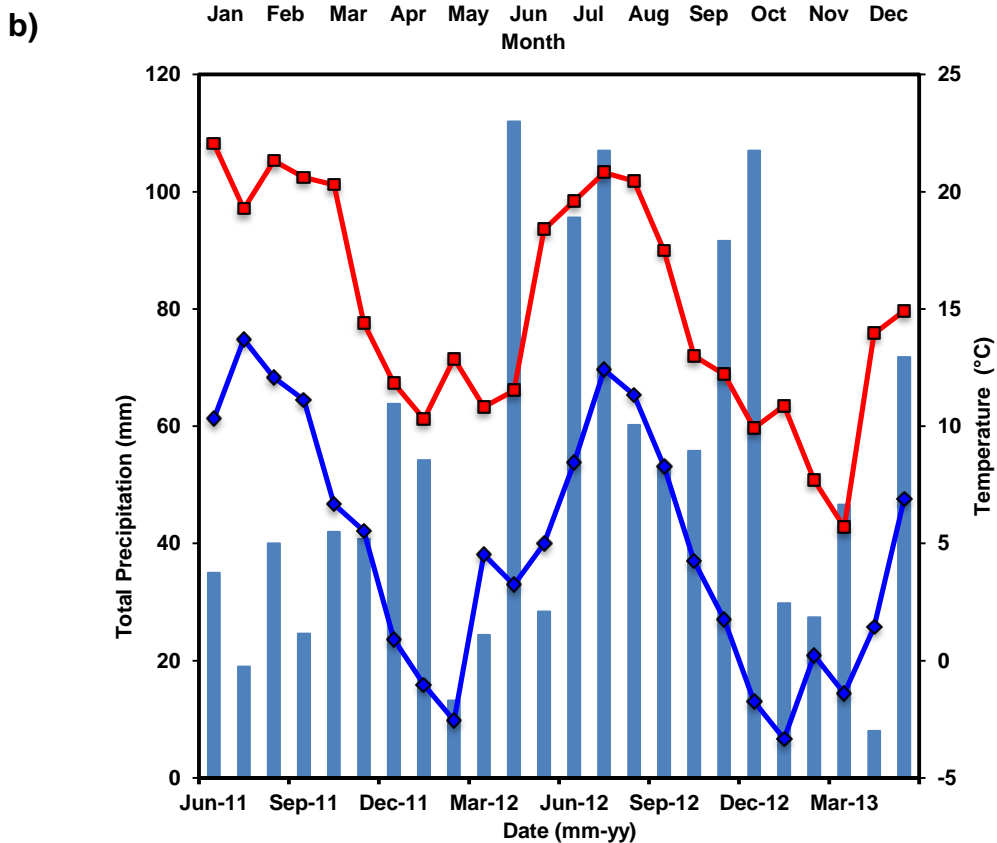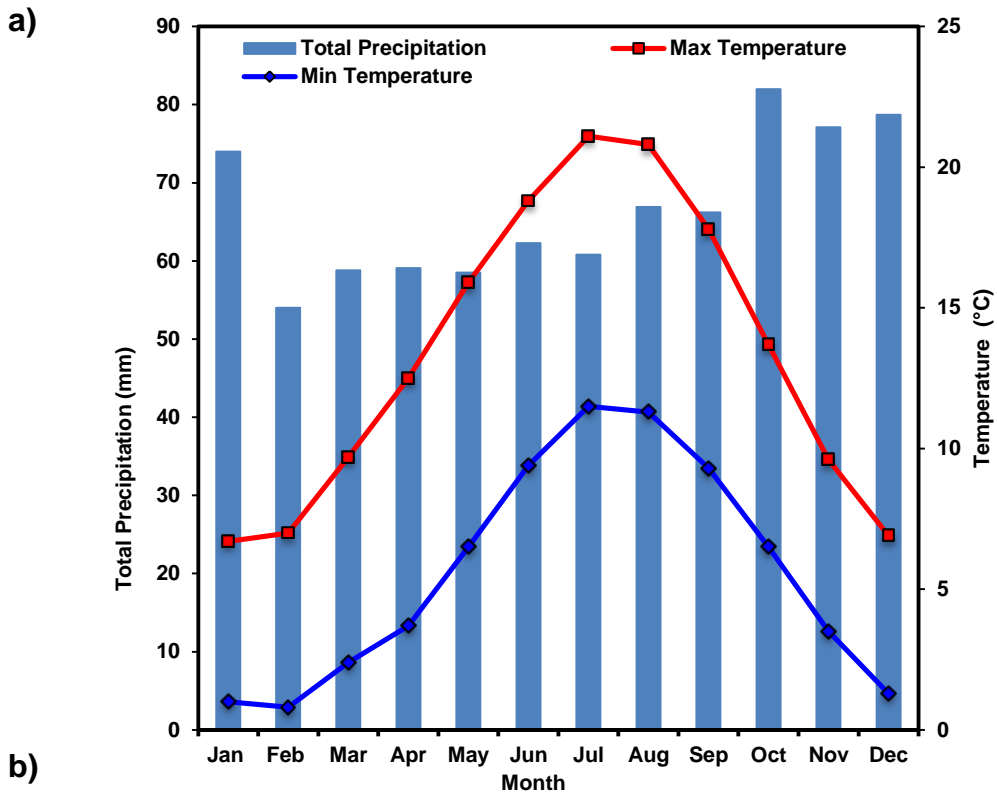
Figure 4-12: a) Minimum and maximum monthly temperature and average monthly precipitation for the East Midlands between 1981 and 2010 (Met Office data). b) Minimum and maximum monthly temperature and total monthly precipitation between July 2011 to May 2013 from University of Nottingham Sutton Bonnington Campus, which is approximately ~11 miles south of the nature reserve (*pers. comm. Matt Jones*).

4.4.2 Sampling

Sampling at the Attenborough Nature Reserve was undertaken in collaboration with Dr. Suzanne McGowan (University of Nottingham). Samples were collected from a fixed point marked by an anchored buoy (Figure 4-11), which was roughly located in the deepest part of each lake.

Water samples- see Section 4.3.2.

Water Chemistry- A YSI 600QS-O-M multi-probe attached to a 650MDS data logger was used to measure vertical profiles for conductivity ($mScc^{-1}$), temperature (°C), dissolved oxygen concentration (mgL^{-1}) and pH of the water column at 50cm intervals. Average values for each of the measured variables are presented in this thesis. The meter was calibrated before use in accordance with manufacturer's procedures

Chironomid Larvae- Sediment samples (two buckets full) were collected using an Ekman grab from each pond. On return to the laboratory the sediments were washed through a 1mm mesh and live chironomid larvae were isolated using fine tipped forceps. The larvae were frozen whole. No attempts were made to differentiate species or instar stage due to low sample abundance, although the coarse sieve size is likely to have resulted in the preferential retention of larger 3rd and 4th instars, since the smaller 1st and 2nd instars will have passed through the mesh.

Following defrosting, head capsules were manually isolated from larval bodies (Section 4.2.2) before undergoing chemical pretreatment (Section 3.6) and $\delta^{18}O$ analysis (Section 2.3).

4.4.3 Results & Discussion

Water temperature

Minimum, maximum and mean monthly lake water temperatures from each lake throughout the sampling period (May 2011- June 2013) are presented in Table 4-8.

Table 4-8: Mean, minimum and maximum water temperature from each lake during the monitoring period.

	Water Temperature (°C)		
Pond	**Mean**	**Minimum**	**Maximum**
Main	10.7 ± 5.9	3.5	20.5
Beeston	11.0 ± 6.0	3.2	20.5
Church	10.5 ± 6.1	2.7	21.8
Clifton	10.7 ± 6.2	3.0	21.0

The main features of water temperature are virtually identical in each of the studied lakes, with maximum temperatures recorded during the summer months and minimum values recorded in the winter (Figure 4-13).
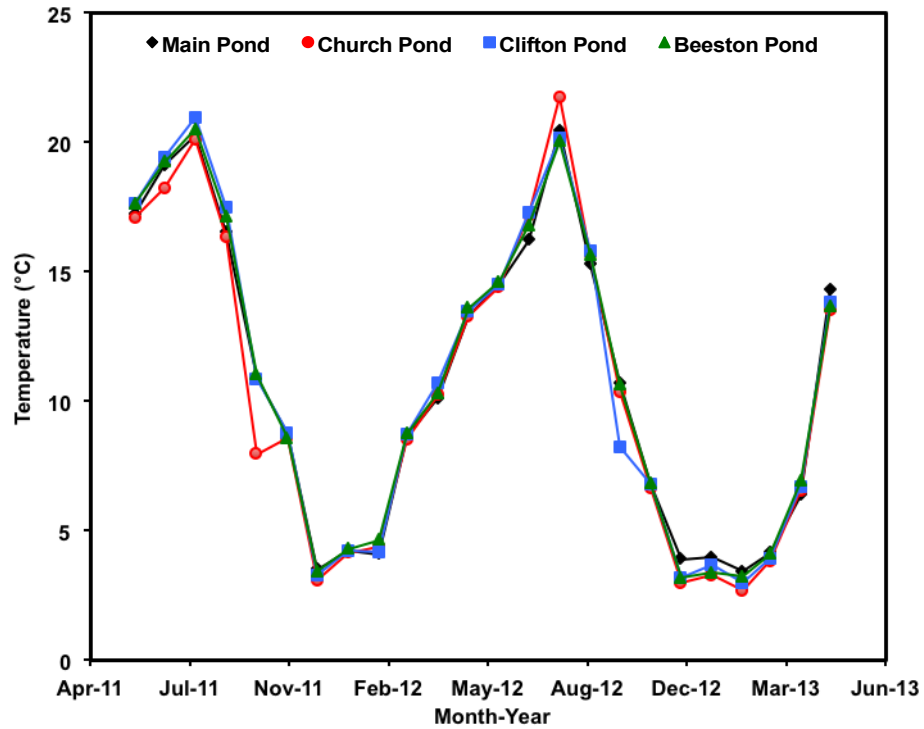
Figure 4-13: Monthly average lake water temperature from each of the monitored ponds over the sampling period.

During the monitoring period water temperature was largely homogenous throughout the water column (Figure 4-14). Some thermal stratification was apparent in all of the lakes during the summer/autumn months probably as a result of the difference in temperature between the colder ground water inflow and the warmer water column.
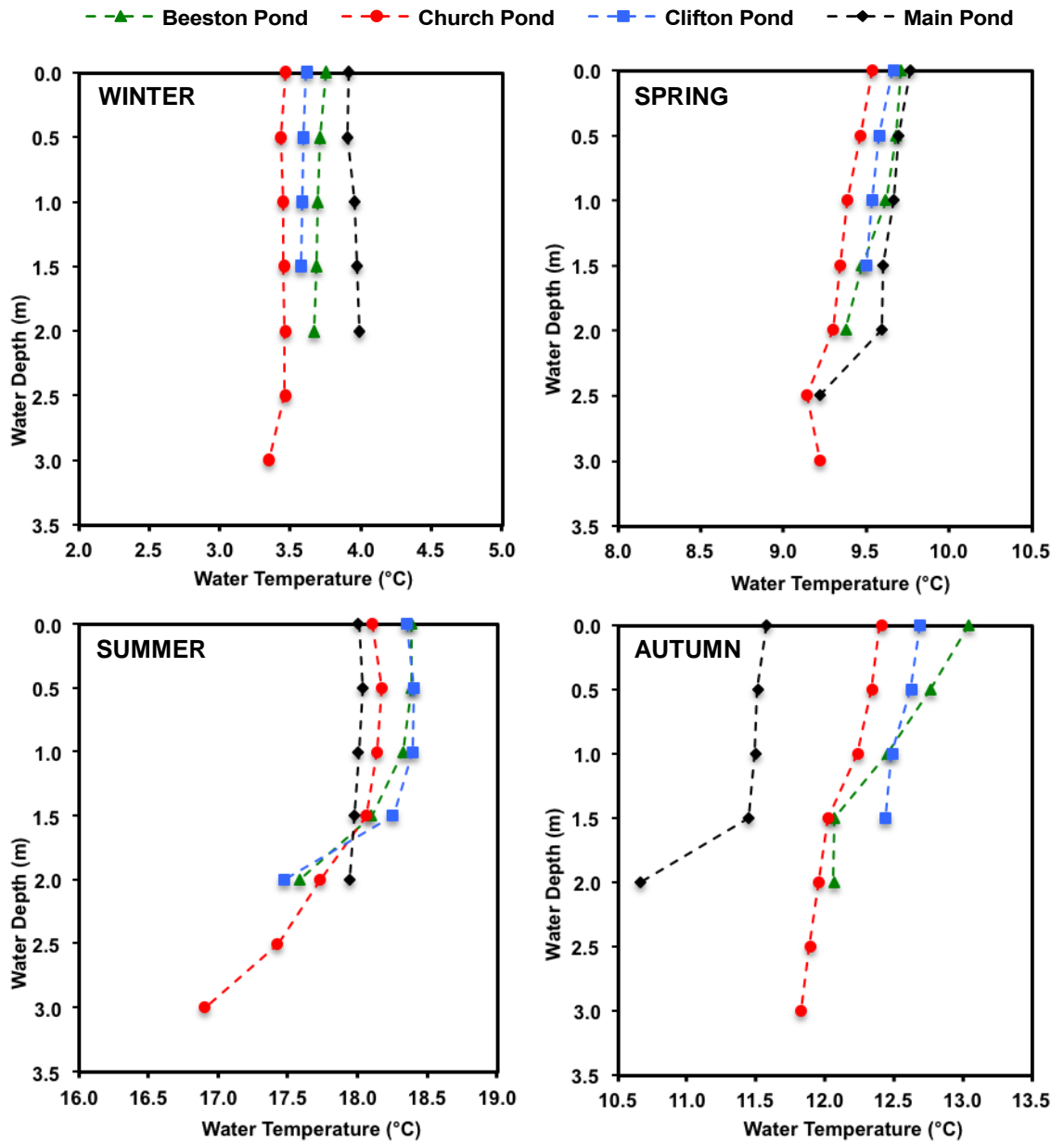
Figure 4-14: Average seasonal temperature profiles for each lake. A degree of thermal stratification can be observed during the summer and autumn months probably related to poor mixing and the cooling influence of ground waters.

Water chemistry

Mean monthly conductivity, dissolved oxygen concentration and pH from each lake throughout the sampling period (May 2011- June 2013) are presented in Table 4-9. The measured parameters in each of the lakes are largely comparable with each other and all showed seasonal variations. The causes for the variations in conductivity, dissolved oxygen concentration and pH are beyond the scope of this study but are likely to be related to changes in local hydrological and/or biological conditions.

Table 4-9: Mean conductivity, dissolved oxygen concentration and pH of lake water at each site from June 2011-May 2013.

Pond	Conductivity $(mScc^{-1})$	Dissolved Oxygen (mgL^{-1})	pH
Main	0.9 ± 0.2	13.1 ± 4.0	8.2 ± 0.6
Beeston	0.6 ± 0.1	12.1 ± 2.0	8.2 ± 0.5
Church	0.5 ± 0.1	12.6 ± 2.1	8.4 ± 0.7
Clifton	0.6 ± 0.0	12.2 ± 2.1	8.4 ± 0.3

Conductivity- Mean monthly conductivity ranged between 0.5 and 1.1 $mScc^{-1}$ across the four lakes during the monitoring period, with the highest value recorded in Main Pond in March 2012 and lowest value recorded in Church Pond in November 2012.

Dissolved oxygen concentration- Mean monthly dissolved oxygen concentration ranged between 5.4 and 19.8 mgL^{-1} across the four lakes during the monitoring period, with the highest value recorded in Main Pond in March 2012 and the lowest value recorded in Church Pond in September 2011.

pH- Mean monthly pH ranged between 7.7 and 10.0 across the four lakes during the monitoring period, with the highest values recorded in Main Pond in July 2011 and lowest values recorded in Main Pond in September 2011.

A summary of mean lake water conductivity, dissolved oxygen concentration and pH from each of the lakes over the duration of the monitoring period is presented in Figure 4-15.
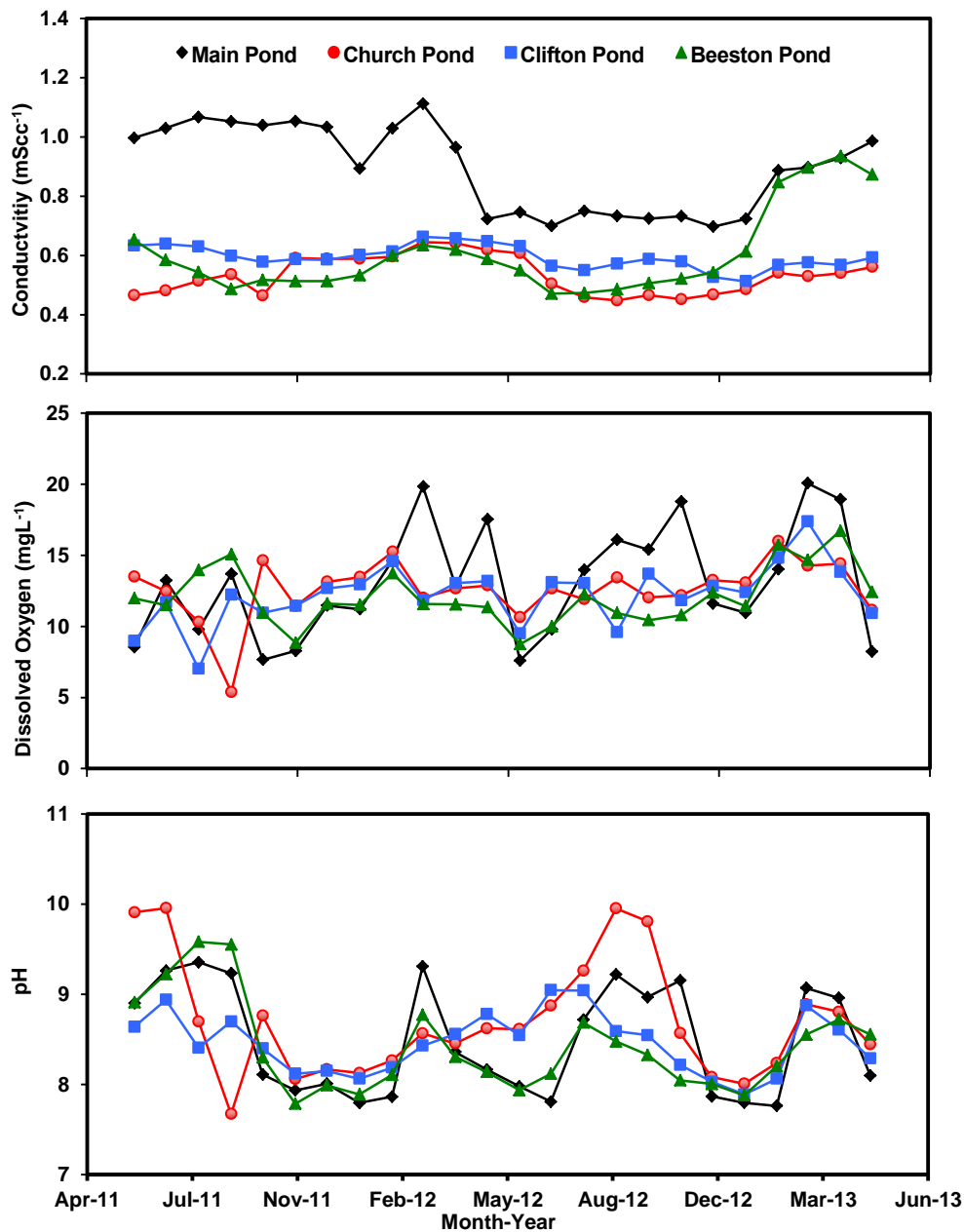
Figure 4-15: Mean monthly lake water conductivity, dissolved oxygen concentration and pH from each of the sampled lakes throughout the duration of the study period.

$\delta^{18}O_{lakewater}$

Stable isotope analyses were performed on surface water samples from each of the lakes on monthly intervals throughout the monitoring period (Table 4-10). Lake water samples collected over the study period yielded $\delta^{18}O$ values ranging from −6.4‰ to +0.1‰, with mean $\delta^{18}O_{lakewater}$ measurements being ~ 4‰ higher in the hydrologically closed lakes (Church and Clifton) than in the open lakes (Main and Beeson) (Table 4-10).

Table 4-10: Summary of mean $\delta^{18}O_{lakewater}$ from each of the sampled sites between June 2011 and May 2013.

<div align="center">

$\delta^{18}O_{lakewater}$ (‰ V-SMOW)

Pond	Mean	Minimum	Maximum
Main	−6.8 ± 1.3	− 9.0	−4.7
Beeston	−6.2 ± 1.5	− 8.9	−4.0
Church	−2.5 ± 2.2	− 6.4	−0.1
Clifton	−2.4 ± 2.3	−6.7	+0.1

</div>

Surface water samples from Main and Beeston ponds plot on, or close to the GMWL, with values becoming more enriched in ^{18}O during periods of greater evaporative enrichment (i.e. during the summer) (Figure 4-16). In contrast, $\delta^{18}O_{lakewater}$ from Church and Clifton ponds generally plot on a LEL, suggesting evaporation had a stronger influence in these lakes probably due to the longer residence times.
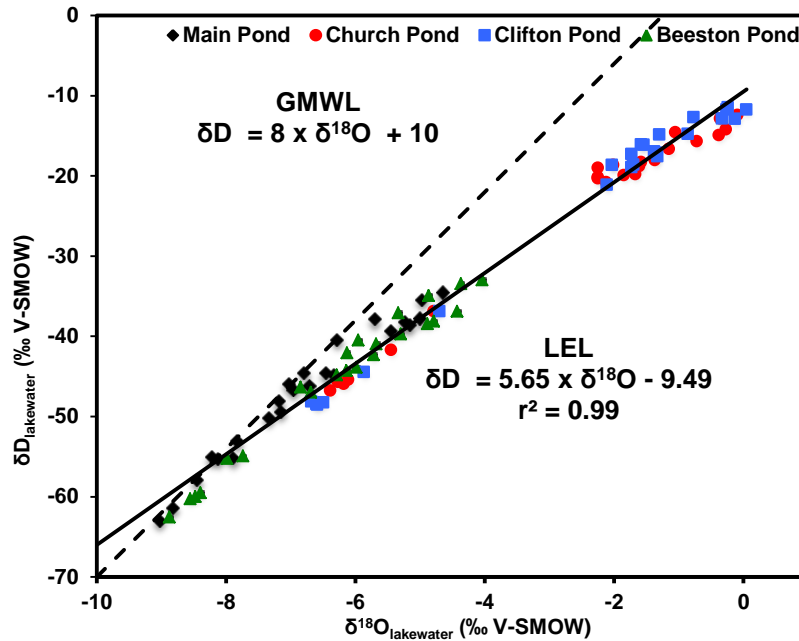
Figure 4-16: Relationship between $\delta^{18}O_{lakewater}$ and $\delta D_{lakewater}$ from each lake throughout the duration of the sampling period. The dashed line represents the GMWL, while the solid line represents the LEL determined from linear regression of all surface water data. The majority of the samples plot below the GMWL, indicating a degree of evaporative enrichment of the heavy isotopes in each lake.

No correlation was observed between monthly $\delta^{18}O_{lakewater}$ and average monthly $\delta^{18}O_{precipitation}$ over the sampling period from Keyworth (Nottinghamshire, UK), the closest available record to the Attenborough Nature Reserve (record provided by British Geological Society *pers. comm.* Melanie Leng) (R= 0.14; r^2 = 0.02; *p* > 0.05; n = 33) prior to the flood event at the site. The offsets between $\delta^{18}O_{lakewater}$ and $\delta^{18}O_{precipitation}$ are likely to have arisen as a consequence of local hydrological conditions at each of the lakes.

The seasonal evolution of $\delta^{18}O_{lakewater}$ (Figure 4-17b) is most likely to reflect the preferential partitioning of water molecules containing light isotopes of hydrogen and oxygen into the vapour phase during evaporation, with the highest values observed in each lake during the summer/early autumn. The influence of the evaporative enrichment is greatest in the closed lakes, with monthly $\delta^{18}O_{lakewater}$ measurements ~ 2.6‰ higher in the summer compared to the winter months; whereas average enrichment of only ~ 1.4‰ is observed between winter and summer $\delta^{18}O_{lakewater}$ measurements in the open lakes (Main and Beeston).
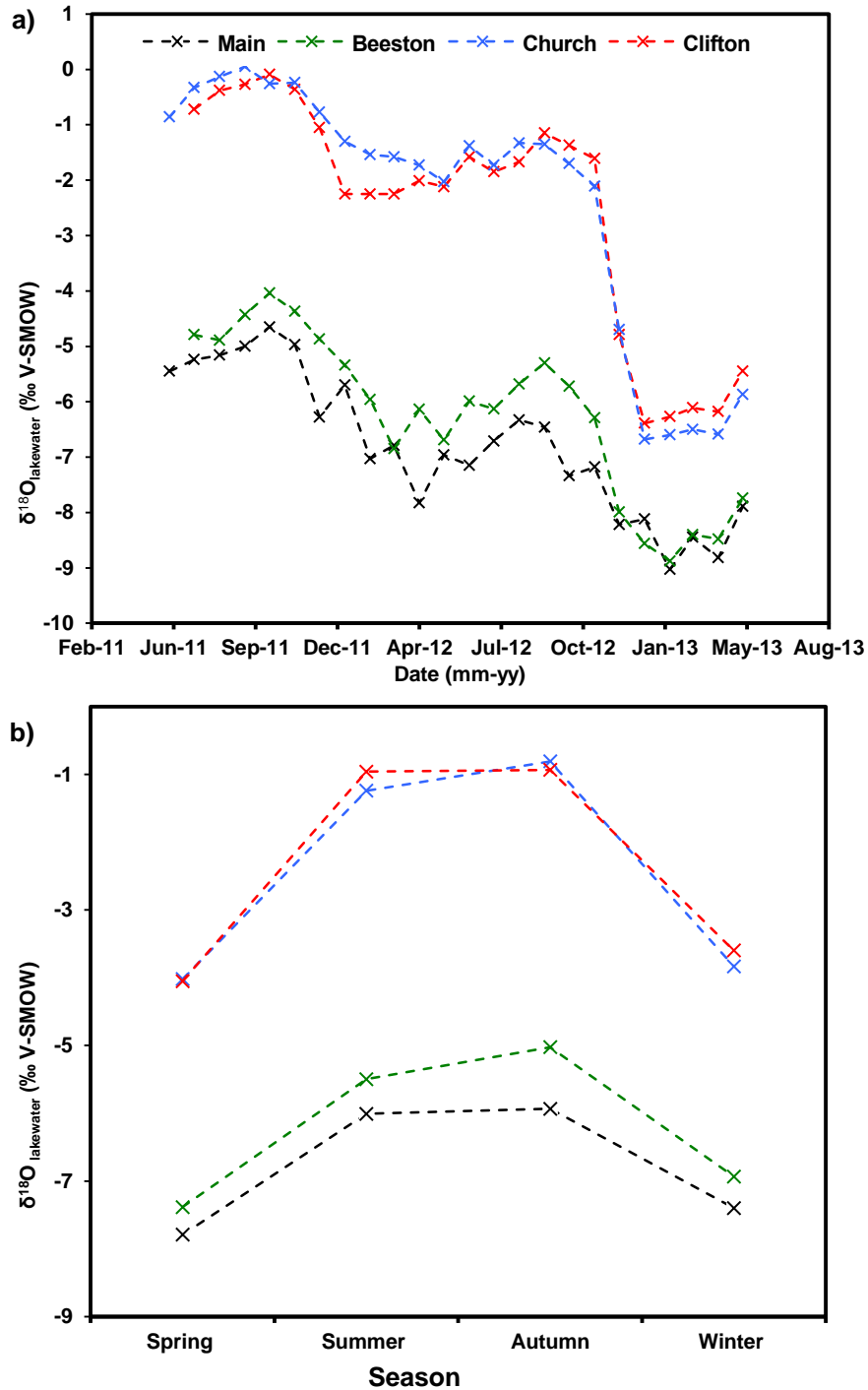
Figure 4-17: a) Evolution of $\delta^{18}O_{lakewater}$ from each lake throughout the duration of the monitoring. b) Average seasonal evolution of $\delta^{18}O_{lakewater}$ from each lake throughout the duration of the monitoring; spring (March, April, May), summer (June, July, August), autumn (September, October, November) and winter (December, January and February).

During periods of high water levels, Church and Clifton ponds are liable to become connected to the main lake chain through a series of overflow pipes and weirs. The substantial negative shift in $\delta^{18}O_{lakewater}$ values observed in all of the sites in the winter of 2012 was associated with a flood event. This flood event was caused by a combination of prolonged intensive precipitation (see Figure 4-12a) and poor maintenance of the system of weirs throughout the lake chain (i.e. weirs became blocked with debris). Interestingly, the isotopic composition of the lake water in the closed lakes (Church and Clifton) failed to fully recover to pre-flood values before the end of the monitoring period, 7 months after the initial flood.

δ^{18}O$_{chironomid}$

Oxygen isotope analyses were performed on purified chironomid head capsules (see Section 3.6 for purification procedure) isolated from larvae on near bi-monthly intervals from each of the studied lakes. Replicates for each sample were prepared for analysis, however at the time of writing these had not been analysed due to laboratory difficulties at Durham University. Since replicate δ^{18}O$_{chironomid}$ analyses were not available, an estimate of analytical uncertainty was based on repeated analyses of IAEA 601 (1σ = ± 0.40‰) (see Section 2.3.1) as its accepted value is closest to the measured δ^{18}O$_{chironomid}$ values.

Spatial and temporal variations were observed in δ^{18}O$_{chironomid}$ measurements throughout the duration of the monitoring period, with values ranging between 13.1 and 20.8‰ (α^{18}O$_{chironomid-H2O}$ = 1.018-1.027) (Table 4-11). The ~ 4‰ disparity between δ^{18}O$_{chironomid}$ from hydrologically open (Main and Beeston) and closed (Church and Clifton) lakes (Table 4-11) is consistent with the offsets observed between δ^{18}O$_{lakewater}$ (Table 4-10).

Table 4-11: Summary of mean, minimum and maximum δ^{18}O$_{chironomid}$ observed at each pond between July 2011- May 2013.

		δ^{18}O$_{chironomid}$ (‰ V-SMOW)		
Pond	**Hydrological Status**	**Mean**	**Minimum**	**Maximum**
Main	**Open**	+14.9 ± 0.9	+13.6	+16.5
Beeston		+15.0 ± 1.0	+13.1	+16.2
Church	**Closed**	+19.0 ±1.1	+16.9	+20.4
Clifton		+19.3 ±1.3	+17.2	+20.8

The evolution of δ^{18}O$_{chironomid}$ and δ^{18}O$_{lakewater}$ throughout the monitoring period is presented in Figure 4-18.
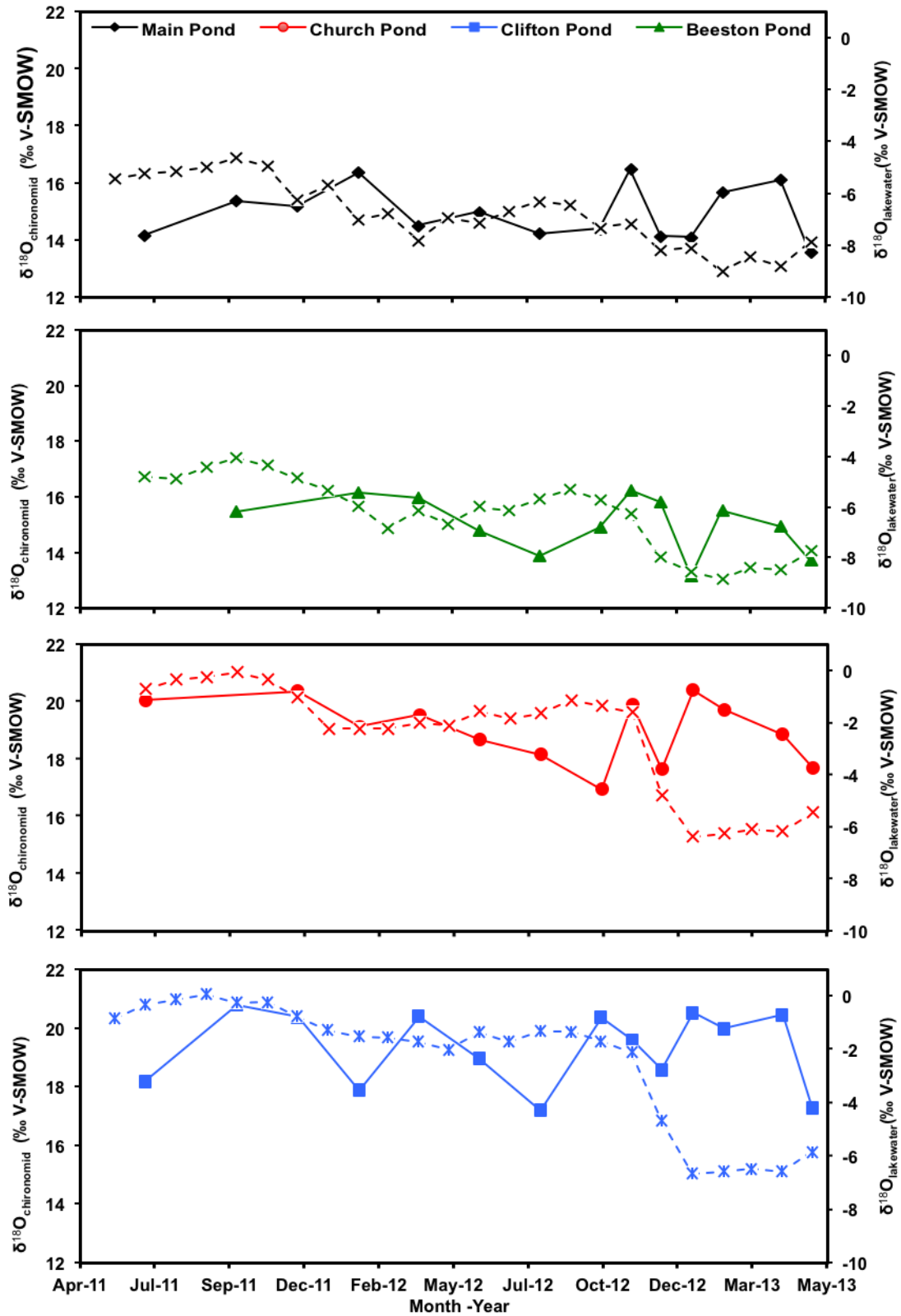
Figure 4-18: Evolution of $\delta^{18}O_{chironomid}$ (solid line) and $\delta^{18}O_{lakewater}$ (dashed line) in each of the lakes between June 2011- May 2013. Note the dramatic decrease in $\delta^{18}O_{lakewater}$ in the hydrologically closed (Church and Clifton) ponds after November 2012 is associated with flooding at the reserve.

142

A moderate linear relationship was observed between $\delta^{18}O_{chironomid}$ and $\delta^{18}O_{lakewater}$ across the lakes monitored in this study (R= 0.65; r^2 = 0.42; *p* < 0.05; n = 53) (Figure 4-19).
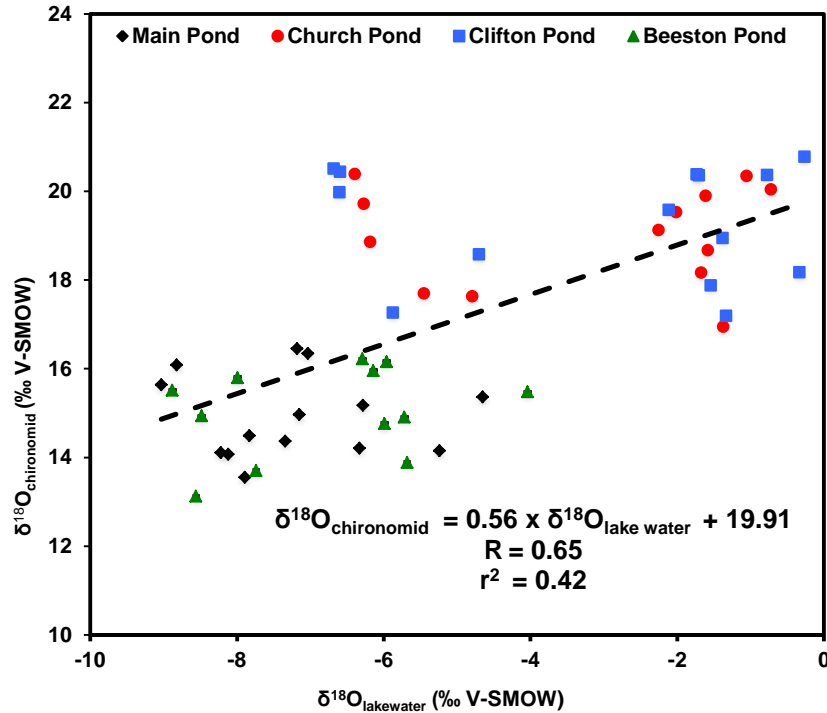
Figure 4-19: Relationship between the measured $\delta^{18}O_{chironomid}$ and measured $\delta^{18}O_{lakewater}$ from July 2011- May 2013. Dashed line represents linear regression between $\delta^{18}O_{chironomid}$ and $\delta^{18}O_{lakewater}$.

The significance of the correlation between $\delta^{18}O_{chironomid}$ and $\delta^{18}O_{lakewater}$ can be improved by removing data following the flood event (R= 0.85; r^2 = 0.73; *p* < 0.05; n = 33) (Figure 4-20). The reassessment of the data excluding measurements after November 2012 reduces the uncertainty of the calibration between $\delta^{18}O_{chironomid}$ and $\delta^{18}O_{lakewater}$ from ±1.8 to ±1.2.

$$\delta^{18}O_{chironomid} = 0.76 \times \delta^{18}O_{lake\ water} + 20.06$$
$$R = 0.85$$
$$r^2 = 0.73$$
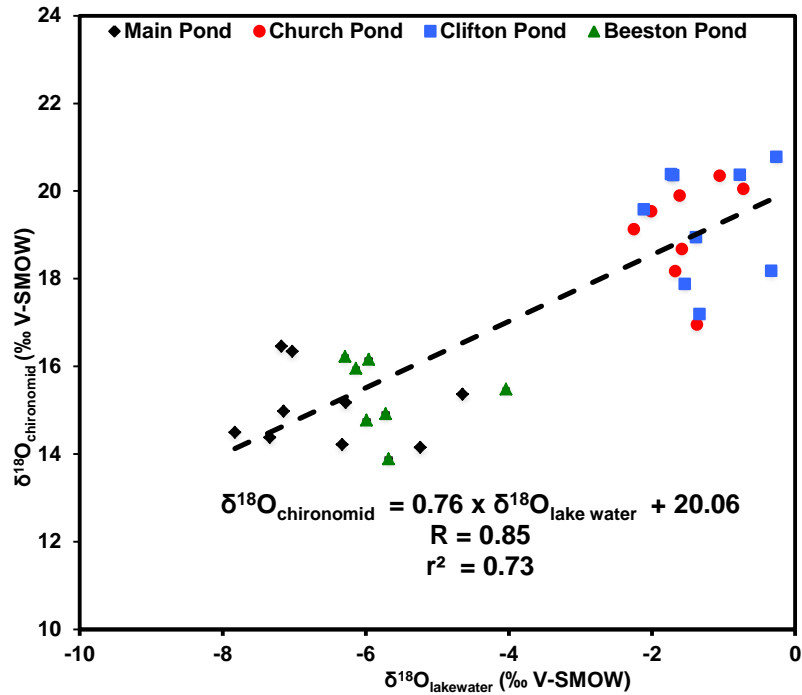
Figure 4-20: $\delta^{18}O_{chironomid}$ vs. $\delta^{18}O_{lakewater}$ from July 2011- November 2012. Samples plotting on the lower left side of the figure are from hydrologically open (Main and Beeston), while data plotting on the upper right side are from hydrologically closed (Church and Clifton) lakes.

The coefficient of determination between $\delta^{18}O_{chironomid}$ and $\delta^{18}O_{lakewater}$ in the reanalysed data (Figure 4-20) is still <1 ($r^2 = 0.73$), implying that other factors may have influenced $\delta^{18}O_{chironomid}$. The cause(s) of the lower than anticipated coefficient of determination must invoke either variable $\alpha^{18}O_{chironomid-H2O}$ or partial equilibration of oxygen atoms incorporated within chironomid head capsules with a source other than lake water. Some of the potential causes of the lower than anticipated coefficient of determination will now be briefly discussed.

Temperature-dependant $\alpha^{18}O_{chironomid-H2O}$

The results presented in Section 4.2 (see Figure 4-3) indicate that $\alpha^{18}O_{chironomid-H2O}$ varies systematically with temperature. A linear relationship is also apparent in the samples collected from Attenborough prior to the November 2012 flooding (R = 0.55; r^2 = 0.31; $p < 0.05$; n = 33) (Figure 4-21).
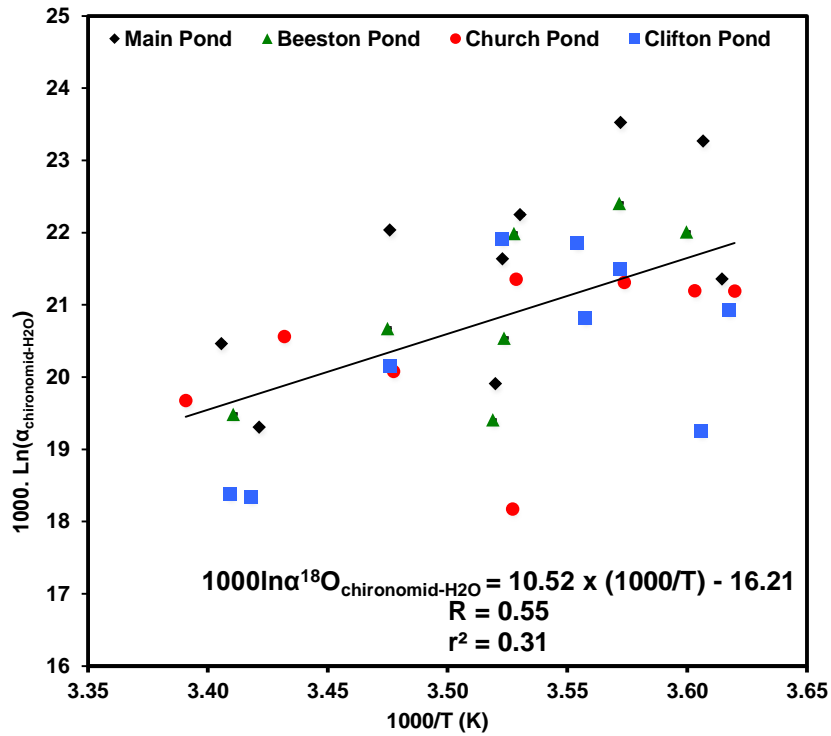
Figure 4-21: 1000ln$\alpha^{18}O_{chironomid-H2O}$ as a function of inverse average monthly water temperature in Kelvin. Temperature decreases from left to right.

The temperature dependence of $\alpha^{18}O_{chironomid-H2O}$ between ~3 and 22°C (temperature range observed in the sampled lakes) can be expressed by the following equation:

$$1000\ln \alpha^{18}O_{chironomid-H2O} = 10.52\ (1000T^{-1}) - 16.21$$

Equation 8

The coefficient of the relationship between $\delta^{18}O_{chironomid}$ and temperature is largely indistinguishable in the laboratory (Section 4.2) and field-based studies (~ −0.1‰/°C^{-1} in both studies). Unsurprisingly the uncertainty of the

calibration is considerably smaller in the controlled laboratory study (±0.63) in comparison to the field data (±1.14). This is most likely to be a reflection of the influence of environmental variability in the field-based calibration studies. It should be noted that offsets are also observed between laboratory and experimentally derived fractionation equations in the carbonate system (Lécuyer *et al.,* 2013).

Diet

Based on the results presented in Section 4.3 it may be speculated that the metabolism of oxygen atoms directly from dietary sources may have contributed to the lower than anticipated correlation coefficient between $\delta^{18}O_{chironomid}$ and $\delta^{18}O_{lakewater}$. However, this could not be assessed in this investigation.

Water chemistry

No correlation was observed between $\delta^{18}O_{chironomid}$ and any of the measured in-lake parameters (e.g. dissolved oxygen concentration, pH and electrical conductivity) (Table 4-12).

Table 4-12: Correlation between $\delta^{18}O_{chironomid}$ and, monthly pH, monthly electrical conductivity, and monthly dissolved oxygen concentration.

	Main and Beeston (Open)				Church and Clifton (Closed)			
	R	r^2	n	*p-value*	R	r^2	n	*p-value*
pH	−0.38	0.15	16	>0.05	−0.39	0.15	17	>0.05
Electrical Conductivity	−0.04	0.00	16	>0.05	0.07	0.00	17	>0.05
Dissolved Oxygen	−0.52	0.27	16	>0.05	0.22	0.05	17	>0.05

$\delta^{18}O_{lakewater}$ *seasonality*

Seasonal changes in chironomid metabolism coupled with seasonality in $\delta^{18}O_{lakewater}$, $\delta^{18}O_{diet}$ and in-lake variables (e.g. photoperiod, water temperature, pH, productivity) provide strong evidence to suggest that $\delta^{18}O_{chironomid}$ may reflect seasonal signals. However, the results from this study indicate that although mean $\delta^{18}O_{chironomid}$ values varied seasonally in each lake, with minimum values generally observed in the late summer, these differences were not statistically significant (one-way ANOVA, $p > 0.05$).
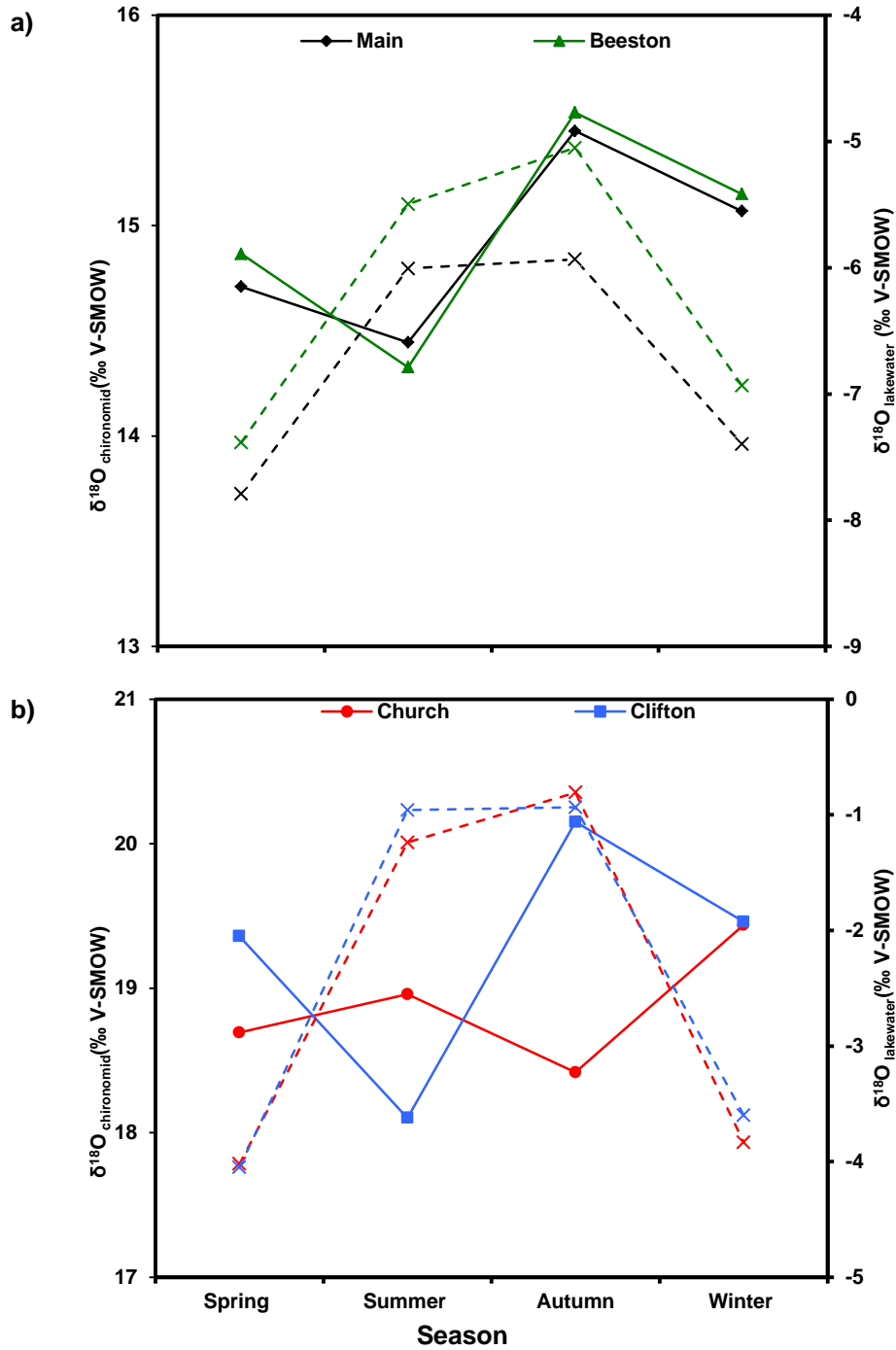
Figure 4-22: a) Mean seasonal changes in $\delta^{18}O_{chironomid}$ (solid line) and $\delta^{18}O_{lakewater}$ (dashed line) observed in the hydrologically open and, b) closed ponds. No statistical significant seasonal differences were observed between $\delta^{18}O_{chironomid}$ (one-way ANOVA, $p > 0.05$). Observed variability in $\delta^{18}O_{chironomid}$ signatures is largely in anti-phase with changes in $\delta^{18}O_{lakewater}$.

Integration of environmental isotopic signature

High-resolution contemporary calibration studies of this nature generally assume that the isotopic composition of a measured compound is reflective of conditions at the time of sampling. In reality isotopic turnover in biologically inert structures, such as chironomid head capsules, is likely to lack sufficient temporal resolution to respond instantaneously to changing environmental conditions. Larval development can only proceed following periodic ecdysis, with the formation of a new cuticle involving the partial re-digestion of the old cuticle, as well as the assimilation of new material (van Hardenbroek *et al.,* 2010; Iovino 1975; Nation 2008). In other insects excessive cuticular sclerotisation in the latter instar stages restricts digestion to structural weak points, facilitating moulting (Nation 2008). Therefore, it can be reasonably assumed that restricted head capsule digestion will occur during $3^{rd}/4^{th}$ instar stages. Since the biosynthesis of chironomid head capsules is not uniform over the year (Heiri *et al.,* 2012), one may anticipate that $\delta^{18}O_{chironmid}$ represents an integrated signal throughout larval development, weighted towards periods of more intense growth (i.e. spring/summer), rather than a discrete set of environmental conditions.

The reassessment of the relationship between $\delta^{18}O_{chironomid}$ and $\delta^{18}O_{lakewater}$ integrated over varying months suggests that isotopic turnover in chironomid head capsules is ~ 5 months (Table 4-13), which is consistent with development rates reported in Section 4.2.3. Delayed isotopic turnover may have contributed to the lower than expected correlation coefficient observed in this investigation and potentially explain the relatively muted response in $\delta^{18}O_{chironomid}$ to the flood event (Figure 4-18).

Table 4-13: Statistical correlation between $\delta^{18}O_{chironomid}$ and $\delta^{18}O_{lakewater}$ with different lake water integration periods, along with associated standard error of the estimate. It should be noted that data after November 2012 were excluded from the data set. The strongest statistical relationship is observed when a 5-month integration is applied.

Number of Months Integrated	R	r^2	p	n	Standard error of the estimate
1	0.85	0.73	< 0.05	33	1.21
2	0.87	0.75	< 0.05	32	1.14
3	0.89	0.79	< 0.05	30	1.05
4	0.90	0.81	< 0.05	30	0.99
5	0.91	0.82	< 0.05	30	0.97
6	0.90	0.82	< 0.05	27	0.97

It appears likely that $\delta^{18}O_{chironomid}$ signatures reflect an integrated environmental signal over the duration of the chironomid life cycle. Further extensive field-based calibration studies assessing seasonal variability in $\delta^{18}O_{chironomid}$ in a wide range of lakes are necessary to validate this hypothesis.

The implications of the findings in terms of palaeoclimate reconstructions are discussed in greater detail in Section 4.5.

4.5 Implications of contemporary calibration studies for palaeoclimate reconstructions

The results presented in this chapter lend support to the hypothesis that contemporary $\delta^{18}O_{chironomid}$ signals are strongly reflective of habitat water in which the larvae grew. The compilation of complementary calibration data sets demonstrates the existence of a strong linear correlation between $\delta^{18}O_{chironomid}$ and $\delta^{18}O_{lakewater}$ (R= 0.95; r^2 = 0.90; $p < 0.05$; n = 58) (Figure 4-23).
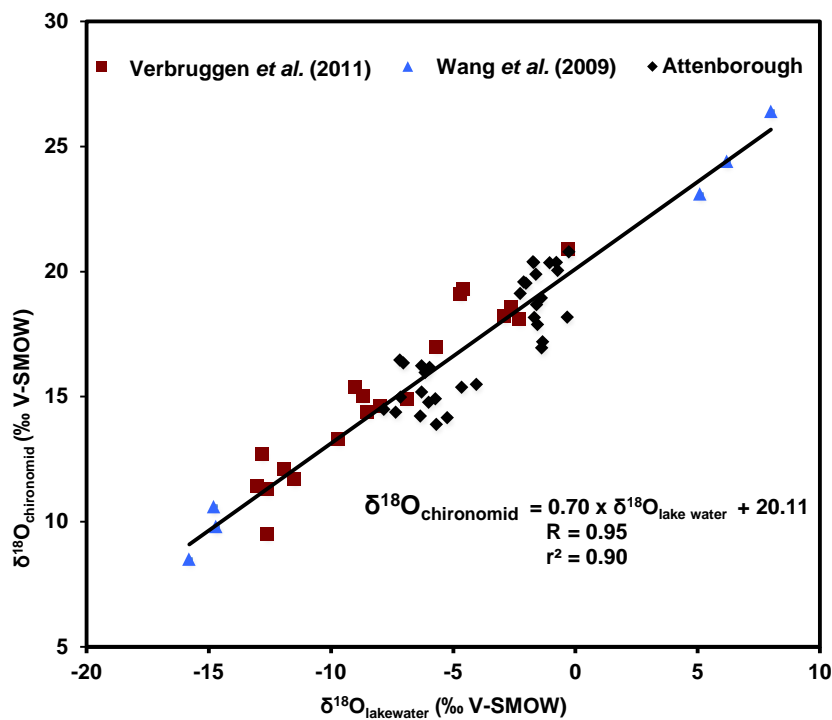
Figure 4-23: Plot of $\delta^{18}O_{chironomid}$ and $\delta^{18}O_{lakewater}$ constructed using data prior to the flood event (data after November 2012 excluded) from Attenborough and published field (Verbruggen *et al.*, 2011) and laboratory (Wang *et al.*, 2009) calibration data sets.

The strength of the linear relationship implies that stratigraphic changes in $\delta^{18}O_{chironomid}$ can be used to directly infer past $\delta^{18}O_{lakewater}$, using the following equation:

$$\delta^{18}O_{lakewater} = \frac{(\delta^{18}O_{chironomid} - 20.11)}{0.70}$$

Equation 9

It should be noted however that no chemical pre-treatments were applied in the studies conducted by Wang *et al.* (2009) or Verburggen *et al.* (2011), with analyses performed on whole chironomid larvae and head capsules isolated from surface sediments respectively. Given the influence of the chemical pre-treatments employed in this investigation (see Chapter 3), direct comparison of the different data sets is potentially problematic.

The predictive power of this model was evaluated by using Equation 9 to estimate average $\delta^{18}O_{lakewater}$ prior to the November 2012 flood event from each of the monitored lakes using average $\delta^{18}O_{chironomid}$ as an input (Table 4-14).

Table 4-14: Assessment of model performance [$\delta^{18}O_{lakewater}$ = ($\delta^{18}O_{chironomid}$ -20.11)/ 0.70] for reconstructing average $\delta^{18}O_{lakewater}$ values at Attenborough lakes prior to the November 2012 flood, using average $\delta^{18}O_{chironomid}$ as an input.

Pond	Average $\delta^{18}O_{chironomid}$	Average $\delta^{18}O_{lakewater}$	Modelled $\delta^{18}O_{lakewater}$	$\Delta^{18}O_{actual-model}$
Main	+15.1	−6.2	−7.2	+0.98
Beeston	+15.3	−5.5	−6.8	+1.32
Church	+19.1	−1.4	−1.5	+0.11
Clifton	+19.3	−1.1	−1.2	+0.04

Although the performance of the model is encouraging, with an average $\Delta^{18}O_{actual\text{-}model}$ of ~ +0.6‰, it is clear from the results presented in Chapter 4 that the interpretation of $\delta^{18}O_{chironomid}$ signals is not as straightforward as originally anticipated.

In contrast to inorganic compounds, temperature-dependant fractionations are expected to be largely absent/negligible during the formation of chironomid head capsules (e.g. Verbruggen *et al.,* 2010b; 2011; Wang *et al.,* 2009; Wooller *et al.,* 2004; 2008). The results from laboratory (Section 4.2) and field (Section 4.4) based calibration studies are the first clear demonstrations that $\delta^{18}O_{chironomid}$ signals are not immune to the complexities surrounding temperature-dependant $\alpha^{18}O_{chironomid\text{-}H2O}$. Both laboratory and field-based studies observed a systematic linear relationship between $\alpha^{18}O_{chironomid\text{-}H2O}$ and temperature; however the linear regressions of the two studies differed greatly from one another (unpaired t-test; $p < 0.05$). The discrepancies between the two studies may be related to the influence of interlinked environmental processes operating in the field-based study. Considering the discrepancies in the relationship between $\alpha^{18}O_{chironomid\text{-}H2O}$ and temperature observed in the calibration studies the two data sets were combined to produce a chironomid-water oxygen isotope fractionation equation (Figure 4-24):

$$1000\ln \alpha^{18}O_{chironomid\text{-}H2O} = 6.30\,(1000T^{-1}) - 0.85$$

Equation 10

Equation 10 can be used to quantify $\alpha^{18}O_{chironomid\text{-}H2O}$ as a function of temperature and will be utilised in the following chapter. It should be considered that the coefficient of the relationship between $\delta^{18}O_{chironomid}$ and temperature (~ -0.1‰/°C^{-1}) observed in the calibration studies presented in this chapter is considerably smaller than the reported analytical uncertainties (Section 2.3). However, the results clearly indicate a statistically significant relationship between $\alpha^{18}O_{chironomid\text{-}H2O}$ and temperature.
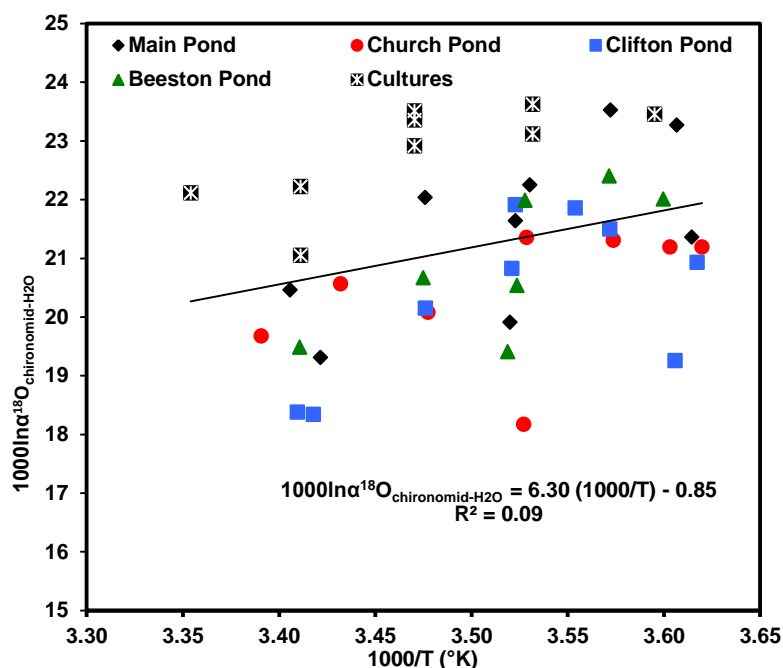
Figure 4-24: Plot of $1000\ln\alpha^{18}O_{chironomid-H2O}$ as a function of inverse temperature. It should be noted that data after November 2012 has been excluded from the Attenborough data set.

The metabolism of oxygen atoms with different dietary isotopic signatures during chitin biosynthesis may also potentially complicate the interpretation of $\delta^{18}O_{chironomid}$ signals (Section 4.3). However, in most cases it may be argued that $\delta^{18}O_{lakewater}$ and $\delta^{18}O_{diet}$ will be strongly correlated since the majority of the dietary components will have formed within the water column (Verbruggen *et al.,* 2011). Future studies should focus on the analyses of larval gut content to establish the influence of $\delta^{18}O_{diet}$ on the $\delta^{18}O_{chironomid}$ signal. It also appears likely that $\delta^{18}O_{chironomid}$ of an assemblage will reflect an integrated environmental isotopic signature weighted towards periods of most intensive growth.

The results presented in this chapter provide the foundation for translating stratigraphic changes in $\delta^{18}O_{chirononmid}$ into estimates of past $\delta^{18}O_{lakewater}$, which will be explored in Chapter 5. However, inherent uncertainties surrounding the confounding influences on $\delta^{18}O_{chironomid}$ signals restrict the predictive power of Equation 9; therefore chironomid-inferred $\delta^{18}O_{lakewater}$ can only really be considered as a first order estimate.

Chapter 5 Lake water palaeothermometry; combined $\delta^{18}O$ analyses of authigenic carbonate and chironomid remains from a Late-glacial sediment core, Hawes Water (UK).

5.1 Introduction

The development of quantitative palaeotemperature proxies is essential for improving our understanding of the likely impacts of future climate change. This chapter focuses on the evaluation of a novel approach for reconstructing palaeotemperatures, by measuring $\delta^{18}O$ of co-occurring chironomid head capsules and bulk carbonate from a Late-glacial sediment sequence retrieved from Hawes Water (UK). The climate of the Late-glacial period is of considerable interest to climate modellers, since it represents one of the most recent periods of natural, high amplitude, climate change; characterised by prolonged cold periods (stadials) interspersed by warmer episodes (interstadials) (Lang *et al.,* 2010). However, terrestrial based palaeoclimate reconstructions from this period are scarce in the UK and are mostly transfer function based (e.g. Atkinson *et al.,* 1987; Bedford *et al.,* 2004; Brooks *et al.,* 2012; Brooks & Birks 2000; Brooks & Langdon 2014). Hawes Water has been the focus of several comprehensive multi-proxy studies, which have demonstrated that the sediment sequence at the site contains a remarkably coherent record of climate change (for review see Bedford *et al.*, 2004, Jones *et al.,* 2002, Marshall *et al.*, 2002). Moreover, sediments from the site have been shown to contain abundant chironomid remains (e.g. Bedford *et al.*, 2004) making Hawes Water an ideal testing ground for the development of the chironomid-carbonate palaeothermometer.

5.1.1 Chapter aims and objectives

This chapter aims to contribute to the development of the chironomid-carbonate palaeothermometer. This will be achieved by: -

- Producing a high-resolution $\delta^{18}O_{chironomid}$ record from Hawes Water.
- Comparing stratigraphic changes in $\delta^{18}O_{chironomid}$ with an existing high-resolution $\delta^{18}O_{bulk\_carbonate}$ (Thomas, unpublished) record from the same sediment core.
- Estimating past lake water temperature from stratigraphic changes in $\delta^{18}O_{chironomid}$ and $\delta^{18}O_{bulk\_carbonate}$.

5.2 Hawes Water: background and context

5.2.1 Setting

Hawes Water is a small (8ha, max depth ~ 12m, ~ 10m above sea level), oligotrophic, hard-water lake ~ 40km north of Lancaster (northwest England) (54°10'58"N, 2°48'10"W; Figure 5-1) (Bedford *et al.,* 2004; Jones *et al.,* 2011). The lake, along with its smaller sister basin (Little Hawes Water), is situated within a shallow depression in a Carboniferous limestone catchment characterised by low limestone hills (Jones *et al.,* 2002).
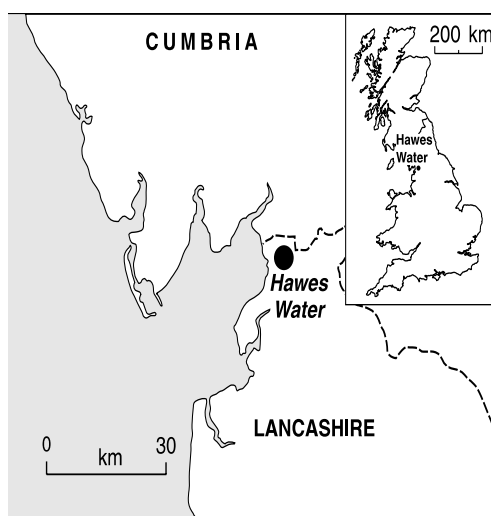
Figure 5-1: A map showing the location of Hawes Water (Jones *et al.*, 2002).

The lake is predominantly groundwater fed but it also receives inputs from precipitation and from its sister basin, via a small stream (Jones *et al.,* 2002). Seepage and stream-flow onto the adjacent Hawes Water Moss are the primary outflows of the lake (Bedford *et al.,* 2004; Jones *et al.,* 2002; 2011; Lang *et al.,* 2010 Marshall *et al.,* 2002). The contemporary $\delta^{18}O_{lakewater}$ (−6.4‰ to −5.5‰) at the site broadly reflects local precipitation, owing to short residence times and a positive precipitation:evaporation balance (Marshall *et al.,* 2002). Furthermore, the site is subject to minimal seasonal evaporative enrichment (~ 0.7‰) between surface and bottom waters during summer months (Marshall *et al.,* 2002).

The contemporary lake is surrounded by a terrestrialised marl bench containing sediments up to 12m thick; with each meter corresponding to roughly 1000 years worth of accumulation based on published sedimentation rates (Marshall *et al.,* 2002). The presence of this terrestrialised marl bench demonstrates that lake levels were once higher than they are today. The sediment sequence at Hawes Water is uninterrupted from the start of the Late-glacial period through to the Holocene (Bedford *et al.,* 2004; Jones *et al.,* 2002; Lang *et al.,* 2010; Oldfield 1960). The composite stratigraphy of the sediments from Hawes Water were first described by Oldfield (1960) and are characterised by a clay section overlain by micrites (limestone formed of calcareous particles), deposited during the Late-glacial interstadial, followed by another clay unit corresponding to the deposition during the Younger Dryas (Marshall *et al.,* 2002). This composite stratigraphy conforms well to the classic tripartite stratigraphic model of Late-glacial sites across North-west Europe (e.g. Lowe & Walker 1997). A detailed interpretation of pollen, chironomid and lithological data have been provided in Jones *et al.* (2002), while Marshall *et al.* (2002) discussed the stable isotope records from Hawes Water (Figure 5-2).

Figure 5-2: Summary diagram of multi-proxy data, including stable isotopic composition of carbonates, lithology, pollen groups and inferred catchment vegetation, and warm and cold chironomid abundances from Hawes Water for the Late-glacial and early Holocene. Stable isotope analyses were conducted on homogenised micrite samples. Abbreviations: AP, arboreal pollen; NAP, non-arboreal pollen; LOI, loss of ignition-used to determine organic matter content (%) of sediment samples through the comparison of sample weights before and after ignition (105°C for 24 hours). Diagram from Marshall *et al.* (2002).

5.3 Materials and methods

5.3.1 Sediment core

Colleagues from the University of Exeter collected three parallel sediment cores from the northern margin of the lake (054°11.032' N, 002°48.119'W, elevation 7m), using a large-diameter Russian corer. The cores were sub-divided into 1cm segments and freeze dried. A limited amount of sediment (10-20g) from selected intervals, spanning the glacial-interstadial transition (HW1), Late-glacial interstadial (HW2) and the Younger Dryas stadial (HW3), were made available for analyses in this investigation. A reliable chronological framework for the site has proved elusive to date (Jones *et al.,* 2002). Efforts have been hampered by a dearth of suitable materials and the plateau effect associated with ^{14}C AMS dating (Ammann & Lotter 1989; Lowe 1991). In the absence of a reliable chronology, the results of this investigation will be presented within the zonal stratigraphic framework, outlined in Marshall *et al.* (2002) (see Figure 5-2), based on the correlation of $\delta^{18}O_{bulk\_carbonate}$ records from the two cores.

The freeze-dried sediment samples (10-20g) were washed through 210 and 90μm mesh sieves with deionised water. The retained residue was briefly (~10 seconds) sonicated, to reduce particles adhering to the surface of the head capsules, before being re-sieved. Aliquots of the sieve residue were transferred into a grooved perspex-sorting tray (Bogorov sorter with grooves 5mm deep, 5mm wide), and chironomid larval head capsules were picked under a binocular microscope (x25). No attempts were made to identify the chironomid species represented in each sub-sample, due to limited sediment availability. Isolated head capsules were stored at 4°C in glass vials containing MilliQ water. The isolated heads were re-examined, providing an opportunity to remove any obvious contamination or miss-identified material, prior to chemical pre-treatment with 2:1 DCM: MeOH. 0.25M HCl, 0.25M NaOH for 24 hours at 20°C (see Section 3.6) and stable isotope analysis (see Section 2.2).

5.4   Results and interpretation

5.4.1   Stratigraphic changes in δ¹⁸O$_{chironomid}$

Oxygen isotope analyses were performed on purified (treated with 2:1 DCM: MeOH, 0.25M HCl, 0.25M NaOH solutions for 24 hours at 20°C) chironomid head capsules isolated from selected sediment horizons. The stratigraphic resolution of the record varied due to sample availability; however where possible analyses were performed every 2cm. No δ¹⁸O$_{chironomid}$ analyses could be performed between 312-320cm due to low head capsule abundance and poor yield following chemical pre-treatment. All samples were measured in replicates (x3) and converted onto the V-SMOW scale. The reproducibility of replicate δ¹⁸O$_{chironomid}$ measurements was ±0.7‰ (1σ). δ¹⁸O$_{chironomid}$ values ranged between +11.6-16.7‰ (mean = +14.1‰; n = 42), with the highest values recorded during Late-glacial interstadial (HW2) and the lowest during the Younger Dryas (HW3) (see Table 5-1 and Figure 5-3). The poor reproducibility of replicate δ¹⁸O$_{chironomid}$ measurements is most likely to be reflective of inter-individual variations, since each analysis was performed on ~ 5-20 individual head capsules equating to a weight of 60 ±10μg. However, it should also be reiterated that the analytical precision based on repeated analyses of IAEA 600, 601 and 602 references materials was between ±0.4-0.6‰ (1σ).

Table 5-1: Summary of average δ^{18}O$_{chironomid}$ in each of the identified sub-divisions.

	Depth (cm)	δ^{18}O$_{chironomid}$ (‰ V-SMOW)		
		Min	Max	Average
Glacial-interstadial transition (HW1)	357-368	+12.7	+15.8	+13.8
Late-glacial interstadial (HW2)	306-356	+13.6	+16.7	+15.1
Younger Dryas (HW3)	268-305	+11.6	+14.6	+12.8

The δ^{18}O$_{chironomid}$ record is presented alongside a high-resolution (1cm) δ^{18}O$_{bulk\_carbonate}$ record (analytical precision = > 0.1‰) (Thomas, *unpublished*) produced from the same sediment sequence, in Figure 5-3. The δ^{18}O records from the independent archives are strikingly similar to one another (R = 0.84, r^2 = 0.70, P < 0.05, n = 44), but the δ^{18}O$_{chironomid}$ record is on average ~ 19‰ higher compared to the δ^{18}O$_{bulk\_carbonate}$ record. The δ^{18}O records indicate climate instability, with lower values associated with demonstrably colder climatic conditions.
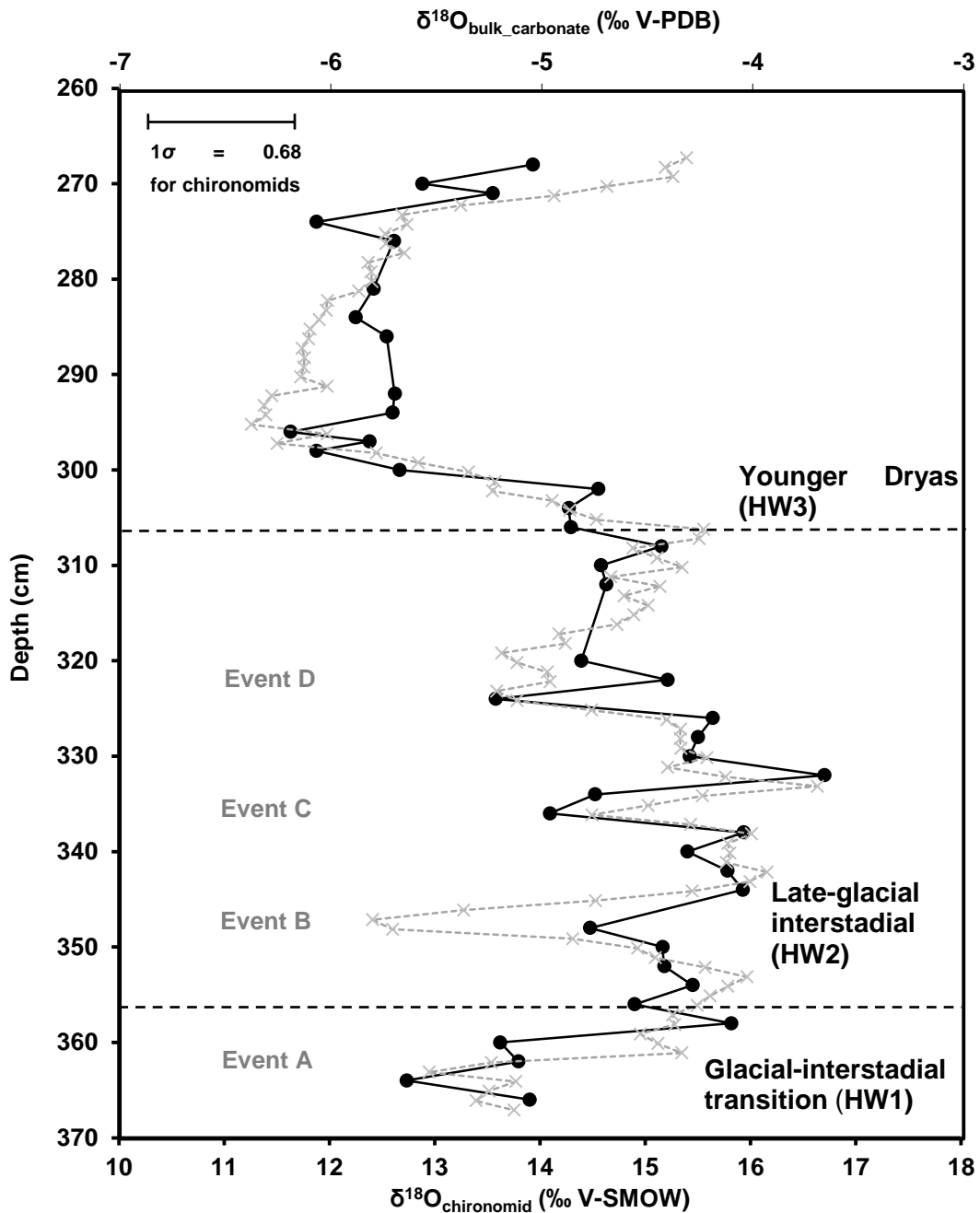
Figure 5-3: Hawes Water $\delta^{18}O_{chironomid}$ (black circle) and $\delta^{18}O_{bulk\_carbonate}$ (grey crosses; Thomas, unpublished) records. The amplitude of the two records differ with $\delta^{18}O_{chironomid}$ varying by 5.1‰, while the $\delta^{18}O_{bulk\_carbonate}$ record varies by 2.7‰ throughout the measured length of the core. Both $\delta^{18}O$ records are characterised by a series of negative isotope excursions (labelled Event A-D) prior to the onset of the Younger Dryas (HW3). Replicate measurements from individual samples were used to estimate uncertainty in the $\delta^{18}O_{chironomid}$ record ($1\sigma = \pm0.68‰$). Note that the two records are presented on separate scales due different reference standards used during the analyses of the two materials.

The $\delta^{18}O_{chironomid}$ and $\delta^{18}O_{bulk\_carbonate}$ records are both characterised by a series of negative isotope excursions (labelled Event A-D in Figure 5-3) prior to the onset of the Younger Dryas (HW3). The negative isotope excursions reflect significant, short-lived deteriorations in climatic conditions and are correlated with changes in other independent climate proxy records reported across the UK (e.g. Brooks & Birks 2000; Mayle *et al.,* 1997; Walker *et al.,* 1993; Walker 1982), Europe (e.g. Eicher & Sigenthaler 1976; von Grafenstein *et al.,* 1999; Lotter *et al.,* 1992) and in ice core records from Greenland (e.g. Johnsen *et al.,* 1992). The characteristics of these negative isotope excursions are summarised in Table 5-2.

Table 5-2: $\delta^{18}O$ characteristics of major negative isotope excursions. * denotes poor sampling resolution restricting the interpretation of the signal.

	$\delta^{18}O_{chironomid}$ (V-SMOW)				$\delta^{18}O_{bulk\_carbonate}$ (V-PBD)			
Event	λ (cm)	-ve	+ve	Shift	λ (cm)	-ve	+ve	Shift
A	362-366	1.2	1.1	−0.1	361-367	0.4	1.1	+0.7
B	344-354	1.0	1.5	+0.5	342-353	1.8	1.9	+0.1
C	332-338	1.8	2.6	+0.8	332-338	0.8	1.1	+0.3
D*	320-326	2.1	0.8	−1.3	314-330	1.0	0.7	−0.3

The evolution of $\delta^{18}O_{chironomid}$ throughout the Late-glacial period will now be discussed in greater detail within the zonal stratigraphic framework outlined in Marshall *et al.* (2002).

357-368 cm: Glacial-interstadial transition (HW1)- In this section $\delta^{18}O_{chironomid}$ values ranged between +12.7 and +15.8‰, fluctuating around a mean of +13.8‰. Increases in $\delta^{18}O_{chironomid}$ are coherent with climate amelioration as indicated by increases in the abundance of thermophilic chironomid taxa (e.g. *Chironomus, Dicrotendipes, Psectrocladius*) (Bedford *et al.,* 2004) and non-arboreal pollen (Jones *et al.,* 2002) (see Figure 5-2).

306-356cm: Late-glacial interstadial (HW2)- Broadly speaking the $\delta^{18}O_{chironomid}$ signature displays a bipartite structure, with values gradually increasing from the base of the zone to a peak of +16.7‰ at 332cm, before steadily declining prior to the onset of the Younger Dryas (HW3). Increases in $\delta^{18}O_{chironomid}$ are again coherent with changes in chironomid taxa (Bedford *et al.,* 2004) and plant communities (Jones *et al.,* 2002) (see Figure 5-2).

The $\delta^{18}O_{chironomid}$ signal is punctuated by three negative isotope excursions (Event B-D). The first of the oscillations (Event B) is associated with a ~ 1.0‰ decline in $\delta^{18}O_{chironomid}$ values, whereas the oscillations in the latter part of the zone are associated with a decline of ~ 1.8‰ (Event C) and ~ 2.1‰ (Event D).

268-305cm: Younger Dryas stadial (HW3)- Mean $\delta^{18}O_{chironomid}$ values for this period are on average ~ 2.5‰ lower than during the Late-glacial interstadial, with values ranging between +11.6 and +14.6‰. The onset of the zone is marked by a rapid decline in $\delta^{18}O_{chironomid}$, after which values increase slightly before stabilising at ~ +12.5‰ and rising again prior to the onset of the Holocene.

Decreases in $\delta^{18}O_{chironomid}$ are associated with a rise in cold water adapted chironomid species (e.g. *Sergentia, Paracladius* and *Heterotrissocladius*) (Bedford *et al.,* 2004) and the expansion of grassland and herb communities (Jones *et al.,* 2002) (see Figure 5-2).

The variability observed in the independent $\delta^{18}O$ archives is largely coherent, although small discrepancies in the magnitude and timing occur in some parts of the core. For example, the response in the $\delta^{18}O_{chironomid}$ following 'Event A' lags a few centimetres behind the $\delta^{18}O_{bulk\_carbonate}$ record; whereas the onset of Younger Dryas (HW3) occurs first in the $\delta^{18}O_{chironomid}$ record. The general coherence of the $\delta^{18}O$ records indicates a strong similarity in the mechanisms involved in the incorporation of $\delta^{18}O$ signals in both archives. In contrast to Verbruggen *et al.* (2011) (Section 1.4.3) the amplitude of variability observed in this study is greatest in the $\delta^{18}O_{chironomid}$ record, which is reflected in the gradient of the relationship between the independent $\delta^{18}O$ archives [$\delta^{18}O_{chironomid}$ = 1.5 x $\delta^{18}O_{bulk\_carbonate}$ + 21.7]. An exception to this general trend is 'Event B', which is less pronounced in the $\delta^{18}O_{chironomid}$ record. This discrepancy is likely to be an artefact of sample resolution, with other stratigraphic records failing to report 'Event B' due to poor sampling resolution.

5.4.2 Quantitative palaeoclimate reconstructions from stratigraphic changes in $\delta^{18}O_{bulk\_carbonate}$ and $\delta^{18}O_{chironomid}$

In his seminal work, Urey (1947) observed that the fractionation of oxygen isotopes between calcite of marine organisms and ocean water ($\alpha^{18}O_{calcite\text{-}H2O}$) was sensitive to temperature. In cases of equilibrium, the measured fractionation between the two phases can be used to estimate temperature at the time of calcification based on the thermodynamics of the mineral that is being precipitated (Epstein *et al.,* 1953; McCrea 1950; Urey 1947). Increases in temperature are associated with a decrease in the fractionation between the water and the measured compound. In contrast to chironomids, $\alpha^{18}O_{calcite\text{-}H2O}$ has been well constrained experimentally and empirically (e.g. McCrea 1950; Epstein *et al.,* 1953; Kim & O'Neil 1997). Based on these findings Craig (1965) developed the first palaeotemperature equation [T (°C) = 16.0 − 4.14 ($\delta^{18}O_{carbaonte}$ - $\delta^{18}O_{water}$) + 0.13 ($\delta^{18}O_{carbonate}$ - $\delta^{18}O_{water}$)^2]. Today, one of the most commonly used palaeotemperature equations is that of Kim and O'Neil (1997), which was re-expressed in a more convenient form by Leng and Marshall (2004):

$$\mathbf{T = 13.8 - 4.58(\delta^{18}O_{carbonate} - \delta^{18}O_{H2O})^2 + 0.08(\delta^{18}O_{carbonate} - \delta^{18}O_{H2O})}$$

Equation 11

where: T refers to water temperature (°C), $\delta^{18}O_{calcite}$ is the oxygen isotope composition of the CO_2 produced by the reaction between the sample calcite with phosphoric acid compared to the V-PDB standard, $\delta^{18}O_{water}$ is the oxygen isotope composition of the water from which the calcite is precipitated from compared to the V-SMOW standard. It should be noted that temperature estimates made using Equation 11 are lower than those calculated using the traditional Craig (1965) palaeotemperature equation or its derivatives (Leng & Marshall 2004).

This approach was first quantitatively applied to estimate past ocean temperatures from foraminifera in deep-sea cores (Emiliani 1954, 1966), and has since been applied in numerous terrestrial and marine-based investigations. However, a fundamental problem of oxygen isotope

palaeothermometry in lacustrine settings is that both $\delta^{18}O_{carbonate}$ and $\delta^{18}O_{lakewater}$ are required in order to resolve a value for temperature (Hodell *et al.,* 2012). In most lacustrine-based studies a value for $\delta^{18}O_{lakewater}$ is often assumed from contemporary calibration studies. However, the assumption that hydrological conditions have remained constant over the time period studied in this investigation is unlikely to be valid (Marshall *et al.,* 2002).

Based on the results presented in Chapter 4 stratigraphic changes in $\delta^{18}O_{chironomid}$ can be used to directly infer past $\delta^{18}O_{lakewater}$, using Equation 9 (see Section 4.5):

$$\delta^{18}O_{lakewater} = \frac{(\delta^{18}O_{chironomid} - 20.11)}{0.70}$$

Equation 9

Chironomid-inferred $\delta^{18}O_{lakewater}$ estimates for Hawes Water using this approach range between −12.1‰ and −4.9‰ (Table 5.3), bracketing contemporary $\delta^{18}O_{lakewater}$ values (−6.4‰ to −5.5‰).

Table 5-3: Summary of chironomid-inferred $\delta^{18}O_{lakewater}$ estimates using the experimental calibration relationship between $\delta^{18}O_{chironomid}$ and $\delta^{18}O_{lakewater}$ [$\delta^{18}O_{lakewater}$ = ($\delta^{18}O_{chironomid}$-20.11)/0.70].

	Reconstructed $\delta^{18}O_{lakewater}$ (V-SMOW)			
	Depth (cm)	**Min**	**Max**	**Average**
Glacial-interstadial transition (HW1)	357-368	−10.5	−6.1	−8.4
Late-glacial interstadial (HW2)	306-356	−9.3	−4.9	−7.2
Younger Dryas (HW3)	268-305	−12.1	−7.9	−10.5

Assuming equilibrium carbonate precipitation, chironomid-inferred $\delta^{18}O_{lakewater}$ estimates were used in conjunction with co-existing $\delta^{18}O_{bulk\_carbonate}$ measurements to estimate calcification temperatures using a palaeotemperature equation (Equation 11), with the resulting values ranging between −9°C and +11°C (~ ±7°C error based on the reproducibility of $\delta^{18}O_{chironomid}$ measurements (±0.68‰)) (Figure 5-4). The uncertainty of the temperature estimates (±7°C) is disconcerting, particularly when considering that chironomid-inferred mean July air temperatures were shown to vary by ~6°C throughout the whole Late-glacial period from the same site (Bedford *et al.,* 2004).
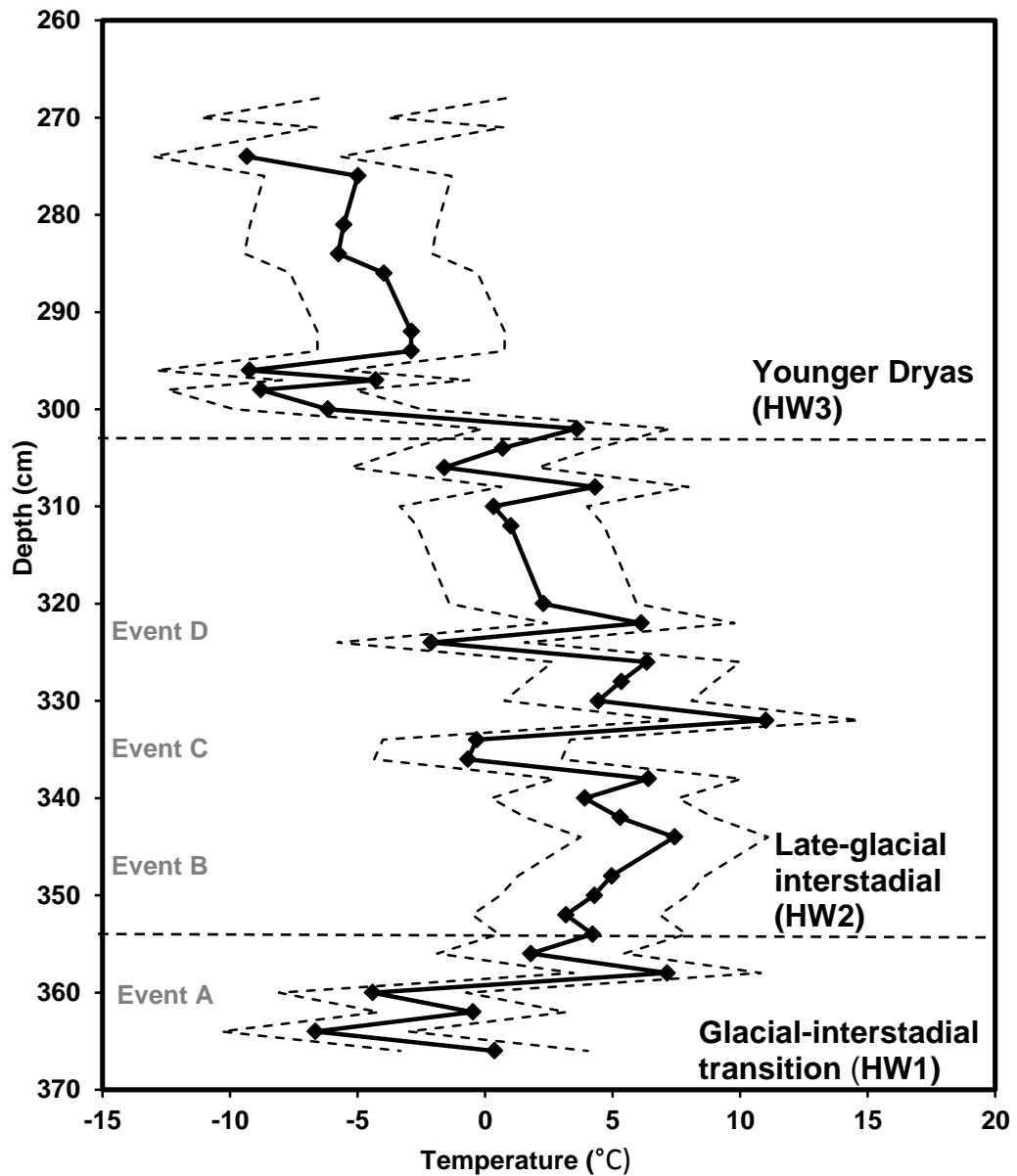
Figure 5-4: Reconstructed summer lake water temperatures (solid line) calculated using the calcite-water equilibrium equation [T°C = 13.8 − 4.58 ($\delta^{18}O_{carbonate}$ -$\delta^{18}O_{lakewater}$) + 0.08 ($\delta^{18}O_{carbonate}$ -$\delta^{18}O_{lakewater}$)] (Leng & Marshall 2004) and chironomid-inferred $\delta^{18}O_{lakewater}$. Temperature estimates are associated with errors of ~ ±7°C (dashed line) based on the reproducibility of $\delta^{18}O_{chironomid}$ measurements (±0.68‰).

Correction for potential isotope exchange induced by the chemical pre-treatments adopted in this investigation (2:1 DCM: MeOH, 0.25M HCl, 0.25M NaOH for 24 hours at 20°C) fails to completely eliminate the unrealistic temperature estimates below zero, although values are moved in a positive direction (Table 5-4).

Table 5-4: Summary of summer lake water temperature and $\delta^{18}O_{lakewater}$ from derived from the conjunctive use of $\delta^{18}O_{bulk\_carbonate}$ and $\delta^{18}O_{chirononmid}$ after +0.88‰ correction has been applied to account for potential isotope exchanges induced during chemical pre-treatment.

	$\delta^{18}O_{lakewater}$ (‰ V-SMOW)			Temperature (°C)		
	Min	Max	Average	Min	Max	Average
Glacial-interstadial transition (HW1)	−9.3	−4.9	−7.5	−1.9	+11.9	+3.4
Late-glacial interstadial (HW2)	−8.1	−3.6	−5.9	+2.6	15.8	8.3
Younger Dryas (HW3)	−10.9	−6.7	−9.2	−4.6	+8.3	+0.2

Although absolute temperature estimates using this approach are largely unrealistic the relative temperature changes obtained are comparable with other studies. For example, the average temperature drop between the Late-glacial interstadial (HW2) and the Younger Drays (HW3) reported in this investigation is ~8°C; in comparison Marshall *et al.* (2002) reported a ~7-8°C drop in average summer temperatures during the same period based on the $\delta^{18}O_{bulk\_carbonate}$, whereas Bedford *et al.* (2004) reported a ~6°C drop during the same period based on C-IT estimates from Hawes Water.

5.5 Potential causes for unrealistic temperature estimate

The chironomid-carbonate palaeothermometer tested in this investigation relies on several fundamental assumptions: i) $\delta^{18}O_{chironomid}$ is a reliable $\delta^{18}O_{lakewater}$ proxy, ii) the independent $\delta^{18}O$ archives must have formed simultaneously from waters with a common $\delta^{18}O_{lakewater}$ and temperature, iii) both archives should be free from contamination and, iv) not be subjected to any post-depositional alterations. The largely unrealistic temperature estimates obtained using this approach implies that one, or more, of these assumptions have been violated in some respect. Each of the assumptions will now be looked at in more detail.

The results presented in Chapter 4 demonstrate that although a strong linear correlation does exist between $\delta^{18}O_{chironomid}$ and $\delta^{18}O_{lakewater}$, confounding factors can complicate the interpretation of $\delta^{18}O_{chironomid}$ signals. The inherent uncertainties surrounding the calibration of the relationship between $\delta^{18}O_{chironomid}$ and $\delta^{18}O_{lakewater}$ are likely to have a deleterious influence on chironomid-inferred $\delta^{18}O_{lakewater}$ estimates, and therefore ultimately temperature reconstructions. Laboratory- (Section 4.2) and field- (Section 4.4) based studies identified that temperature has a confounding influence on $\delta^{18}O_{chironomid}$ signals. Although this relationship is poorly characterised the results presented in Chapter 4 were used to define a chironomid-water oxygen isotope fractionation equation, which can be used to quantify $\alpha^{18}O_{chironomid-H2O}$ as a function of temperature (see Section 4.5):

$$1000\ln \alpha^{18}O_{chironomid-H2O} = 6.30\ (1000T^{-1}) - 0.85$$

Equation 10

The chironomid-water oxygen isotope fractionation equation (Equation 10) can be used in conjunction with the carbonate-water oxygen isotope fractionation equation [$1000\ln\alpha^{18}O_{calcite-H2O} = 18.03\ (1000\ T^{-1}) - 32.42$] (Kim & O'Neil 1997) to simultaneously infer changes in temperature and $\delta^{18}O_{lakewater}$ from paired $\delta^{18}O_{chironomid}$ and $\delta^{18}O_{bulk\_carbonate}$ measurements, using the following methodology:

For carbonate

$$1000\ln\alpha^{18}O_{carb-H2O} = a_{carb} + b_{carb} \cdot \frac{1}{T}$$

For chironomids

$$1000\ln\alpha^{18}O_{chiron-H2O} = a_{chiron} + b_{chiron} \cdot \frac{1}{T}$$

Note that:

$$\alpha^{18}O_{carb-H2O} = \frac{1000 + \delta^{18}O_{carb}}{1000 + \delta^{18}O_{H2O}} \quad \text{and} \quad \alpha^{18}O_{chiron-H2O} = \frac{1000 + \delta^{18}O_{chiron}}{1000 + \delta^{18}O_{H2O}}$$

Therefore

$$\alpha^{18}O_{carb-chiron} = \frac{1000 + \delta^{18}O_{carb}}{1000 + \delta^{18}O_{chiron}} = \frac{\alpha^{18}O_{carb-H2O}}{\alpha^{18}O_{chiron-H2O}}$$

and

$$\ln\alpha^{18}O_{carb-chiron} = \ln\alpha^{18}O_{carb-H2O} - \ln\alpha^{18}O_{chiron-H2O}$$

Substituting Equation 12 and Equation 13 into Equation 14 and Equation 15

$$1000 \ln \left\{ \frac{1000 + \delta^{18}O_{carb}}{1000 + \delta^{18}O_{chiron}} \right\} = (a_{carb} - a_{chiron}) + (b_{carb} - b_{chiron}) \cdot \frac{1}{T}$$

Equation 16

$\delta^{18}O_{chirononmid}$ and $\delta^{18}O_{bulk\_carbonate}$ are the measured values for each sample, a_{carb} and b_{carb} are constant values published in Kim and O'Neil (1997), while a_{chiron} and b_{chiron} are derived from Equation 10. Substitution of the appropriate values into Equation 16 allows the calculation of 1/T in K, which can then be used in either Equation 12 or Equation 13 to calculate a value for $\alpha^{18}O_{chiron-H2O}$ or $\alpha^{18}O_{carb-H2O}$, and thus permit the calculation of $\delta^{18}O_{lakewater}$.

However, even when accounting for the influence of temperature, the chironomid-carbonate palaeothermometer still produces results that are largely below zero (~ −10°C and ~ +11°C) (Table 5-5). This implies that; i) the characterisation of the relationship between $\alpha^{18}O_{chironomid-H2O}$ and temperature is not valid in this circumstance, ii) one or more of the fundamental assumptions (see above) have been violated during the adoption of this approach or iii) variables that influence $\alpha^{18}O_{chironomid-H2O}$ have been overlooked. For example inaccurate determination of growth water temperature and/or $\delta^{18}O$ of environmental water can lead to imprecise fractionation equations.

Table 5-5: Summary of summer lake water temperature and $\delta^{18}O_{lakewater}$ derived from the conjunctive use of $\delta^{18}O_{bulk\_carbonate}$ and $\delta^{18}O_{chirononmid}$ measurements.

	$\delta^{18}O_{lakewater}$ (‰ V-SMOW)			Temperature (°C)		
	Min	Max	Average	Min	Max	Average
Glacial-interstadial transition (HW1)	−10.2	−5.9	−18.4	−7.6	+6.9	−1.4
Late-glacial interstadial (HW2)	−8.9	−4.7	−7.0	−3.7	+11.1	+2.8
Younger Dryas (HW3)	−11.5	−7.4	−9.9	−9.6	+4.4	−4.7

Disparities in the temporal resolution of the two independent $\delta^{18}O$ archives may have contributed to the deleterious palaeotemperature reconstructions obtained using this approach. For example, the analysed 1cm bulk carbonate segments may represent several years worth of accumulation whereas the chironomid head capsules isolated from the same layer may only represent a few months/years worth of accumulation. Furthermore, disparities in the timing of calcification and chironomid development could potentially account for the unrealistic temperature estimates obtained using the chironomid-carbonate palaeothermometer. An existing contemporary monitoring program reported that authigenic carbonates are precipitated close to conventional carbonate isotopic equilibrium at Hawes Water, in response to increased photosynthetic activity during the summer months (June – August) (Marshall *et al.,* 2002). Subsequently $\delta^{18}O_{bulk\_carbonate}$ is likely to reflect summer lake water conditions. In contrast, $\delta^{18}O_{chironomid}$ is likely to reflect an integrated environmental signal throughout the life of the larvae, weighted towards periods of more intense growth (Section 4.4.3). However, the strong correlation between the two records (Figure 5-3) implies that the independent archives are likely to have recorded the same environmental signal, although

the higher variability observed in the $\delta^{18}O_{chironomid}$ record may reflect the incorporation of different seasonal signals within the $\delta^{18}O_{chironomid}$ signature and/or differences in the temporal resolution of the two archives. This discrepancy may also reflect genuine differences in the sensitivity of the independent $\delta^{18}O$ archives. Such an observation should be treated with a degree of caution since comparisons are being drawn from records with different sampling resolutions and analytical precisions. In order to fully evaluate potential differences in the sensitivity of the two proxies, the resolution of the $\delta^{18}O_{chironomid}$ record needs to be improved, particularly during periods of demonstrably colder conditions. However, such periods are associated with low head capsule abundances and therefore would require extensive sediment processing to obtain sufficient samples (> 50µg) for $\delta^{18}O$ analyses.

Due to insufficient quantities of individual carbonate micro and macrofossils colleagues from the University of Exeter performed $\delta^{18}O$ analyses on bulk sediments, which are likely to have contained both authigenic and biogenic carbonates (including marl, molluscs, ostracods as well as detrital carbonates). If possible $\delta^{18}O$ analyses should not be performed on bulk sediments since individual carbonate components are associated with unique mineral-water isotope fractionation effects (von Grafenstein *et al.,* 1999; Leng & Marshall 2004). Marshall *et al.* (2002) have indicated that the Late-glacial carbonate sequence at Hawes Waters is likely to be predominantly composed of authigenic carbonates. However, varying contributions from different carbonate components throughout the length of the Hawes Water core may have contributed to the unrealistic palaeotemperature reconstructions obtained in this investigation.

It is assumed that the sequential treatment of chironomid samples with DCM: MeOH (2:1), HCl (0.25M), NaOH (0.25M) for 24 hours at 20°C, yielded samples of a sufficient purity so that contamination did not have a detrimental influence on $\delta^{18}O$ analysis. The effectiveness of the chemical pre-treatments could not be confirmed since no assessment of the level of contamination was made prior to or after chemical pre-treatment. However, the chemical pre-treatments adopted in this investigation were associated with average $\Delta^{18}O_{\text{untreated-treated}}$ of -3.3‰ (n= 28; $1\sigma = 1.4$) (Table 5-6), with the statistical correlation between $\delta^{18}O_{\text{bulk\_carbonate}}$ and $\delta^{18}O_{\text{chironomid}}$ increasing slightly following chemical pre-treatment (Figure 5-5).

Table 5-6: Comparison of $\delta^{18}O_{chironomid}$ from chironomid samples that have and have not been subjected to chemical pre-treatment.

	$\delta^{18}O_{chironomid}$ (‰ V-SMOW)		
Depth (cm)	**Treated**	**Untreated**	$\Delta^{18}O_{Untreated\text{-}treated}$
268	13.9	19.7	5.8
270	12.9	18.8	5.9
286	12.5	14.3	1.7
296	11.6	13.3	1.7
297	12.4	14.9	2.5
298	11.9	14.9	3.0
300	12.7	17.1	4.4
302	14.6	18.5	3.9
304	14.3	20.7	6.4
306	14.3	16.8	2.5
308	15.2	17.6	2.4
310	14.6	17.5	2.9
312	14.6	18.7	4.1
326	15.6	19.3	3.7
330	15.4	18.3	2.9
332	16.7	19.4	2.7
334	14.5	19.3	4.8
336	14.1	18.0	3.9
338	15.9	19.8	3.9
342	15.8	19.2	3.4
348	14.8	17.3	2.8
354	15.5	18.3	2.9
356	14.4	18.4	4.0
358	15.8	20.1	4.3
360	13.6	16.8	3.2
362	13.8	14.3	0.5
364	12.7	15.2	2.5
366	13.9	14.7	0.8
Average			**3.3**
1σ			**1.4**
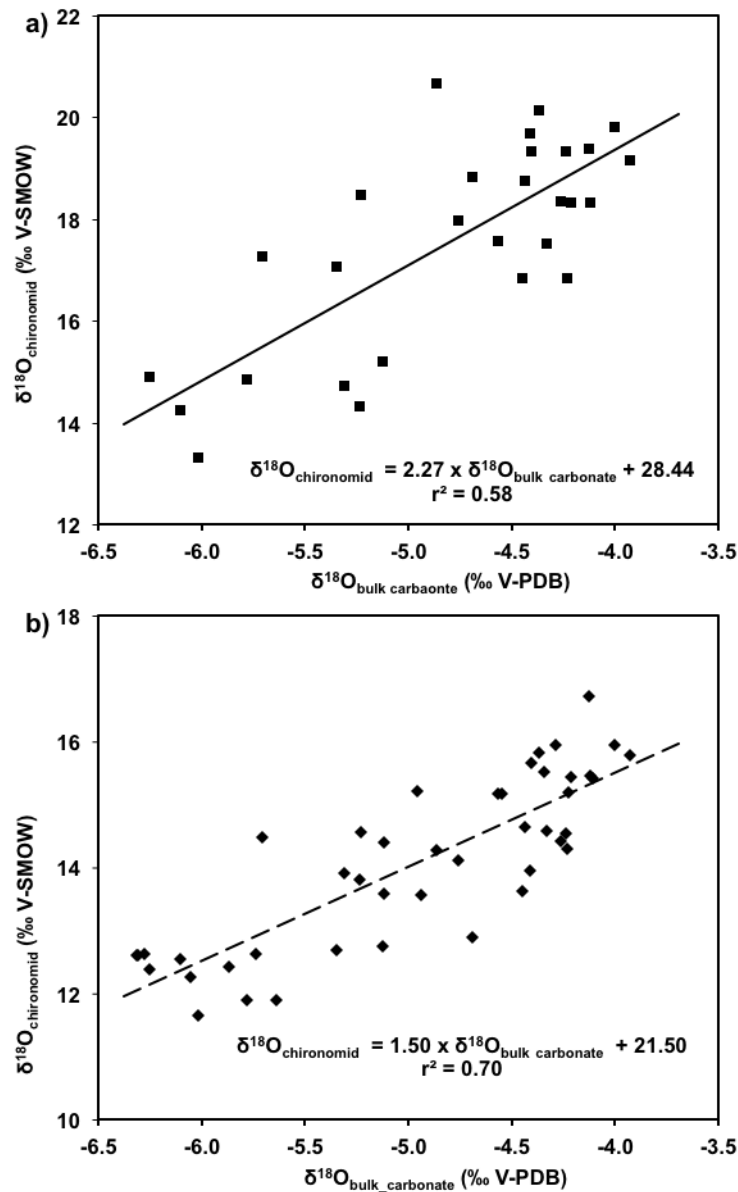
Figure 5-5: Correlation between a) untreated (square) and b) treated (diamond) $\delta^{18}O_{chironomid}$ vs. $\delta^{18}O_{bulk\_carbonate}$. The correlation between the archives improves after chemical pre-treatment.

The chemical composition of chitin is thought to remain largely unchanged for tens of thousands of years under favourable depositional environments (e.g. high sedimentation rates and anoxia) (Stankiewicz *et al*., 1997a; 1997b). Verbruggen *et al.* (2010a) reported the presence of chitin-derived moieties in Late-glacial chironomid remains. In contrast, preliminarily chromatographic screening of chironomid remains in this investigation, using pyrolysis gas chromatography mass spectrometry (Py-GC-MS) techniques, suggests that chitin-derived complexes were largely absent in the limited

number of samples tested (*pers. comm.* Reichart, Utrecht University). The chironomid remains analysed were largely composed of protein-derived compounds along with a series of alkene/alkanes. The macromolecular structure of the tested chironomid remains from Hawes Water are characteristic of the formation of aliphatic (geo)polymers during diagenesis, via the polymerisation of liberated lipid molecules (Baas *et al.,* 1995; Briggs 1999; Cody *et al.*, 2011; Gupta *et al.,* 2009; Stankiewicz *et al.,* 2000). The alphatic component of fossil arthropods is bound to the degraded chitin-protein residue through ester linkage to form the geopolymer (Cody *et al.,* 2011). The conditions governing the kinetics of this transformation are largely unknown, therefore the influence of the formation of geopolymers on the $\delta^{18}O_{chironomid}$ signature at Hawes Water is difficult to ascertain. However, clearly diagenetic alterations have the potential to reset, or at least alter, the original $\delta^{18}O_{chironomid}$ signature. Additionally, chitin-protein complexes within chitinous biomass are known to undergo various condensation reactions post mortem, resulting in the formation of numerous compounds that may or may not be indigenous to the original insect remains (Tripp *et al.,* 2004). Based on the observation made in this investigation it is recommended that the integrity of the chironomid remains should be assessed through chromatographic separation prior to $\delta^{18}O$ analyses.

Since the formation of geopolymers involves the diagenesis of oxygen-bearing compounds present in the original material, a large proportion of oxygen atoms may be derived from the original head capsules. Given the similarity between the $\delta^{18}O_{chironomid}$ and the $\delta^{18}O_{bulk\_carbonate}$ records, one may argue that any diagenetic alterations that took place at Hawes Water must have produced a systematic offset (i.e. shifted $\delta^{18}O_{chironomid}$ by more or less a fixed value). For example, an average shift of ~ +2.5‰ is necessary to largely eliminate unrealistic temperature estimates below 0°C. However, it should be noted that this offset produces some unrealistically high temperature estimates indicating that the diagenetic processes may not have been systematic (Table 5-7).

Table 5-7: Summary of $\delta^{18}O_{lakewater}$ and temperature estimates derived using chironomid-carbonate palaeothermometer with a +2.5‰ offset applied for diagenetic alteration.

	$\delta^{18}O_{lakewater}$ (‰ V-SMOW)			Temperature (°C)		
Zone	Min	Max	Average	Min	Max	Average
Glacial-interstadial transition (HW1)	−7.0	−2.6	−5.2	+6.8	+20.6	+12.6
Late-glacial interstadial (HW2)	−5.8	−1.3	−3.6	+11.4	+24.5	+17.0
Younger Dryas (HW3)	−8.5	−4.4	−6.9	+4.2	+17.1	+8.9

Ultimately the true cause(s) of the unrealistic temperature estimates returned by the chironomid-carbonate palaeothermometer is difficult to establish. However, the available preliminary results tentatively indicate that both confounding influences on $\delta^{18}O_{chironomid}$ and diagenetic alteration of the chironomid remains are the principal mechanisms responsible for the unrealistic temperature reconstructions obtained using the chironomid-carbonate approach.

Chapter 6 Conclusion

The remains of chironomid larvae are often one of the most abundant biogenic components preserved in lacustrine sediments and have recently received increasing attention as a tool for inferring past $\delta^{18}O_{lakewater}$, and indirectly past climate. The main aims of this research (as described in Section 1.5) were focused on the development of $\delta^{18}O_{chironomid}$ as a tool for inferring past climates. The early chapters of this thesis concentrated on the development of analytical and preparatory procedures in the analyses of $\delta^{18}O_{chironomid}$, whereas the latter chapters focused on the interpretation of $\delta^{18}O_{chironomid}$ signals in contemporary and stratigraphic settings.

The absence of a standardised procedure for the preparation of chironomid remains for $\delta^{18}O$ analysis has prevented inter-laboratory comparisons, hampering the development of the $\delta^{18}O_{chironomid}$ approach. Non-amino polysaccharide impurities (both compositional and exogenous) present within chitinous biomass have a deleterious influence on $\delta^{18}O$ determinations. Therefore, in order to produce meaningful $\delta^{18}O_{chironomid}$ measurements efforts should be made to limit impurities. Based on the results of a systematic investigation presented in Chapter 3, it is recommend that chironomid samples are sequentially soaked in DCM: MeOH (2:1), HCl (0.25M), NaOH (0.25M) solutions for 24 hours at 20°C, prior to $\delta^{18}O$ analysis. It is hoped that this procedure can form the basis for the standardisation of preparatory procedures in future $\delta^{18}O_{chirononmid}$ analysis.

Organic compounds preserved in lacustrine sediments are anticipated to be largely independent of kinetic (temperature related) and disequilibrium effects. However, the interpretation of $\delta^{18}O_{chirononmid}$ is not as straightforward as one may expect. Laboratory- (Section 4.2) and field- (Section 4.4) based calibration studies presented in this thesis indicate that $\delta^{18}O_{chironomid}$ signals are not immune to the complexities surrounding temperature-dependant $\alpha^{18}O_{chironomid-H2O}$. The metabolism of oxygen atoms with dietary isotopic signatures during chitin biosynthesis was also shown to potentially complicate the interpretation of $\delta^{18}O_{chironomid}$ signals (Section 4.3), although in

most circumstances $\delta^{18}O$ of dietary components formed within a lake will be reflective of $\delta^{18}O_{lakewater}$. Furthermore, it should be acknowledged that vital effects might also influence $\delta^{18}O_{chironomid}$ signals. The possibility that distinct chironomid species fractionate oxygen differently to one another due to autoecological preferences is potentially problematic to the wider adoption of this approach, since changing abundances may preclude the analyses of a single species throughout a sediment core. The autoecological preferences of different communities may potentially be reflected in $\delta^{18}O_{chirononmid}$ signals.

The findings of the contemporary calibration studies, presented in Chapter 4, provided the foundations for the interpretation of stratigraphic changes in $\delta^{18}O_{chirononmid}$ from a Late-glacial sediment sequence (Hawes Water, England) (Chapter 5). The $\delta^{18}O_{chirononmid}$ record produced from this site was strikingly similar to an existing high-resolution $\delta^{18}O_{bulk\_carbonate}$ record, indicating that the two independent proxies recorded the same broad environmental signal. In addition, the results of the contemporary calibration studies were used to develop a chironomid-carbonate palaeothermometer. Although the general climate trends reported by this approach are largely in good agreement with other palaeoclimate reconstructions from the region, absolute temperature estimates were unrealistically low (ranging between −9°C and +11°C). However, relative temperature changes reported throughout the length of the core were comparable to palaeotemperature estimates from other proxy records at Hawes Water. The spurious absolute palaeotemperature estimates obtained in this investigation indicate that the fundamental assumption that $\delta^{18}O_{chirononmid}$ represents an uncorrupted $\delta^{18}O_{lakewater}$ proxy is not valid in all instances. Based on the limited available data the spurious temperature estimates were attributed to diagenetic alterations of the original $\delta^{18}O_{chironomid}$ signature.

The results presented in this thesis demonstrate that in carefully selected locations (e.g. free from excessive diagenetic alterations) $\delta^{18}O_{chironomid}$ can potentially become a powerful addition to the analytical arsenal available for inferring terrestrial palaeoclimates. In particular, this approach can become

an important tool in elucidating past climates in environments that have sparse or inherently difficult to interpret proxy records. However, the successful application of this approach relies on understanding the inherent $\alpha^{18}O_{chironomid\text{-}H2O}$ associated with the incorporation of environmental signals into chironomid larval head capsules.

One of the most important aspects of this approach that needs to be resolved is the large error associated with $\delta^{18}O_{chironomid}$ measurements. These errors are propagated through the palaeotemperature reconstructions resulting in large uncertainties in temperature estimates. Furthermore, future studies should focus on the experimental verification of the empirical relationships between $\delta^{18}O_{chironomid}$, $\delta^{18}O_{lakewater}$, local environment (e.g. temperature, diet, water chemistry) and autoecological constraints. In the absence of such studies this approach can only be considered as a qualitative or at best semi-quantitative tool for reconstructing past climates. However, it is hoped that the findings presented in this thesis will contribute to the development of a theoretical framework within which stratigraphic changes in $\delta^{18}O_{chironomid}$ signals can be interpreted.

Bibliography

Abdullin, V.F., Artemenko, S.E., Ovchinnikova, G.P. & Arzamastev, O.S. 2008. Extraction processes in extraction of the biopolymer chitin from crab shells. *Fibre Chemistry*, 40: 513–516.

Accoe, F., Berglund, M., Geypens, B. & Taylor, P. 2008. Methods to reduce interference effects in thermal conversion elemental analyzer/continuous flow isotope ratio mass spectrometry $\delta^{18}O$ measurements of nitrogen-containing compounds. *Rapid Communications in Mass Spectrometry*, 22: 2280–2286.

Acosta, N., Jiménez, C., Boraut, V. & Heras, A. 1993. Extraction and characterization of chitin from crustaceans. *Biomass and Bioenergy*, 5: 145–153.

Alley, R. B. & Cuffey, K.M. 2001. Oxygen and hydrogen isotopic ratios of water in precipitation: beyond paleothermometry. *Reviews Mineralogy and Geochemistry*, 43: 527-553.

Alley, R.B., Marotzke, J., Nordhaus, W.D., Overpeck, J.T., Peteet, D.M., Pielke, R.A., Pierrehumbert, R.T., Rhines, P.B., Stokcer, T.F., Talley, L.D. & Wallace, J.M. 2003. Abrupt climate change. Science, 299: 2005-2010.

Ammann, B. & Lotter, A.F. 1989. Late-glacial radiocarbon stratigraphy and palynostratigraphy on the Swiss plateau. *Bores,* 18: 109-126.

Andersen, S.O. 1979. Biochemistry of insect cuticle. *Annual Review of Entomology*, 24: 29–59.

Anderson, L., Abbott, M.B. & Finney, B.P. 2001. Holocene Climate Inferred from oxygen isotope ratios in lake sediments, Central Brooks Range, Alaska. *Quaternary Research*, 55: 313–321.

Araguás Araguás, L., Froehlich, K. & Rozanski, K. 2000. Deuterium and oxygen- 18 isotope composition of precipitation and atmospheric moisture. *Hydrological Processes*, 14: 1341–1355.

Aranaz, I., Mengíbar, M., Harris, H., Paños, I., Miralles, B., Acosta, N., Galed, G. & Heras, Á. 2009. Functional characterization of chitin and chitosan. *Current Chemical Biology*, 3: 203–230.

Armitage, P.D., Cranston, P.S., & Pinder, L.C.V (Eds). 1995. The Chironomidae. The biology and ecology of non-biting midges. Chapman and Hall, London, 572 p.

Atkinson, T.C., Briffa, K.R. & Coope, G.R. 1987. Seasonal temperatures in Britain during the past 22,000 years, reconstructed using beetle remains. *Nature*, 325: 587–592.

Baas, M., Briggs , D.E.G., van Heemst, J.D.H., Kear, A.J. & de Leeuw, J.W.1995. Selective preservation of chitin during the decay of shrimp. *Geochimica et Cosmochimica Acta*, 59: 945–951.

Barbakadze, N., Enders, S., Gorb, S. & Arzt, E. 2006. Local mechanical properties of the head articulation cuticle in the beetle Pachnoda marginata (Coleoptera, Scarabaeidae). *Journal of Experimental Biology*, 209: 722–730.

Battarbee, R. W. 2000. Palaeolimnological approaches to climate change, with special regard to the biological record. *Quaternary Science Reviews* 19: 107-124

Bedford, A. Jones, R., Langm B., Brooks, S. & Marshall, J.D. 2004. A Late-glacial chironomid record from Hawes Water, northwest England. *Journal of Quaternary Science*, 19: 281–290.

Bigler, C., Larocque, I., Peglar, S.M., Birks, H.J.B. & Hall, R.I. 2002. Quantitative multiproxy assessment of long-term patterns of Holocene environmental change from a small lake near Abisko, northern Sweden. *The Holocene*, 12: 481–496.

Birks, H.H., Battarbee, R.W. & Birks, H.J.B. 2000. The development of the aquatic ecosystem at Kråkenes Lake, western Norway, during the Late-glacial and early Holocene-a synthesis. *Journal of Paleolimnology*, 23: 91–114.

Borda, P. 1985. Application of a new catalyst based on molybdenum for direct determination of oxygen by pyrolytic gas chromatography. *Microchemical Journal*, 31: 183-191.

Boschetti, T. & Iacumin, P. 2005. Continuous- flow $\delta^{18}O$ measurements: new approach to standardization, high- temperature thermodynamic and sulfate analysis. *Rapid Communications in Mass Spectrometry*, 19: 3007–3014.

Bouchard, R.W., Jr. & Ferrington, L.C. 2008. Identification Guide and Key to Chironomid Pupal Exuviae in Mongolian Lakes. Chironomid Research Group, 72. p.

Brand, W.A. 1996. High precision isotope ratio monitoring techniques in mass spectrometry. *Journal of Mass Spectrometry*, 31: 225–235.

Brand, W.A., Coplen, T.B., Aerts-Bijma, A.T., Böhlke, J.K., Gehre, M., Geilmann, H., Gröning, M., Jansen, H.G., Meijer, H.A.J., Mroczkowski, S.J., Qi, H., Soergel, K., Stuart-Williams, Weise, S.M. & Werner, R.A. 2009. Comprehensive inter-laboratory calibration of reference materials for $\delta^{18}O$ versus VSMOW using various on-line high-temperature conversion techniques. *Rapid Communications in Mass Spectrometry*, 23: 999–1019.

Brandriss, M.E. O'Neil, J.R., Edlund, M.B. & Stoermer, E.F. 1998. Oxygen isotope fractionation between diatomaceous silica and water. *Geochimica et Cosmochimica Acta*, 62: 1119–1125.

Brenna, J.T., Corso, T.N., Tobias, H.J. & Caimi, R.J. 1997. High- precision continuous- flow isotope ratio mass spectrometry. *Mass spectrometry reviews*, 16: 227–258.

Brine, C.J. & Austin, P.R. 1981. Chitin variability with species and method of preparation. *Comparative Biochemistry and Physiology*, 69: 283–286.

Brodersen, K.P. & Lindegaard, C. 1999. Classification and Trophic Reconstruction. *Freshwater Biology*, 42: 143–157.

Brooks, S.J., Mayle, F.E. & Lowe, J. 1997. Chironomid-based Late-glacial climatic reconstruction for southeast Scotland. *Journal of Quaternary Science*, 12: 161-167.

Brooks, S.J., 2000. Late-glacial fossil midge stratigraphies (Insecta: Diptera: Chironomidae) from the Swiss Alps. *Palaeogeography, Palaeoclimatology, Palaeoecology*, 159: 261–279.

Brooks, S.J. & Birks, H.J.B. 2000. Chironomid- inferred Late- glacial air temperatures at Whitrig Bog, Southeast Scotland. *Journal of Quaternary Science*, 15: 759–764.

Brooks, S.J. & Birks, H.J.B. 2001. Chironomid-inferred air temperatures from Late-glacial and Holocene sites in north-west Europe: progress and problems. *Quaternary Science Reviews*, 20: 1723–1741.

Brooks, S.J. 2006. Fossil midges (Diptera: Chironomidae) as palaeoclimatic indicators for the Eurasian region. *Quaternary Science Reviews*, 25: 1894–1910.

Brooks S.J., Langdon P.G. & Heiri O. 2007. The identification and use of palaearctic chironomidae larvae in palaeoecology. Quaternary Research Association Technical Guide No. 10. London, 276 p.

Brooks, S.J. Axford, Y., Heiri, O., Langdon, P.G. & Larocque-Tobler, I. 2012. Chironomids can be reliable proxies for Holocene temperatures. A comment on Velle et al. (2010). *The Holocene*, 22: 1495–1500.

Brooks, S.J. & Langdon, P.G. 2014. Summer temperature gradients in northwest Europe during the Late-glacial to early Holocene transition (15–8 ka BP) inferred from chironomid assemblages. *Quaternary International*, 341: 80-90.

Buhay, W.M., Wolfe, B.B. & Schwalb, A. 2012. Lakewater paleothermometry from Deep Lake, Minnesota during the deglacial-Holocene transition from combined & $\delta^{18}O$ analyses of authigenic carbonate and aquatic cellulose. *Quaternary International*, 260: 76–82.

Carlström, D. 1957. The crystal structure of α-chitin (poly-N-acetyl-D-glucosamine). *The Journal of Biophysical and Biochemical Cytology*, 3: 669–683.

Charoenvuttitham, P., Shi, J. & Mittal, G.S. 2006. Chitin extraction from black tiger shrimp (*Penaeus monodon*) waste using organic acids. *Separation Science and Technology*, 41: 1135–1153.

Clark, I.D. & Fritz, P. 1997. Environmental isotopes in hydrogeology, Lewis Publishers, Boca Raton, 328 p.

Cody, G.D., Gupta, N.S., Briggs, D.E.G., Kilcoyne, A.L.D., Summons, R.E., Kenig, F., Plotnick, R.E. & Scott, A.C. 2011. Molecular signature of chitin-protein complex in Paleozoic arthropods. *Geology*, 39: 255-258.

Cohen, E. 1987. Chitin biochemistry: synthesis and inhibition. *Annual Review of Entomology*, 32: 71–93.

Cohen, E. 2001. Chitin synthesis and inhibition: a revisit. *Pest Management Science*, 57: 946–950.

Cotton, F.A. & Wilkinson, G. 1966. Advanced inorganic chemistry: a comprehensive text, (2nd edn.). Wiley-Interscience Publication, 1376 p.

Craig, H. 1961. Isotopic variations in meteoric waters. *Science*, 133: 1702–1703.

Cranston, P.S. 1985. *Eretmoptera murphyi Schaeffer* (Diptera: Chironomidae) an apparently parthenogenetic Antarctic midge. *British Antarctic Survey Bulletin*, 66: 35–45.

Criss, R.E., 1999. Principles of Stable Isotope Distribution. Oxford University Press, New York. 264 p.

Cross, I. D. 2009. The effects of nutrients and hydrology on shallow lake plankton at Attenborough nature reserve, Nottinghamshire. PhD dissertation, University of Nottingham, Nottingham, England, 424 p.

Dansgaard, W. 1964. Stable isotopes in precipitation. *Tellus*, 16: 436–468.

Daley, T.J., Barber, K.E., Street-Perrott, F.A., Loader, N.J., Marshall, J.D, Crowley, S.F. & Fisher, E.H. 2010. Holocene claimte variability revealed by oxygen isotope analysis of *Sphagnum* cellulose from Walton Moss, northern England. *Quaternary Science Reviews*, 29: 1590–1601.

Darling W. G., Talbot J. C. and Brownless M. A. (1996) The stable isotopic content of rainfall and groundwater in the British Isles. In: *Isotopes in Water Resources Management* 1, International Atomic Energy Proceedings Series (Vienna): 434–437.

Darling, W.G. & Talbot, J.C. 2003. The O and H stable isotope composition of freshwaters in the British Isles. 1. Rainfall. *Hydrology and Earth System Sciences Discussions*, 7: 163–181.

Darling G.W., Bath A.H., Gibson J.J., Rozanski K., 2006. Isotopes in Water. In: Isotopes in Palaeoenvironmental Research, Leng, M.J. (Ed.), Springer, Dordrecht: pp. 1-66.

Das, S. & Ganesh, E.A. 2010. Extraction of chitin from trash crabs (Podophthalmus vigil) by an eccentric method. *Current Research Journal of Biological Sciences,* 2: 72–75.

DeNiro, M.J. & Epstein, S. 1981. Isotopic composition of cellulose from aquatic organisms. *Geochimica et Cosmochimica Acta*, 45: 1885–1894.

Dutta, P.K., Ravikumar, M.N.V. & Dutta, J. 2002. Chitin and chitosan for versatile applications. *Journal of Macromolecular Science, Part C: Polymer Reviews*, 42: 307–354.

Dutta, P.K., Dutta, J. & Tripathi, V.S. 2004. Chitin and chitosan: Chemistry, properties and applications. *Journal of Scientific and industrial research*, 63: 20–31.

Edwards T. W. & McAndrews J. H. 1989. Paleohydrology of a Canadian Shield lake inferred from ^{18}O in sediment cellulose. *Canadian Journal of Earth Sciences*, 26: 1850-1859.

Eggermont, H., Heiri, O. & Verschuren, D. 2006. Subfossil Chironomidae (Insecta: Diptera) as quantitative indicators for past salinity variation in African lakes. *Quaternary Science Reviews*. 25: 1966–1994.

Eggermont, H. & Heiri, O. 2012. The chironomid- temperature relationship: expression in nature and palaeoenvironmental implications. *Biological Reviews*. 87: 430-456.

Eicher, U. & Sigenthaler, U. 1976. Palynological and oxygen isotope investigations on late-Glacial sediment cores from Swiss lakes. *Boreas,* 5: 109-117.

Einbu, A., 2007. Characterisation of chitin and a study of its acid-catalysed hydrolysis. PhD dissertation, Norwegian University of Science and Technology, Trondheim, Norway.

Emiliani, C. 1954. Temperature of Pacific bottom waters and polar superficial waters during the Tertiary. *Science,* 119: 853–855

Emiliani, C. 1966. Isotopic paleotemperatures. *Science,* 154: 851–857.

Epler, J.H., 2001. Identification manual for the larval Chironomidae (Diptera) of North and South Carolina: a guide to the taxonomy of the midges of the southeastern United States, including Florida. St. Johns River Water Management District.

Epstein, S. Buchsbaum, R., Lowenstam, H.A. & Urey, H.C. 1953. Revised carbaonte-water isotopic temperature scale. *Geological Society of America Bulletin*, 64: 1315-1326.

Epstein, S., Thompson, P. & Yapp, C.J. 1977. Oxygen and hydrogen isotopic ratios in plant cellulose. *Science,* 198: 1209–1215.

Farquhar, G.D., Henry, B.K. & Styles, J.M. 1997. A rapid on-line technique for determination of oxygen isotope composition of nitrogen-containing organic matter and water. *Rapid Communications in Mass Spectrometry*, 11: 1554–1560.

Ferrington, L.C. 2008. Global diversity of non-biting midges (Chironomidae; Insecta-Diptera) in freshwater. *Hydrobiologia*, 595: 447–455.

Fleitmann, D., Burns, S.J., Neff, U., Mudelsee, M., Mangini, A. & Matter, A. 2004. Palaeoclimatic interpretation of high-resolution oxygen isotope profiles derived from annually laminated speleothems from Southern Oman. *Quaternary Science Reviews*, 23: 935–945.

Fricke, H.C & O'Neil, J.R. 1999. The correlation between $^{18}O/^{16}O$ ratios of meteoric water and surface water temperature: its use in investigating terrestrial climate change over geologic time. *Earth Planet Science Letters.* 170: 181-196.

Fritz, S.C. 1996. Paleolimnological records of climatic change in North America. *Limnology and Oceanography*, 41: 882–889.

Gannes, L.Z., O'Brien, D.M. & Del Rio, C.M. 1997. Stable isotopes in animal ecology: assumptions, caveats, and a call for more laboratory experiments. *Ecology*, 78: 1271–1276.

Gat, J.R. 1996. Oxygen and hydrogen isotopes in the hydrologic cycle. *Annual Review of Earth and Planetary Sciences*, 24: 225–262.

Gat, J.R. 2000. Atmospheric water balance—the isotopic perspective. *Hydrological Processes*, 14: 1357–1369.

Gehre, M. & Strauch, G. 2003. High-temperature elemental analysis and pyrolysis techniques for stable isotope analysis. *Rapid Communications in Mass Spectrometry*, 17: 1497–1503.

Gehre, M. Geilmann, H. Richter, J., Werner, R.A. & Brand, W.A. 2004. Continuous flow $^{2}H/^{1}H$ and $^{18}O/^{16}O$ analysis of water samples with dual inlet precision. *Rapid Communications in Mass Spectrometry*, 18: 2650–2660.

Gillet, E., Chiaren, J.C. & Gillet, M. 1976. Decomposition thermique du monoxide de carbon sur une surface de molybdene: Foramtion de couches superficielles de caron et de carbure. *Surface Science*, 55: 126-140.

Gilson, T.R., & Hendra, P.J. 1970. Laser Raman Spectroscopy. Wiley-Interscience, 266 pp.

Godlewski, J., Kludkiewicz, B., Grzelak, K. & Cymborowski, B. 2001. Expression of larval hemolymph proteins (Lhp) genes and protein synthesis in the fat body of greater wax moth (*Galleria mellonella*) larvae during diapause. *Journal of Insect Physiology*, 47: 759–66

Goldstein, J., Newbury, D.E., Joy, D.C., Lyman, C.E., Echlin, P., Lifshin, E., Sawyer, L. & Michael. J. 1992. Scanning electron microscopy and x-ray microanalysis: a text for biologists, materias scientists, and geologists (2nd edn.). Springer, New York, 840 pp.

von Grafenstein, U., Erlenkeuser, H., Müller, H., Trimborn, J. & Alefs, P. 1996. A 200 year mid-European air temperature record preserved in lake sediments: an extension of the $\delta^{18}O_{precipitation}$ - air temperature relation into the past. *Geochimica et Cosmochimica Acta,* 60: 4025-4036.

von Grafenstein, U., Erlernkeuser, H. & Trimborn, P. 1999. Oxygen and carbon isotopes in modern fresh-water ostracod valves: assessing vital offsets and autecological effects of interest for palaeoclimate studies. *Palaeogeography, Palaeoclimatology, Palaeoecology*, 148: 133–152.

von Grafenstein, U., Belmecheri, S., Eicher, U., van Raden, U.J., Erlenkeuser, H., Andersen, N. & Ammann, B. 2013. The oxygen and carbon isotopic signatures of biogenic carbonates in Gerzensee, Switzerland, during the rapid warming around 14, 685 years BP and the following interstadial. *Palaeogeography, Palaeoclimatology, Palaeoecology*, 391: 25–32.

Grey, J., Kelly, A., Ward, S., Sommerweek, N. & Jones, R.I. 2004. Seasonal changes in the stable isotope values of lake- dwelling chironomid larvae in relation to feeding and life cycle variability. *Freshwater Biology*, 49: 681–689.

Gröcke, D.R. Schimmelmann, A., Elias, S. & Miller, R.F. 2006. Stable hydrogen-isotope ratios in beetle chitin: preliminary European data and re-interpretation of North American data. *Quaternary Science Reviews*, 25: 1850–1864.

Gupta, N.S., Cody, G.D., Tetlie, O.E., Briggs, D.E.G., & Summons, R.E. 2009. Rapid incorporation of lipids into macromolecules during experimental decay of invertebrates: Initiation of geopolymer formation. *Organic Geochemistry,* 40: 589–594.

Gygli, A. 1993. Microdetermination of oxygen in organic compounds using a glassy carbon pyrolysis tube and nondispersive infrared detection. *Microchimica Acta*, 111: 37–43.

Hagopian, W.M. & Jahren, A.H. 2012. Elimination of nitrogen interference during online oxygen isotope analysis of nitrogen-doped organics using the "NiCat" nickel reduction system. *Rapid Communications in Mass Spectrometry*, 26: 1776–1782.

Hahn, D.A. & Denlinger, D.L. 2011. Energetics of Insect Diapause. *Annual Review of Entomology*, 56: 103–121.

van Hardenbroek, M. Heiri, O., Grey, J., Bodelier, P.L.E., Verbruggen, F. & Lotter. 2010. Fossil chironomid δ^{13}C as a proxy for past methanogenic contribution to benthic food webs in lakes? *Journal of Paleolimnol*ogy, 43: 235-245.

Hargreaves, J.C. & Annan, J.D. 2009. On the importance of paleoclimate modelling for improving predictions of future climate change. *Climate of the Past*, 5: 803–814.

Hayes, J.M. 1983. Practice and principles of isotopic measurements in organic geochemistry. In: Organic geochemistry of contemporaneous and ancient sediments, Great Lakees Section, Meinschein, W.G. (Ed.), Society of economic palaeontologists and mineralogists, Bloomington, 143 p.

Heiri, O., Cremer, H., Engels, S., Hoek, W.Z., Peeters, W. & Lotter, A.F. 2007. Lateglacial summer temperatures in the Northwest European lowlands: a chironomid record from Hijkermeer, the Netherlands. *Quaternary Science Reviews*, 26: 2420–2437.

Heiri, O., Schilder, J. & van Hardenbroek, M. 2012. Stable isotopic analysis of fossil chironomids as an approach to environmental reconstruction: state of development and future challenges. *Fauna Norvegica*, 31: 7-18.

Henderson, A.C.G. & Holmes, J.A. 2009. Palaeolimnological evidence for environmental change over the past millennium from Lake Qinghai sediments: a review and future research prospective. *Quaternary International*, 194: 134-147.

Henrikson, L., Olafsson, J.B. & Oskarsson, H.G. 1982. The impact of acidification on Chironomidae (Diptera) as indicated by subfossil stratification. *Hydrobiologia.* 86: 223–229.

Heslop, R.B. & Jones, K.1976. Inorganic chemistry: A guide to advanced Study (2nd Ed.). Elsevier, Amsterdam, 838 p.

Hodell, D.A., Turchyn, A.V., Wiseman, C.J., Escoba, J., Curtis, J.H., Brenner, M., Gilli, A., Mueller, A.D., Anselmetti, F., Ariztegui, D. & Brown, E.T. 2012. Late Glacial temperature and precipitation changes in the lowland Neotropics by tandem measurement of water. *Geochimica et Cosmochimica Acta*, 77: 352–368.

Hodgins, G., Thorpe, J.L. & Hedges, R.E.M. 2001. Protocol development for purification and characterization of sub-fossil insect chitin for stable isotopic analysis and radiocarbon dating. *Radiocarbon*, 43:199–208.

Hoefs, J. 2009. Stable isotope geochemistry (6th Ed.). Springer, 288 p.

Hofmann, W. 1998. Cladocerans and chironomids as indicators of lake level changes in north temperate lakes. *Journal of Paleolimnology*, 19: 55–62.

Hogenkamp, D.G. 2006. Chitin metabolism in insects: chitin synthases and beta-N-acetylglucosaminidases. PhD dissertation. Kansas State University. Manhattan, Kansas, USA, 126 p.

Holleman, A.F. & Wiberg, E. 2001. Inorganic chemistry, academic press, New York, 1924 p.

Hopkins, T.L. & Kramer, K.J. 1992. Insect cuticle sclerotization. *Annual Review of Entomology*, 37: 273–302.

Hopley, P.J., Marshall, J.D. & Latham, A.G. 2009. Speleothem preservation and diagenesis in South African hominin sites implications for paleoenvironments and geochronology. *Geoarchaeology*, 24: 519–547.

Hostetler, S.W. & Benson, L.V. 1994. Behavior of the stable isotopes of oxygen and hydrogen in the Truckee River-Pyramid Lake surface-water system, Part 2: A predictive model of $\delta^{18}O$ and $\delta^{2}H$ in Pyramid Lake. *Limnology and Oceanography*, 39: 356-364.

Iovino, A. J. 1975. Extant chironomid larval populations and the representativeness and nature of their remains in lake sediments. PhD dissertation. Indiana University, Bloomington Indiana, USA, 60 p.

IPCC 2013. 5th Assessment report. Stocker, T.F., Qin, D., Plattner, G-K., Tignar, M.M.B., Allen ,S.K., Bosching, J., Nauels, A., Xia, Y., Bex, V. & Midgley, P.M (eds). Contribution of working group 1 to the fifth assessment report of the intergovernmental panel on claimte change. Cambridge University Press, UK and New York.

Ito, E., De Deckker, P. & Eggins, S.M. 2003. Ostracodes and their shell chemistry: implications for paleohydrologic and paleoclimatologic

applications. *Paleontological Society Papers*, 9:119-152

Johnson R.K. & Pejler, B. 1987. Life histories and coexistence of the two profundal Chironomus species in Lake Erken, Sweden. E*ntomologica scandinavica Supplements*, 29: 233–238.

Johnsen, S.J., Clausen, H.B., Dansgaard, W., Fuhrer, K., Gundestrup, N., Hammer, C.U., Iversen, P., Jouzel, J., Stauffer, B. & Steffensen, J.P. 1992. Irregular glacial interstadials recorded in new Greenland ice core. *Nature,* 359: 311-313.

Jones, P.D., Briffa, K.R., Osborn, T.J., Lough, J.M., van Ommen, T.D., Vintherm B.M., Luterbacher, J., Wahl, E.R., Zwiers, F.W., Mann, M.E., Schmidt, G.A., Ammann, C.M., Buckely, B.M., Cobb, K.M., Esper, J., Goosse, H., Graham, N., Jansen, E., Kiefer, T., Kull, C., Küttel, M., Mosley-Thompson, E., Overpeck, J.T., Riedwyl, N., Schulz, M., Tudhope, A.W., Villalba, R., Wanner, H., Wolff, E. & Xoplaki, E. 2009. High-resolution palaeoclimatology of the last millennium: a review of current status and future prospects. *The Holocene*, 19: 3–49.

Jones, R.I. & Grey, J. 2004. Stable isotope analysis of chironomid larvae from some Finnish forest lakes indicates dietary contribution from biogenic methane. *Boreal Environment Research*, 9: 17–24.

Jones, R.T., Marshall, J.D., Crowley, S.F., Bedford A., Richardson, N., Bloemendal, J. & Oldfield. 2002. A high resolution, multiproxy Late-glacial record of climate change and intrasystem responses in northwest England. *Journal of Quaternary Science*, 17: 329–340.

Jones, R.T., Marshall, J.D., Fisher, E., Hatton, J., Patrick, C., Anderson, K., Lang, B., Bedford, A. & Oldfield, F. 2011. Controls on lake level in the early to mid Holocene, Hawes Water, Lancashire, UK. *The Holocene*, 21: 1061–1072.

Jones, M.D., Cuthbert, M., Leng, M.J., McGowan, S., Mariethoz, G., Arrowsmith, C., Solane, H., Humphrey, K. & Cross, I. *in prep.* Data based models of lake δ^{18}O variability.

Jouzel, J., Alley, R.B., Cuffey, K.M., Dansgaard, W., Grootes, P., Hoffmann, G., Johnsen. S.J., Koster, R.D., Peel. D., Shuman, C.A., Stievenard, M., Stuiver, M. & White, J. 1997. Validity of the temperature reconstruction from water isotopes in ice cores. *Journal of Geophysical Research: Oceans*, 102: 26471–26487.

Jouzel, J., Hoffmann, G., Kosterm R.D. & Masson, V. 2000. Water isotopes

in precipitation: data/model comparison for present-day and past climates. *Quaternary Science Reviews*, 19: 363–379.

Juillet-Leclerc A. & Labeyrie L. 1987. Temperature dependence of the oxygen isotopic fractionation between diatom silica and water. *Earth Planetary Science Letter,* 84: 69–74.

Juillet-Leclerc, A., Reynaud, S., Rollion-Bard, C., Cuif, J.P., Dauphin, Y., Blamart, Ferrier-Pagès. & Allemand, D. 2009. Oxygen isotopic signature of the skeletal microstructures in cultured corals: Identification of vital effects. *Geochimica et Cosmochimica Acta*, 73: 5320–5332.

Keatings, K.W. & Holmes, J.A. 2002. Carbon and oxygen isotope fractionation in non-marine ostracods: results from a "natural culture" environment. *Geochimica et Cosmochimica Acta*, 66: 1701–1711.

Kim, S.T. & O'Neil, J.R. 1997. Equilibrium and nonequilibrium oxygen isotope effects in synthetic carbonates. *Geochimica et Cosmochimica Acta*, 61: 3461–3475.

Koch, P.L. 1998. Isotopic reconstruction of past continental environments. *Annual Review of Earth and Planetary Sciences*, 26: 573–613.

Korhola, A., Olander, H. & Blom, T. 2000. Cladoceran and chironomid assemblages as qualitative indicators of water depth in subarctic Fennoscandian lakes. *Journal of Paleolimnology*, 24: 43–54.

Kornexl, B.E., Gehre, M., Höfling, R. & Werner, R.A. 1999. On-line δ^{18}O measurement of organic and inorganic substances. *Rapid Communications in Mass Spectrometry*, 13: 1685–1693.

Koziet, J. 1997. Isotope ratio mass spectrometric method for the on-line determination of oxygen-18 in organic matter. *Journal of Mass Spectrometry*, 32: 103–108.

Kramer, K.J. & Koga, D. 1986. Insect chitin: physical state, synthesis, degradation and metabolic regulation. *Insect biochemistry*, 16: 851–877.

Kurek, J. 2008. Past climate and environmental change in eastern Beringia inferred from chironomids. PhD dissertation. The University of New Brunswick, Fredericton, Canada, 180 p.

Kurita, K. 2006. Chitin and Chitosan: Functional Biopolymers from Marine Crustaceans. *Marine Biotechnology*, 8: 203–226.

Lamb, A.L., Leng, M.J., Sloane, H.J. & Telford, R.J. 2005. A comparison of

the palaeoclimate signals from diatom oxygen isotope ratios and carbonate oxygen isotope ratios from a low latitude crater lake. *Palaeogeography, Palaeoclimatology, Palaeoecology*, 223: 290-302.

Lamb, A.L., Brewer, T.S., Leng, M.J., Sloane, H.J. & Lamb, H.F. 2007. A geochemical method for removing the effect of tephra on lake diatom oxygen isotope records. *Journal of Paleolimnology*, 37: 499-516.

Lang, B., Bedford, A., Brooks, S.J., Jones, R.J., Richardson, N., Birks, H.J. & Marshall, J.D. 2010. Early-Holocene temperature variability inferred from chironomid assemblages at Hawes Water, northwest England. *The Holocene*, 20: 943–954.

Langdon, P.G., Barber, K.E. & Lomas-Clarke, S.H. 2004. Reconstructing climate and environmental change in northern England through chironomid and pollen analyses: evidence from Talkin Tarn, Cumbria. *Journal of Paleolimnology*, 32: 197–213.

Larocque, I. & Hall, R.I. 2003. Chironomids as quantitative indicators of mean July air temperature: validation by comparison with century-long meteorological records from northern Sweden. *Journal of Paleolimnology*, 29: 475–493.

Leng, M.J. & Henderson, A.C. G. 2013. Recent advances in isotopes as palaeolimnological proxies. *Journal of Paleolimnology*, 49: 481–496.

Leng, M.J., Lamb, A., Heaton, T.E., Marshall, J.D., Wolfe, B.B., Jones, M.D., Holmes, J.A. & Arrowsmith, C. 2006. Isotopes in lake sediments. In: Isotopes in Palaeoenvironmental Research, Leng, M.J. (Ed.), Springer, Dordrecht: 147-184 p.

Leng, M.J. & Barker, P.A. 2006. A review of the oxygen isotope composition of lacustrine diatom silica for palaeoclimate reconstruction. *Earth-Science Reviews*, 75: 5–27.

Leng, M.J. & Marshall, J.D. 2004. Palaeoclimate interpretation of stable isotope data from lake sediment archives. *Quaternary Science Reviews*, 23: 811–831.

Lécuyer, C., Amiot, R., Touzeau, A. & Trotter, J. 2013. Calibration of the phosphate $\delta^{18}O$ thermometer with carbonate- water oxygen isotope fractionation equations. *Chemical Geology*, 347: 217–226.

Little, J.L. & Smol, J.P. 2001. A chironomid- based model for inferring late-summer hypolimnetic oxygen in southeastern Ontario lakes. *Journal of Paleolimnology*, 26: 259–270.

Loader, N.J., Santillo, P.M., Woodman-Ralph, J.P., Rolfe, J.E., Hall, M.A., Gagen, M., Robertson, I., Wilson, R., Froyd, F. & McCarroll,D. 2008. Multiple stable isotopes from oak trees in southwestern Scotland and the potential for stable isotope dendroclimatology in maritime climatic regions. *Chemical Geology*, 252: 62–71.

Lombino, A., Atkinson, T. & Firth, S. 2012. $\delta^{18}O$ analysis of organic compounds: problems with pyrolysis in molybdenum- lined reactors. *Rapid Communications in Mass Spectrometry*, 26: 2407–2412.

Lotter, A.F., Eicher, U., Siegenthalar, U. & Birks, H.J.B. 1992. Late-glacial climatic oscillations as recorded in Swiss lake sediemnts. *Journal of Quaternary Science*, 7: 187-204.

Lotter, A.F., Birks, H.J.B., Hofmann, W. & Marchetto, W. 1997. Modern diatom, cladocera, chironomid, and chrysophyte cyst assemblages as quantitative indicators for the reconstruction of past environmental conditions in the Alps. I. Climate. *Journal of Paleolimnology*, 18: 395–420.

Lotter, A.F., Lotter, AF; Birks, HJB; Hofmann, W, & Marchetto, A. 1998. Modern diatom, cladocera, chironomid, and chrysophyte cyst assemblages as quantitative indicators for the reconstruction of past environmental conditions in the Alps. II. Nutrients. *Journal of Paleolimnology*, 19: 443–463.

Lowe, J.J. 1991. Stratigraphic resolution and radiocarbon dating of Devensian lateglacial sediments. *Quaternary Proceedings*, 1: 19-26.

Lowe, J.J. & Walker, M.J.C. 1997. Reconstructing Quaternary Environments. (2nd ed). Longman, London, 446 p.

Majtán, J. et al. Bíliková, K., Markovič, O., Gróf, J., Kogan, G. & Šimúth, J. 2007. Isolation and characterization of chitin from bumblebee (Bombus terrestris). *International Journal of Biological Macromolecules*, 40: 237–241.

Marshall, J.D. Jones, R.T., Crowley, S.F., Oldfield, F., Nash, S. Bedford, A. 2002. A high resolution late-glacial isotopic record from Hawes Water, northwest England: Climatic oscillations: Calibration and comparison of palaeotemperature proxies. *Palaeogeography, Palaeoclimatology, Palaeoecology*, 185: 25–40.

Mayle. F. E., Lowe, J. J. & Sheldrick, C. 1997: The Devensian Lateglacial palaeoenvironmental record from Whitrig Bog, SE Scotland. 1.

Lithostratigraphy and palacobotany. *Boreas,* 26: 279 295.

McCarroll, D., & Loader, N.J. 2004. Stable isotopes in tree rings. Q*uaternary Science Reviews*, 23: 771–801.

McCrea, J.M. 1950. On the isotopic chemistry of carbonates and a paleotemperature scale. *The Journal of Chemical Physics*, 18: 849-857.

Merzendorfer, H. & Zimoch, L. 2003. Chitin metabolism in insects: structure, function and regulation of chitin synthases and chitinases. *Journal of Experimental Biology*, 206: 4393–4412.

Merzendorfer, H. 2006. Insect chitin synthases: a review. *Journal of Comparative Physiology Biology*, 176: 1–15.

Miller, R.F. 1991. Chitin paleoecology. *Biochemical Systematics and Ecology*, 19: 401–411.

Morley, D.W., Leng, M.J., Mackay, A.W. & Solane, H.J. 2005, Late glacial and Holocene environmental change in the Lake Baikal region documented by oxygen isotopes from diatom silica, *Global and Planetary Change*, 46: 221-233.

Motz, J.E. 2000. Oxygen and hydrogen isotopes in fossil insect chitin as paleoenvironmental indicators. PhD dissertation, University of Waterloo, Ontario, Canda, 152 p.

Nation, J.L. 2008. Insect physiology and biochemistry (2nd ed). CRC Press. 560 p.

Nemtsev, S.V. Zueva, O.Y., Khismatullin, M.R., Albulov, A.I. & Varlamov, V.P. 2004. Isolation of chitin and chitosan from honeybees. *Applied Biochemistry and Microbiology*, 40: 39–43.

Neville, A.C. 1975. Biology of the Arthropod Cuticle. Springer, 448 p.

Nielson, K.E. & Bowen, G.J. 2010. Hydrogen and oxygen in brine shrimp chitin reflect environmental water and dietary isotopic composition. *Geochimica et Cosmochimica Acta*, 74: 1812–1822.

Nier, A.O. 1950. A re-determination of the relative abundances of the isotopes of carbon, nitrogen, oxygen, argon, and potassium. *Physical Review*, 77: 789-793.

Oldfield, F. 1960. Studies in the post-glacial history of British vegetation: lowland Lonsdale. New Phytologist. 59: 192-217.

Oliver, D.R. 1971. Life history of the Chironomidae. *Annual Review of Entomology*, 16: 211–230.

Overpeck J.T. 2007. Paleoclimate perspectives on climate change., The science of climate change: A Royal Society showcase of the IPCC 4th Assessment Working Group 1 report. The Royal Society, London.

Partington, J. R. 1958. General and Inorganic Chemistry (3rd edn.). Macmillan and Co, 927 p.

Percot, A., Viton, C. & Domard, A. 2003a. Characterization of Shrimp Shell Deproteinization. *Biomacromolecules*, 4: 1380–1385.

Percot, A., Viton, C. & Domard, A. 2003b. Optimization of Chitin Extraction from Shrimp Shells. *Biomacromolecules*, 4: 12–18.

Pinder, L. 1986. Biology of freshwater Chironomidae. *Annual Review of Entomology*, 31: 1–23.

Płóciennik, M. Self, A., H.J.B. Birks. & Brooks, S.J. 2011. Chironomidae (Insecta: Diptera) succession in Żabieniec bog and its palaeo-lake (central Poland) through the Late Weichselian and Holocene. *Palaeogeography, Palaeoclimatology, Palaeoecology*, 307: 150–167.

Poage, M.A. & Chamberlain, C.P. 2001. Empirical relationships between elevation and the stable isotope composition of precipitation and surface waters: Considerations for studies of paleoelevation change. *American Journal of Science*, 301: 1–15.

Quinlan, R., Smol, J.P. & Hall, R.I. 1998. Quantitative inferences of past hypolimnetic anoxia in south-central Ontario lakes using fossil midges (Diptera: Chironomidae). *Canadian Journal of Fisheries and Aquatic Sciences*, 55: 587–596.

Ravi-Kumar, M.N. 1999. Chitin and chitosan fibres: a review. *Bulletin of Materials Science*, 22: 905–915.

Rinaudo, M. 2006. Chitin and chitosan: Properties and applications. *Progress in Polymer Science*, 31: 603–632.

Rozanski, K., Araguás-Araguás, L. & Gonfiantini, R. 1993. Isotopic patterns in modern global precipitation. *Geophysical Monograph Series*, 78: 1–36.

Rozanski, K., Klisch, M., Wachiew, P., Gorczyca, Z., Goslar, T., Edwards, T.W.D. & Shemesh A. 2010. Oxygen-isotope geothermometers in lacustrine sediments: New insights through combined $\delta^{18}O$ analyses of

aquatic cellulose, authigenic calcite and biogenic silica in Lake Gościąż, central Poland. *Geochimica et Cosmochimica Acta*, 74: 2957–2969.

Ruiz, Z., Brown, A.G. & Langdon, P.G., 2006. The potential of chironomid (Insecta: Diptera) larvae in archaeological investigations of floodplain and lake settlements. *Journal of Archaeological Science*, 33: 14–33.

Sauer, P.E., Miller, G.H. & Overpeck, J.T. 2001. Oxygen isotope ratios of organic matter in arctic lakes as a paleoclimate proxy: field and laboratory investigations. *Journal of Paleolimnology*, 25: 43–64.

Sayer, C.D. & Roberts, N. 2001. Establishing realistic restoration targets for nutrient-enriched shallow lakes: linking diatom ecology and palaeoecology at the Attenborough Ponds, UK. *Hydrobiologia*, 448: 117–142.

Schimmelmann, A. 2010. Carbon, nitrogen and oxygen stable isotope Ratios in chitin. In: Chitin formation and diagenesis, topics in geobiology. Gupta, N.S (Ed.), Springer, Dordrecht, Netherlands: 81–103.

Schimmelmann, A. & DeNiro, M.J. 1986. Stable isotopic studies on chitin. III. The D/H and ^{18}O/^{16}O ratios in arthropod chitin. *Geochimica et Cosmochimica Acta*, 50: 1485–1496.

Schimmelmann, A., DeNiro, M.J., Poulicek, M., Voss-Foucart, M.F., Goffinet. & Jeuniaux, C. 1986. Stable isotopic composition of chitin from arthropods recovered in archaeological contexts as palaeoenvironmental indicators. *Journal of Archaeological Science*, 13: 553–566.

Self, A.E., 2010. The relationship between chironomids and climate in high latitude Eurasian lakes: implications for reconstructing Late Quaternary climate variability from subfossil chironomid assemblages in lake sediments from northern Russia. PhD dissertation, University College London, England, 454 p.

Sensuła, B. Böttger, T., Pazdur, A., Piotrowska, N. & Wagner, R. 2006. Carbon and oxygen isotope composition of organic matter and carbonates in recent lacustrine sediments. *Geochronometria,* 25: 77.94.

Shackleton, N. J. 1967. Oxygen isotope analyses and Pleistocene temperatures re-assessed. *Nature*, 215: 15–17.

Shackleton N. J. 2000. The 100,000-year ice-age cycle identified and found to lag temperature, carbon dioxide and orbital eccentricity. *Science,* 289: 1897–902.

Sidgwick, N.V. 1950. The Chemical Elements and their Compounds (Vol. II) Clarendon Press, 1730 p.

Sonoda S, Fukumoto K, Izumi Y, Ashfaq M, Yoshida H. & Tsumuki H. 2007. Expression profile of arylphorin gene during diapause and cold acclimation in the rice stem borer, Chilo suppressalis Walker (Lepidoptera: Crambidae). A*pplied Entomology Zoology*, 42: 35–40.

Stankiewicz, B.A. Briggsm D.E.G., Evershed, R.P., Flannery, M.B. & Wuttke, M. 1997a. Preservation of chitin in 25-million-year-old fossils. *Science*, 276: 1541–1543.

Stankiewicz, B.A, Briggs, D.E.G., Evershed, R.P. & Duncan, I.J. 1997b. Chemical preservation of insect cuticle from the Pleistocene asphalt deposits of California, USA. *Geochimica et Cosmochimica Acta*, 61: 2247–2252.

Stankiewicz, B.A. Briggs, D.E.G., Michels, R., Collinson, M.E., Flannery, M.B. & Evershed, R.P. 2000. Alternative origin of aliphatic polymer in kerogen. *Geology*, 28: 559-562.

Stuiver, M. 1970. Oxygen and carbon isotope ratios of freshwater carbonates as climatic indicators. *Journal of Geophysical Research,* 75: 5247-5257.

Stuart-Williams, H., Wong, C.S., Farquhar, G.D., Keitel, C. & Clayton, S. 2008. An innovative molybdenum column liner for oxygen and hydrogen stable isotope analysis by pyrolysis. *Rapid Communications in Mass Spectrometry*, 22: 1117–1126.

Swann, G.E.A., Maslin, M.A., Leng, M.J., Sloane, H.J. & Haug, G.H. 2006. Diatom $\delta^{18}O$ evidence for the development of the modern halocline system in the subarctic northwest Pacific at the onset of major Northern Hemisphere glaciation. *Paleoceanography*, 21: 1-12.

Tokeshi, M., 1995. Life cycles and population dynamics. In: The Chironomidae: Biology and Ecology of Non-biting Midges, Armitage P. D., P. S. Cranston & L. V. C. Pinder (Eds), Chapman & Hall: 225–268.

Talbot, M. R. 1990. A review of the paleohydrological interpretation of carbon and oxygen isotopic ratios in primary lacustrine carbonates. *Chemical Geology,* 80: 261– 279.

Tripp, J.A., Higham, T. & Hedges, R. 2004. A pretreatment procedure for the AMS radiocarbon dating of sub-fossil insect remains. *Radiocarbon*, 46: 147–154.

Urey, H.C. 1947. The thermodynamic properties of isotopic substances. *Journal of the Chemical Society,* 0: 562–581.

Velle, G., Brooks, S.J., Birks, H.J.B. & Willassen, E. 2005. Chironomids as a tool for inferring Holocene climate: an assessment based on six sites in southern Scandinavia. *Quaternary Science Reviews*, 24: 1429–1462.

Velle, G., Brodersen, K.P., Birks, H.J.B & Willassen, E. 2010. Midges as quantitative temperature indicator species: Lessons for palaeoecology. *The Holocene*, 20: 989–1002.

Verbruggen, F., Heiri, O., Richart G.J., de Leeuw, J.W., Nierop, K.G.J. & Loter, A.F. 2010a. Effects of chemical pretreatments on $\delta^{18}O$ measurements, chemical composition, and morphology of chironomid head capsules. *Journal of Paleolimnology*, 43: 857–872.

Verbruggen, F., Heiri, O., Richart G.J. & Lotter, A.F. 2010b. Chironomid $\delta^{18}O$ as a proxy for past lake water $\delta^{18}O$: a Lateglacial record from Rotsee (Switzerland). *Quaternary Science Reviews*, 29: 2271–2279.

Verbruggen, F., Heiri, O., Richart G.J., Blaga, C. & Lotter, A.F. 2011. Stable oxygen isotopes in chironomid and cladoceran remains as indicators for lake water $\delta^{18}O$. *Limnology and Oceanography*, 56: 2071–2079.

Waelbroeck, C., Labeyrie, L., Michel, E., Duplessy, J.C., McManus, J.F., Lambeck, K., Balbon, E. & Labracherie, M. 2002. Sea-level and deep water temperature changes derived from benthic foraminifera isotopic records. *Quaternary Science Reviews*, 21: 295–305.

Walker, M.J.C. 1982. The Late-glacial and early Flandrian deposit at Traeth Mawr, Brecon Beacons, South Wales. *New Phytologist*, 90: 177-194.

Walker, I.R. 1987. Chironomidae (Diptera) in paleoecology. *Quaternary Science Reviews*, 6: 29–40.

Walker, I.R. & Mathewes. R.W. 1987. Chironomidae (Diptera) and postglacial climate at Marion Lake, British Columbia, Canada. *Quaternary Research*, 27: 89–102.

Walker, I.R., Mott, R.J. & Smol, J.P., 1991. Allerod-younger dryas lake temperatures from midge fossils in atlantic Canada. *Science*, 253: 1010-1012.

Walker, M.J.C., Coope, G.R., Lowe, J.J. 1993. The Devensian (Weichsellian) Late-glacial palaeoenvironmental record from Gransmoor, East Yorkshire, England. *Quaternary Science Reviews*, 12: 659-680.

Walker, I.R. & Cwynar, L.C. 2006. Midges and palaeotemperature reconstruction-the North American experience. *Quaternary Science Reviews*, 25: 1911–1925.

Wang, Y.V. Francis, D., O'Brien, D.M. & Wooller, M.J. 2008. A protocol for preparing subfossil chironomid head capsules (Diptera: Chironomidae) for stable isotope analysis in paleoclimate reconstruction and consideration of contamination sources. *Journal of Palaeolimnology,* 40: 771-781.

Wang, Y.V. O'Brien, D.M., Jenson, J., Francis, D. & Wooller, M.J. 2009. The influence of diet and water on the stable oxygen and hydrogen isotope composition of Chironomidae (Diptera) with paleoecological implications. *Oecologia*, 160: 225–233.

Ward, C. M. & Cummins, K. W. 1979. Effect of food quality on growth of a stream detritivore, Paratendipes albimanus (Meigen) (Diptera: Chironomidae). *Ecology*, 60: 57-64

Werner, R. 2003. The Online ^{18}O/ ^{16}O Analysis: Development and application. *Isotopes in Environmental and Health Studies*, 39: 85–104.

Werner, R.A. & Brand, W.A. 2001. Referencing strategies and techniques in stable isotope ratio analysis. *Rapid Communications in Mass Spectrometry*, 15: 501–519.

Wolfe, B.B., Edwards, T.W. & Elgood, R. 2001. Carbon and oxygen isotope analysis of lake sediment cellulose: methods and applications. In: Tracking environmental change using lake sediments (Vol. 1), Last, W,M. & Smol, J.P (Eds), Kluwer Academnic Publishers, Dordrecht: 373–400.

Wolfe, B.B., Falcone, M.D., Clogg-Wright, K.P., Mongeon, C.L., Yi, Y., Brock, E., Amour, N.A.S., Mark, W.A. & Edwards, T. W.D. 2007. Progress in isotope paleohydrology using lake sediment cellulose. *Journal of Paleolimnology*, 37: 221–231.

Wooller, M., Wang, Y. & Axford, Y. 2008. A multiple stable isotope record of Late Quaternary limnological changes and chironomid paleoecology from northeastern Iceland. *Journal of Paleolimnology*, 40: 63–77.

Wooller, M.J., Francis, D., Fogel, M.L., Miller, G.H., Walker, I.R. & Wolfe, A.P. 2004. Quantitative paleotemperature estimates from δ^{18}O of chironomid head capsules preserved in arctic lake sediments. *Journal of Paleolimnology*, 31: 267–274.

Zhang, M., Haga, A., Sekiguchi, H. & Hirano, S. 2000. Structure of insect

chitin isolated from beetle larva cuticle and silkworm (Bombyx mori) pupa exuvia. *International Journal of Biological Macromolecules*, 27: 99–105.

Zhang, E., Bedford, A., Jones, R., Shen, J., Wang, S. & Tang, H. 2006. A subfossil chironomid-total phosphorus inference model for lakes in the middle and lower reaches of the Yangtze River. *Chinese Science Bulletin*, 51: 2125–2132.

Appendices

A-I: δ^{18}O Analysis of Organic Compounds: Problems with Pyrolysis in Molybdenum-lined Reactors

Introduction- δ^{18}O determinations on organic compounds are typically made using high temperature pyrolysis systems (HTP) [1-7]. Classical HTP reactors consist of a bed of glassy carbon granules inside a glassy carbon tube that lines an outer alumina (Al_2O_3) tube[1-6]. A recent paper by Stuart-Williams et al.[8] evaluated an HTP reactor that employed molybdenum (Mo) foil as a barrier liner instead of a glassy carbon tube. The Mo-lined reactor gave a precision <0.25‰ (1σ) during δ^{18}O analysis of solid organic compounds and waters[8]. Mo is an attractive alternative as it conforms well to the interior of the outer column, is resistant to high temperatures and is relatively cheap[8].

However, when we adopted a Mo-lined Al_2O_3 reactor in a standard TC/EA (High Temperature Conversion Elemental Analyser) and ConFlo III (both Thermo Scientific, Germany) system for δ^{18}O analysis of benzoic acid, we encountered unexpectedly poor precision, variable CO yields, and severe scale compression during analysis of reference materials IAEA-601 and -602 (www.Nucleus.iaea.org/rpst/RefrenceMaterials/Stable_Isotopes/index). The TC/EA EA was fitted with a zero-blank auto sampler (Costech International, Italy) and was coupled to a Thermo Delta+XP isotope ratio mass spectrometer. This poor performance suggests that quantitative sample conversion to CO gas was not achieved in our system. Non-quantitative reduction will cause isotopic fractionation and can either be due to incomplete pyrolysis, which is unlikely in this case, or partitioning of oxygen into phases other than gaseous CO. The absence of CO_2 from the gases emerging from our reactor implied that the partitioning was likely to have been into non-gaseous phases. In order to investigate this hypothesis we conducted scanning electron microscope- energy dispersive X-ray spectroscopy (SEM-EDX)[9] and Raman spectroscopy[10] on two used Mo-lined reactors. In this letter we illustrate the results and discuss their implications.

Reactor Configuration- The TC/EA reactor consisted of a Al_2O_3 tube (i.d. 13 mm; o.d. 17 mm; length 470mm) that was lined with high purity (99.95%) 0.1mm thick Mo-foil (supplied by SerCon, UK. www.sercongroup.com) (*Fig.1a*). A 60 mm deep bed of glassy carbon granules (3-4 mm) was supported in the hottest part of the reactor by a plug of folded Mo-foil (*Fig.1a*).

The tube diameter and glassy carbon bed thickness were both constrained by the construction of the TC/EA furnace, so there were important differences from the reactor employed by Stuart-Williams et al.[8]. Their furnace had a deeper hot-zone, as shown in *Fig. 1b*, and a wider Al_2O_3 tube (i.d. 16mm). Based on Stuart-Williams et al.[8] we infer that their glassy carbon bed was approximately twice as deep as ours (~110 -120mm).

Testing and Reactor Performance- Aliquots of 150ug ±10µg oven-dried benzoic acid, folded into Ag foil capsules, were dropped sequentially from the fully purged auto-sampler directly onto the carbon bed where they underwent flash pyrolysis. The gaseous products were entrained by a carrier gas (99.999% He) and separated by passage through the TC/EA's standard GC column (5 Å molecular sieve, 80 -100 mesh at 60°C). The carrier and sample gases were admitted to the mass spectrometer via the ConFlo III open split, which provides a parallel gas stream to enable injections of a CO reference gas. Most analyses were carried out at 1400°C although temperatures were occasionally varied in the range 1350 – 1430°C to search for conditions that would improve precision. Carrier gas flow rates were varied systematically from 60 – 90 mL/minute.

During runs at various flow rates but at 1400°C the Mo-lined reactors suffered from scale compressions of up to 20‰ relative to our reference gas, between IAEA reference materials with $\delta^{18}O$ values 48‰ apart on the SMOW scale. Reproducibility of $\delta^{18}O$ was poor (0.4 - 3‰ (1σ)). CO yields per unit weight of benzoic acid varied considerably even at constant flow rate (*Fig. 2*). CO yields were higher at lower flow rates because of longer residence times of the gases within the carbon bed, at temperatures >1100°C (*Fig. 2*).

Examination and analysis of used reactor liners- Two reactors were examined after 207 and 160 analyses and analysed for elemental composition by SEM-EDX and Raman spectroscopy (Note that the atomic % values given for C, N and O have relatively large uncertainties due to both the lack of sensitivity of the EDX detectors to the x-ray emissions of light elements and the absorption of oxygen onto the surface of the samples before analysis). The outer alumina tubes were broken open by tapping with a hammer. The Mo-liners had become brittle, and were severely corroded and pitted in the hottest part of the furnace. Based on visual examination both reactors could be divided into five zones (*Fig. 3a*):

Zone I spanned 130 mm from the top of the Mo-liner, with temperatures ~450 to ~1150°C (*Fig. 1b*). The Mo-foil had a violet/brown lustre, consistent with MoO[11-14] (*Fig. 3a*).

Zone II is 40 mm long and characterised by bronze/gold patina (*Fig. 3a*), that gives way downwards to bright metal just above the top of the carbon bed where temperatures were ~1400°C. EDX analysis of the inner surface of the Mo-liner confirmed the presence of Mo and oxygen (nominal proportions Mo: 30 atom%, O: ~69 atom%) (*Fig. 3b*). EDX spectra from the outer surface indicated similar proportions of Mo and oxygen as the inner surface, plus trace amounts of Al.

Zone III is 25mm long with temperatures >1350°C in the upper part of the carbon bed (*Fig. 1b).* The Mo-liner shows extensive pitting and dulling with surface encrustations both inside and out (*Fig. 3a*). The outer encrustations contained O (nominally ~58 %), Al (29 %), N (10 %) and Mo (2 %) (*Fig. 3c*). The inner surface contained Mo (85 %) and O (~15 %).

Zone IV spans the lower 35 mm of the carbon bed, with temperatures >1100°C (*Fig. 1b*). The inner surface of the Mo-liner was dulled and covered by globules of soft metal up to several mm in diameter (*Fig. 3a*). They consisted of silver with substantial proportions of carbon and oxygen (Ag: 51%, C: 32 %, O: ~15 %) (*Fig. 3d*).

Zone V spans the cooler region below the Mo-plug with temperatures ~400 – 1100°C (*Fig. 1b).* Both inner and outer surfaces carried a patina of Mo-oxides (Mo: 41%, O: ~52%) on which fine globules of silver had been deposited (*Fig. 3e*).

A few silver globules occurred on the inner surface in Zone II and in the lowest part of Zone I. As these were above the bed of glassy carbon granules, they most likely represent splashes of molten silver thrown out by the gases released during pyrolysis. In the lower part of Zone IV and through most of Zone V both surfaces carried many closely spaced hemispherical silver globules that were finer and more closely spaced downwards. Like the large globules in the upper part of Zone IV, they contained both carbon (up to 30 %) and oxygen (up to 10 %).

In Zone III and the upper part of Zone IV the inner surface of the Al_2O_3 tube was stained black. Raman spectroscopy showed the presence of graphite. Above and below this graphitic deposit the Al_2O_3 retained its original white colour.

Discussion- The severe pitting and corrosion of the original Mo metal in Zones III and IV is associated with deposition of patinas of Mo-oxides on almost the entire surface of the liner.   There are three possible sources of reactive oxygen in our system: (a) diffusion of atmospheric oxygen and nitrogen through the hot Al_2O_3 wall of the reactor, (b) diffusion of oxygen atoms from the heated Al_2O_3 itself, or more likely direct reaction of Al_2O_3 with the Mo metal where the two came into contact (c) oxygen-bearing gases released by pyrolysis of the samples. The first two sources might account for Mo-oxides forming on the outer surface of the liner, but are less likely to be responsible for the much more extensive patinas seen on the inside. The detection of nitrogen in an EDX spectrum from the outer surface of Zone III (*Fig. 3c*) is consistent with air having diffused through the Al_2O_3 column wall, so atmospheric oxygen is likely to be a source of corrosion. However it is unlikely to have been the principal source. The corrosion of the outside surface of the Mo liner was comparatively slight whereas the inside surface was deeply pitted and holed, with oxide deposits apparently lining the pits. One would not expect this pattern if the principal source lay on the outside of the liner.

The oxygen-bearing gases produced by pyrolysis of benzoic acid could include CO, CO_2, H_2O but reaction with the carbon bed at 1400°C would reduce CO_2 and H_2O to CO and H_2, so these must be the principal gases present inside the Mo-liner, apart from carrier He. Mo metal reacts with gaseous CO to produce Mo-oxides and carbon[14]:

$$Mo + mCO \rightarrow MoO_m + mC.$$

The presence of graphitic carbon on the inner surface of the Al_2O_3 column strongly supports this reaction as being responsible for some, if not all, of the corrosion of Mo and formation of oxides. The carbon deposit occurred where CO could easily escape through holes, cracks and pitted regions of the Mo-liner and attack the outer surface of the metal. The principal oxides of Mo are MoO_2 and MoO_3. They have melting and boiling points far lower than the 1400°C in the hottest part of the reactor (MoO_2 MP 782°C, BP 1257°C; MoO_3 MP 795°C, BP 1155°C[11-14]) which would permit them to exist there as vapour, condensing to form patinas and crystalline coatings in the cooler parts.

The consumption of CO in the production of new Mo-oxides is a probable explanation for the variability observed in yields of CO gas per unit weight of benzoic acid (*Fig. 2)* and would directly cause isotopic fractionation of the residual CO. To account for the scale compression between the reference materials IAEA 601 and 602, such fractionation would have to vary systematically with the $\delta^{18}O$ of the sample, which seems unlikely in such a high-temperature system, but cannot be ruled out. An alternative explanation may lie in the fact that the build-up of Mo-oxides forms a reservoir of oxygen with which gaseous CO could exchange both isotopically and through bulk chemical reactions. Another product of pyrolysis is hydrogen, and above 500°C MoO_2 reacts with H_2 to form Mo metal and water[11, 15]. At temperatures over 1000°C the water produced will be partially reduced on glassy carbon and will re-form as H_2 and CO. Thus Mo and C in the reactor will take part in a circular series of reactions with the gases:
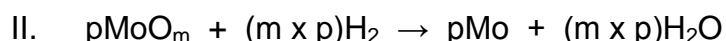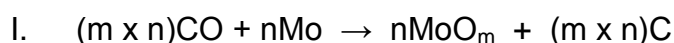
$$\text{I.} \quad (m \times n)CO + nMo \rightarrow nMoO_m + (m \times n)C$$

$$\text{II.} \quad pMoO_m + (m \times p)H_2 \rightarrow pMo + (m \times p)H_2O$$

$$\text{III.} \quad (m \times p)H_2O + (m \times p)C \rightarrow (m \times p)H_2 + (m \times p)CO.$$

Reaction I will sequester a portion of the oxygen in the original CO into Mo-oxides. Reaction II followed by III will return some of this oxygen to gaseous form as CO. This return will only be complete in the case that n=p in the above scheme, and also that Reaction III runs to completion. If both were so, the Mo-liner would show pitting and corrosion, but would lack any patina of Mo-oxides. The fact that our Mo-liners were coated by Mo-oxides indicates that in our case p<n, and the return of oxygen to gaseous CO is

incomplete. It is known from experimentation with analysis of water in glassy-carbon lined reactors that Reaction III does not run to completion unless temperatures exceed 1350 – 1400°C [2,5], catalysis by Ni being required at lower temperatures. Thus there is scope for additional isotopic fractionation of the final CO leaving the reactor, through kinetic effects in both Reactions II and III. We speculate that the varying scale compressions observed in $\delta^{18}O$ of the final CO may be a function of differential fractionations between Reaction I and Reactions II and III, as well as the degree of inequality p<n and other possible factors. The latter include the possibility that Reactions II and III take place over a range of temperatures as the gases stream downwards from the hottest zone into cooler regions and Mo-oxides condense from the vapour to the liquid and solid phases. Once the Mo-liner has been pierced by corrosion due to Reaction I, as seems to have occurred quite quickly in our reactors, some of the gases and vapours may migrate down the annulus between the Mo-liner and the outer Al_2O_3 tube, where there is no access to solid carbon apart from that produced by Reaction I, which as noted above was confined to the hottest region. Thus, Reaction III will not affect these gases to any significant extent, and the water that results from Reaction II will mostly remain unconverted back to CO and H_2. In the core of reactor, where carbon is abundant, Reaction III can be expected to run to completion in Zone III where the local temperature is high enough, but may not do so in the cooler lower part of the carbon bed (Zone IV), and cannot do so where carbon is absent (Zone V). The yield of CO gas, its isotopic composition and resultant scale compression, are likely to depend upon the interplay of reaction rates, local temperatures, carrier gas flow rates and the residence times of the gases in the parts of the reactor that are most favourable for Reactions II and III. The condition of the reactor liner, especially whether it is pierced by corrosion, and the amount of Mo-oxide deposit that has built up over time are further factors. The Mo-oxide deposit is a potential locus for Reaction II, so the fractionation it causes in the final output of CO may depend on the whole history of reactor use and the $\delta^{18}O$ values of the samples that have been analysed previously, as there will be a memory of these in the Mo-oxide $\delta^{18}O$.

If the scheme of reactions envisaged is correct, then successful, accurate analysis of benzoic acid and other compounds would require conditions such that Reactions II and III can return all oxygen to gaseous form as CO, so that Mo-oxides would not build up in the reactor. This is most likely to be achieved if the sample gases have a long residence time in contact with carbon in the hottest part of the reactor, optimising recovery of oxygen to CO via Reaction III. As Stuart-Williams et al.[8] were able to achieve good precision without scale compression (see Table 3 of Brand et al.[16]), these

conditions probably were met in their reactor which had a longer hot zone (*Fig.1b*) and larger diameter than ours. Rough estimation suggests that if volumetric gas flows were equal in the two systems, the gas residence time in the hottest part of Stuart-Williams' reactor would be 2-3 times greater than in our TC/EA. We strongly suspect, therefore, that it is the residence time of gas in contact with carbon at ~1400°C that is critical.

A possible line of development for reactors such as the TC/EA, which has a narrow hot-zone (Fig. 1B), might be to inactivate the Mo surface of the liner. Mo is known to form a variety of carbides by reaction with CO[17] and a coating of these may inhibit the corrosion reactions with the metal. Border[18] describes the use of Mo-Carbide coated carbon as a catalyst for the conversion of oxygen in organic compounds into CO at 1080°C. Inactivation might also slow down corrosion of the outside surface of the Mo-liner by oxygen diffusion through the alumina tube or by direct reaction with the Al_2O_3. Direct measurement of air diffusion through the alumina tubes under operating temperatures would help to establish the relative importance of these sources of oxygen in causing the corrosion we have observed, but so far we have not attempted this.

Conclusion- To our knowledge no previously published studies have investigated the chemical composition of HTP reactors after use. Molybdenum liners are inexpensive and easy to fabricate but they are unsuitable for the popular Thermo TC/EA. The principal reason for this appears to be production and build up of Mo-oxides as a patina or coating on the liner as a result of the reaction between Mo metal and CO gas, causing poor precision and variable CO-yields. To some extent the loss of CO is compensated by reactions between Mo-oxides and hydrogen gas derived from the sample, producing water, followed by reduction of the water to CO and H_2 by reaction with glassy carbon. However, these restoring reactions probably introduce further fractionation effects and may be responsible for scale compression. Despite all this, it is possible to obtain a precision of 0.25‰ from Mo-liners, as demonstrated by Stuart-Williams et al.[8]. From comparison of reactor designs, we conclude that the depth of the hottest zone and the time that the pyrolysis products spend within it are critical factors, although differences in diffusion of atmospheric oxygen through the walls of the alumina tubes may also have played a part. Analysts intending to develop a Mo-lined HTP system should ensure that their furnace and reactor designs follow those of Stuart-Williams et al.[8] and provide a residence time at ~1400°C for the produced gases of at least 4 seconds. The approximate residence times in our TC/EA system varied from ~1.3 to ~2 seconds which was not sufficient to promote 100% net conversion of oxygen from the sample into CO. Although molybdenum lined reactors have

potential for $\delta^{18}O$ determinations within some HTP systems, it is clear from our experience that the chemistry of reactions is not straightforward and that Mo-liners seem unsuitable for use within TC/EA units in the configuration tested by this study.
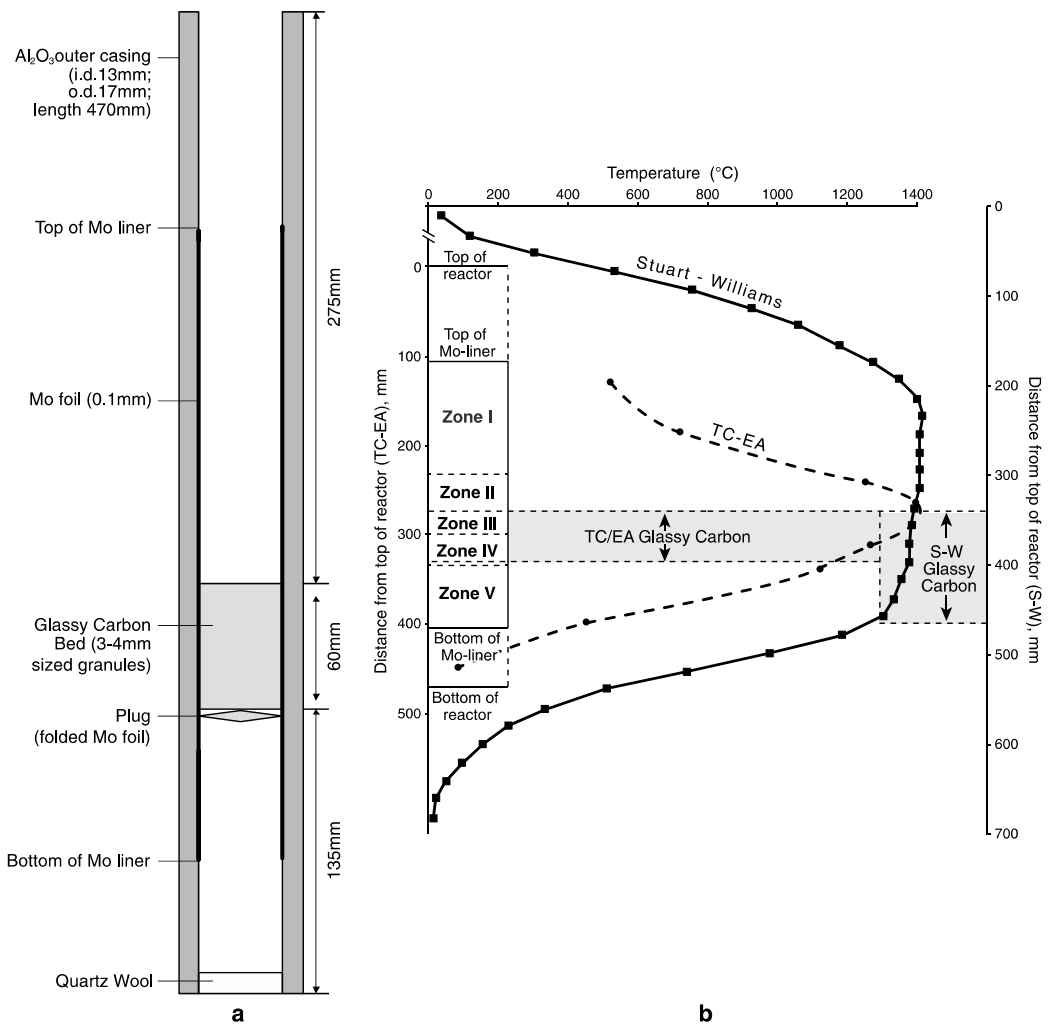
Figure 1. (a) Construction of the Mo-lined reactor for the TC/EA system. (b) Comparison between the temperature profiles and glassy carbon bed thickness for TC/EA and the Mo-lined reactor used by Stuart-Williams et al.[8] The vertical scales are offset so that the tops of the glassy carbon beds are aligned. Zones of corrosion damage in TC/EA reactor shown on the left.
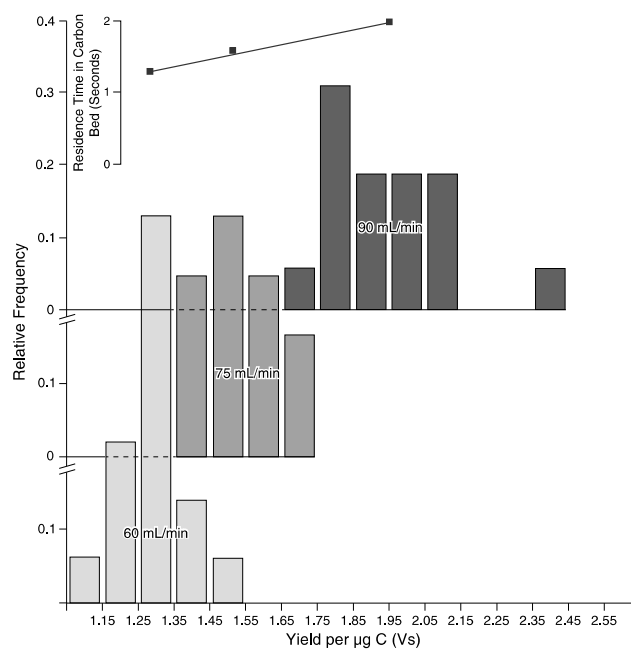
Figure 2. Variability of CO gas yield with carrier gas flow rate and inferred residence time in contact with glassy carbon at temperature >1100 °C. Histograms show grouped data from individual analyses; square symbols show mean for each flow rate plotted against residence time.
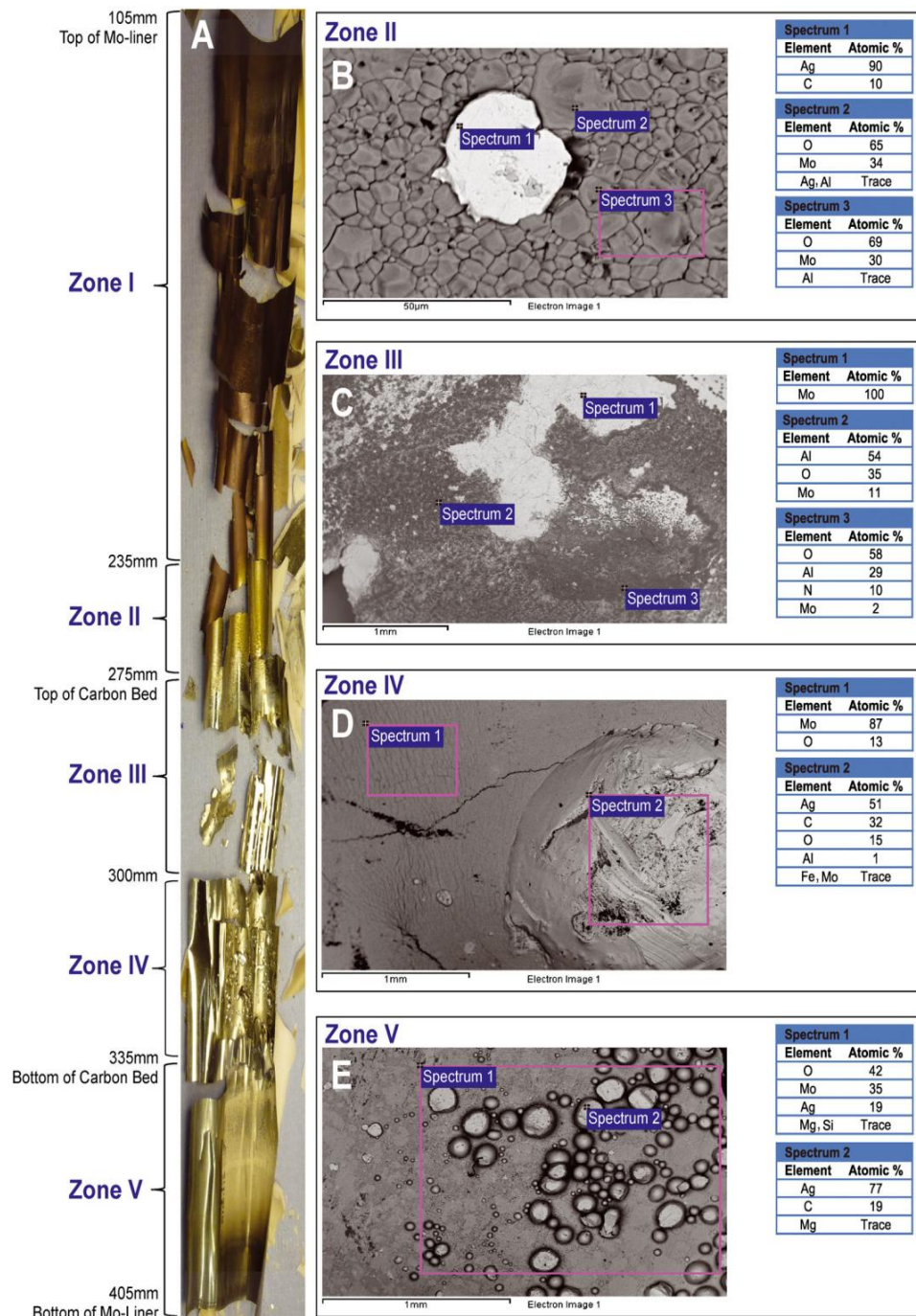
Figure 3. (a) Photograph of used Mo-liner, 300 mm long, broken during extraction and unrolling. For division into zones (left), see text. (b) SEM image and EDX analyses of inner liner surface from Zone II, showing silver globule (spectrum 1) adhering to mosaic-like patina of Mo-oxides (spectra 2 and 3). (c) SEM image and EDX analyses of outer liner surface from Zone III, showing areas of light-coloured Mo metal (spectrum 1) and darker patina containing Al and Mo oxides (spectrum 2) and a nitrogen-bearing phase (spectrum 3). (d) SEM image and EDX analyses of inner liner surface from Zone IV, showing cracked patina of Mo-oxide (spectrum 1), plus 2 mm diameter blob of silver containing carbon and oxygen (spectrum 2). (e) SEM image and EDX analyses of inner liner surface from Zone V with ~0.1 mm globules of silver containing carbon (spectrum 2) on a patina of Mo-oxide. Spectrum 1 contains both components.

216

A-II: Raw data from δ^{18}O analyses of reference materials IAEA 601 and 602, which should differ by 48.1‰

Reactor Temp (°C)	Carrier Pressure (mL/min)	Material	δ^{18}O (‰)	Δ^{18}O$_{602-601}$
		601	12.8	
			13.1	
			13.2	
1450	**1000**		10.8	
		602	33.5	
			32.0	
			32.5	**20.5**
		601	23.8	
			23.3	
			22.7	
1400	**1000**		23.1	
		602	53.1	
			53.3	
			54.6	
			52.9	**30.3**

			-23.0	
		601	-24.9	
			-21.5	
1400	**800**		-21.8	
			0.4	
		602	4.1	
			-1.7	
			4.4	**24.5**
			23.9	
		601	22.8	
			23.2	
1350	1000		22.7	
			62.7	
		602	62.1	
			61.8	
			62.0	**39.0**

B-I: Sample size analyses

Weight (µg)	$\delta^{18}O_{corrected}$				
	1	2	3	$\bar{x}$	1σ
10 (±2)	23.1	24.6	23.7	23.8	0.8
20 (±2)	25.3	26.2	26.6	26.0	0.7
30 (±2)	25.6	26.6	26.9	26.4	0.7
40 (±2)	27.3	26.7	26.0	26.7	0.7
50 (±2)	25.8	26.4	26.9	26.4	0.6
60 (±2)	26.1	27.1	26.6	26.6	0.5
70 (±2)	27.0	26.5	26.1	26.5	0.5
80 (±2)	26.6	26.1	27.0	26.6	0.5
90 (±2)	26.8	26.3	25.9	26.3	0.5
100 (±2)	26.3	25.8	26.7	26.3	0.5

B-II: Table 3.2 raw data

Chitin Standard	ID								Weight loss			δ^{18}O$_{corr}$ (V-SMOW ‰)		
Treatment	Concentration			Temperature		Duration			Start (µg)	End (µg)	% Loss	1	2	3
	2:1	0.25	1M	20°C	70°C	1 hr	24 hr							
DCM: MeOH	X			X		X			2058	1346	35	28.2		
	X			X			X		2042	1328	35	28.7	29.0	
	X				X	X			2035	1255	39	28.3		
	x				x		X		1995	807	60	28.6		
HCl	N/A	X		X		X			2033	1127	45	28.9		
		X		X			X		2077	1204	42	29.1		
		X			X	X			2094	872	58	28.8		
		X			X		X		1977	1588	20	28.9		
			X	X		X			1933	1458	25	28.4	29.2	
			X	X			X		1987	1198	40	28.9		
			X		X	X			1950	904	54	28.2	29.4	
			X		X		X		2022	0	100			
NaOH	N/A	X		X		X			2071	1716	17	29.1	28.9	
		X		X			X		1969	1577	20	28.6		
		X			X	X			2069	1489	28	29.2	28.9	
		X			X		X		1939	1391	28	28.8		
			X	X		X			2077	1319	36	28.5	27.4	
			X	X			X		2016	1132	44	29.0		
			X		X	X			2019	1596	21	28.2		

			X		X		X		2031	1470	28	28.6	29.5	
DCM:	X	X		X		X		2081	954	54	28.0		
	X	X		X			X	2032	829	59	28.9		
MeOH +	X	X			X	X		2067	1382	33	28.7		
HCl +	X	X			X		X	2017	1295	36	28.5		
	X		X	X		X		1977	883	55	29.5	30.0	
NaOH	X		X	X			X	1962	1052	48	29.3	30.0	
	X		X		X	X		2011	432	79	29.0		
	X		X		X		X	1960	1221	38	27.7		
Control	N/A			X		X		1951	1265	35	28.1	27.3	
				X			X	2021	1343	34	27.8	28.0	
					X	X		2044	1102	46	28.2	27.3	
					X		X	2049	1082	47	27.8	28.6	28.4

Head Capsules	ID							Weight loss			$\delta^{18}O_{corr}$ (V-SMOW ‰)		
Treatment	Concentration			Temperature		Duration		Start (µg)	End (µg)	% Loss	1	2	3
	2:1	0.25 M	1M	20°C	70°C	1 hr	24 hr						
DCM: MeOH	X			X		X		1020	420	59	15.9		
	X			X			X	1005	430	57	13.6	13.0	
	X				X	X		1021	417	59	15.2	14.2	
	x				x		X	1011	421	58	12.3	12.8	
HCl	N/A	X		X		X		1998	1230	38	13.2	13.4	15.1
		X		X			X	2014	1384	31	15.1	15.5	15.3
		X			X	X		2045	1398	32	14.8		
		X			X		X	1934	1343	31	16.2	14.3	15.7
			X	X		X		2010	1271	37	15.0		
			X	X			X	2030	1029	49	15.3		
			X		X	X		1974	1008	49	16.0		
			X		X		X	1973	560	72	17.8		
NaOH	N/A	X		X		X		1949	586	70	16.0	15.6	
		X		X			X	1938	308	84	18.1		
		X			X	X		1990	313	84	17.1		
		X			X		X	1003	85	92	17.1	16.2	
			X	X		X		1004	52	95	16.0		
			X	X			X	1003	61	94	19.0		
			X		X	X		1015	24	98	16.0		

Group								ID					
			X		X		X	1001	492	51	22.4		
DCM: MeOH + HCl + NaOH	X	X		X		X		1014	243	76	15.9	14.9	
	X	X		X			X	1006	110	89	16.3	16.5	
	X	X			X	X		1015	240	76	15.9	16.2	
	X	X			X		X	1027	55	95	16.1	18.6	
	X		X	X		X		1047	270	74	14.6		
	X		X	X			X	1003	57	94	17.7		
	X		X		X	X		1035	109	89	17.7	16.6	
	X		X		X		X	1010	53	95	12.9		
Control	N/A			X		X		1037	457	56	14.1	12.9	13.4
				X			X	1061	653	38	15.6		
					X	X		1062	554	48	14.7	14.0	15.0
					X		X	1035	617	40	14.2	14.5	14.0

C-I: Monthly $\delta^{18}O_{lakewater}$ from Attenborough Nature Reserve between June 2011-May 2013

Monthly $\delta^{18}O_{lakewater}$ measurements from each of the sampled ponds at the Attenborough Nature Reserve between June 2011-May 2013, average data is presented in Table 4-10.

Month-Year	$\delta^{18}O_{lakewater}$ (V-SMOW ‰)			
	Main	**Beeston**	**Church**	**Clifton**
June 2011	−5.45			−0.86
July 2011	−5.24	−4.79	−0.72	−0.33
August 2011	−5.16	−4.89	−0.38	−0.13
September 2011	−5.00	−4.43	−0.27	0.05
October 2011	−4.65	−4.04	−0.09	−0.26
November 2011	−4.97	−4.37	−0.36	−0.24
December 2011	−6.28	−4.87	−1.05	−0.77
January 2012	−5.70	−5.34	−2.25	−1.30
February 2012	−7.03	−5.96	−2.25	−1.54
March 2012	−6.79	−6.85	−2.25	−1.58
April 2012	−7.83	−6.14	−2.01	−1.73
May 2012	−6.96	−6.69	−2.12	−2.03
June 2012	−7.15	−5.99	−1.58	−1.38
July 2012	−6.71	−6.13	−1.85	−1.73
August 2012	−6.33	−5.68	−1.67	−1.33
September 2012	−6.46	−5.30	−1.15	−1.35
October 2012	−7.34	−5.72	−1.37	−1.70
November 2012	−7.18	−6.29	−1.61	−2.11

December 2012	−8.22	−7.99	−4.79	−4.70
January 2013	−8.12	−8.56	−6.39	−6.68
February 2013	−9.03	−8.88	−6.27	−6.60
March 2013	−8.45	−8.40	−6.11	−6.50
April 2013	−8.82	−8.48	−6.18	−6.59
May 2013	−7.89	−7.74	−5.45	−5.87

C-II: Monthly $\delta^{18}O_{chironomid}$ from Attenborough Nature Reserve between June 2011-May 2013

Monthly $\delta^{18}O_{chironomid}$ measurements from each of the sampled ponds at the Attenborough Nature Reserve between June 2011-May 2013, average data is presented in Table 4-11.

Month-Year	Main	Beeston	Church	Clifton
		$\delta^{18}O_{chironomid}$ (V-SMOW ‰)		
July 2011	14.15		20.04	18.17
October 2011	15.36	15.48		20.78
December 2011	15.17		20.34	20.36
February 2012	16.34	16.16	19.12	17.87
April 2012	14.49	15.95	19.53	20.38
June 2012	14.97	14.77	18.67	18.94
August 2012	14.21	13.88	18.16	17.19
October 2012	14.37	14.91	16.94	20.36
November 2012	16.45	16.22	19.89	19.57
December 2012	14.11	15.80	17.63	18.57
January 2013	14.08	13.13	20.39	20.51
February 2013	15.64	15.51	19.71	19.98
April 2013	16.09	14.94	18.86	20.44
May 2013	13.55	13.70	17.69	17.26